



THE UNIVERSITY OF ADELAIDE

Department of Civil & Environmental Engineering

**DEFORMATIONS in NAILED
PLYWOOD GUSSET PLATE JOINTS
due to DYNAMIC LOADING**

BY WADE STEVENS

**Thesis submitted for the degree of
Master of Engineering Science**

ABSTRACT

Multi-nail, plywood gusset plate 'knee' joints provide the structural integrity of large, LVL timber portal frames. One example is the "Yttrup" Joint. An extensive literature review discusses the relevance of current timber engineering knowledge to moment resisting joints. The long term effect on the stiffness and ultimate strength of these joints, due to the dynamic action of lateral wind loadings, is discussed. A measurement technique is described which simultaneously records the magnitudes of the deformation responses of one "Yttrup" Joint and the incident gust wind speed for an Adelaide structure. This information acts as a record of the performance of an actual joint already 'pre-softened' by several years of random, 'in-service' wind loadings. Recordings are compared to a 2D computer structural model and concurrent laboratory tests on half scale "Yttrup" Joint models. Both of these represented the LVL members and joint only, and highlight the importance of the three dimensional action of the structure.

DECLARATION of ORIGINALITY

This work contains no material which has been accepted for the award of any other degree or diploma in any university or other tertiary institution and, to the best of my knowledge and belief, contains no material previously published or written by another person, except where due reference has been made in the text.

I give consent to this copy of my Thesis, when deposited in the University Library, being available for loan and photocopying.

SIGNED: .

DATE: 13/1/95

ACKNOWLEDGEMENTS

The timber engineering research project, of which this study was part, was funded by a grant from the Australian Research Council.

Dr. Michael Griffith was a constant source of encouragement and assistance throughout the project, on both a technical and personal level, and deserves the highest praise for his patient supervision.

Thanks are also extended to Dr. Malcolm Hirst, who acted as my co-supervisor. Also, his experiences from previous research investigations involving strain and thermal measurements proved invaluable.

A significant proportion of the project comprised the design and development of an accurate and reliable instrumentation system for measuring the deformations in the portal frame 'knee' joint. The injection of ideas, and the enthusiastic attitude of the instrumentation and technical staff in the Department were particularly encouraging. Credit for the many innovative components of the data collection set-up belongs to Bruce Lucas, Stan Woithe, Bob Marcussen and Colin Haese.

Dr. George Sved, an Honorary Visiting Research Fellow in the Department of Civil Engineering, was consulted on several occasions. His experience in the timber engineering field, and his fundamental approach to problem solving, were particularly useful, especially during the development of suitable methods for rafter strain and joint rotation measurement.

In addition, I would like to express thanks to my research colleague, Gregg Klopp, a fellow research postgraduate, for his constant technical assistance, contribution of ideas, encouragement and comradeship throughout the duration of my project. Many of the structural dynamic measurement and analysis techniques used in this study were developed with his help. Gregg also proved to be an invaluable asset on our CD buying raids to the city centre record stores at lunchtimes.

Mr. Rob Rundle and Len Lovis of Signature Joinery, the tenants of the Wingfield building, generously allowed us to instrument the structure, and accommodated all of our requests. Discussions with Mr. Peter Ytrup, the designer of the Wingfield structure, were of great help, as was his provision of the structural drawings for the structure. A current employee of his structural engineering consultancy, Keith Nicholls, completed his final year research project under the direction of Dr. Griffith during 1990. His report is referenced in this thesis, and that study helped to rekindle interest in timber research in the Department. The links with industry established during his project have been continued, and have provided a healthy exchange of ideas between all of those mentioned above.

Mr. Peter Llewellyn, Executive Director of the Timber Development Association of South Australia was always supportive. During the literature search for the overall project, his help, along with that of Ms. Kay Leverett of the Barr-Smith Library at the University, and Ms. Meredith Isbell of the S.A. Woods and Forests Department, made this time-consuming task much easier.

The assistance and advice from Mr. Jack Ewers, Senior Lecturer (Water Engineering) in the Department of Civil Engineering, during the calibration of the wind anemometer, was greatly appreciated.

TABLE of CONTENTS

1. INTRODUCTION	1
2. The NAIL-WOOD FAILURE MECHANISM	3
3. LITERATURE REVIEW	
Introduction	7
3.1 Number and Arrangement of Nails	9
3.2 Member Materials and Dimensions	15
3.3 Nail Head Restraint	21
3.4 Interface Characteristics	27
3.5 Cyclic Loading Characteristics	31
4. PREDICTION of YTTRUP JOINT PERFORMANCE	
4.1. Summary of the Literature Review	37
4.2. Prediction of Load Capacity - A Review of Theoretical Methods	38
5. The INSTRUMENTATION SYSTEM	
5.1 The Instrumentation System	45
5.2 Rafter Bending Moment and Axial Force	53
5.3 Joint Rotation	65
5.4 Wind Measurements	73
5.5 Lateral Displacement of Knee Joint	77
6. PREDICTIONS for RAFTER STRAINS and JOINT DEFORMATIONS due to WIND LOAD	81
6.1 Structural Model Features	82
6.2 Derivation of Rotational Spring Constant K_0	83
6.3 Wind Loading	89
6.4 Structural Model Estimates	91
6.5 Estimates for Rafter Strains	93
6.6 Estimates Based on Refined K_0	94
7. RESULTS and DISCUSSION	
7.1 Joint Moment-Rotation	95
7.2 Joint Stiffness	103
7.3 Lateral Displacement of Knee Joint	105
7.4 Frequency of Response	109
8. COMPARISONS of RESULTS	
8.1 Comparison with Structural Model	111
8.2 Comparison with Laboratory Tests	117
9. CONCLUSIONS	121
APPENDICES	
A. Strain Gauge Calibration Test	123
B. RVDT Calibration Test	127
C. Anemometer Calibration Test	129
D. Calculations for the Ultimate Moment Capacity of the Yttrup Joint	131
E. Testing Variables	137
F. IMAGES-3D™ Output	145
G. Moment-Rotation Calculations	159
BIBLIOGRAPHY	171

32 — The Advertiser, Monday, March 8, 1993

YAMAHA V
8 PM Parts
quest

WANTED TO

...ne to
...ne 200th floor."
...ers say they are investigating
...ch system which could deal with
... an emergency — but they haven't
disclosed any details. — AAP

ing.
Adelaide.
Paris.
Sydney.
New York.

S-E jobs boost in \$5m timber move

An extra 28 jobs would be created at IPL Australia's Nangwarry plant in the South-East following a State Cabinet decision to double production capacity of laminated veneer lumber products, the Primary Industries Minister, Mr Groom, said yesterday.

Mr Groom said Cabinet's decision to approve the installation of a second laminated veneer lumber production line at the plant this week followed recent shortages of large-section building timbers from overseas. The move would immediately create

six new full-time jobs, followed by a further 22 when production lifted to full capacity, he said. IPL, a subsidiary of a South Australian Timber Corporation company — Forwood Products — would spend \$5.5 million on the project.

TRADE

Call Phonefind for any MAIL OUTLETS

Introduction

1. INTRODUCTION

The investigation reported in this Thesis formed part of a larger timber engineering research project, examining the fatigue strength of moment resisting 'knee' joints in large timber portal frames. This project focused on a joint which connects the LVL column and rafter members in the frame with a plywood gusset plate on each side of the joint, fastened by two large nail groups (or 'rings'), as seen in Figure 1.1. Hardened nails were pneumatically driven through the gusset plate without pre-drilling to form a 'tight' connection. For the sake of brevity, this joint has been referred to throughout the report as the "Yttrup Joint", after its designer, Mr. Peter Yttrup.

These joints provide the structural integrity for portal frame buildings. They are commonly designed in Australia for 'static' loading only. Limited guidance is provided by the Australian Timber Structures Code, AS1720-1988, for the design of moment resisting joints, in particular those containing gusset plates or hardened nails. Also, research conducted in New Zealand on similar joints has only focused on "earthquake" type loading, involving relatively few load repetitions at very high amplitudes of deformation. However, the predominant loading on these lightweight structures is that of wind. This represents an almost continuous buffeting of varying intensity over the life of the structure, and may be categorized more generally as 'dynamic lateral loading'. In direct contrast with seismic loading, it causes a seemingly infinite number of load applications at relatively low level deformations. Over time, this type of loading could be expected to progressively 'soften' the joint by causing ever increasing local deformations at the nail sites, thus reducing the stiffness and load carrying capacity of the joint in the long term.

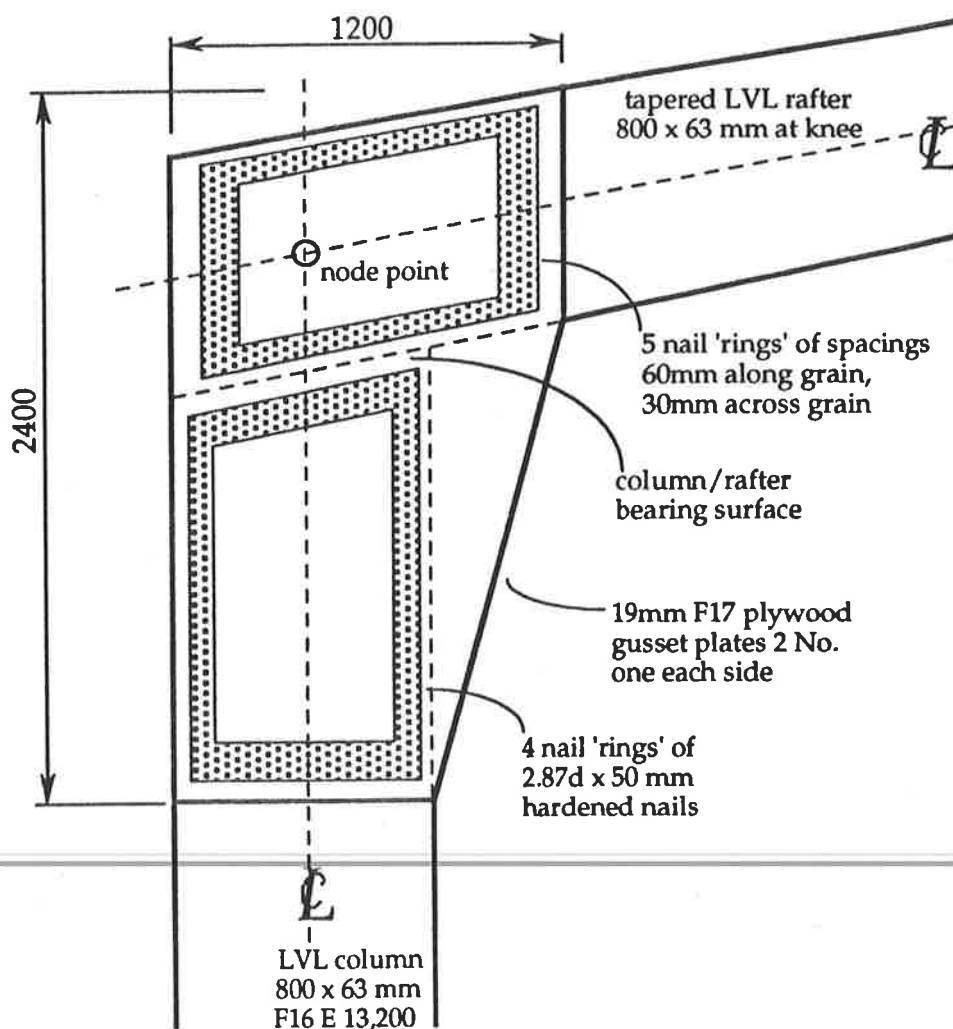


Figure 1.1. The "Yttrup Joint"

This study investigated the performance of an 'in-service' example of the Yttrup Joint at the 'serviceability' load level. A full scale joint in a typical portal frame structure was instrumented to measure its response to ambient wind excitation. Because the building had been constructed three years prior to measurements, this served to document the performance of the joint in the 'softened' condition. A concurrent study (D. Lee, M.Eng.Sc. Thesis, 1993) conducted laboratory fatigue tests on half-scale models of the Yttrup Joint to determine their 'ultimate' moment capacity, failure mode and fatigue strength. The field measurements also gave perspective to the amplitudes of load applied to the model specimens during the laboratory tests.

The structural responses measured for the building were:

- a) bending moment carried by the 'knee' joint,
- b) joint rotation,
- c) joint stiffness (being the quotient of moment and rotation),
- d) lateral frame 'sidesway' (horizontal displacement at the 'knee') and
- e) frequency of response for the structural frame.

The deformation responses of the portal frame can be regarded as equivalent to the responses of the building as a whole, due to compatibility constraints. However, deformations experienced by the frame would have been reduced by the considerable stiffening effect provided by the exterior cladding, 'rigid' end walls and bracing.

No attempt was made to quantify the wind loads applied to the structure, other than recording the instantaneous gust speed of the wind events for which the structural responses were measured. To estimate the external moment applied to the building by the wind, it would have been necessary to establish (and then integrate) the pressure distribution over the frame. This highly specialized (and time consuming) exercise was outside the scope of this study. Since the key focus was 'timber' (not 'wind') engineering, the "responses" were measured in detail and the "action" recorded in an "inexact" manner, as explained in Sections 5.1. & 5.4. Responses were recorded for a nominal ten second duration, since the "design gust" defined by the Australian Wind Loading Code, AS1170.2-1989, is based on a two to three second gust.

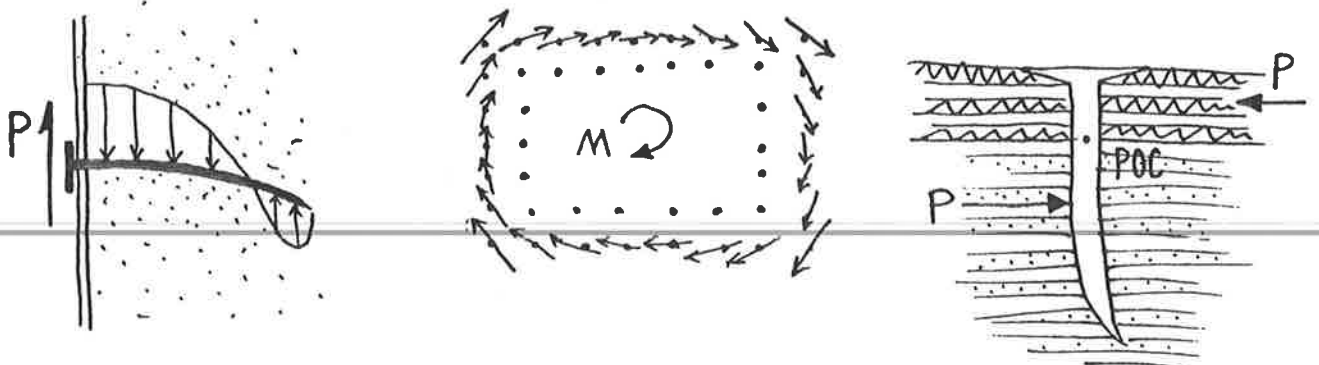
In order to maximize the (serviceability level) loads and deformations measured, and minimize the measuring errors, high wind "events" were needed. The chosen building was located in the light industrial suburb of Wingfield, Adelaide. In the prevailing wind directions for Adelaide (SW in winter, NW during spring), the surrounding area represented "Terrain Category 2" as defined by AS1170.2. Being less 'sheltered' than the standard residential "TC3" category, this provided higher wind gust speeds at the building site, and larger structural responses.

Advantage was taken of the dynamic, high frequency nature of the responses to wind loading in comparison to those due to dead load, creep or temperature effects. By measuring only the short term *changes* in strains, rotations etc., these more 'static' effects were negated, and measuring ranges could be narrowed to improve resolutions and signal to noise ratios. Most of the measurement techniques involved some compromise due to the adverse environment inside the fully operational building, used as a timber joinery workshop. As far as possible, techniques similar to those employed in the laboratory tests were used, to facilitate data correlation. Particular care had to be taken during the design of this system to ensure that the expected amplitudes of response could be reliably measured.

The measured responses were compared with those predicted by computer analysis using a structural analysis package. Rather than recreating the design process however, special attention was given to modelling the behaviour of the joint, using a rotational spring element. Two values for its stiffness were used, one based on previous New Zealand research on similar joints, the other taken from the concurrent laboratory tests on the Yttrup Joint.

Although the project was confined to the Yttrup Joint, many of its conclusions will assist the understanding of the behaviour of other similar timber moment resisting joints.

The Nail-Wood Failure Mechanism



2. The NAIL-WOOD FAILURE MECHANISM

Within the Literature Review in the following Chapter, many references are made to the "Yield Theory" of nail failure. This section has been included to facilitate the understanding of these references, to give a perspective on its wide ranging applicability and an appreciation of its limitations.

The preferred failure mode for timber joints involves the yielding of the nail fasteners. However, the high local stresses generated in the timber prior to yielding can cause the adjacent wood fibres to crush in bearing under the nail shank. Ideally, these two 'failures' would occur simultaneously. This (non-linear) nail-wood interaction is an important contributor to the overall joint load-slip performance.

An empirical approach is adopted by the Australian Timber Structures Code for estimating the allowable lateral load capacity of a single nail. A 'basic allowable' load for each of six broad timber grading groups is quoted for a 'simple' joint involving one low carbon steel nail hand-driven into two members of same wood type. Modification factors allow for divergences from this basic case. This method cannot account for all combinations of joint variables, and modification factors are not given for features used in many joint types now in common use, including the Yttrup Joint.

To predict the failure load of a laterally loaded timber joint more accurately, for a wider range of joint types, more rational 'first principles' approaches have been used. Two main methods exist, namely 'Yield Theory' and finite element based theoretical models. Both of these incorporate the dimensions and material properties for both the timber and nail as input variables. As such, their application is not limited to any particular joint type or 'basic case'. To ensure accuracy when inputting the parameters of timber embedment stress (F_e) or nail yield stress (F_y) into prediction equations from either of these methods, many investigators have chosen to obtain them from their own tests. Both F_e and F_y have been shown to exhibit a nail diameter dependency (see Section 3.2.).

2.1. FINITE ELEMENT ANALYSES

Finite element models are impractical for design use, but are very important tools during theoretical studies. Their chief application is to model the behaviour of a joint so that sensitivity analyses may be undertaken free of the material variabilities common in experimental testing. Many examples of this have been referenced in this study:

The nail-wood interaction described above has been theoretically modelled as a semi-rigid beam on an elastic (wooden) foundation by Foschi (1974) [after Hetenyi (1946) and Winkler (1867)]. His study considered only the nail head fixity conditions of 'fully fixed' (rigid side plate) and 'free' or 'pinned' (thin, soft wood side plate), for single-nailed joints. Later, Malhotra and Thomas developed this to model the timber as a bi-linear foundation (1984), and to also include the effect of interface characteristics in multi-nail joints, over the entire load-slip behaviour spectrum (1985). Nicholls (Nov 1990) included the case of 'partially restrained' nail head, to represent a joint with a thin steel side plate, in his own extension of the theoretical considerations of Foschi (1974).

2.2. YIELD THEORY

Yield Theory based 'ultimate limit state' equations were first derived by Johansen (1941), to predict the lateral load capacities of nailed timber joints. These were later developed by Moeller (1951) and Larsen (1977), and were subsequently incorporated into Scandinavian design codes. At present they form the basis of the draft Eurocode No. 5, "Common unified rules for timber structures", currently used by all EEC countries in parallel with their own. Aune and Patton-Mallory (1986a,b) extended the theory further, and

recommended its adoption in the USA. Their comprehensive papers form the basis for this Section. The extensive programs of Smith and Whale et al (1987-8) to derive embedment characteristics for nailed and bolted joints incorporated Yield Theory considerations. Their simplified prediction equations were compared with those of the 'working stress' British Timber Code BS 5268.2-1984 in Hilson and Whale (1990).

Lheude (1988) successfully gained the inclusion of reduced timber thickness to nail diameter (t/d) ratios, justified by Yield Theory, into the current Australian Code, AS1720.1-1988. As seen below, the t/d ratio is a key indicator of the mode of failure for a joint. Further studies (1990) showed that the capacities of joints incorporating recent construction practices and materials (such as those found in the Yttrup Joint) exceed AS1720 estimates for their allowable nail loads by as much as 100%.

The Yield Theory model assumes plasticity in both the wood and the fastener, and that yield occurs by 'ideal plastic' deformation, as seen in Figure 2.1. This infers that there is no limit on joint deformation. The 'ideal plastic' assumption has been shown to provide adequate load predictions during experimental verification by several authors. For more exact considerations, Aune and Patton-Mallory (1986) demonstrated that the substitution of a "fourth-root curve" for the ideal plastic 'embedment stress-deformation' assumption removes any consequent error or limitation to the Theory. With this modification, it would also be possible to obtain estimates for the joint slip (lateral deformation).

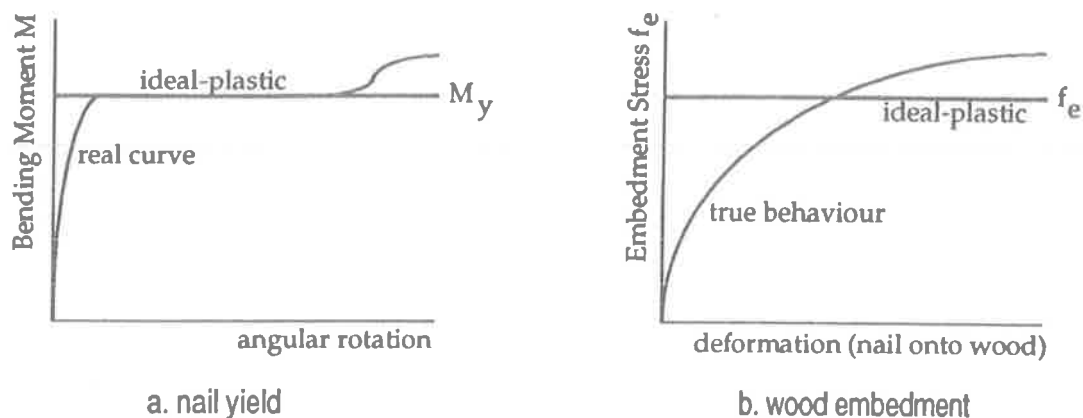


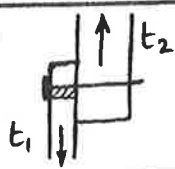
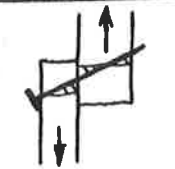
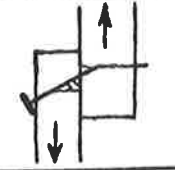
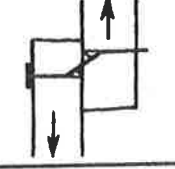
Figure 2.1. Assumed nail yield and wood embedment behaviour in Yield Theory.

Yield loads were derived for each of the likely failure scenarios (or "modes"), as shown in Figure 2.2, for the example of a timber joint with two members of equal embedment strength F_e . For any particular joint, the boundary conditions of timber F_e and thickness 't' and nail F_y and diameter 'd' are used to determine which of the failure modes applies. In this way, the equations are not 'continuous', but rather they categorize similar joints into groups having the same 'yield load'. The AS1720 method effectively limits joint failures to only the strongest of these scenarios with design rules governing allowable member thicknesses and the 'basic case' approach described earlier.

The basic failure modes for the example shown in Figure 2.2., in ascending order of nail yield load are:

- Mode 1. wood yield ('slotting') in the *side* member only
- Mode 2. wood yield in both members (no nail yield)
- Mode 3. wood yield and *one-point* nail yield in *main* member only
- Mode 4. wood yield and *two-point* nail yield

“Mode 1” failures do not involve the formation of a yield point in the nail, and are by definition premature, brittle failures of the timber due to crushing. As may be seen in Figure 2.2., they depend on the thicknesses of the timber members only (Lheude, 1990). “Splitting” failures are not considered in the Theory, as explained in Section 2.3.

mode	failure geometry	Yield Load F_u (N)	thickness conditions
1		$F_u = f_{e1} d t_1$	$\frac{t_1}{\sqrt{\gamma}} \leq 1$ $\alpha \geq 3$
2		$F_u = \frac{f_{e1} d t_1}{2} [\sqrt{3\alpha^2 + 2\alpha + 3} - (1+\alpha)]$	$\frac{t_1}{\sqrt{\gamma}} < \frac{4}{(1+3\alpha) - \sqrt{3\alpha^2 + 2\alpha + 3}}$ $1 < \alpha < 3$
3		$F_u = \frac{f_{e1} d}{3} [2 \sqrt{t_1^2 + 3\gamma} - t_1]$	$1 < \frac{t_1}{\sqrt{\gamma}} < 2 + \sqrt{2}$ $t_2 \geq \frac{2}{3} \sqrt{t_1^2 + 3\gamma} - \frac{1}{3} t_1 + 2\sqrt{\gamma}$
4		$F_u = \frac{\sqrt{2} f_{e1} d M_y}{d^2 \sqrt{f_{e1} F_y}}$ $= \frac{\sqrt{2}}{\sqrt{3}} \sqrt{f_{e1} F_y}$	$\frac{t_1}{\sqrt{\gamma}}$ and $\frac{t_2}{\sqrt{\gamma}} \geq 2 + \sqrt{2}$

$\alpha = t_2/t_1$, f_e = wood embedment strength (MPa), M_y = nail yield moment = $1/6 F_y d^3$, F_y = nail yield stress (MPa)

Figure 2.2. Nail yield formulae and failure modes for a joint with two members of equal f_e ($\beta = 1$).

Nails in the Yttrup Joint may be regarded as ‘two-member’ joints, despite the presence of three members, since the 50mm nails extend only 31mm into the 63mm wide LVL ‘main’ member. For two member joints having *unequal* embedment strengths, such as found in the Yttrup Joint, two additional failure modes are possible:

- Mode 1A. wood yield (‘slotting’) in the *main* member only
- Mode 3A. wood yield and one-point nail yield in *side* member only

The ratio of member embedment strengths (β) was $72/98 = 0.85$ for the Yttrup Joint. Calculations for its nail yield load showed that Mode 4 governed, and that the difference between the $\beta = 1$ and 0.85 cases was acceptable ($\approx 4\%$). Mode 3A (nail yield within the plywood side member) was seen to have a very low likelihood of occurrence. (see Section D.4.). As such, the simpler prediction equations of the $\beta = 1$ case could be used.

Similar expressions were developed by Aune and Patton-Mallory for the cases of joints with steel side members, three timber members and two member joints with a gap of known magnitude. This enabled a comparison of their yield loads. One notable similarity was that the yield load for Mode 4 for the above joint type (e.g. Yttrup Joint) was equal to the Mode 3 yield load for a joint involving a thin steel side plate joined to a timber main member. This is because these joints offer a similar amount of restraint to rotations of the nail head: this is explained in detail in Section 3.3. The level of nail head restraint determines how many yield points or ‘hinges’ form in the nail at failure. In Mode 4, restraint is high enough (“fixed” nail head case) to enable two hinges to form, resulting in the highest yield load for that joint configuration. For the “pinned” head restraint case

of Modes 1 and 2, side members are so thin that failure occurs at a much lower load, before yield can occur in the nail. The Yttrup Joint can be considered to fall into the "fixed" head category of nail head restraint (refer to Sections 3.3., 4.1.c.).

2.3. LIMITATIONS of the YIELD THEORY

(1) The Yield Theory makes no attempt to predict failures caused by premature, brittle rupture of the wood material. These may be induced by close nail spacings, local defects in the timber or small end distances (see Section 3.1.). (2) No account is made of friction at the interface between the joined members, or the influence of the (ever changing) magnitude of the gap between joint members undergoing the large deformations implied in the Theory (see 3.3.). (3) Also, for joints having steel side plates, the plate thickness is assumed to have no effect on the nail yield load (see 3.2. and 3.3.).

(4) By concentrating on the capacity of a single nail, only local or 'micro' scale effects are considered, effectively defining two-dimensional behaviour. Yield Theory then suffers the limitation of other prediction methods when extrapolating this nail strength to an estimate for the total capacity of a multi-nail joint (see 3.1.).

This is even more difficult in the case of moment resisting joints. Within large, multi-nail groups, the lateral load applied to individual nails is not uniformly distributed: it depends on nail position and the type of loading. "Perimeter" nails will be most highly stressed due to bending action, while under shear loading, nails along the loading axis most remote from the centroid of the group will attract a greater load, as seen in multi-nail rows. (See 3.1.). Due to the presence of bi-directional shear and moment in moment resisting joints, every nail will experience a different lateral load, in a unique direction.

(5) To further compound the complication of this lack of loading uniformity are the orthotropic properties of the wood material in response to its action. For example, Yield Theory incorporates no allowance for the different load-slip behaviour experienced 'along' or 'across' the grain, nor any intermediate angle. Even the "fourth root curve" modification introduced above is limited by this consideration.

2.4. BOLTED JOINT ANALOGY

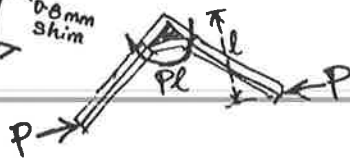
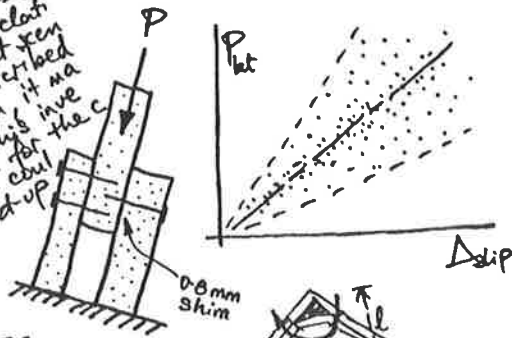
As a final note, it has been recognized that the bolted joint may be a useful analogy for the topic of nail-wood failure mechanism, on the premise that nails and bolts are usually tested as 'pins of a certain diameter'. However, the limitation of this is evidenced by the following examples, where differences have been noted.

Humphrey and Ostman (1989) developed an innovative wafer technique to model wood deformation around bolts, sandwiching 0.8mm thick wafers of Douglas fir between two sheets of glass to observe them loaded in tension by a steel pin. It was noted that the complex state of stress around this pin was quite different for smaller pins (e.g. nails), where diameter approached the magnitude of material growth rings or fibre size. The obvious difference in bending strength between the more ductile nail fastener and the generally larger diameter bolts has an obvious implication on failure modes.

In addition, multi-nail rows exhibit a more uniform and predictable load distribution than rows containing many bolts. The peak load in a row of nails is seen in the end nails, together with a 'prying moment' causing withdrawal (Nicholls, 1990). This causes failure of the end nail, and the resultant load redistribution as this fastener 'sheds' load causes a 'progressive' failure of the row (or "zippering"). However, in a multi-bolt row, any one of the bolts may initially carry almost all of the applied load, until load increases and slips in each individual bolt allows load sharing, until any of the bolts may become "critical". In both cases it has been shown that the capacity of the row of ' n ' fasteners is less than n multiplied by the single fastener capacity, with the reduction being more significant for the bolted case. This is explained in the following Section 3.1.

Literature Review

ent resisting joints in
but the effect was found to be
tunately in this case no relation
responded to the default seen
owever, with the above described
no doubt. In conclusion it ma
whatever to do with this in ve
ngworth (1975) showed that the c
rather friction effects coul
tically determinate set-up
clusively though.



INTRODUCTION

The 'reductionalistic' approach to understanding a large, complex problem is to dismantle it into many smaller component ones, which may then be treated in isolation, where they may be more easily understood. From the results of this, the now-quantified components are reassembled to provide an accurate theoretical model, in the manner begun in Australia by Mack (1966), viz:

$$\text{total phenomena} = \text{function (effect 1)} \times \text{f(effect 2)} \times \dots \times \text{Basic Value.}$$

This seems preferable in the present study to the empirical, holistic approach of examining the total phenomena without regard for its make up, producing an

$$\text{"ACTUAL total phenomena} = \text{variable} \times \text{OBSERVED total phenomena"}$$

type conclusion.

The LVL timber - plywood gusset plate joint (Yttrup 1990), which is fastened (initially with a tight interface) by large multi-nail "ring" groups, and subjected to cyclic, dynamic loading in both shear and bending, is a multi-variable problem. Timber researchers have examined individual parts of this highly complex problem since the early 1960's. From the simple case of a single nail, two member joint loaded statically in shear, variations have been made to materials, fastener arrangements and loadings. For example, Soltis and Mtenga took up dynamic loading of the simple joint, while Karacabeyli and Foschi investigated a square shaped nail group loaded by a static bending moment. The literature survey has found that while no previous investigation exactly matches this study, there has been a large number of related or useful ones.

Following on from the work of Hunt and Bryant (1990), a comparison in terms of the topics introduced above between the two extremes of nailed timber joint complexity, the "simple" and "Yttrup" joints, is presented in the table below:

	"SIMPLE" JOINT	"YTTRUP" JOINT
nail group	single low strength nail or one multi-nail row	hollow rectangular 'ring', with six multi-nail rows of 50 hardened nails each
joined members	two of same species, thickness, roughness, moisture content	63mm LVL member plated on two sides by 19mm plywood gusset plates
nail head restraint	pre-bored hole, parallel driving of single nail, head flush to wood	on site, pneumatically driven flat head nails; variable depth and angle of driving
interface gap and friction	members having same roughness and moisture content, one nail only influencing contact pressure	surfaces open to air (possibly wetted) prior to non-uniform, tight nailing pressure due to multi-nail group
loading type	lateral (shear) only, load applied in plane of joint interface	bi-directional shear plus bending moment at nail group centroid
load duration	short term (minutes), one application	long term (years), infinite applications
loading function	'ramp' load, steady build up to one value without reversal	reversed, cyclic pulses of erratically fluctuating magnitude

Table 3.A. Comparison of "simple" and "Yttrup" joint types

The components evident within the Yttrup joint, as studied individually by other researchers, are introduced below:

1. number and arrangement of nails (from single nail to multi-nail rows, to multi-row nail groups);
2. materials and dimensions of joined members;
3. nail head restraint (incl. nail head type and extent of driving, and side plate material);
4. interface characteristics (friction and gap magnitude);
5. static loading type (shear and moment combinations); and
6. cyclic loading characteristics (load magnitude, rate, frequency, shape, history and duration)

The use of these joints to resist bending moments in portal frames, without steel side plates, and hence act as the sole provider of structural integrity of these buildings, is only a recent development. The Australian Standard for timber structures, AS1720.1, provides very little guidance for the design of this joint type. Rules pertain to only the first two topics listed above. Lheude (1990) has shown the Code coverage of nail head restraint to be highly conservative. Its treatment of moment loading does not apply to gusset plate joints, and no mention is made of any loading type other than statically applied, non-reversed forces.

Very similar research to the present study has been undertaken in New Zealand on essentially identical joint types (Batchelar and Cavanagh; Boulton; Hunt and Bryant; and Walford), but emphasizing earthquake instead of wind-type cyclic loading. Also, an analogy may be drawn between nailed and bolted joints in many areas of behaviour, by regarding both fasteners as 'pins' of a certain diameter, and comparisons are made to the concurrent research in that related field.

Many topics such as creep slip due to long-term lateral loads, the effect of drying on interface gap, joint arrangement effects on damping and hysteresis, and the relative merits of steel and timber side plates have been mentioned only briefly. Firstly, where they are specifically compared by an author to the characteristics found in our joint, or when they serve to provide a useful perspective to our necessarily narrowly defined topic.

The developments in each of the above areas of research are considered in turn in this Chapter, with reference to the behaviour of the Yttrup Joint.

3.1. NUMBER and ARRANGEMENT of NAILS

Of the six topics outlined above, the multi-nail versus single nail joint question is probably the best example of the reductionalistic research philosophy. This approach of extrapolating the strength of a multi-nail joint from that of a single nail or single row joint is seemingly universal in Codes, including the Australian Timber Structures Code, AS 1720 (Clause 4.2.1.2). Modification factors invariably operate on this basic relationship, to account for the effects of nail group geometry.

Discussion of multi-nail joints is inexorably linked to the loading type for which the joint is designed. Economic constraints dictate that where multiple nails are required to form the connections to truss members, (that is, acted upon by pure tension or compression), nail plates are used. These standard connectors consist of a base plate with many transversely protruding 'spikes', stamped from a thin steel plate. When bending moment is introduced, the geometry of the nail group must be adapted so that nails are placed where they are most effective, namely remote from the centre of rotation of the joint (see Figure 3.1.1.b). A 'ring' of nails optimizes the joint's use of materials, reducing stress concentrations in the brittle timber material, in contrast to bolted joints which usually contain a small number of fasteners. In large moment resisting joints, nail plate connectors are not more economic than many individually driven nails, due to their sheer size and non-standard nature.

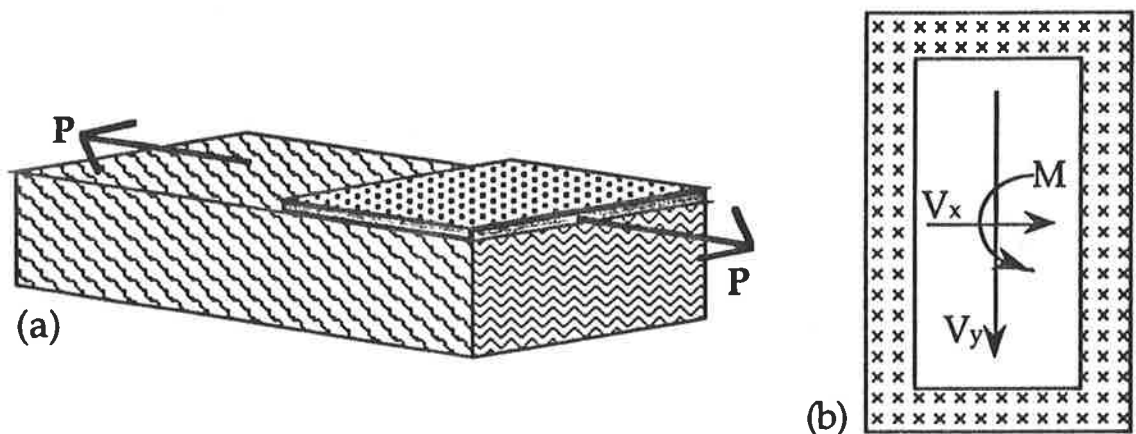


Figure 3.1.1. (a) typical rectangular (multi-) nail group (single shear), and (b) 'ring' type nail group

Overview of referenced papers: Foschi and Longworth (1975) investigated connections between Douglas fir members and pre-drilled steel plates, joined by high strength Glulam rivets in a tightly packed rectangular group, i.e. with a number of identical rows of the same number of fasteners. They studied the influence of the connection's geometry on the stress distribution around the nail group, in order to predict the failure mode and ultimate static strength of such joints concentrically loaded parallel to the grain. Karacabeyli and Foschi (1987) extended this work to include eccentric loading and refined the predictions for ultimate load capacity of the same joint configuration. Thomas and Malhotra (1985) quantified the distribution of the lateral load resistance of individual nails within a single row, oriented parallel to the grain, for joints with and without interface friction between the joined members.

Two failure models need to be considered for multi-nail joints with a rectangular nail pattern (i.e. more than one row), laterally loaded parallel to the grain in single shear. The first failure mode features the nails yielding in bending while the wood under their shanks fails in bearing, and in the second mode, the wood fails in shear such that the wood volume containing the embedded nails detaches completely from the member of which it was a part, as seen in Figure 3.1.2. below. For this to happen, shear failure must occur in the plane joining the points of the nails in the group, and the cross-section

most remote from the member end must fail in tension (or 'plucking'). Other planes experience splitting to permit this brittle failure. Ordinarily, this 'premature' failure mode is considered to 'limit' the preferred 'ductile' failure mode.

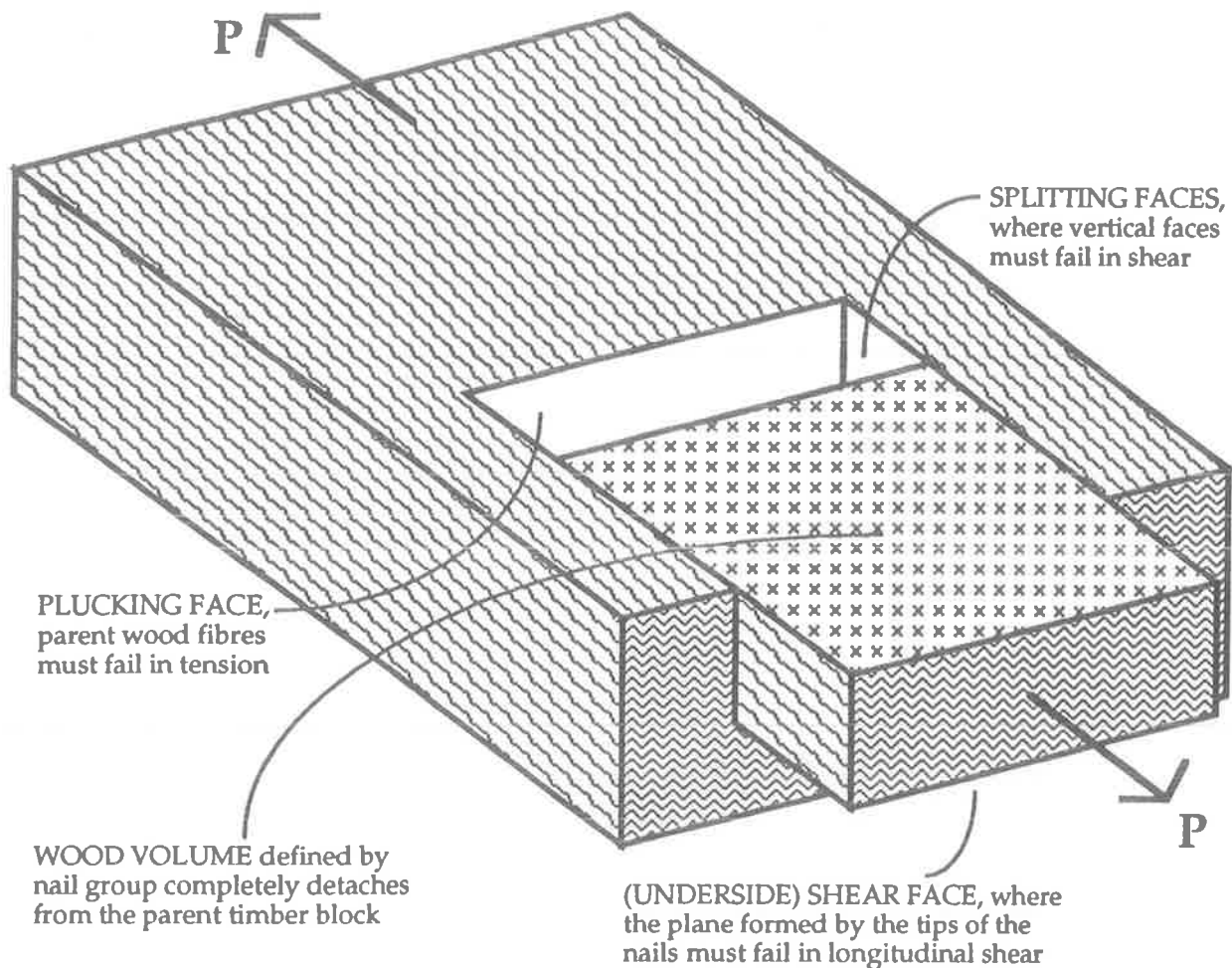


Figure 3.1.2. Brittle (timber) failure mode of a laterally loaded multi-nailed joint

Due to the size, 'ring' arrangement and the dominance of moment loading of the Yttrup joint, the 'nail yielding-wood bearing' failure mode is the most likely of the two modes described above. Failure of the parent members in bending, at a section immediately adjacent the gusset plate edge, or splitting failure of the plywood gusset plate itself, are also possible. These 'failure' scenarios are outside the scope of this study, which is concerned with quantifying the 'in-service' (serviceability level) loadings and responses of an actual structure possessing the Yttrup joint. The concurrent study of Mr. Daniel Siu-Cheung Lee (M.Eng.Sc. Thesis, 1993) attempted to directly address this issue.

Thomas and Malhotra (1985) confirmed the work by Lantos (1969),¹ from whose report on bolted joints they cited the conclusion that:

"...the fasteners in a row of a joint do not transmit the load applied to the joint uniformly".

For multi-nail joints, Thomas and Malhotra indicated that

"...the lateral load carried by each of the multiple nails in a row of a joint is not the same as that carried by a corresponding joint fabricated with a single nail".

¹ LANTOS (1969). "Load distribution in a row of fasteners subjected to lateral load", *Wood Science*, 1(3), 129-136.

Nails at both ends of the row tend to carry a larger share of the applied lateral load than that carried by the nails at the centre, while the joint is still within its linear elastic range.

This characteristic of multi-nail rows differs completely from the case of a row of bolts. Wilkinson (1986) discovered that *“the load distribution for any particular row of bolts is unique”*. Due to fabrication effects, *“any one of the bolts (in the row) may be the major load carrier”*, until slip at this bolt site sees any further load applied to the remaining bolts in the row. Furthermore, *“any bolt hole may be misdrilled causing that bolt to transmit almost no load for a major portion of the joint loading”*.

Thomas and Malhotra also introduced the concept of a modification factor C_N to scale the joint capacity equation:

$$P_n = C_N n P_1$$

where P_n is the capacity of a joint with n nails in a single row, related to the capacity of a single nail joint P_1 . The factor C_N was found to vary slightly with joint slip (i.e. load), the reduction in strength being of the order of 0-10% ($C_N = 1.0-0.9$) at proportional limit slip for joints with 2-8 nails in a row, and 0-7% at ultimate slip.

Similarly, Mack (1966) noted that the German Standard for Building Construction, DIN 1052 (1947), specified a reduction in the nailed joint basic design load of 10% for every 10 nails, corresponding to a factor of 0.9. Their own tests, for one single shear joint configuration with twelve nails, gave an average load factor of 0.94.

Foschi and Longworth (1975) incorporated the Lantos (bolted joint) conclusion, without confirmation, into their model for the behaviour of a multi-nail joint under increasing load. But Thomas and Malhotra were later to find that:

“...the reduction of strength in the case of joints fabricated with common wire nails is relatively very much lower than that in the case of joints with bolts”.

C_N was found to reduce to 0.55 for a joint with 8 bolts in a row, compared to 0.9 for the 8 nail equivalent. The conclusions of Foschi and Longworth also did not include the modification factor approach, effectively assuming a $C_N = 1.0$. However, their joint behaviour model remains valid:

“As the (applied lateral) load P increased (past the linear range), the nails at the ends (of a row) start to yield and bend, while the wood under the shanks starts to fail in bearing. As these nails reach their maximum load-carrying capacity, additional increases in P must be transferred to the less-loaded nails at the centre of the group. Eventually, the load P reaches an ultimate value corresponding to a situation in which every nail in the connection has reached its ultimate capacity. Under this condition (only), the distribution of load among the nails is uniform and the ultimate load, P_n , for the connection equals:

$$P_n = NR.NC P_1$$

where NR indicates the number of rows parallel to the grain, each of NC nails.”

AS 1720 defines the permissible load of a (single) laterally loaded nail as $Q = k Q'$, where k' is a product of five modification factors, including k_{17} , which relates to the number of nails in a joint. (No allowance is made for timber grade in the design of fasteners/connections). An approach similar to that of the C_N modification factor is thus stipulated, with joint design capacity deemed to fall short of the $“P_n = n P_1”$ prediction for an increase in the number of nails orientated parallel to the principal direction of loading (n_a). Table 4.2 (A) from AS1720 is reproduced overleaf:

Condition of Timber	Values of k_{17}			
	number of fasteners n_a			
	$n_a < 4$	$n_a = 5$	$n_a = 10$	$n_a > 20$
Unseasoned	1.00	0.90	0.80	0.75
Seasoned	1.00	0.94	0.90	0.85

Table 3.1.A. AS1720 Table 4.2.(A), for "multi-nail" type joints

The 'nail yielding' failure mode described above is only possible if the premature, brittle shear failure of the wood surrounding the nail group is avoided. Only then will the full load carrying capacity of the nails be realised. This may be achieved with good detailing of the nail group geometry. The study of Foschi and Longworth considered this failure model in detail, and the influence of variations in the nail group geometry on its ultimate load capacity. Variations were made to the number of rows, number of fasteners in each row, fastener penetration depth, fastener spacings (parallel and perpendicular to the grain), and the distances from the group to the edges of the host member (side, end and bottom). The effect of this was seen in the three-dimensional stress state around the nail cluster, the knowledge of which enabled a prediction of the failure mode and ultimate load. They found that nail spacings were the primary influence on joint strength and failure mode, for a given number and arrangement of nails, nail penetration etc., "with a wider spacing producing nail yielding mode". Also, "for the same nail spacing, a longer end distance (from the end of the timber member to the 'first' nail) increases the ultimate load based on shear failure", thus delaying premature failure.

The Australian Timber Structures Code, AS1720, makes recommendations for nail spacings, edge distances and minimum penetration according to the nail diameter and pre-boring, to which the Yttrup nailed joint complies. Interestingly though, Glulam rivets were not selected, and are not generally used in multi-nail joints in Australia or New Zealand, in contrast to overseas practice. "Blunt end" connectors such as these tend to 'break' the wood fibres rather than 'splitting' them as nails do, which can "create micro-shear planes within the wood structure, thus inducing an inherent weakness in the timber member" (Crews, 1992).

The 'nail yielding' model also assumes that after a nail has yielded, the wood supporting its shank has sufficient reserve bearing capacity to not fail before all of the central nails have reached their yield loads. For this to occur in larger multi-nail groups under lateral load (only), considerable "plastic" behaviour (and load sharing) would be required: as the nails under initially higher load yield, and wood deformation under their shanks increases, load is "shed" to other nails. The load-deformation curve for bearing parallel to the grain has such a flat 'post-yield' plateau, but in contrast to the rising curve seen when loading is perpendicular to the grain (refer to Figure 4.2.2.). Should the wood supporting an outer nail suffer brittle failure in bearing, even more load will be transferred quite suddenly to the innermost nails. This may then produce a progressive, splitting failure in the host timber member². At best, this brittle wood failure would reduce the joint P_n , commensurate with the number of failed nail sites. For the Yttrup Joint, it would be optimistic to expect the realisation of the full capacity of the joint P_n where *all* the nails in the joint have yielded, having avoided such a premature "brittle" failure.

Failure mode assumptions made when calculating the moment capacity for these joints are described in detail in Section 4.2. Generally, they assume that "failure" occurs when either the *first* nail reaches its yield stress, or when *all* nails have yielded. Load distribution differs from that produced by pure lateral load, where the "end" nails in the

² The work of Hunt and Bryant (1988-90) documented these premature, brittle "splitting" failures, seen at nominal stresses well below the modulus of rupture for the LVL, and caused by stress concentrations introduced by the close nail patterns of multi-nail, moment resisting joints.

line of loading attract the highest load, in that those nails most remote from the group centroid are most highly stressed. To achieve the pure "nail yielding" mode capacity under moment loading, all nails must reach ultimate slip (at $P = P_1$), before the laminates fail in bearing. No guidance was available from the New Zealand testing of Batchelar and Cavanagh (1984), since all recorded failures occurred in the plywood gusset plates or parent LVL members adjacent to the joint region.

The ability of the outermost nails to yield, and remain as load carrying fasteners in their plastic behaviour, without inducing brittle wood failure, until load distribution within the joint has induced yield at the less remote nail sites, is crucial to determining the failure mode during this final, non-linear phase of the joint's performance.

Subsequently, only one of the seven half scale models tested by Lee (1993) failed in this "nail yielding" mode. Nails at the most remote locations of the "inside" (tension) region of the gusset plate yielded, leaving the nails closer to the centroid or on the "outside" of the joint much less distressed. The LVL and plywood at these 'failed nail' sites appeared less crushed than expected. Evidently, the possibility for the "nail yielding" failure mode to occur within such an "over-designed" joint (see Appendix D) had been confirmed.

AS1720 uses a similar approach to that for laterally loaded joints to allow for the large numbers of nails (n_a) in these joints. The factor k_{17} is once again used, as seen below in the AS1720 Table 4.2(B):

n_a (whose $r > 0.7 r_{max}$)*	k_{17}
2	1.00
5	1.05
10	1.10
20	1.15
100 or greater	1.20

* r = distance to individual nail from nail group centroid

Table 3.1.B. AS1720 Table 4.2.(B), for "ring" type joints

3.2. MEMBER MATERIALS and DIMENSIONS

The Australian Standard AS1720 stipulates the permissible load Q of a (single) laterally loaded *nail* as:

$$Q = k_1 k_{13} k_{14} k_{16} k_{17} Q'$$

where Q' is a basic working load, quoted for seasoned and unseasoned timber, for particular nail diameters and each of the six species groups in the Code. (For simplicity, some 43 major species have been sorted into six broad groups for both strength (design of member) and joint considerations (design of connections)). These values for Q' are unified to represent "*an arbitrarily chosen, but constant, basic reference set of conditions*", with due allowance for variable factors such as those covered by the modification factors, and a safety factor.

[Note that the values of Q' are quoted from test joints of all-solid wood with hand-driven, low carbon steel nails, with the effects of interface friction removed (unknown magnitude of gap). 'Tight' joints made with gun-driven, high strength nails such as the 'Yttrup' joint are not covered, and no provision is made to increase these basic loads despite the obvious improvements made to the joint configuration.]

The modification factors (k) relate respectively to load duration, nail position in the grain, number of shear planes, material used for the 'side' member and multi-nail joints. AS 1720 Clause 4.1.3 states that "*no allowance for grade of timber has been made in design data for fasteners*", providing that defects (such as knots, veins, splits and severe sloping grain) are avoided at the fastener location. As such, no prediction is made of ultimate loads for other failure modes other than nail yielding, such as brittle shear failure of the wood or fastener pullout at the member end. (Minimum end and edge distances are given to prevent the latter).

Factor k_1 (load duration) is discussed in Section 3.5. "Cyclic Loading Characteristics", and k_{17} (multi-nail joints) in the previous section. This section is concerned with how the materials or species of the connected members and their relative sizes affects joint performance. As such, k_{16} is of relevance.

AS 1720 recognizes the increased strength of timber joints made by driving nails through close fitting holes in metal side plates by setting k_{16} to 1.2, compared with 1.1 for plywood gusset plates and 1.0 for the basic case of an all solid wood joint. These allowances are due to the increased resistances of both steel and plywood against nail head rotation and movement of the loaded nail through the side plate material. The extent of the *lateral* passage of a nail through the joined members is affected by their material properties such as embedment strength, density and moisture content, and are elaborated on later.

3.2.1. STEEL SIDE PLATES

Being inextricably linked, the influence of steel side plates and nail head restraint on joint behaviour is discussed in detail in the following Section 3.3. If an embedded nail is imagined to act as a semi-rigid beam on an elastic (wooden) foundation, then simple beam theory predicts that the rotational restraint offered to either end of the nail will influence nail curvatures and deformations. Increased resistance to rotation at the nail head will control curvature (and hence bending over the nail length), limit deflections at the head (and hence slip of the joint) and result in a stiffer nail 'beam'. This high level of resistance is offered in descending order by thick steel side plates with tightly fitted nails, thinner steel plate, looser fitting nails, then plywood gussets with pneumatically driven high strength nails.

3.2.2. TIMBER SIDE PLATES

Since plywood side plates feature in the Yttrup Joint, their influence on joint behaviour is now examined. **Thickness** and **embedment stress** (or 'bearing resistance') are the two most important parameters of timber side plates which influence joint performance. In turn, it is generally accepted that bearing resistance is proportional to the wood density.

3.2.2.A. THICKNESS

The timber side plate thickness influences the extent of nail head restraint and the failure mode of the joint, and is expanded on in the following Section 3.3. For a given timber material, thicker side members provide considerable nail head restraint, and achieve the highest lateral load capacities, while thinner plates are more likely to fail by timber crushing due to bearing of the nail, at lower loads. The ratio of timber side plate thickness (t) to nail diameter (d) enables the identification of 'thin' plate failures, at t/d ratios of 1.5 or lower. Side members are considered to be 'thick' where t/d is greater than approximately four.

a) SOLID WOOD

AS 1720 Clause 4.2.1.4 allows the use of the quoted basic permissible lateral loads Q' for thicknesses of all-solid wood joint members above prescribed minimums. For two-member joints (nail in single shear), members must be a minimum of 10 nail diameters thick, while in the double shear case of three-member joints, outer members must be a minimum of $7.5d$ and central ones $10d$. Nails are to be assumed non-load bearing for thicknesses less than $5d$, with a proportional reduction allowed for intermediate 't' values.

There are obvious t/d inferences in these clauses. In AS1720, the strength of *solid wood* joints is assumed to follow the relationship shown in Figure 3.2.1. below.

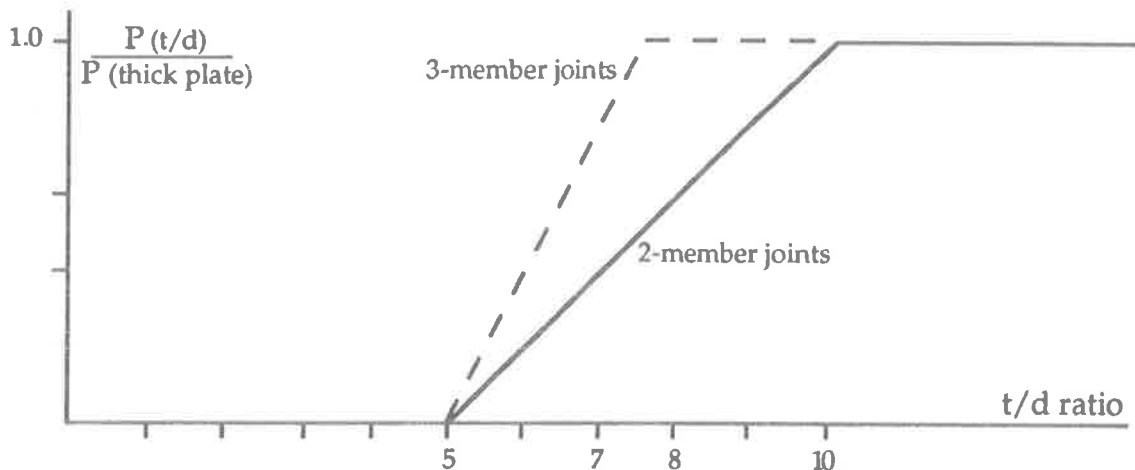


Figure 3.2.1. Influence of t/d ratio on the strength of solid wood joints.

b) PLYWOOD

Due to the presence of transverse layers (or 'cross bands') in plywood, it demonstrates a reduced tendency to fail prematurely by splitting than solid wood. Along with many other Codes, the Australian Timber Structures Code, AS 1720, recognizes the increased strength of joints with plywood side plates over those of solid wood, by setting its

aforementioned modification factor k_{16} to 1.1 for joints with t/d ratios of 1.5 or greater. In comparison, the equivalent Canadian and United States Code modification factors are both higher (at 1.3), but both apply only for joints with much thicker side members, with the t/d ratios of 5 and 10 respectively.

Based on research by Lheude (1988), AS 1720 was revised in 1988 to permit a *linear reduction* in permissible lateral load for the plywood joint t/d ratios below 1.5, disappearing at the theoretical zero t/d . Most other Codes disallow *any* plywood joint capacity below their quoted minimum t/d ratio, notably Canada (min $t/d = 2.2$), New Zealand (2.7-3.0), United States (3.2) and Norway (4.8). This was made possible by Lheude's work, which recognized the existence of the failure mode (for low values of t/d) where the nail moves laterally through the side plate material as a rigid body. This was referred to as "Mode 1" in the Yield Theory considerations of Chapter 2.

As seen in Figure 3.2.2. below, AS 1720 predicts that the lateral load capacity of a joint with plywood side plates exceeds an equivalent one with (exact same dimension) solid wood members (i.e. $P_{ply} > P_{solid}$) for all t/d ratios greater than 1.36. This 'cut-off' point varies between Codes, currently being 3.8, 7.0 and 7.8 in the Canadian, Norwegian and U.S. Codes respectively. The different treatments of the effect of side plate thickness by these national Codes is seen in Figure 3.2.2. (from Lheude, 1990).

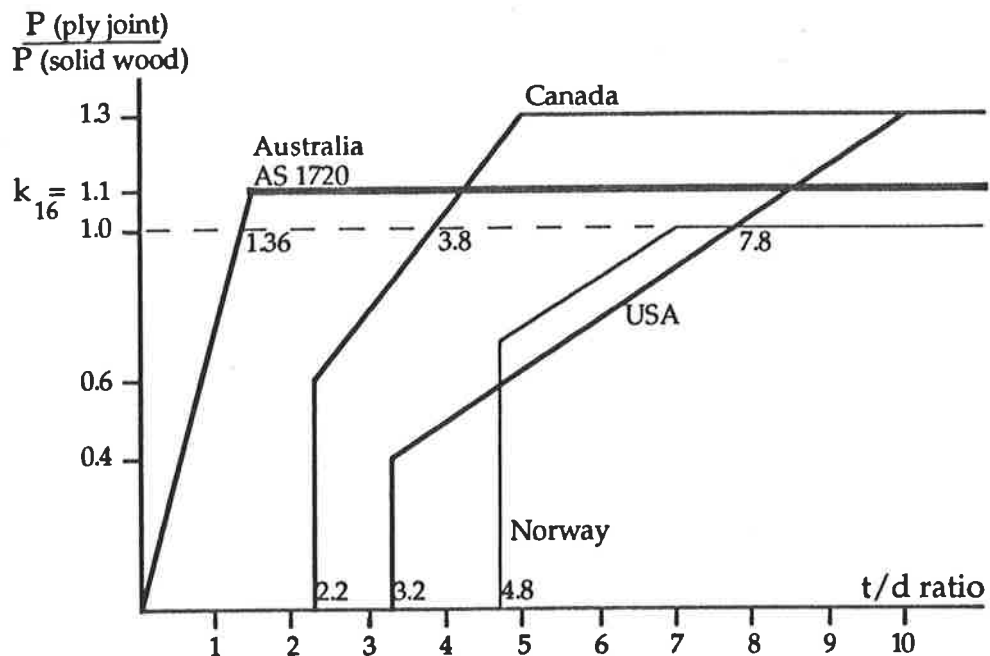


Figure 3.2.2. Comparison of Code Lateral Load Capacity vs. t/d ratio relationships for plywood joints.

3.2.2.B. TIMBER MATERIAL PROPERTIES

Important properties to be considered for the timber members are embedment strength, density/specific gravity and moisture content.

a) EMBEDMENT (or BEARING) STRESS

Experimentally, the nail-on-wood bearing resistance may be derived from one of two approximate methods. Historically, researchers have used the side shank of a typical nail to apply a true, uniformly distributed ram load to an external surface of the timber (Foschi, Nicholls, Komatsu et al). However, Girhammar and Anderson (1988), Smith and Whale et al (1988) and later Hunt and Bryant (1990), tested a nail embedded in an

actual joint, thus fully surrounded by wood, with the load being applied to the nail by rigid steel clamps as close as possible to the timber surface in order to eliminate bending in the nail as much as possible. This test setup enables the loading of the timber to be at any direction relative to the grain. Hunt and Bryant found that *"...these tests led to better theoretical predictions of nail joint behaviour....than the predictions given by the Foschi-type bearing tests"*.

Girhammar-Anderson varied the rate of application of single pulse loads, and found that the maximum timber bearing strength increased proportionally to the logarithm of the imposed deformation rate, for both parallel and perpendicular to grain loading. No trend was recorded between deformation rate and elastic modulus.

Smith and Whale et al (1988) conducted a major (ongoing) study into the properties of laterally loaded, single nailed or bolted joints, concentrating their materials testing programme upon deriving reliable "embedment characteristics". Large numbers of tests were conducted, on many solid woods and sheet materials, over a wide range of fastener diameters, to serve as input into yield theory based limit state design formulae for joint strength. They found that

"...the differences between the (embedment) strength properties of specimens loaded in different directions, or in a tensile or compressive mode, were only very small."

To confirm this, Hunt and Bryant (1990) concluded that *"there is not a simple relationship between ...bearing resistance and direction of loading"*.

The loadings applied by individual nails to the wood volume in a moment resisting joint are necessarily unique in both direction and magnitude. Generally, data is only available for the two principal directions of loading, parallel and perpendicular to the grain, as in the case of Smith and Whale above. While the 'failure' stress in embedment may not differ between these two extreme directions, the shapes of their load-slip traces (over a range of load levels) may be quite different. The importance of this is discussed in Section 4.2. "Prediction of Yttrup Joint Performance".

b) EMBEDMENT STRESS and DENSITY

The strength of timber is directly related to the amount of wood substance present, and given wood's cellular construction, this is determined by the cell size and the thickness of cell walls. Density (and in turn, specific gravity) acts as indicator to this. As such, hardwoods may be expected to possess greater strength than softwoods. However, variations to wood density within a given species also occur. Apart from the natural variation in wood properties from different parts of the tree, this may be caused by other factors which increase density but not strength, including abnormal growth features such as compression wood, large amounts of gum or resin and the presence of knots (higher density branch wood)....(Silvester, 1967). Fortunately, the production process for glue laminated timbers such as LVL mitigates these effects.

This reasoning was used by Lheude in 1988 to explain the higher embedment strengths found for plywood over solid wood of the same Radiata Pine species, being 65 and 45 MPa respectively, along with a 10% difference in their densities.

However, Hunt and Bryant (1990) reported bearing resistance vs. displacement data for Radiata Pine solid wood, parallel and perpendicular to the grain, at four densities, and concluded that *"...there is not a simple relationship between density (and) bearing resistance...."* A plot of their data did reveal the general trend of increasing resistance for an increase in density, except that two of the four traces were reversed from the expected order. It is suggested that account for material abnormalities and the relatively low number of tests conducted allows confidence in the original relationship, which was shown to be true for all of their "perpendicular to grain" data.

Certainly, from some 3200 embedment tests, Smith and Whale plotted *linear* traces between maximum embedment strength (F_e) and density (ρ), noting that F_e demonstrated a negative nail diameter (d) trend in these. Thereafter they established a power law relationship between timber embedment strength, density and nail diameter.

Values for F_e varied little between the two loading modes of tension and compression and the two directions of loading, parallel and perpendicular to the grain, as found by Hunt and Bryant (1990).

In a similar way, Komatsu et al (1988) extended the work of Hirai to establish the non-linear correlation between (initial) embedment stiffness (k_s), fastener diameter (d_n) and the modulus of elasticity (E_w) of the parent timber, of the form:

$$k_s = \frac{E_w}{(A + B d_n)}$$

where A and B are empirical curve-fitting constants.

All the above bearing tests provide convenient values for the timber bearing resistance. However, they do not model the true wood-nail interaction, that of a nail loaded laterally *at its head* whilst embedded in the non-linear wood volume. The theoretical work of Nicholls (1990) reflected this aspect, but without experimental verification (3.2.1.). This consideration introduces the additional effects caused by the interaction of the nail head with the side member, and are discussed in the following Section 3.3. "Nail Head Restraint".

3.2.3. NAIL PROPERTIES

Relevant factors concerning the nail fastener in a single nail joint are diameter, yield stress (these two together giving yield moment), nail head characteristics (shape, size) and depth of penetration.

Nail head characteristics pertain mostly to the extent of restraint against rotation offered to the nail head by the side plate, and are mentioned in the following Section 3.3, "Nail Head Restraint." Depth of penetration has a role to play in restraining the nail head also, since without sufficient frictional resistance to withdrawal of the nail shank, the nail head would be pried clear of the side plate under reversed loading. Nail diameter has been shown to affect both timber embedment strength (discussed above) and the yield stress of the nail.

a) YIELD STRESS F_y

Yield theory incorporates the yield moment of the fastener in its prediction of the lateral load capacity of a timber joint failing in the 'nail yielding' mode. To ensure accuracy when inputting this parameter into Yield Theory derived ultimate load equations, or finite element based theoretical models for joint capacity, many investigators have chosen to obtain nail yield stress F_y from their own tests.

As for embedment strength F_e , the nail yield strength F_y is an important parameter when predicting nailed joint capacity. However, it has been shown by Loferski-McLain (1991) that "*nail properties are notthe same as wire properties*" due to cold working of the source steel during manufacture. As a further consequence of this, the nail F_y exhibits a ("linear and negative") diameter dependency. F_y for the nail product is often not available, and the definition of "hardened" nails appears to differ between manufacturers and engineers. A similar lack of uniformity exists in the test methods used to experimentally define F_y . As another example of how experimental findings may be influenced by test procedure, this aspect is discussed in Appendix E, "Testing Variables."

b) NAIL PENETRATION

Hunt-Bryant (1990) varied the depth of penetration of 2.5mm diameter nails with 'clamped' heads, holding all other joint variables constant, and found that ultimate load increased with penetration. Steady increases in capacity were seen between the cases of 4d, 6d, 10d and 14d depths, but above this, only a marginal gain was made by the identical cases of 18d and 22d.

The extreme case of 4d penetration and clamped head represented the 'ideal' case of a very stiff cantilevered nail 'beam', for which the nail-wood interaction was near-uniform compression down the full length of the nail shank. In this case, the nail does not bend, so the preferred 'yielding' mode of failure is not seen. Naturally, withdrawal resistance is a minimum for this case also.

3.2.4. The YTTTRUP JOINT

In the Yttrup Joint, 50mm long x 2.87mm diameter hardened nails are used to fix two side plates of thickness 19mm to both sides of a 63mm parent member, with no over-driving. Since the t/d ratio of $19/2.87 = 6.62$ is comfortably above four, the work of Lheude (1990) into plywood joints indicates that the side plate may be considered 'thick' in terms of the extent of restraint offered to the nail head. As such, the head 'clamping' restraint would be significant, sufficient to ensure a "nail yielding" failure mode. (see also Sections 2.1. and D.4.).

From the work of Hunt and Bryant (1990) above, an embedment of about sixteen nail diameters would be required to fully realise the lateral load capacity of a single nail joint. The nail embedment depth of 31mm (10.8d) found in both sides of the Yttrup Joint could be expected to provide in the order of 70-80% of this theoretical maximum.

3.3. NAIL HEAD RESTRAINT

Increased nail head restraint (against rotation) has been shown to improve the stiffness and strength of nailed timber joints by many researchers. In 1984, Lowe and Edwards expressed the widely held view that:

"...joint stiffness is greatly influenced by the head (rotational) fixity of the nails"

Improved nail head restraint increases the stiffness of the upper portion (headside) of the nail, limiting bending (curvatures) in the nail, thus delaying the failure of the joint in the 'nail yielding' mode.

Nail head restraint in joints possessing a timber side member may be improved by increasing the side member thickness, or if 'thick' plates are used (i.e. more than 14mm), by increasing the nail fastener head size or yield moment. The latter may be achieved through increasing either the nail diameter or yield stress. Stiffer and stronger again are joints with steel side plates, the chief influences being thickness of plate and snugness of fit between the nail and its hole in the plate. Nail head shape is also important, more so in the case of steel side plates, with a flat underside achieving the greatest degree of fixity at the nail head.

Overview of referenced papers: Hunt and Bryant (1990) presented a comprehensive report on the main factors affecting nailed joint behaviour, including side member material and thickness, nail diameter, head shape, head restraint and extent of driving. They extended a finite element analysis of laterally loaded, single-nail joints, developed by Foschi (1974), to study joints of varying configuration and incorporated experimentally derived non-linear material properties. Lheude (1990) predicted an increase in ultimate strength over the allowable loads in AS1720 of a joint featuring high strength nails, gun-driven through steel side plates to form a 'tight' interface. The Code values are based on friction-free, all-solid wood joints with plain wire nails. Earlier, in 1988, he showed how the failure mode and capacity of joints with solid or ply-wood side members depended on the ratio of the side plate thickness to nail diameter (t/d). Lowe and Edwards (1984) compared the relative merits of 3mm steel and plywood nail plates, with or without interface friction present in the joint, under the action of a fully reversed cyclic (shear) loading regime. Nicholls (1990) contributed findings on a recently adopted joint type, representing an example of 'partial fixity' of the nail head.

3.3.1. STEEL vs. TIMBER SIDE MEMBER

All the above references suggest that the strongest and stiffest joint would be achieved by using thick steel side plates and high strength nails driven at least 10-18 diameters through 'tight-fit' holes into the parent timber member.

In support of timber side plates, Lowe and Edwards suggested that:

"...steel nail plates produce stiffer joints in the small load amplitude region, though at larger amplitudes, the difference (in residual stiffness) between steel and plywood joints is not so pronounced...."

and that

"...the use of plywood (side) plates results in a softer more ductile joint, with little difference in (its) dynamic properties for loading along the grain and loading across the grain...."

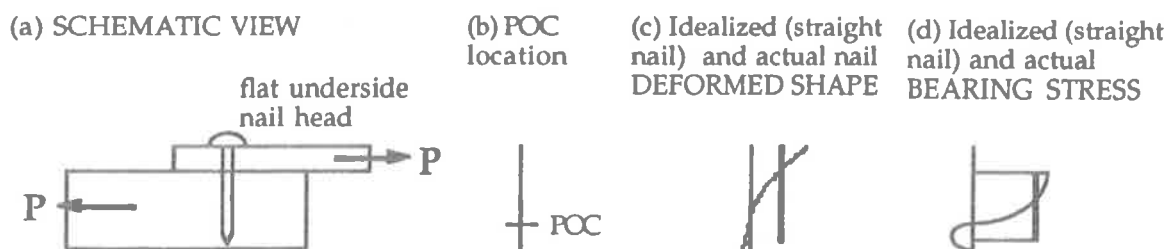
From these findings, they conclude that *"plywood joints would seem to have some advantages over steel when a ductile (nailed) timber joint is required for seismic considerations"*.

Yield theory, as outlined by Aune and Patton-Mallory (1986), ignores both interface friction, thickness of steel side plates and nail head shape. Even so, it predicts that the ultimate load capacity of a steel side plate joint with fully restrained ('clamped') nail heads will exceed one with unrestrained heads by a factor of 1.4. Also, the same factor applies between steel and wood joints where both have clamped heads. These have been confirmed respectively by Foschi and Longworth (1975) and Lheude (1990), as well as by the original authors (1986 b).

The Australian Standard AS 1720 applies a modification factor (k_{16}) to allow for side plate material when determining the lateral load capacity of a joint. This is set to 1.2 for mild steel and 1.1 for plywood side plates. Lheude (1990) has claimed that the k_{16} factor for steel plates was conservative, and that "...*(even) relatively thin (1.6mm) steel side-plates provide a high degree of restraint to the nail.*" He proposed an increase in k_{16} to at least 1.41, the value predicted by Yield Theory. Walford (1988, NZ) and Komatsu (1989, Japan) have both suggested similar improvements of 2.0 and 1.56 to 2.13 respectively, above their own Code values, both 1.25.

The influence that nail head restraint has on joint behaviour is explained by its effect on the position of the point of contraflexure for the nail prior to 'failure', the formation of a plastic hinge. This point of contraflexure (POC) can only exist where a moment of resistance is provided near the head of the nail, to produce double curvature in the nail. This may be achieved by either embedment in a 'thick' timber side member or steel (rigid) side plate. The degree of restraint offered by timber side members depends on the embedment strength of the timber and its thickness, and in the case of steel side plates, on thickness and the 'snugness of fit' of the nail in its hole in the plate.

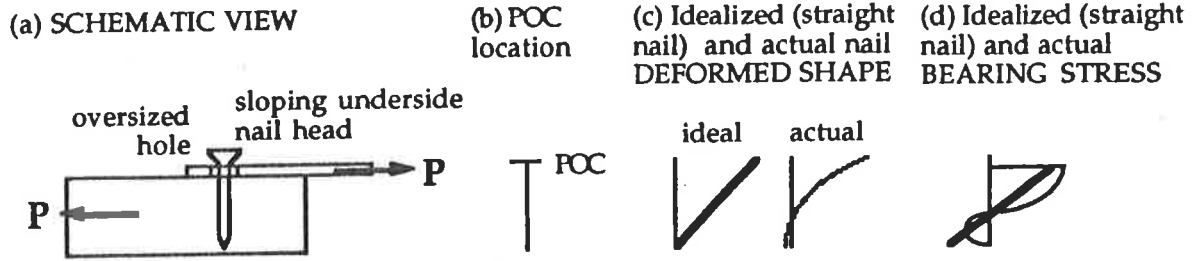
In the case of an unrestrained nail head, this POC may be said to "remain at the nail head location". For greater degrees of fixity at the nail head, the POC moves towards the point of the nail. For an infinitely stiff nail fixed from rotating at the head, the stress distribution of bearing on the timber would be uniform. The lateral load resistance is thus maximized for this case. For realistic nail bending stiffnesses, the bearing stress distribution is non-linear, with a POC close to the nail point. Hunt and Bryant (1990) indicated that the "fully fixed" case may be practically achieved only with thick steel side plates with close fitting nails.



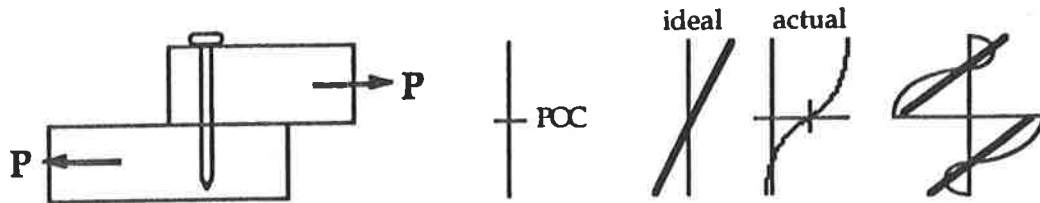
1. "Fully fixed" case, high nail head restraint. Thick steel side plate, flat undersided nail head.

The stiffest *timber* joint has two equally "thick" members, possessing a POC at the interface. Should a joint possess a *thin* steel side plate, offering *no* rotational head restraint, it will also have a POC at the interface. But since total joint displacement is taken as the sum of the deformations at the head and point of the nail, displacements for this steel configuration will be half those of the stiffest timber arrangement, since it is in effect 'one half' of that joint. Even the stiffest timber case can never provide the stiffness of the (unrestrained nail head) steel side-plate joint. However, according to yield theory, these two joints will have identical ultimate (nail yield) lateral load capacities.

The Yttrup Joint is an example of this scenario, due to the high bearing strength of the component timber members. (refer Sections 2.1., D.4.).



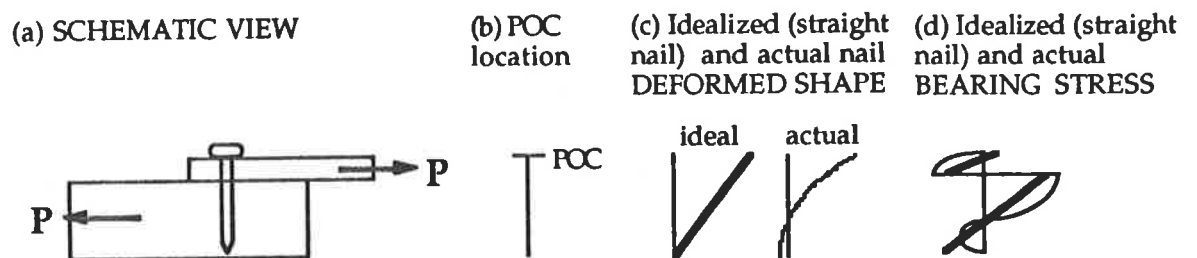
2. "Pinned" or "Free" case, low nail head restraint. Thin steel side plate, "sloppy" nail fit.



3. "Stiffest timber arrangement", high nail head restraint. Two 'thick' timber members.

Joints with common wire nails driven into oversized holes in thin steel side plates are considered to represent "pinned" heads. Since in practise it is impossible to precisely achieve the theoretical extremes of either 'fully fixed' or 'pinned' nail heads, references to joints with these nail head conditions actually imply that the 'most rigid' or 'most free' situation exists. The question then arises as to what behaviour is seen in the large zone between these two extremes.

The case of 'partial' restraint to the nail head is distinguished from that of 'restrained' or 'fixed' head in that a point of contraflexure will never form in the joint. (As for the case of an unrestrained head, the POC may be said to remain at the head). The failure mode will involve rotation of the nail head and the upper portion of the nail (often referred to as the 'headside'), and bearing failure ('crushing') of the host timber member(s). The failure mode and ultimate strength for such joints are influenced greatly by the many joint variables such as member thicknesses, material strengths, nail strength etc. and are covered more completely in Sections 3.2., 3.3.2. and 4.2.



4. "Pinned" or "Free" case, no nail head restraint. 'Thin' timber side plate.

Nicholls (1990) used a bi-linear rotational spring to model the nail head rotational stiffness in a 2-D model of the nail-wood interaction. Extending earlier investigations, he modelled the nail as an elasto-plastic beam on a wood foundation, represented by a

series of bi-linear axial spring supports. This enabled a study of intermediate degrees of fixity of the nail head between the theoretical 'fully fixed' and 'free' conditions. The 'partially fixed' example chosen by Nicholls was that of high strength nails gun-driven straight through thin steel side plates, as used in recent construction practice. He concluded that these joints behaved as for 'fully fixed' head joints at low slips, then rapidly converged to the 'free' (or 'pinned') condition near 1.2mm slip, and beyond to ultimate slip. Interestingly, the theoretical (FEM) plot for these "partial fixity" joints at no time accurately described the tested joint's load-slip behaviour.

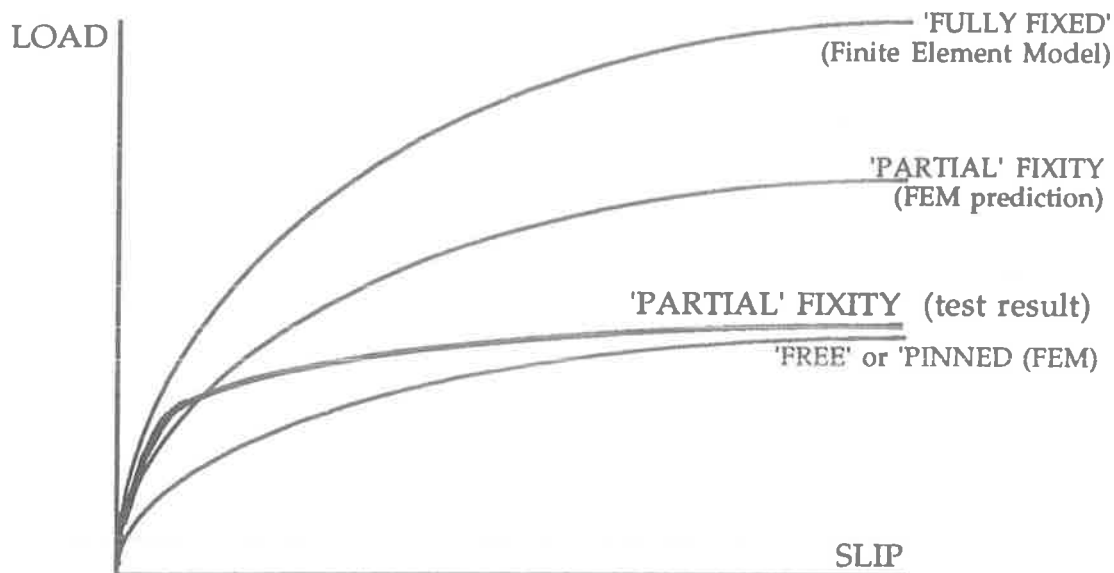


Figure 3.3.1. Theoretical LOAD-SLIP traces for joint studied by Nicholls (1990) over the full range of nail head fixity states from 'free' to 'fixed', compared to tests on 'partially fixed' head case.

Nail head *shape* also has an effect on the load-slip behaviour of steel side plated joints, according to Hunt-Bryant (1990). The withdrawal resistance of the nail shank allows a clamping effect by the underside of the nail head on the steel plate, effectively increasing the restraint of nail head rotation. This is most noticeable for nail heads with flat undersides, in which case restraint is offered at all levels of loading. For nail heads with sloping or rounded 'shoulders' however, restraint is only offered after significant rotation has already occurred, and the head is brought to bear against the side plate. As such, this restraining effect is seen in the load-slip trace only at higher levels of loading (i.e. after considerable slip). Flat head nails can be expected to provide stiffer joints than those using sloping shoulder nail heads.

3.3.2. TIMBER SIDE MEMBERS

By varying side member thickness for plywood joints, Hunt and Bryant noticed that:

"...even at large (nail) displacements, head rotations are small when the plywood thickness is 20mm or more" and "when the plywood thickness is 18mm or more, there are insignificant changes in joint stiffness or strength with plywood thickness".

Thus, thicknesses above 18mm may be regarded as "thick", providing considerable nail head restraint, such that the nail bends in double curvature to form a point of contraflexure near the joint interface. As explained by Lheude (1988), the dimensionless parameter t/d , the ratio of timber side plate thickness to nail diameter, is relevant here. Since Hunt-Bryant held nail diameter constant at 2.5mm, their conclusion may be read as "...for t/d greater than 7.2."

For **thinner** side members,

"...stiffness at lower loads as well as ultimate strength increase with the plywood thickness".

For these joints, *"the point of contraflexure moves into the side-member, resulting in a less stiff and weaker joint"*. They also noted that even for these thinner members, *"head restraining effects can be significant"*, explaining that *"some lateral restraint can be provided by the resistance to rotation of the nail heads in bearing"*.

A lower bound exists at which the thickness of the thin timber side plate becomes small enough that it is insufficiently rigid to restrain the portion of the nail embedded in it. The headside of the nail then moves laterally as a rigid body, to produce a crushing failure of the side plate timber in bearing, instead of bending into the preferable nail yielding mode. Lheude found that this phenomena occurred in plywood below the t/d ratio of approximately 1.2. Since this failure mode relates more to side member thickness, it was discussed in the previous Section 3.2. "Member Materials....".

Lheude (1988) explored the **intermediate zone** between the two extremes of 'thick' side members (t/d greater than say 4), with their significant nail head restraint, and the very 'thin' side plates (t/d below 1.2), for which the failure mode degrades to a brittle type bearing-crushing failure. For joints in this middle range of t/d ratios, the side plate is stiff enough to bend the nail into single curvature, leading to failure in the 'nail yielding' mode. However, this restraint is lower than that of the thicker side plates, where double curvature is achieved, along with higher ultimate lateral capacities.

Also, Hunt-Bryant proved that the nail head restraining effect (and hence joint strength and stiffness) will *"increase with (nail) head size"*. They used a joint with a 'thin' 7.5mm plywood side-plate and 2.5mm diameter nails, varying nail head sizes through 4,2 and 1 (no head) times the shank diameter. The improvement in lateral load resistance at ultimate slip (5 mm) gained by doubling the head size from a typical 2d to 4d was 26%.

Nail head **shape** has also been shown to be significant in timber joint performance by both Lheude (1988) and Hunt-Bryant. Lheude compared bullet and flat head nails, in two joint types, 'thick' to 'thick' (48mm) solid wood and 'thick' solid wood to 'thin' (4.8mm) plywood, using 4.5mm nails in Radiata Pine throughout. Nail head diameters were different however, being 9mm for flat and 6.8mm for bullet head nails (*cf. Hunt-Bryant conclusion above*). As expected from the findings for steel side plates outlined above, in the 'thick to thick' case, the flat head nail provided an initially stiffer joint than the bullet head nail, which has sloping 'shoulders'. However, for the case with 4.8mm plywood side plates, the reverse was true: but since the plate thickness/nail diameter ratio here is 1.0, the failure mode would have been crushing of the plywood in bearing under the lateral movement of the nail. Nail head restraint effects are only relevant in the 'nail yielding' mode.

3.4. INTERFACE CHARACTERISTICS

The two characteristics of interest are *friction* between the two joined members and the *magnitude of the gap* between them. In the Yttrup joint, this relates to the contact surfaces between the gusset plate and the two incident structural members, namely column and rafter. The theoretical model developed by Thomas and Malhotra (1985) showed the significance of the effect of friction when predicting joint behaviour. They, and earlier Antonides et al (1980), showed experimentally that joint behaviour was directly related to the magnitude of the interface gap.

Under increasing static load, it is commonly accepted that the interface gap increases, reducing and then negating the effect of friction between the contact surfaces. The performance of joints subjected to reversed cyclic loading (within their elastic range), exhibiting constantly varying gap size, is unclear. This is the case for the Yttrup joint under the action of ambient wind loads.

Overview of referenced papers: Malhotra and Thomas (1984/5) cover this topic extensively in the context of timber joints with multiple nails, loaded to ultimate slip. Atherton et al (1980) incorporated the aspect of friction as a variable into their comprehensive program to examine the damping and slip of cyclically loaded single nail joints. Also to use a fully reversed cyclic loading regime were Lowe and Edwards (1984), when comparing the performances of plywood and steel side plates. Jenkins et al (1979) extended their study of the effect of duration of load on the stiffness of single nail joints to examine the effect of joint-interface friction. Chou and Polensek (1987) and later, Polensek (1988) studied the effect of nailing pressure and presence of interface gap on the damping and stiffness of single nail joints. However in their study, the interface gap was introduced by a reduction in moisture content of the wood, rather than by the more common employment of shims during assembly. Antonides et al (1980) compared these two techniques for gap variation in two and three member joints, in their pilot study of the effect of gap magnitude.

Their respective conclusions were not markedly different, but because it is very difficult to completely isolate this problem, a convincing quantification of the effect of interface characteristics on joint behaviour has proven elusive. This is evident in the conclusions of Atherton et al (1980), who could only qualitatively describe how these mechanisms influenced joint performance in conjunction with other joint characteristics.

A further complicating factor, as discussed in Appendix E, "Testing Variables", is the lack of uniformity between the experimental loading devices used by the referenced authors, and the presence of varying degrees of out-of-plane eccentricity in their two-member arrangements (see Figure E.2.). This eccentricity produces a tendency for the loaded specimen to rotate in the plane of the members, which subsequently mobilises an additional prying moment at the nail site, further widening the gap between members under increasing load. Since it is an uncontrolled effect, related to the geometry of the testing rig and not to joint behaviour, comparisons between the conclusions of different researchers must be made with additional care. Of those listed above, Atherton, Chou-Polensek, Jenkins and Polensek employed the same (Oregon State Univ.) test rig, but differed from Antonides (Colorado State Univ.). Malhotra-Thomas used a three member arrangement, which substantially removes the eccentricity problem.

No mention is made in the report of Soltis-Mtenga (1985) about the influence of interface characteristics. They tested single nail joints to failure with a reversed cyclic loading regime of step-wise increased deformations, also without the eccentricity mentioned above. The repetitive opening-closing of the joint would have seen it experience, in turn, extremes of both interface friction (as the gap closed between the reversed cycles) then gap magnitude effects (at the end of each 'push' or 'pull' cycle). Their conclusions on joint performance however, deal exclusively with the influence of loading characteristics. The inference is that interface effects are secondary for reversals of

deformation up to ultimate levels, modifying rather than dominating the load-slip trace for cyclically loaded joints.

The most likely explanation for this observation is that for these single nail tests, the "clamping effect" seen in multi-nail joints was not present. Other conclusions cited by the authors above suggest that the majority of resistance to each new (and higher) load level in the cyclic loading regime was experienced during the very first application of that load level. Together, these points would indicate that the joint fully 'closed' only during the *first* cycle, and as such, friction was not seen during the majority of the tests. The assumption, by these researchers at least, that their effect is secondary, exemplifies the difficulty in quantifying them for cyclically loaded joints.

3.4.1. INTERFACE FRICTION

Thomas and Malhotra (1985) concluded that:

"...for practical purposes, it can be said that for multi-nailed joints, the effect of friction on joint stiffness at ultimate slip is rather insignificant...", and that "...with the increase in the number of nails in a row, the effect of interface friction becomes less significant, both at proportional slip¹ (0.38mm) and at ultimate slip (5.08mm)."

The maximum effect (of friction on joint stiffness) reported was about 10%.

They also tested single nail joints (1984). For these, a slight increase in stiffness due to the presence of friction was observed, being 15% at proportional limit slip and 5% at ultimate slip. Atherton agreed, reporting that for both gypsum board and plywood joints, slip moduli was "greater with than without friction at low loads", and "at high loads, friction has no effect". And Lowe and Edwards (1984) regarded "the contribution of friction to residual stiffness to be small and of the order of 10% or less" in both plywood and 3mm steel side-plated joints, "significant only at smaller amplitudes (of slip)".

From their short term loading tests on single nail joints, Jenkins et al (1979) admitted that their number of specimens prevented a reliable trend to be ascertained. Nevertheless, by comparing their load-slip results with those of Mack (1966), they concluded that :

"...the (shear) loads for slips of (up to) 0.12in (3.0mm) were not affected by (interface) friction...."

In apparent contradiction to the bulk of evidence outlined above, accumulated during lateral load tests of varying duration, Jenkins recorded total slips due to (low level) long term loads as being two to three times larger for specimens 'without friction' than those 'with friction'. This was despite concluding that for short term loading, stiffness was "not affected by interlayer friction". This apparent contradiction was attributed to the *static* coefficient of friction, associated with sliding under short term loads, being 50 percent greater than the *dynamic* coefficient of friction relevant to the long term creep tests. However, since this result was obtained in the context of permanent (e.g. 'dead') loading, and this investigation is primarily interested in the dynamic, short term action of wind loads, it is only of interest value.

Nailing pressure affects friction, and was studied by Chou and Polensek (1987) and Polensek (1988), using both fully driven nails (giving a 'tight' joint) and nails that were incompletely driven, then pushed in the remainder using a ram ('loose' joint). Their discovery confirmed the intuition that a nail driven through a thin (deformable) side member engages interlayer friction, in the form of a local zone of higher contact pressure at the nail site. Coupled with the higher static coefficient of friction, this produces a high initial slip modulus. But after initial slip, friction effects disappear.

¹ see Figure E.3. for definition of terms

Atherton et al (1980) also employed this method to fabricate their 'with friction' joints, pushing their 1/2cm proud nails to 0.4mm (1/64 inch) below the surface, but Polensek (1988) later found that the likelihood of initial over-driving made the method unreliable.

Of direct relevance to this study is the finding of Thomas and Malhotra that the magnitude of the frictional force in the interface increases linearly with the number of nails until three nails are present in the joint, after which the frictional force is constant.

The Yttrup joint, with its thick side plates of structural plywood, will negate the effect of nailing pressure mentioned above. As agreed by all the referenced researchers, the effect of interface friction may be safely neglected at ultimate loads. However, friction will be an important factor in the joint's performance at the serviceability level loads relevant to this study. This is particularly true in view of the high number of nails present, whose collective withdrawal resistance provides a considerable clamping effect, which serves to maintain the initial 'tightness' of the joint.

The research of Boulton (1987) provides experimental evidence to confirm the presence of this 'clamping' effect. He developed a finite element model to predict the deformations in steel side plated moment resisting timber joints. After calibrating the model to actual test data, it was noted that the predicted plate movements were over-estimated. Since his model neglected the restraining effect of interface friction, he suggested from this result that "*interface friction would amount to approximately 15% of the moment transfer.*" By expressing this as a percentage, the implication is that it applies throughout the full range of loading up to 'ultimate'. Realistically, the entire error between the experimental and analytical results could not be attributed solely to the presence of interface friction, and it is unlikely that the effect of friction remains proportional at the higher load levels. However, this finding does show that the influence of friction exists at much greater loads than would be expected in an equivalent joint with relatively few nails.

As discussed earlier, the 'nail yielding' failure mechanism involves separation of the joined members for increased lateral loading. The effect of the introduction of this gap is now discussed.

3.4.2. INTERFACE GAP

"As stated by Mack (1966), it has generally been accepted that a specific level of interlayer/interface friction is difficult to achieve and maintain over a period, even with dry wood, and the conservative approach of testing nailed joints (...for their ultimate capacity...) with an initial gap provides a more reliable value of design loads for structures subject to long term loading..." (Lheude, 1990). Nevertheless, Antonides et al (1980) developed a testing apparatus at Colorado State University which maintains the gap at the initial value throughout the test.

In the case of a simple (single nail) nailed joint, laterally loaded in single shear, with a 'static' load application in one direction only, it may be said that the effects of interface friction disappear once a gap is introduced between the members. Indeed, should an initially 'tight' joint receive a large magnitude load, sufficient to cause plastic deformation through yielding of the nails, it will perform thereafter as a joint with an initial slip and interface gap. All the references indicate that the magnitude of the gap present in a nailed timber joint directly affects its lateral resistance. As gap increases, the stiffness of the exposed nail portion decreases, causing a drop in joint resistance. But the range of different methods used to actually achieve varying gap magnitudes, and the limitations of each of them, means direct comparisons of their conclusions must be made with due regard to test method. This topic is discussed in detail in Appendix E. Also, many investigators treat the problem as a 'secondary' effect, generally adopting only one value of gap. It was considered unlikely that such a gap would appear during serviceability level loads on the Yttrup Joint. Observations during the half scale model laboratory tests reported by Lee (1993) confirmed this hypothesis.

3.4.3. COLUMN - RAFTER BEARING JOINT

The design intention for the Yttrup joint is for the rafter to bear on the top of the column. The innovative construction method used for erecting the structural frame of this building involved the on-site pre-fabrication of the roof assembly, at ground level. The columns were hinged in a slotted hole to the gusset plate, which was attached to the rafter only, such that when the multi-bay roof assembly was lifted, the columns swung into place underneath. Ties were used between the exterior ends of the two rafters in each frame to hold the roof into its triangular shape during the lift. The 'nail ring' connection of the gusset plate was made to the top of the column whilst the weight of the rafter and roof assembly was supported by crane (or stiff bracing). The weight of the stiff roof assembly was then released onto the columns.

As a consequence, the dead load is permanently shared by the gusset-column connection and column-rafter bearing surface. Certainly, in an uplifting wind situation, the nail groups would carry the net upward force. However, two scenarios exist whereby this gap might have varied from the design intention, thus altering the proportion of load carried by the nail groups under downward loads. Firstly, during erection, where tolerances may have increased or misalignment of the structural components may have occurred. And secondly, if the moisture contents of either the rafter or the column reduced (due to shrinking or seasoning) after the frame was sealed inside its weatherproof cladding. LVL is much more susceptible to moisture cycling than solid timber, being highly permeable along the grain. In either case, the effect would be to produce a non-uniform bearing of the rafter onto the column top, thus throwing the remainder of downward vertical load unevenly onto the gusset-column nail group (refer to Figure 5.2.1.).

As the joint rotates under the action of bending moment, the presence of this bearing surface would be beneficial. Neglecting local deformation of the top of the column in compression, contact would see the centre of rotation for the overall joint lie towards one end of this surface (outside end for 'opening' and inside end for a 'closing' joint). Should a gap exist between the rafter and column, this centre would lie close to the geometrical centroid of the two nail groups, for elastic response. The greater lever arm in the former case would result in lower lateral loads for nails remote from the centre of rotation. Despite the benefits, the New Zealand practice is to deliberately introduce this gap.

It can be seen that the presence or absence of a gap between the two structural members is of great consequence to joint behaviour under both downward vertical load and bending moment. Advice from the structural engineer responsible for the design and construction of the Wingfield building, Mr. Peter Yttrup, suggests that full contact was indeed made, and a reasonably uniform bearing achieved. As such, there would be no gap in the 'knee' joints in this structure. (see also discussion in Section 5.3.).

3.5. CYCLIC LOADING CHARACTERISTICS

Repetitive application of lateral load to a nailed joint produces a progressively increasing local deformation in the timber members at the fastener sites. Over time, this causes a gradual loss of static strength and stiffness (or 'softening') of the joint. Central to this research project is the determination of the level of cyclic loading at which long term degradation becomes significant in the Yttrup joint, both in terms of load amplitude and the number of load cycles.

Classic fatigue theory predicts a deteriorating static strength for an increasing number of cycles at a particular stress level. Miner's linear cumulative damage rule states that the summation of the fatigue effects of cycling at a progression of stress levels, (each for a number of cycles less than that which would induce failure individually), should be equivalent to the same total number of cycles at a higher level. The critical number of cycles at each level is found from a series of constant-amplitude tests. Since wind loading is random by nature, with an infinite number of impulse amplitudes, the direct application of this theory would be impractical. However, it has been used as a basis by previous researchers to examine the effect of cyclic loading on timber joints, as is evident in their loading regimes.

All of the reported dynamic cyclic loading profiles, either of load vs. time or, if deformation controlled, slip vs. time, have hinted at an earthquake application: i.e. relatively few cycles of large amplitude loads. This contrasts with the case of serviceability level wind loading, which features many repetitions of relatively low amplitude impulses.

Overview of referenced papers: Of the previous studies which included cyclic loading, many chose a loading regime with the imposed deformation (or load) increased in a stepwise fashion, after a number of fully reversed cycles at that level. A non-cyclically loaded 'control' joint is generally used for comparison. Soltis and Mtenga (1985) tested single nail joints under such a reversed cyclic deformation regime in a 'ramp' function, at two frequencies (1 and 10Hz). Lowe and Edwards (1984) also used deformation control, but with a sinusoidal function, and 1200 frequency-amplitude combinations within a study of the relative merits of plywood and 3mm steel side plates. Atherton et al (1980) and Polensek (1988) both employed load control, Atherton with a constant loading rate of 67N/second. Polensek also incorporated deformation rate control in his load-limited cycles, to study the loading rate effect on joint performance, which was also studied by Girhammar and Anderson (1988), but by using deformation control of a non-reversed single pulse shear load.

The testing programs of these researchers is summarized in Table 3.5.1 below, and discussed in more detail in Section 3.5.3.

	loading control	static control rate	load function	no. cycles @ amplitude	load frequency	loading rate
Soltis-Mtenga	deformation control	6.35mm/min (0.25in/min)	triangular	40 cycles @ 4 slip levels	1 and 10 Hz	varied rate= 4A/T or 4Af
Atherton	load	-	ramp	4 @ 5 loads	-	66.72N/sec.
Polensek	load and defm~n rate	3.8mm/min. (0.15in/min.) ASTM	triangular or sinusoidal	3 cycles @ 4 load levels til 3mm slip	0.1,1.0,2.5,7, 15 and 20 Hz (sinusoidal)	0.38 or 38mm/min (triangular)
Lowe-Edwards	deformation		sinusoidal	6 cycles @ 4 slip levels	1200 freq.- Amp. sets	(unspecified)
Girhammar-Anderson	deformation	2.0mm/min	ramp	n.a.	n.a.	5 rates b/t. 1.25 & 1250 mm/min

n.a. = not applicable

Table 3.5.A. Testing programs of other researchers

The main characteristics of cyclic loading (3.5.1.) are magnitude (3.5.2.), rate/frequency (3.5.3.) and the number of cycles applied at any prescribed level. The effects of load shape (as a function of time) (3.5.4.), and the influence of loading history (3.5.5.) on joint performance are also of interest.

To compare the results of deformation controlled tests with those using load control, a decrease in lateral load resistance after many cycles at a specific slip (in a deformation control test), may be equated to a higher slip at many applications of one load magnitude (in a load control test). That is, an increase in slip at constant load suggests a decrease in resistance at a given slip.

Note that varying either loading rate or frequency infers a variation in the other.

The close similarity of the imposed loading profiles of the four cyclic load investigations mentioned above (i.e. a number of cycles at one level, followed by the same number at a series of larger amplitudes) suggests easy comparison between their conclusions about joint performance. Unfortunately, their different emphases, and the brevity of the journal articles, prevents a more detailed analysis of their data. A comparison of the relative merits of the above researchers' chosen loading profiles was similarly thwarted.

The Australian Standard, AS 1720, defines the permissible load of a (single) laterally loaded nail as $Q = k Q'$, where k is a product of five modification factors, including k_1 , relating to load duration. For connections, this factor is linearly varied with respect to logarithmic time from 2.0 for "instantaneous" loads (with a peak load duration of 5 seconds or less) to 1.0 for durations of 50 years or greater, namely "permanent" loads. The transient, fluctuating nature of wind loading as examined in this study approximates to many applications of varying amplitude loads of very short duration. AS 1720 makes no mention of cyclic loading (3.5.1. below), nor is any guidance given about the influence on joint performance of loading rate (3.5.3.) or concerning the residual capacity after the application of near-ultimate level loads (3.5.2., 3.5.5.).

3.5.1. STATIC vs. CYCLIC LOADING

The task of formally concluding that the presence of cyclic (instead of static) loading affects the lateral load resistance of a joint was left to Soltis and Mtenga (1985). Interpreting the transition from static to dynamic as primarily an increase in loading rate, they reported an (initial) increase in joint resistance with this higher loading rate, and a (steady) decrease in resistance after a number of load cycles. At small (elastic range) amplitude deformations and low number of cycles, these two effects were seen to offset each other. But:

"...at higher deformations and increased number of cycles, there is a decreased joint resistance under cyclic loading"

The ratio of joint resistance after a number of cycles to the resistance after one application of each load level was seen to decrease for increased number of cycles. This phenomena was seen to be accentuated by higher loading frequency, when comparing their 1 and 10 Hz results. This trend is discernible in Figure 3.5.1.

This is confirmed by the load controlled studies of Mack (1960) and Wilkinson (1976). Mack indicated that after 1,000 and 10,000 cycles of low level, non-reversed load, the joint static ultimate load was the same as that of joints not exposed to repetitive loading. However, for increasing initial slip, about which the joint was cycled, he observed "considerable slip increases" for increased number of cycles, "the increase (in slip) being greater for higher initial slip". Atherton et al (1980) concur, showing that the effect of the number of reversed cycles on residual slip (after removal of load) is most important at higher load magnitudes.

Conclusions concerning **stiffness** were not as unanimous. Atherton also found that:

"...the effect of load cycling on....slip modulus....is minimal compared to the effects of load (magnitude) and joint friction"

Nevertheless, their load-controlled tests showed that after initial friction effects were removed during the stepwise-increasing loading, the slip moduli of all their joints *gradually reduced* for increasing load. This 'slip modulus' is actually the slope of the chord joining successive points on the load-slip curve which represent the *very first* application of each new (higher) load level in their loading regime.

This is also seen from the graph of Soltis-Mtenga's Table 1 below [not from their paper]. As (both) deformation level and loading rate increased during their test, the initial resistance of the joint to the very first cycle at each higher imposed deformation, did not change markedly. Interestingly, resistance actually *increased* slightly despite the accumulating damage to the joint. This is true even when comparing the results for their two different frequencies of loading.

But both these statements are only relevant for an application of load *higher* than that previously experienced. In more realistic loading cases such as wind loading, load level is continually fluctuating, and the 'previous highest load' will be exceeded very rarely. The load-slip trace of Atherton does however show that for repeated applications of the *same* load, the shape of the curve does not change markedly until, as expected, plastic behaviour is seen at higher (near ultimate) loads.

Soltis-Mtenga (1985) Table 1

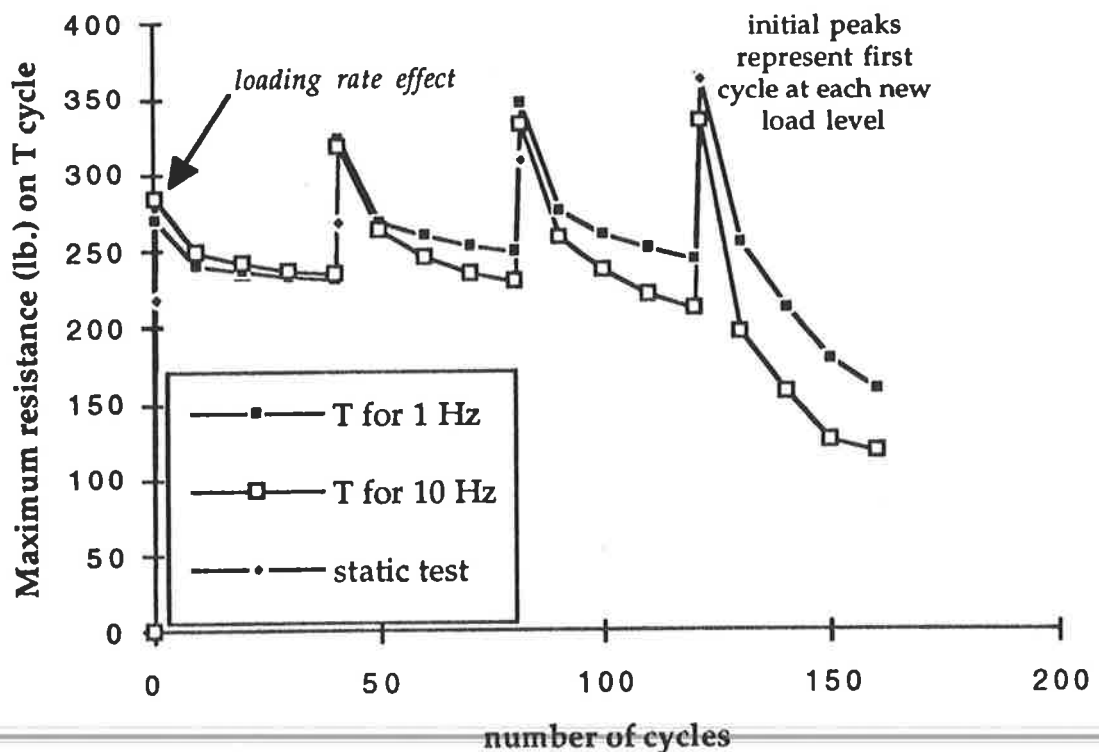


Figure 3.5.1. Soltis-Mtenga (1985) deformation controlled test on joint between 2"x4" Douglas Fir and 5-ply, 1/2" plywood side member. 40 cycles were applied at each of four discrete deformation amplitudes of 0.03", 0.06", 0.10" and 0.15".

For convenience, researchers often use a 'secant' modulus as an indicator of 'stiffness', making conclusions by comparing the load resistance at a standard slip value, as seen in Mack (1960). This gives the expected result, found by inverting the 'decreased resistance' conclusion, that stiffness is reduced after cyclic loading. This convention appears to have been developed for non-reversed loading. In the case of reversed cyclic loading, whose load-slip trace is a hysteresis loop, using the 'chord' definition for stiffness would seem to be more appropriate.

In light of the observations above, it may be concluded that **stiffness** (as defined by chord slip modulus) at serviceability level loads is largely *independent* of cyclic loading, but will gradually deteriorate at higher loads.

It is clear that by introducing cyclic loading to a timber joint, its **resistance** to repeated loading decays and its static strength is reduced. This equates to saying that **slips** increase with load repetition. The modification of these two relationships by the loading characteristics of magnitude, rate or frequency, and the number of cycles experienced are discussed in detail below.

3.5.2. LOADING MAGNITUDE

The previous section indicated the importance of the *magnitude* of the imposed loading on behaviour. For the situation where the amplitude is low enough such that the joint is well within its elastic limit, any number of repetitions should not cause the dynamic case to differ greatly from the static.

From their load controlled tests, Atherton et al stated that "*load (magnitude) affects slip modulus more than any other factor, but much less for non-friction than friction joints*", but that in both types of joints, "*load level was by far the greatest effect on energy absorption*", which increased rapidly for increasing load.

Loading magnitude was not varied in isolation within tests with controlled deformation or deformation rate; it was invariably in conjunction with an increase in loading rate, as was seen earlier in the summary of loading profiles in Table 3.5.A. As such, conclusions concerning the effect of magnitude on joint resistance may not be made from deformation controlled tests.

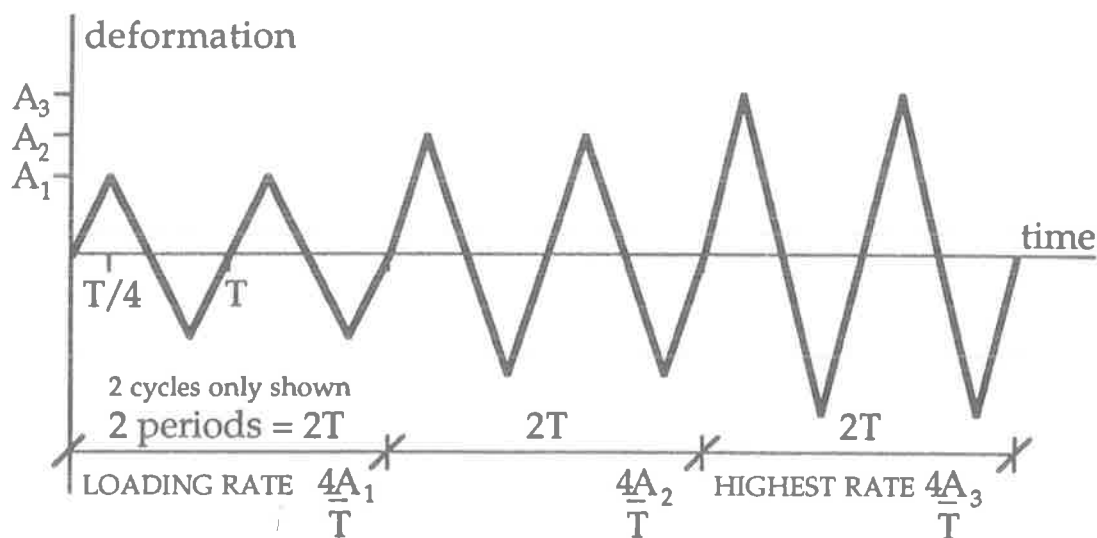


Figure 3.5.2. Loading profile for Deformation Control test, showing the increase in loading rate for an increase in deformation level, whilst keeping frequency constant.

However, Polensek (1988) incorporated deformation *rate* control into his load-limited testing. Consequently, his loading profile took the same shape as the above (although plotted as *load* vs. time), but maintained a constant slope, so that loading rate was not affected by increases in load level throughout the test.

He performed a two-factor linear regression to ascertain the significance of the relationship between **maximum slip** and loading frequency and magnitude. The regression equation also included a term for the natural logarithm of the load magnitude, $\ln(P)$. The overall correlation coefficient (r) was 0.77, with those of frequency and $\ln(P)$ being slightly below this, but for magnitude, $r=0.14$. He limits the validity of this finding to joints of the same materials and type as their study, Douglas fir-plywood joints with a 'non-tight' interface. Nevertheless, the correlation coefficients suggest that only a frequency effect was discernible.

Polensek and Atherton have both discussed the effect of loading magnitude on **damping**, and both made conclusions based on analyses of variance. Polensek again proposed two regression equations for damping ratio, both including the (again) highest correlation term, frequency, one containing load magnitude, the other joint slip. However, all the component and overall correlation coefficients are below 0.48 and 0.72 respectively, so trends only may be observed, without strict quantification. Polensek observed that "*in tight joints, damping decreased as load increased for all cyclic frequencies*", but for "*joints with gap, damping changed little or even increased under increased load*". This apparent contradiction was discussed earlier in relation to interface gap.

It would appear that the primary effect of loading magnitude is to modify the effects of other loading or joint characteristics. For example, at higher loads, the effect on joint resistance due to interface friction becomes insignificant (Thomas-Malhotra, Atherton). The effect due to loading frequency, to reduce maximum slip at higher frequencies, only manifests itself at higher loads (Polensek). In addition, the reduction in joint resistance after a number of cycles is accentuated at higher loading amplitudes (Soltis-Mtenga, Atherton, Mack).

To expand the knowledge of the influence of load magnitude on joint behaviour, it is necessary to conduct tests similar to those outlined above, but without the stepwise increase of amplitude during the course of each loading; that is, the constant amplitude tests inherent in the application of Miner's linear cumulative damage rule.

3.5.3. LOADING RATE AND FREQUENCY

Polensek studied the frequency effect using both a ramp cyclic loading function with 'static' level rates of 3.8 (ASTM D 1761 standard) and 38.0mm/minute, and a sinusoidal cyclic loading function, with frequencies of 0.1, 1.0, 2.5, 7, 15 and 20 Hz for plywood side plate joints; the latter being in line with timber structures oscillating at their natural frequencies due to extreme wind or earthquake excitation. As described previously in the Section 3.5.2, these two effects were not isolated, but frequency was easily the highest correlating factor influencing both maximum slip and damping ratio.

The effect of loading frequency to reduce **maximum slip** (sinusoidal tests only) for increasing frequency was greatest for the larger load magnitudes (up to 2.3 times working design level), but virtually non-existent at the lower loads (1.0 to 1.5 times working design level). He inferred that this reduction in maximum slip corresponded to an increase in joint stiffness. This would appear to agree with Wilkinson (1976), who found that:

"...increasing the frequency of vibrational loading increased the stiffness of nailed and bolted joints".

His vibration tests were also designed to simulate earthquake-like conditions, but did not include a varied load magnitude.

Soltis and Mtenga (1985) proved that *“as the rate of loading increased from static to dynamic, the lateral nail resistance at the end of the first cycle (of four) increased”*. Quantitative conclusions beyond this are invalid since load magnitude and rate/frequency were varied simultaneously, rather than in isolation, as for Polensek’s cyclic tests.

Girhammar and Anderson (1988) investigated the effect of loading rate on the load-slip behaviour and ultimate capacity of a four nail joint by varying the rate at which a single shear pulse load was applied, and also by varying the thickness of the three members joined. They concluded, convincingly, that for an increase in the deformation rate of their non-cyclic loading, the **ultimate strength** increases and deformation capacity (**ultimate slip**) decreases. The increase in dynamic strength over static was “substantial” for both ‘thick’ (34mm) and ‘thin’ (17mm) joint types, regardless of the direction of load relative to grain direction. Bearing tests on the wood and bending tests on the nails were also conducted at various deformation rates, the influence on their **material strengths** being greater in the case of wood. Since the ultimate capacity of ‘thin’ member joints is limited by wood failure, these joints are most affected by the deformation rate effect.

“Test results show that (for both the joint thicknesses and load directions), the increase in ultimate load is linearly dependent on the logarithmic deformation rate”,

with very high correlation factors. The **stiffness** in the elastic range did not appear to be affected by the deformation rate.

3.5.4. LOAD FUNCTION

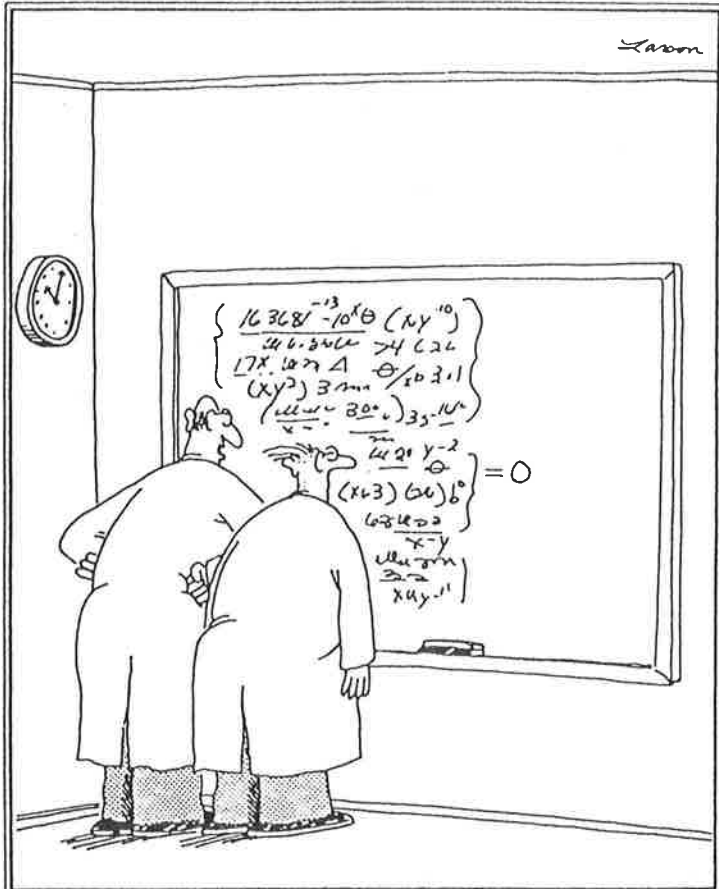
Jenkins et al (1979) discussed the enormous complexity introduced to the question of load-slip behaviour when load was considered as a function of time, as in the case of wind loading. So that the validity of their results was not limited to the chosen function, they *“developed an alternative procedure that estimated the creep-dependent joint modulus for any numerically defined load function from the experimental data for creep under constant shear loads”*. Since their method specifically quantifies joint behaviour due to the action of long term loads, in contrast to the load function for wind load, which is highly erratic, their results cannot be directly applied to this research.

3.5.5. LOAD HISTORY

Soltis and Mtenga conducted a test wherein one set of specimens was loaded directly at the second largest of the four deformation levels (2.5mm) they considered, without first cycling at the two lower levels (0.75mm and 1.5mm). The close similarity in specimen behaviours for both of these regimes indicates that the effect of load history is negligible, when considering increasing load. There is, however, an obvious magnitude implication in this: were the joint to experience considerable yielding of the nails, and retain a large residual slip, performance would undoubtedly be degraded. It was for this reason that Soltis and Mtenga did not compare performance after progressive cycling to the result from a test at their *highest* deformation level (3.8mm), during which they observed low cycle fatigue of the nails, and a rapid reduction in joint resistance for the number of cycles applied.

The question of whether the Yttrup joint’s behaviour is significantly affected by the entirely random, cyclic loading history that it has undergone is central to this investigation. That history comprises the influences of all the major factors detailed in this Section, most of which interact to affect each other individually as well. The laboratory tests of Lee (1993) on half scale Yttrup Joint models were an attempt to further the understanding of the effects of the cyclic loading characteristics above.

A summary of the Literature Review chapter is presented in the following Section 4.1.



"No doubt about it, Ellington—we've mathematically expressed the purpose of the universe. Gad, how I love the thrill of scientific discovery!"

Prediction of Yttrup Joint Performance

4.1. PREDICTION of Yttrup Joint PERFORMANCE

In the preceding chapter, timber engineering research relevant to multi-nail joints was examined, in the context of the Introductory remarks. A great deal of this research was undertaken using 'simple' joints, or connections not involving a force eccentricity about the nail group centroid. An attempt will now be made to distil from these findings a prediction for the performance of the moment resisting Yttrup Joint. This serves as a summary to Chapter 3, and topics appear in the same order as before.

4.1.a) NUMBER of NAILS

- spacing of nails determines the failure mode of the *nail group* for a given joint
- a "nail yielding" mode is preferable to a brittle "splitting" failure of wood volume, and the most likely mode for the Yttrup Joint *nail group* (as opposed to LVL or plywood failures)
- lateral load capacity of $P_n = C_N n P_1$ unlikely to develop for the 400+ nail group

4.1.b) MEMBER MATERIALS and DIMENSIONS

- the presence of a side plate made of *plywood* as against solid wood is significant, due to its greater uniformity and high embedment strength. AS1720 k_{16} factor = $P_{ply}/P_{solid} = 1.1$
- t/d determines 'global' failure mode of joint. Yttrup $t/d = 6.6 > 4$, \therefore "nail yielding" mode.
- Yttrup depth of nail penetration = $10.8d$ \therefore certain to obtain 70-80% of max. possible P_1

4.1.c) NAIL HEAD RESTRAINT

- Since $t/d = 6.6 \approx 7.2$ and $t_{ply} = 19 \approx 20\text{mm}$, may regard the side plate as "thick".
- Yield Theory predicts double curvature nail shape and "Mode 4" failure (see Section D.4.), hence two yield points (hinges) in the nail at failure.
- Thus, nail head restraint is very high. (Flat nail head shape also contributes).
- Lheude (1990) advised AS1720 k_{16} factor (see above) should be at least 1.4 for such joints.

4.1.d) INTERFACE CHARACTERISTICS

- Small scale joint tests indicate friction between the joined members is likely to contribute 10-20% of the moment resistance at serviceability level loads.
- "Clamping" effect of high number of nails in Yttrup Joint (\therefore high collective withdrawal resistance) should retain friction over longer portion of loading range, and create amore uniform contact over gusset plate area: especially due to remote location of 'ring' nails.
- Pneumatic nailing unlikely to locally affect contact pressure, due to thickness of plywood.
- Moment resisting joint research in New Zealand suggested that friction effects are more important for joints with high numbers of nails than for 'simple' joints.
- A "gap" is unlikely to form in the Yttrup Joint at serviceability level loads.

4.1.e) CYCLIC LOADING CHARACTERISTICS

- Once again, these characteristics (e.g. loading rate, number of cycles) will influence all findings based on 'static' load tests. Load amplitude influences the effect of all the other cyclic load characteristics.
- Stiffness independent of load cycling (repetition) and rate of loading/deformation at serviceability level deformations.
- Lateral load resistance reduces with higher deformation and higher numbers of cycles.
- Load resistance increases logarithmically with the rate of loading, at all levels of load.

4.1.f) MOMENT LOADING

- Presence of load eccentricity influences all of the above effects. Principal effect is to alter the distribution of load around the nail group (see 3.1.). Most of the referenced research occurred in New Zealand, where ultimate level, "earthquake" type loading was studied.

4.2. PREDICTION of LOAD CAPACITY - A REVIEW of THEORETICAL METHODS

Any prediction of the capacity of a moment resisting joint must deal with the issue of non-uniformity of load distribution (and hence nail slip) throughout the nail group. A plethora of approximate methods exist, of varying sophistication, for the case of steel side plated joints, as compared by Walford (1988).

The two main methods of modelling nail group behaviour during the "nail yielding" failure mode are the 'torsion stress' and 'discrete' methods. The five prediction methods reviewed by Walford appear in summary form in Table 4.2.A. below. The first two are examples of the 'torsion' approach, while the final three use the 'discrete' method. This is evident from an examination of the geometric term (K) used in each model to express the nail group characteristics of size, shape and number of nails. The underlying assumptions behind these models will now be examined, and later, these formulae will be used to compute the strength of the Yttrup Joint. Finally, the numerical results predicted by the various methods will be discussed (see Table 4.2.B. and Appendix D).

prediction model	formula for joint $M = K P_1$	major assumption
"Thin Tube Wall" Analogy	$\frac{4 n A B}{p} \cos\theta P_1$	shear flow = P/cp around the enclosed ring is constant.
Mitchell Method (1979) (Shared Nail Group Analogy)	$\frac{2 I_{polar}}{c p r_{max}} P_1$	"stress = $M.r/I_p$ " at any point within the nail group area.
Discrete Nail Group Analogy Non-Linear DRG Analogy AS1720-1988, NAFI ($m = 1, 0.7, 0.5$ respectively).	$\frac{\sum (r_i)^{m+1}}{(r_{max})^m} P_1$	$M_n = \sum P_i r_i$ $P_i = k (r_i)^m$ and slip (Δ_i) $\propto r_i$ with $k = P_1/(r_{max})^m$

where 'M' = moment capacity of the nail group, 'P_o' = "allowable nail load", 'n' = the number of rows of nails, 'p' and 'c' are the nail pitch and nail row spacing respectively, 'r' = "radius" of a nail from the group centroid, 'A' and 'B' = centreline dimensions of the nail ring 'enclosed area', and I_{polar} = the polar moment of inertia of this area about the nail group centroid.

Table 4.2.A. Summary of five major moment capacity prediction equations (see also Table 4.2.B.).

4.2.1. FAILURE MODE ASSUMED

All the methods mentioned in the Table above concentrate on the 'nail yielding' failure mode, ignoring the likelihood of premature brittle wood failure. (see also 3.1.).

Hunt-Bryant (1988,90) demonstrated the danger of ignoring the brittle wood failure mode, as their "finite element analyses of the region of the nail plate in joints between laminated timber members showed that....timber stresses can be significantly higher than given by usual timber engineering calculation". Their experimental work, and that of other researchers at Auckland University, including Boulton (1987), found that "some joints failed at embarrassingly low nominal timber stresses (based on My/I and P/A)."

These findings confirm, for moment resisting joints, the earlier work on this brittle failure mode by Foschi-Longworth (1975) for laterally loaded multi-nail joints *without* load eccentricity.

The reversed cyclic loading tests by Batchelar (1984) on joints very similar to the Yttrup Joint showed that the most likely mode of failure was rupture of the tension edge of the *plywood gusset plate* in bending, during the closing cycle. Reinforcements to the joint, in the form of either timber or thin steel strips, were added at this critical stress site in an

attempt to fully realise the bending capacity of the connected Glulam members. Two of the specimens exhibited this failure mode, but none of the joints produced the 'nail yielding' mode.

Karacabeyli and Foschi (1987) were the only researchers to develop prediction formulae for both of the main failure modes of rivet (or nail) fastener yielding *and* brittle splitting of the parent timber, given a known eccentricity of load. Their work is examined in detail later.

4.2.2 MOMENT-SHEAR LOAD COMBINATION

The effect of the combination of loading by lateral load and moment is notably absent from all the above 'approximate' prediction methods. The presence of bi-directional shear on the nail groups of moment resisting joints such as the Yttrup joint is thus ignored by them all. Such an interaction was shown by Karacabeyli-Foschi to be significant, as seen below:

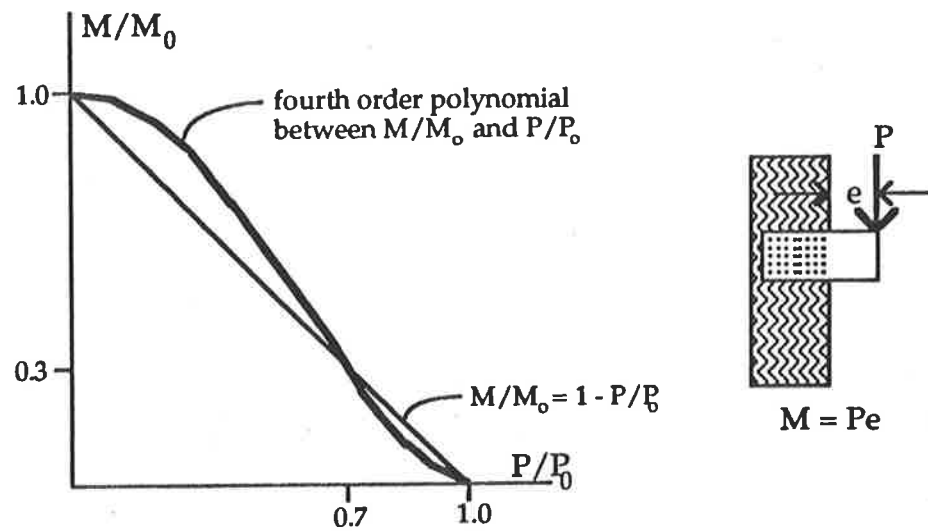


Figure 4.2.1. Interaction relationship as derived by Karacabeyli-Foschi for "nail yielding" failure mode. P_0 is the capacity in lateral shear without moment, M_0 the (theoretical) moment equivalent. [Their Fig. 6.]

Clearly, the moment capacity of a nail group is overestimated when no account is made for the presence of lateral load. This becomes most significant for joints whose moment to shear ratio (M/V) is low.

An approximate analysis of the relative importance of moment and shear loadings on the Yttrup Joint revealed that the ratio of applied moment to moment capacity for the joint (M/M_0) is about seven times that of the shear equivalent (P/P_0). In practice then, it would be possible to ignore this interaction in the design of the joint: in the above Figure, the intersection of the line $M/M_0 = 7 P/P_0$ with that of the 'design' interaction $M/M_0 = 1 - P/P_0$ would indicate an error in the order of 10-15%.

$$\frac{M/M_0}{P/P_0} = \frac{M \times P_0}{M_0 \times P} = \frac{P e \times n F_u}{K F_u \times P} = \frac{n e}{K} = \frac{3000 \times 410}{175,000} \approx 7.$$

The assumption of " $P_0 = n F_u$ " implies that the shear capacity of a joint containing 'n' nails is a linear magnification from the capacity of a single nail joint, F_u . It was made for the sake of convenience here, despite research showing its inaccuracy, as discussed in Section 3.1. The 'upper' nail group in the Yttrup Joint contains approximately 410 nails. Defining

'e' = M/V = moment to shear ratio, an examination of three loading cases of dead load and the two wind loading cases (West and North) showed that 'e' varied from 2.6 to 3.2, so a representative value of 3.0 was used (refer to Appendix F). In addition, an average value for the geometric term 'K' introduced in Table 4.2.A is 175,000.

4.2.3. USE of "ALLOWABLE NAIL LOAD P_o "

All of the capacity prediction models in current use rely on an estimate for the allowable nail load for that nail considered most likely to 'fail' first, generally the most remote from the joint centroid. As seen from the work of Aune & Patton-Mallory (1986,USA), Smith-Whale (1987,UK), Lheude (1990,Aus) and the discussions of Walford (1988,NZ), there is international agreement that the use of Codified values for this allowable nail load in *multi-nail* joints is invalid and conservative (see Sections 3.2, 3.3.). Code values, as in the case of AS1720, are obtained from tests on joints of quite simple geometry (usually with a single nail), which involve materials and methods no longer relevant to moment resisting joints. Also, the "allowable loads" are obtained as those loads at an "allowable slip", making the results highly dependent on the timber bearing resistance (itself a function of slip) and the subjective choice of the "allowable slip" level. From the work of Lheude (1990), the materials and techniques used in the Yttrup Joint should produce an improvement over the AS1720 allowable nail load of at least 200%. (seen in Table 4.2.B.).

The first two researchers above showed that from Yield Theory considerations, the "nail yielding" failure load is greatly affected by the characteristics of timber thickness and embedment strength, and nail diameter and yield stress. Other influencing factors, not covered by Yield Theory, are steel side plate thickness (Lheude, 1990), interface friction (Thomas-Malhotra, 1985) and the unifying effect of joints possessing large numbers of nails (Walford, 1988). These matters were discussed in detail in the preceding Sections.

It can be seen therefore, that regardless of the geometrical elegance of a moment prediction equation (of the form $M = K P_o$), the use of even a modified Code "allowable nail load" P_o will inevitably limit its accuracy. As will be seen in the numerical comparisons later (Table 4.2.B.), the use of a Yield Theory nail load based on the true joint geometry and material properties offers much improved accuracy.

4.2.4. "FAILURE" = "FAILURE of FIRST NAIL" ASSUMPTION

In addition, even the most "exact" of the approximate methods considers the load-slip curve only during its initial 'elastic' phase. For example, the various "Discrete Nail Group Analogy" methods employ relationships between fastener load P and slip (limited to proportional slips, of the order of 1mm), where $P = (\text{slip})^m$, and 'm' ranges between 0.5 and 1.0. There are two flawed assumptions with this approach.

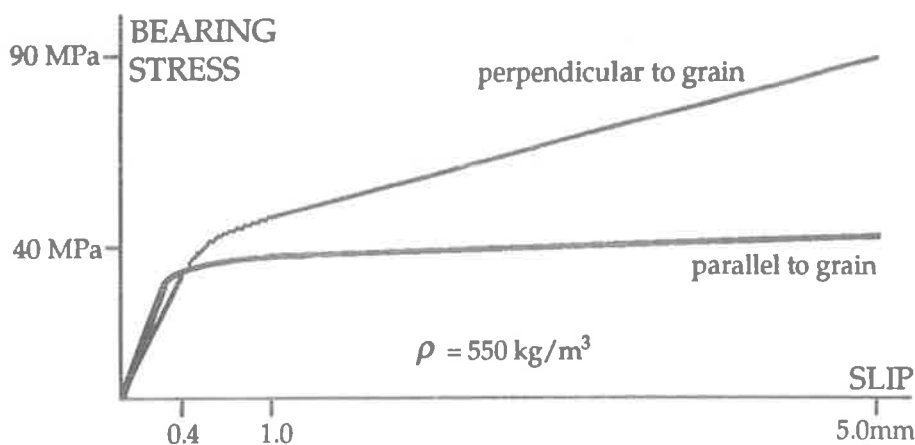


Figure 4.2.2. Hunt-Bryant (1990) tests on Pinus Radiata timber, using 3.55mm diameter nails.

Firstly, by using the same expression between nail load and slip for all nails in the group, the inference is that a nail loaded perpendicular to the grain behaves exactly as a nail loaded parallel to the grain. This is demonstrably false, for any nailed timber joint, as seen in the Figure 4.2.2. for the example of wood bearing resistance.

Furthermore, in the case of moment resisting joints, the influence of the moment loading is to create a load component tangential to the radius between an individual nail and the nail group centroid. For the overwhelming majority of nails in the group, the resultant load will be at some angle to the grain between the extremes of parallel and perpendicular.

For these unique directions, generally no load-slip data is available. Karacabeyli-Foschi employed a mathematical interpolation for the general load-slip relationship for angles of loading relative to the grain between these two extremes. AS1720 allows the use of this approach only when determining the basic working load for a *bolted* joint (Clause 4.4.2.3).

Secondly, by limiting the extent of the load-slip expression to only the elastic phase of behaviour, the implication is that 'failure' is said to occur in the joint as soon as the very first nail is seen to begin yielding, at the onset of its plastic performance. While serving to provide a conservative "working stress" type design value, this underestimates the true failure moment of a joint and limits the application of the model to *small* rotations (nail slip less than 1mm). Karacabeyli-Foschi define joint failure as when rotation of the rigid side plate begins to rapidly increase. It is only at this time that the applied load to individual nails begins to unify (i.e. they are all 'at' or 'near' yield) throughout the group.

One prediction method, the "thin walled tube analogy", introduces the "uniform nail load" assumption in the form of a constant shear flow around a nail 'ring', implying that as the extreme nails fail, all others in the group are 'on the point of failure'. This is only valid at very *high* joint rotations, in the case of nail groups with an aspect ratio close to unity. However, the method also uses an elastic region "allowable" nail load, which is inconsistent with the constant shear flow assumption, since this is only true in the 'ultimate' condition. Since some of the prediction models are based on assumptions which are only valid in the 'ultimate' condition, nail "yield" loads should be used in order to satisfy the principles of mechanics. [*In the absence of nail test data, the Yield Theory equations relevant to the joint could be used (Aune and Patton-Mallory, 1987). This approach has been adopted in the numerical comparisons at the end of this Section.*]

Another (more refined) example of the 'torsion stress' approach, the "Mitchell Method" (1979), was shown by Walford (analytically) to compare best to the "exact" method, that of the "Non-linear nail group analogy", itself an example of the 'discrete' approach. However, this may only be because both models make identical failure mode assumptions, essentially differing only in their geometrical approach. These assumptions are:

- (a) ignoring the potentially premature and brittle wood splitting failure mode,
- (b) ignoring the load combination of lateral load (bi-directional) and bending moment,
- (c) the use of a Code "allowable nail load",
- (d) using a single nail failure as the basis for defining overall nail group failure, effectively
 - (i) curtailing load-slip performance to the 'elastic' phase and (ii) disregarding the orthotropic behaviour of the wood material.

All of these assumptions, from the above discussion, are seen to be flawed.

4.2.5. KARACABEYLI - FOSCHI MODELS

The work of Karacabeyli-Foschi (1987) is the only theoretical model not limited by the above points. They established computation methods for the theoretical interaction relationships between lateral load and bending moment, for both modes of failure and for any joint geometry. Their experiments verified their analytical models, for two examples of wood failure and one in the nail yielding mode.

Their 'discrete' type "nail yielding" model has a failure mechanism based on failure of the joint as a whole, not that of a single nail. It was based on the known nail-slip performances (for single nails) in the directions parallel and perpendicular to the timber grain. As a true "ultimate" load level method, it can be readily used in accordance with the Limit-State philosophy.

For the purposes of this study, the direct relevance of their work should not be dismissed on account of the simplifying presence of a rigid (steel) side plate.

4.2.6. EXTRAPOLATION of the K-F METHOD to the YTTRUP JOINT

While their work concentrated on the example of (steel) Glulam rivets fastening a steel side plate to Douglas Fir Glulam, with a rectangular group of rivets and a specific spacing and embedment depth, there is scope for use of their theoretical approach outside of this joint type. In order to apply the *method* described in their work to the Yttrup Joint, those elements of their work which may be adapted to *any* joint type must be isolated.

For the two failure modes, these elements are as follows:

I. For the 'nail yielding' failure mode:

(a) The use of experimentally derived load-slip relationships for a single nail joint of equivalent geometry at angles to the grain (β) of 0° (parallel) and 90° (perpendicular).

(b) The interpolation between these known values in (a) for any value of β using Hankinson's formula (1921). The use of this specific equation was contended by Smith and Whale in the Discussion of the Karacabeyli-Foschi paper. Despite a rebuttal in their "Author's Reply", it would appear that the error has been proven.¹ Even so, as noted by the original authors,²

"...I do not think the Hankinson's formula for strength has ever been proven from principles of mechanics, and may be seen as just an interpolating equation which seems, in some cases, (to) provide a reasonably good fit at different angles to the grain. Other such functions can be equally used."

II. For the brittle wood failure mode:

Their prediction method considers three-dimensional deformations in the wood member, which is treated as a linear orthotropic solid. Strain energy considerations are used to derive stresses in the three orthogonal directions for each rivet. These were then numerically integrated over the volume of the wood member.

(a) The computation of external strain energy in this method involves the use of an assumed bearing distribution for the embedded fastener. A triangular distribution extending from a surface maximum to zero at half penetration depth (of 50mm) is used for the Glulam rivets (found to be valid from previous testing).

(b) *"The numerical integration of the stresses over the member volume required some judgement and approximations."* Two of these are important:

(i) Among the terms excluded from the function integrated were the forces parallel to the nail shank causing withdrawal of the rivet from the member, considered negligible for the case of 50mm Glulam rivets.

(ii) The wood area defining the bounds of integration was defined in order to give good calibration of the theoretical prediction to *test results* from one of the connections tested.

¹ personal correspondence with Dr. Ian Smith, Director, Wood Science And Technology Centre, University of New Brunswick, Canada.

² personal correspondence with Professor Ricardo O. Foschi, Department of Civil Engineering, University of British Columbia, Vancouver, Canada.

The validity of the above assumptions should be tested before application of the Karacabeyli-Foschi models to other moment-resisting joints, including the Yttrup Joint. With this considered, their described *method* may be used to provide more reliable (and indeed rational) theoretical predictions for joint capacity than possible at present. This process is outside the scope of this study. If this was to be undertaken, the additional question of cyclic loading, not covered by Karacabeyli-Foschi, would need to be addressed:

In their static loading case, the total lateral load applied to the joint is divided evenly between all nails in the group (their Eq.13). Even for statically loaded joints, this is only approximately true, and then only in the ultimate condition, as shown by Thomas-Malhotra (1985). (See discussion in Section 3.1). In the (present) case of a cyclically loaded moment resisting joint, this is not at all true, as demonstrated in reversed cyclic load tests by Batchelar-Cavanagh (1984):

"...it was clear from nail hole deformation patterns that nails on the inside of the joint were worked considerably harder than those in the outer bands".

Thus, the considerable mathematical simplification that this assumption affords a moment capacity prediction model using the "discrete" method would be inadmissible. Considering also that the orthotropic nature of the wood material and the complexity of the loading present in these joints requires the development of a unique load-slip relationship for each individual nail in the group,

"...Overall you can see that (the) use of non-linear load-slip functions makes calculations messy in the case of a gusset plate joint transferring a moment."³

The concurrent research at the University of Adelaide of Mr. Daniel Siu-Cheung Lee (M.Eng.Sc. Thesis, 1993) experimentally studied the fatigue strength of the Yttrup Joint, and the results of this work intends to promote greater understanding of this highly complex problem.

4.2.7. RESULTS of the NUMERICAL EVALUATIONS

Each of the five methods introduced in Table 4.2.A. were evaluated (see Section D.3.) for the Yttrup Joint using two different nail loads (D.4.). The AS1720 value represents an 'allowable' nail load, but was factored up by 1.4 (Lheude, 1990) to account for the considerable nail head restraint offered by the Yttrup joint members (Section 3.3.). Yield Theory represents an 'ultimate' load for the nail, and is commensurately higher. Being finite element based, it implicitly incorporates several of the modification factors used in the AS1720 approach, most notably k_{16} , used to allow for the "presence" of a plywood side plate (of higher embedment strength f_e) and k_{17} , which allows for the number of nails present in the group. Therefore, moment capacities evaluated from the Yield Theory nail load may be regarded as predictions of the 'ultimate' condition, while AS1720 values represent 'design' capacities.

As described in Section 4.2.4., the "Thin Tube Wall" Analogy requires a nail 'yield' load to satisfy the principles of mechanics. As such, the moment capacity using the 'allowable' nail load is given for the purposes of comparison only. As would be expected, this method recorded the highest 'geometric term', thus giving the greatest moment capacity estimates.

Moment capacities in Table 4.2.B. represent the estimates for *one side* of a single group in the overall joint. Since each group must transmit the same applied moment, the same design is commonly used for both upper and lower nail groups. Space restrictions caused by the gusset plate size dictated two different groups in the Yttrup Joint, but as evidenced below, they achieved remarkably similar theoretical capacities.

³ personal correspondence with Dr. Ian Smith, Director, Wood Science And Technology Centre, University of New Brunswick, Canada.

prediction model	equation $M = K P_1$	geometric term K [mm]	$M = K F_u$ (kNm) (Yield Theory) ($F_u = 1515$ N)	$M = K Q'$ (kNm) (AS1720-1988) ($Q' = 440$ N)*
Thin Tube Wall	$\frac{4 n A B}{p} \cos\theta P_1$	upper 290,553 lower 282,310	440.2 427.7	(127.8) (124.2)
"Mitchell Method" (1979)	$\frac{2 I_{polar}}{c p r_{max}} P_1$	u 203,578 l 201,319	308.4 305.0	89.6 88.6
Discrete Group Analogy ($m = 1.0$)	$\frac{\sum (r_i)^{m+1}}{(r_{max})^m} P_1$	u 165,511 (lower not calculated)	250.7 -	72.8 -
Non-Linear DRG ($m = 0.7$)	as above	u 177,352	268.7 -	78.0 -
AS1720, NAFI ($m = 0.5$)	as above	u 185,115	280.4 -	81.5 -

" P_1 " represents the assumed lateral load capacity for one nail.

Load duration factor k_1 was set to 1.0 for both nail loads, equivalent to "dead" load case.

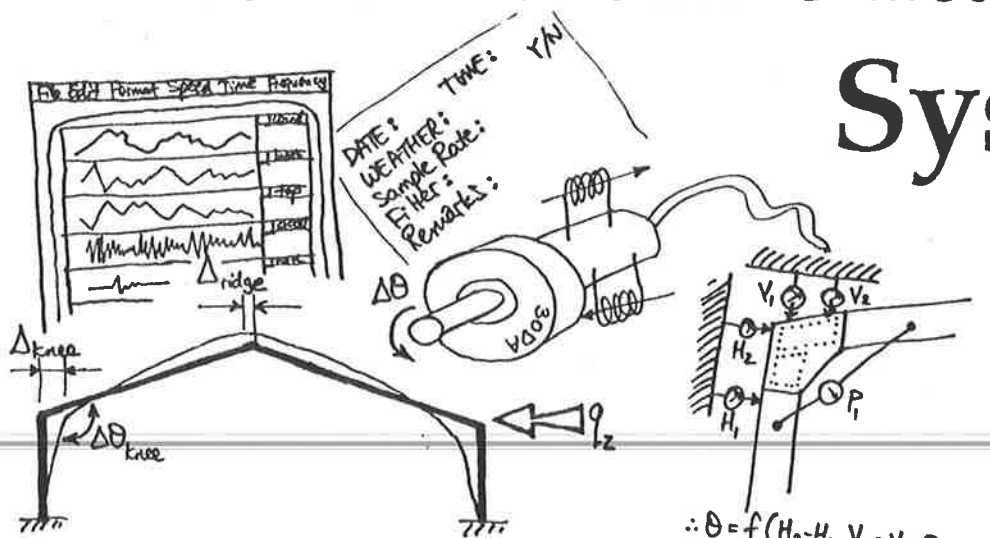
* includes an additional modification factor for hardened nails of 1.4, from Lheude (1990): see Section D.4.

Table 4.2.B. Numerical comparison of five major prediction methods for Yttrup joint moment capacity

During the laboratory tests on half scale models (Lee, 1993), one specimen was seen to fail in the 'nail yielding' mode (Test 7). Failure occurred in the most remote "inside" nails first, confirming the Batchelar-Cavanagh (1984) observation of above (4.2.6.), after 157,028 cycles at a ram load of 25 ± 15 kN. This represented a scale model opening moment range of 44.6 ± 26.8 kNm, equivalent to node moments in the full scale joint of 178.6 ± 107.1 kNm. The maximum moment applied was 285.7 kNm, over 150,000 times. This provided an excellent confirmation of the Yield Theory predictions above (which assumed one repetition). As expected, the "Thin Wall Tube Analogy" over-estimated the failure moment, providing test confirmation of the discussions in Sections 3.1. and 4.2.

Also of interest was the result for Test 6, which was cyclically loaded with an equivalent full scale moment range of 178.6 ± 142.8 kNm, giving a maximum of 321.4 kNm. However, this specimen suffered a bending failure on the LVL rafter tension face, not a nail yield.

The Instrumentation System



DATE: _____
 WEATHER: _____
 Sample Rate: _____
 Filter: _____
 Remarks: _____

$$\begin{aligned} \therefore \theta &= f(H_2 - H_1, V_2 - V_1, P_1, \text{ and } \\ &= \arctan(V_2 - \\ &\Rightarrow \text{inv sin} \end{aligned}$$

5.1. THE INSTRUMENTATION SYSTEM

As outlined previously, the primary task in this study was the on-site instrumentation of an existing large timber portal frame structure, to ascertain the magnitude of dynamic lateral loadings and the response and performance of an actual moment resisting nailed joint under their action.

The loading history of ambient and gust wind events experienced by the joint causes progressive localized deformation around the nails, gradually 'softening' the initially tightly formed joint over time. By examining an existing joint, the structural response in this 'pre-softened' condition may be documented: structural response being in the form of a moment versus curvature relationship. The measurement of these two parameters is discussed in detail in the following sections.

Wind speed and direction data was not used to empirically derive an approximate loading on the structure or to estimate the bending moment applied to the joint, as allowed in AS1170.2-1989. Wind data was only recorded to estimate over what range of wind loadings that the derived moment vs. curvature relationship was valid. As such, a continual record was needed to simultaneously log the wind and structural (i.e. action vs. response) data.

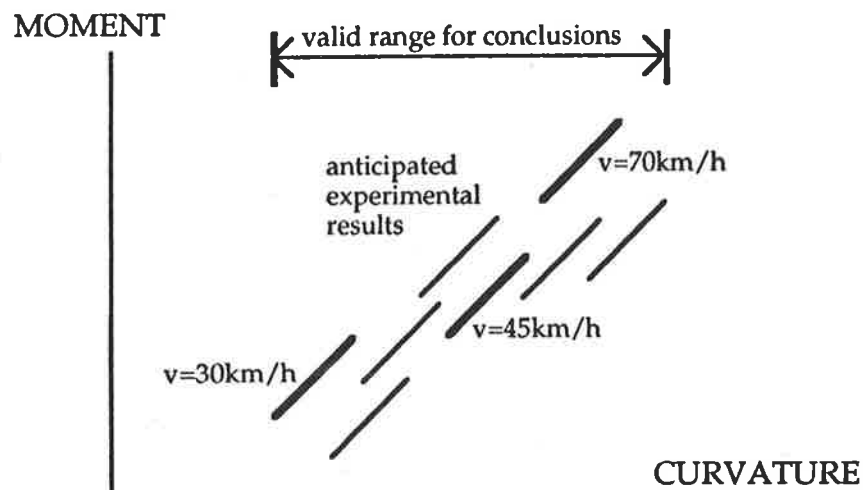


Figure 5.1.1. Expected moment-curvature relationship (linear), for anticipated range of wind velocities.

5.1.1. SELECTION of the ON-SITE LOCATION for the INSTRUMENTATION SYSTEM

In plan, the Wingfield building is a simple rectangle comprising 7 open bays. The southern end wall is made "rigid" by external cladding (without an East-West running portal frame), while lateral stability for the northern half of the structure has been provided by partially filling in the first portal frame from the northern end. The northern 'face' of the building consists of a facade of full-height glass. Numbering the portal frames from the Southern end, as one to seven inclusive, the fourth portal frame is equidistant from these two 'rigid' bays (see Figure 5.4.1.). As such, the lateral sway of this frame was expected to be greatest. By instrumenting this frame, deformation response data was maximized relative to measuring errors and signal noise.

Wind measuring equipment was sited on the Western side of the building, since the prevailing wind direction in Adelaide is Westerly. The exact site was then influenced by the need to not impair access nor car parking on this side of the building, while keeping as

close as possible to being in line with the fourth frame. This then influenced the choice between which of the two 'knee' joints in the fourth portal frame to instrument for the structural responses (East or West). Since a common data logging site was needed for both wind and structural data, choosing the Eastern side joint would have clearly introduced large cable lengths to the data logger, resulting in increased signal noise, so all instrumentation was undertaken on the Western side. Another advantage of this was that for a given Westerly wind, the deformations of the Western joint (opening) were greater than those of the Eastern joint (closing), theoretically by a factor of 1.5. (See Chapter 6).

The form of the joint instrumentation was strongly influenced by the uses and clearance requirements of the interior space of the building. Having cladding attached directly to the outside of the frame made access difficult (and subject to weather) on that side of the joint, and its steel sheeting exacerbated the effect of temperature on strain measuring apparatus. Since the major use of the building was to house a timber joinery workshop, the presence of large machinery, compressors and wood dust had to be accounted for. And finally, special attention was warranted by the recording site being off-campus, and the constraints of equipment availability and use sharing. The solutions to these specific site constraints are detailed in subsequent sections.

5.1.2. LOW PASS FILTER

In order to minimize signal noise and electrical interference, a 6 channel mechanical "low pass" filter was introduced for all output signals at the 'post-amplification, pre-data recording stage'. It was designed within the Civil Engineering Department, operating at 11.5 Hertz, +/- 5V. The classical Nyquist "sampling theory" required the sampling frequency to be twice that of the highest frequency of the observed phenomena. In practice, a level *four* times that of the estimated frequency for the *second* mode of response was chosen, giving a $4 \times 10 = 40$ Hertz sampling frequency for the collection of data. The practical limitations of mechanical (low pass) filter design dictated a 'cut-off' frequency of about one fifth that of the sampling frequency (8 Hz), but at least 50% above the phenomena frequency ($1.5 \times 10 = 15$ Hz). Increasing the sampling frequency was not possible, due to the sampling volume limitation of the 8 channel ⌘ MacLab data logger. The compromise 11.5 Hz was chosen, equivalent to 29% of the sampling frequency, but well above the structure natural frequency of 3 to 4 Hz.

Wind vane signal output fluctuated 0 to 10 V, so bypassed the filter en-route to the data logger. Later, with the introduction of two additional ('glued') strain gauges (see 5.2.2. & 7), the anemometer (wind speed) signal also bypassed the filter. At this time, it was discovered that the filter affected the anemometer output, by a proportional amount (c.mid Sept '92). After further investigation, the 'post-filter' signal was found to be nearly constant at 0.6 times the 'pre-filter' signal. Examination with a Cathode Ray Oscilloscope by the Departmental Instrumentation staff could not satisfactorily establish the cause.

5.1.3. ⌘ MacLab DATA LOGGER

Used in conjunction with an ⌘ Apple Macintosh computer and the ⌘ Chart/8 recording package, the 8 channel ⌘ MacLab Data Logger provided a simple, reliable and highly portable data acquisition system.

"The hardware unit has considerable computing power of its own and performs all urgent tasks required during measurements. This means that the actual data capture rate is not affected by the controlling Macintosh."

A summary of its specifications and features is seen below:

- 8 channel single ended input: 10mV-10 V full scale (FS) range
- Maximum sampling rate: 100,000 samples per second

- 'Trigger' the commencement of data acquisition relative to a preset value for one of the acquired channels. Recording time either fixed length or relative to same 'trigger value'.
- Input noise: <3 microV rms referred to input
- Channel crosstalk: better than -110 dB or >1/4 LSB
- Variable input accuracy (with consequences for full scale range and effective resolution).
- Resolution: $1/2^{12}$, or $1/4096$, of full scale (FS) range. For example, 5microV resolution for the most sensitive 2mV/division range ($\pm 10\text{mV FS}$), to 2.5mV for 1V/div ($\pm 5\text{V FS}$).

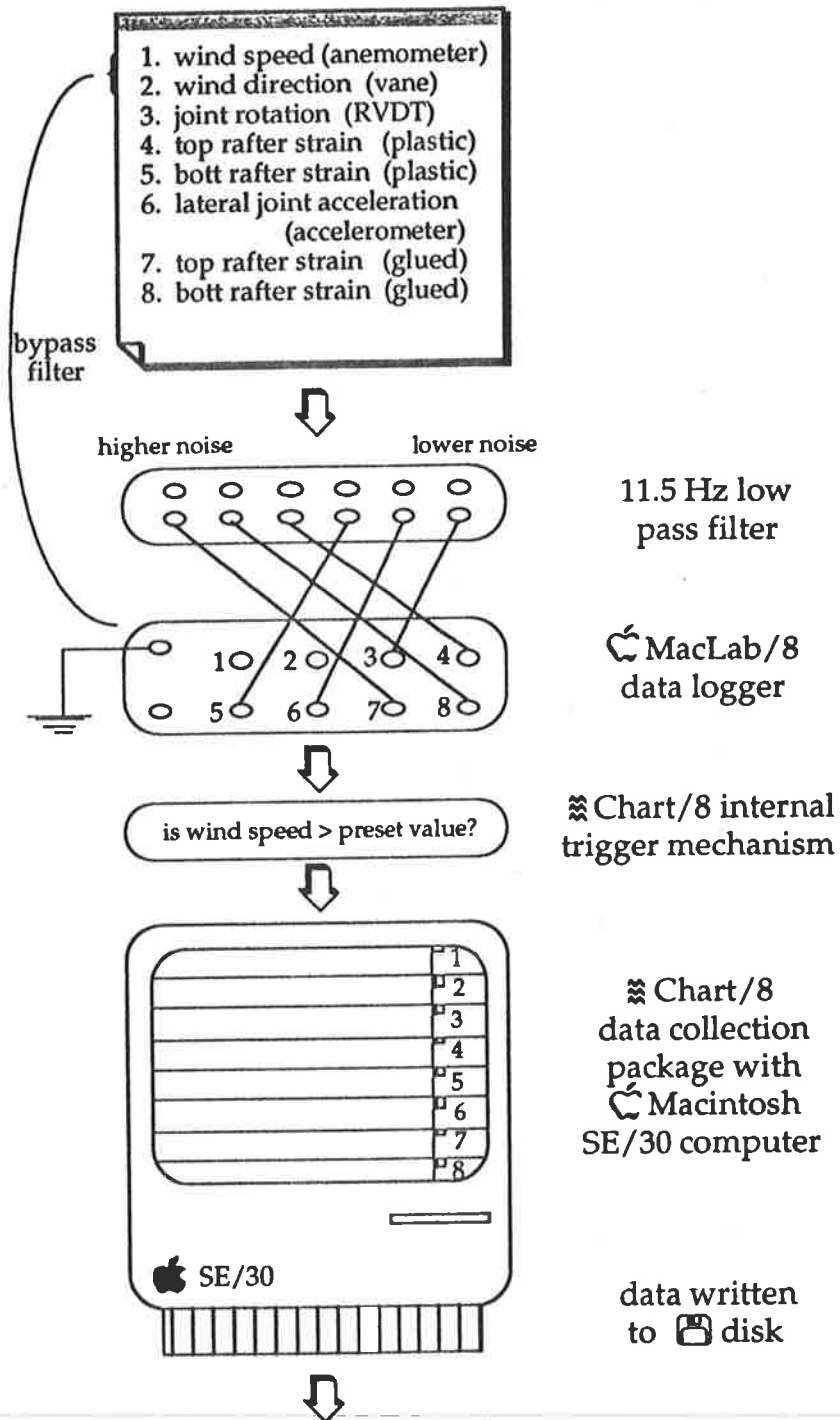


Figure 5.1.2. Schematic view of the measuring system in its final form

A discussion of the resolution of this equipment must necessarily involve consideration of the expected magnitude of the data to be acquired and the associated instrument measuring errors. Details of these will be found in later Sections. A summary is presented in Table 5.1.A. below. It should be noted that all of the predictions for the structural responses, required to select and design instrumentation, were based on simple portal frame action. Due to the stiffening effect of the exterior cladding and 'rigid' end bays on the structure, 'knee' joint forces and deformations could be expected to be significantly less than those calculated with this "upper bound" assumption.

Ch. No.	channel title	Gain/ Div	MacLab resolution	calibration error***	total system error**	expected min value
1	wind speed	1 V	2.5 mV	2% = 30mV	≈ 35 mV ≈1.2 km/hr	<5 km/hr
2	wind dir~n	2 V	5 mV	.5% = 50mV	≈ 56 mV ≈2 degrees	<10 deg.
3	RVDT	10 mV	25 microV	0.092 mV	≈ 0.1 mV ≈0.8mdeg.	1mdeg.
4	top SG	20 mV	50 microV	2% =0.1mV	≈ 0.2 mV ≈0.8ms	20 ms
5	bott SG	20 mV	50 microV	2% =0.1mV	≈ 0.2 mV ≈0.8ms	20 ms
6	accel~n	10 mV	25 microV	-	≈ 0.1 mV ≈0.001g	0.0005g
7	top glSG	10 mV	25 microV	2% =0.1mV	≈ 0.2 mV ≈0.8ms	20 ms
8	bott glSG	10 mV	25 microV	2% =0.1mV	≈ 0.2 mV ≈0.8ms	20 ms

* see relevant Section 5.# (or associated Appendix) for calculations. ("ms" = microstrain $\mu\epsilon$).

** includes the filter contribution (varies between channels, but always less than 0.1mV).

*** % errors converted to output voltages at the min. expected value level, using the derived relationship.

Table 5.1.A. A comparison of measuring errors and expected minimum values for structural responses.

When comparing the expected system measuring errors and the minimum expected values for each of the phenomena in the above table, it is clear that errors are insignificant for all but the RVDT (rotation) system. The minimum value approaches the predicted system error, which in this case is dominated by the error associated with the instrument calibration test. Fortunately, since these 'calibration test' errors only increase the *uncertainty* of output accuracy, rather than increasing the error in the system itself, a significant calibration error does not necessarily mean that recordings are themselves insufficiently accurate. The total error of 0.1 mV could only be estimated, since neither the "board wobble" error (see 5.3.1.) nor filter noise contribution could be exactly determined. To minimize the latter of these two, special care was taken with the connections and positioning of RVDT cables.

Examination of the RVDT output for all wind events of significance (rafter strains > 20 microstrain) revealed that the proportion of 'noise' in the output signal was acceptable, and typically less than 5%. The uniformity of the final results suggests that gross errors could not have been present in any of the measuring systems, especially when considering that wind events were recorded over a period of 10 weeks. (see also 6.5.).

5.1.4. EXPERIMENTAL TIME FRAME

Due to the seasonal nature of these high speed wind events in Adelaide, most wind recordings occurred during June to September of 1992. The system overall had been designed so that instruments themselves could be left in place for months at a time, and either the recording unit or just the data itself (written to disk) removed easily. To avoid most of the electrical noise and vibration from machinery operated during the working week, 'thermal strain' recordings were routinely made on weekends or overnight. The practical difficulties involved in establishing an 'absolute zeroed' strain gauge measuring apparatus meant that each recording 'session' could only be of several days duration before strain drift became significant (see Section 5.2.5.).

Data was sensitive to “amplitude” rather than “frequency”, so large wind events were required to maximize responses and diminish the influence of signal noise and measuring errors. The relative proximity of the structure to Adelaide University meant that as soon as large wind events were anticipated, travelling to the site allowed instrumentation to be ‘zeroed’ and the recording initiated. This was crucial when minimizing measuring errors, since the ζ MacLab package allowed a selection of data collection ‘gains’ for each individual channel. Resolution was linked directly to the ‘gain’ of a channel and set at 1/4096 of the full scale range. Therefore, operating the system *whilst a wind event was in progress* allowed instruments to be fine-tuned, ‘zeroed’ and measuring ranges narrowed: hence greater resolution. This ‘zeroing’ also removed residual or extraneous influences on the data. By concentrating solely on the dynamic, short term *changes* in the structural responses, ‘static’ effects such as long term creep, instrument drift and, most importantly, temperature effects were eliminated (see 5.2.5. & 6.).

To reduce the volume of data collected, the ζ MacLab ‘trigger’ facility was employed. The unit continually monitored the wind speed signal, and when it rose above a predetermined value, recording would commence. Data was then collected for a specified time (nominally 10 seconds during wind events) in preference to the alternative, that of continuous recording until the wind speed signal fell below the ‘trigger’ value. A pre- or post-trigger delay could also be set, so that the collection of data could be delayed or ‘pre-empted’ relative to the time of the trigger. This facility was used during the wind events, to collect the 1 to 2 seconds of data *before* the ‘trigger’ time. This was most useful during very gusty wind events, when high speed winds followed calmer ‘lulls’, producing very steep velocity records and maximizing the dynamic effect of wind loading on the structure.

An example copy of the site sheet is seen overleaf. On each visit to the structure to initiate or collect data recordings, weather and wind conditions, background machinery noise and vibration levels and data logger settings such as channel gains, trigger levels, sampling frequency were noted. This provided a permanent record and manual check on instrument outputs and of the daily conditions.

5.1.5. LITERATURE REVIEW of ALTERNATIVE SYSTEMS

Similar research has been conducted into this type of moment resisting joint in New Zealand, but with an emphasis on earthquake loading. During laboratory controlled testing on newly formed joints, a low number of high amplitude cyclic impulses are applied, in contrast to the wind loading phenomena of very large numbers of low amplitude loads.

Of the reports in literature on instrumenting full scale frame testing, all have used laboratory sited programs. Of interest is the intuitive method used by Kivell-Moss-Carr (1982), who also sought a moment-curvature relationship for a three member timber portal. A single lateral cyclic force was applied to the ‘knee’ node, and frame deformations monitored. With a known lever arm between the pinned column bases and point of load application, the total bending moment is known for any instantaneous force.

“.....Five dial gauges were placed on the underside of the beam at approximately even spacing. From these deflections, approximate curvatures were determined for each end of the beam, and hence the known moment input could be apportioned accordingly.”

Steel side plates were used to form the moment resisting joints, and their rigidity in the plane of the frame considerably simplified the measurement of joint deformation, as also seen in Karacabeyli-Foschi (1987). With this type of joint, net rotations and translations of the joint as a whole may be monitored by simply recording the movement of this effectively rigid plate relative to both a fixed datum and to the timber members. Rotations of the two nail groups can be assumed to occur at the respective centroids of the nail groups, and curvature of the joint as a whole becomes a function of the distance between these two centroids, ready for use in the moment-curvature relationship.

Actual Deformations in the Semi-Rigid Nailed Plywood Gusset Plate Joints of Large Timber Portal Frames

START-UP DATE _____ day / / 92 AM/PM WEEKEND Y
 COLLECTED DATE _____ day / / 92 AM/PM DATA ? N

FILENAME SJ _____ SAMPLE RATE _____ Hz (40)
 d d m m (x10 Hz) FILTER RATE _____ Hz (11.5)

WIND DESCRIPTION: _____ start day _____ collection day
 DIRECTION: _____ | _____ |
 WEATHER DESCRIPTION _____ start day _____ collection day
 MACHINERY OPERATING? Y/N _____ Y/N _____

MacLab Chart/8 Channel Gains

Ch.	Label	Gain/Div	Initial Value	Zeroed?	Collection Day Value
1.	wind speed(1) V	_____ V	N.A.	_____ V
2.	wind dir'n(2) V	_____ V	N.A.	_____ V
3.	RVDT(10) mV	_____ mV	Y/N (‘zeroed’ to mV on / / 92)	_____ mV
4.	top SG(20) mV	_____ mV	Y/N	_____ mV
5.	bot SG(20) mV	_____ mV	Y/N	_____ mV
5.	accel'n(10) mV	_____ mV	Y/N (amp (0.1) g's per Volt)	_____ mV
7.	glue top SG(20) mV	_____ mV	Y/N	_____ mV
3.	glue bot SG(20) mV	_____ mV	Y/N	_____ mV

TRIGGER VALUE V = km/h V = 0.02881 v_{km/h}

⇒ After set time _____ secs (10) Delay Mode Pre-trigger _____ secs (1.0)
 or _____ min (0.2) or Post-trigger _____ min (5)
 At end of trigger

REMARKS:

$$\text{curvature } (\chi) = \frac{(\text{net rotation } \theta_{\text{upper nail group}} + \theta_{\text{lower nail group}} + \theta_{\text{plate bending}})}{\text{distance between nail group centroids}}$$

This simplicity is not offered by the timber gusset plate, as it cannot be assumed to act as a rigid plate, but an alternative technique was developed by Batchelar-Cavanagh (1984). This is similar to the method adopted by Mr. Daniel Siu-Cheung Lee (M.Eng.Sc. Thesis, 1993), in his concurrent laboratory tests on the Yttrup joint.

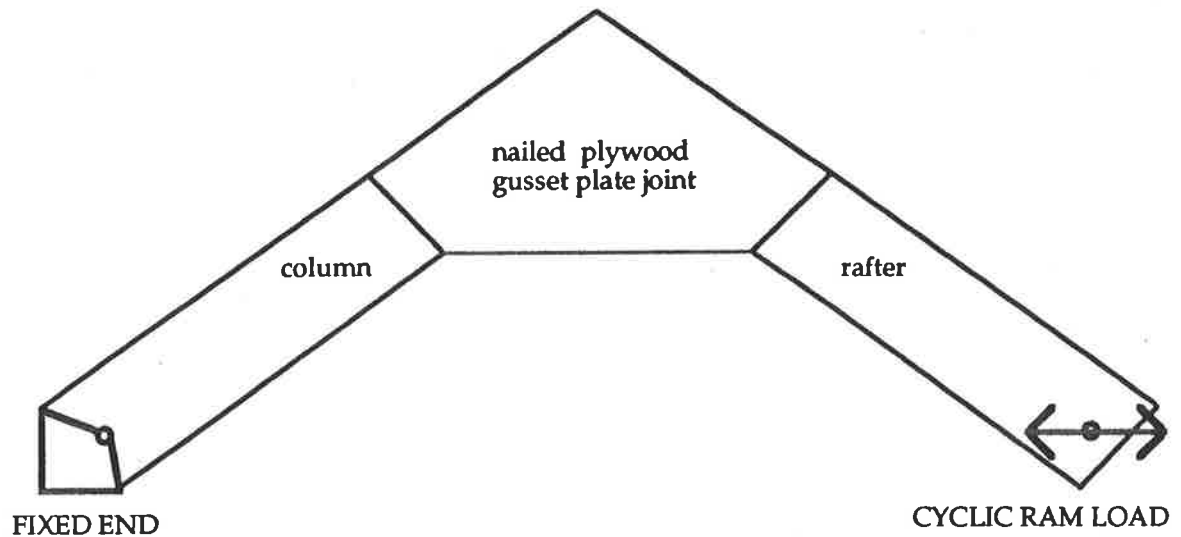


Figure 5.1.3. Experimental set-up first used by Batchelar-Cavanagh (1984)

Their set-up used only one plywood gusset plate joint, comprising a full length column and a rafter segment of same length. These members formed the two equal sides of an isosceles triangle, with the load applied at the extreme ends of the members along the line of the third imaginary side, whose length increased or decreased according to the action of a reverse cyclic ram load. A moment-curvature relationship was derived from the instantaneously known applied force, measured change in length of the third side and a consideration of geometry. This 'remote' method negates the need to measure deformations at the joint directly, and avoids the complex state of stress in the gusset plate and within the nail groups.

However, common to all these laboratory based experiments is the facility to base all deflection measurements from a fixed reference datum. For example, acquiring the lateral sway deflection of the portal frame is a simple matter of installing a gauge between the column-rafter node and the rigid datum.

The use of such a rigid reference frame was not possible in the case of an existing structure containing working machinery. A frame located within the interior of the building would have the advantage of not being loaded directly, especially by large wind events. If located externally, wind would buffet this purportedly 'rigid datum', reducing its effectiveness. An external frame was also impractical for the Western side of the building due to the presence of vehicular access. An early proposal for such a reference frame took the form of a steel truss mounted rigidly from the floor slab, extending to eaves height adjacent the relevant joint, with its plane orientated parallel to that of the portals, and its overall width limited so as to not exceed the structural depth of the column member. Instrumentation could then have been conveniently mounted from this rigid vertical 'post'. But the security of even this minimal intrusion on space could not be guaranteed on a long term basis, so was not adopted.

5.2. RAFTER BENDING MOMENT and AXIAL FORCE

5.2.1. THE CHOICE of CROSS-SECTION

Moment resisting joints in (traditionally steel) portal frames are generally designed for the bending moment at the **column-rafter node** of an 'idealized frame' model representing the 'true' structure. This investigation is concerned with the measurement of the 'actual' joint bending moment of an existing structure. Inevitably, this moment will be measured at a site somewhat remote from the node point of the joint. For the portal frame in this study, an estimate of the 'actual' bending moment diagram shape due to the action of wind forces could be obtained from the theoretical loading of the Australian Wind Loading Code, AS1170.2, applied to the idealized frame. The bending moment at the node could then be estimated from the moment measured at the chosen (remote) site by assuming that the bending moment diagram for the 'true' (measured) case closely matched that produced by the 'idealized' method above.

However, this information is of only theoretical use (e.g. in a joint moment-curvature relationship) since the capacity of the knee-joint is limited by the capacity of either the nail groups in the joint (nail yielding), or the parent structural members (brittle timber splitting). Full scale frame testing by Komatsu et al (1988,9) and moment resisting joint research by Karacabeyli-Foschi (1987) showed that incident structural members invariably fail at a site immediately adjacent to the gusset plate, initiated by local splitting at a perimeter nail site. The limit state in the design of the Yttrup joint was the serviceability case of long term creep deflection.¹ The lack of guidance provided by AS1720 and the more practical considerations of construction method and available plywood sheeting (gusset) sizes governed during consideration of the structural capacity limit state. The resulting conservative nailed joint design would suggest that failure of the structural members will also precede failure of this joint.

It is unknown from which cross-section the design moment for the "knee" joint should be obtained. Many possibilities exist, as seen in Figure 5.2.1. Conventions vary in New Zealand between joints with different configurations, as described by Walford (1988). Accepted Australian practice for the design of timber portal frames is to use the cross-section immediately adjacent to the gusset plate on the rafter, tilted to be normal to the idealized frame used to obtain the bending moment (2). During the instrumentation of this joint, the bending moment was obtained near the first section perpendicular to the rafter centreline which was unaffected by the stiffening effect of the adjacent gusset plate (3). Consideration of the strain distributions in the vicinity of the complex joint region (see 5.2.3.) led to the adoption of the offset location on the rafter (4). The rafter site was chosen over the column equivalent because it was less remote from the centre of the joint. Since the gusset plate was cut from the largest commercially available plywood sheet, its aspect ratio was 2:1, orientated such that the plate occupies almost the entire upper half of the column member.

New Zealand practice is to deliberately introduce a gap between the top of the column and the underside of the rafter, so that all loads transferred between the two members are transmitted through the nailed joint and gusset plates. This means that the joint bending moment may be more easily obtained, by simply attaching strain gauges to the gusset plate surface, in a row coinciding with this column-rafter gap (e.g. Batchelar, 1984). The 'measured' moment is also obtained much closer to the 'node' of the joint, reducing errors during estimation of the 'node' moment. However, this gap is not present in the Yttrup joint. By not measuring extreme fibre strains on the gusset plate, the uncertainty of the stress distribution within the nail group region, as described by Batchelar and Cavanagh (1984) and Boulton (1987), was avoided. By assuming that the main structural members remained within their material elastic behaviour range, both axial force and bending moment for them were obtained from only two strain gauges.

¹ personal consultation with Mr. Peter Yttrup, designer of the Wingfield structure.

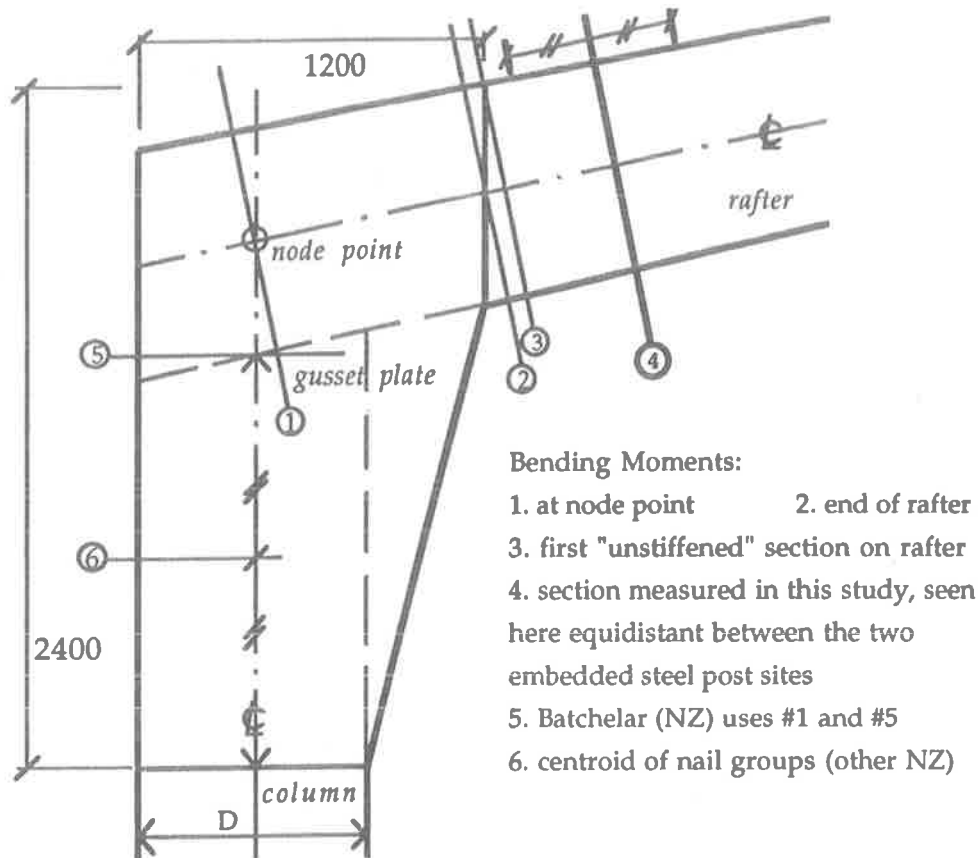


Figure 5.2.1. "Knee joint" showing bending moments at various cross-sections.

5.2.2. STRAIN GAUGE ATTACHMENT

With steel flexural members, bending and axial strains may be obtained by attaching two strain gauges *directly* to one side face of the bending member, one each near the top and bottom, approximately the same distance from the respective extreme fibres, to provide a compression and tension strain. The assumption of an elastic strain distribution and the geometry of the arrangement is then used to calculate the two extreme fibre strains from the measured values. Since longitudinal strains are measured, the average of these gives the axial strain, while half the difference provides the bending strain.

In practice, direct measurement of surface fibre strains is difficult to achieve for a cellular structured and non-homogeneous material such as wood. It was considered inaccurate to attempt a direct attachment of the strain gauges to the side-face of the rafter². Since the size of the strain gauge approaches the dimension of individual fibres in the cellular wood structure, erratic results might be expected from adjacent gauges, attached to different, neighbouring fibres. This was despite reference to the technique developed by Sliker (1989), who used nitrocellulose adhesive to bond 1-mil constantan wire gauges directly to five layer laminate specimens to measure strains in *all three* orthogonal directions. He showed that it was possible to accurately measure 10^{-7} strains by direct attachment to the surface fibres. The accuracy of Sliker's arrangement was not required in this study, and a much less complicated solution adopted.

Strain gauges were directly attached to the LVL members in the concurrent research on the Yttrup joint carried out by Mr. Daniel Siu-Cheung Lee (M.Eng.Sc. Thesis, 1993). A preliminary study compared seven alternative gauges, with various lengths and backing materials, and their surface strains compared with theory in a simple three-point load beam test (Lee, 1993). The KYOWA "KC-70-A1-1" strain gauges were chosen, and

² personal consultation with Dr. George Sved, Honorary Visiting Research Fellow, Department of Civil Engineering, University of Adelaide

subsequently used throughout the laboratory tests. Their exceptional length (70mm) was considered advantageous in negating localized surface strain fluctuations. To correlate strains measured in the two studies, and to confirm the accuracy of the "steel post-plastic strip" method, these gauges were also installed directly on the LVL rafter (see 5.2.6.).

In addition, Batchelar (1984) and Batchelar-Cavanagh (1984) fixed 60mm strain gauges directly to the exterior face of the *plywood* gusset plates of their moment-resisting 'knee' joints, using cynoacrylate adhesive. The more uniform manufacture of plywood means that adjacent strain gauges attached to its surface could be expected to return similar results.

5.2.3. RAFTER STRAIN DISTRIBUTION

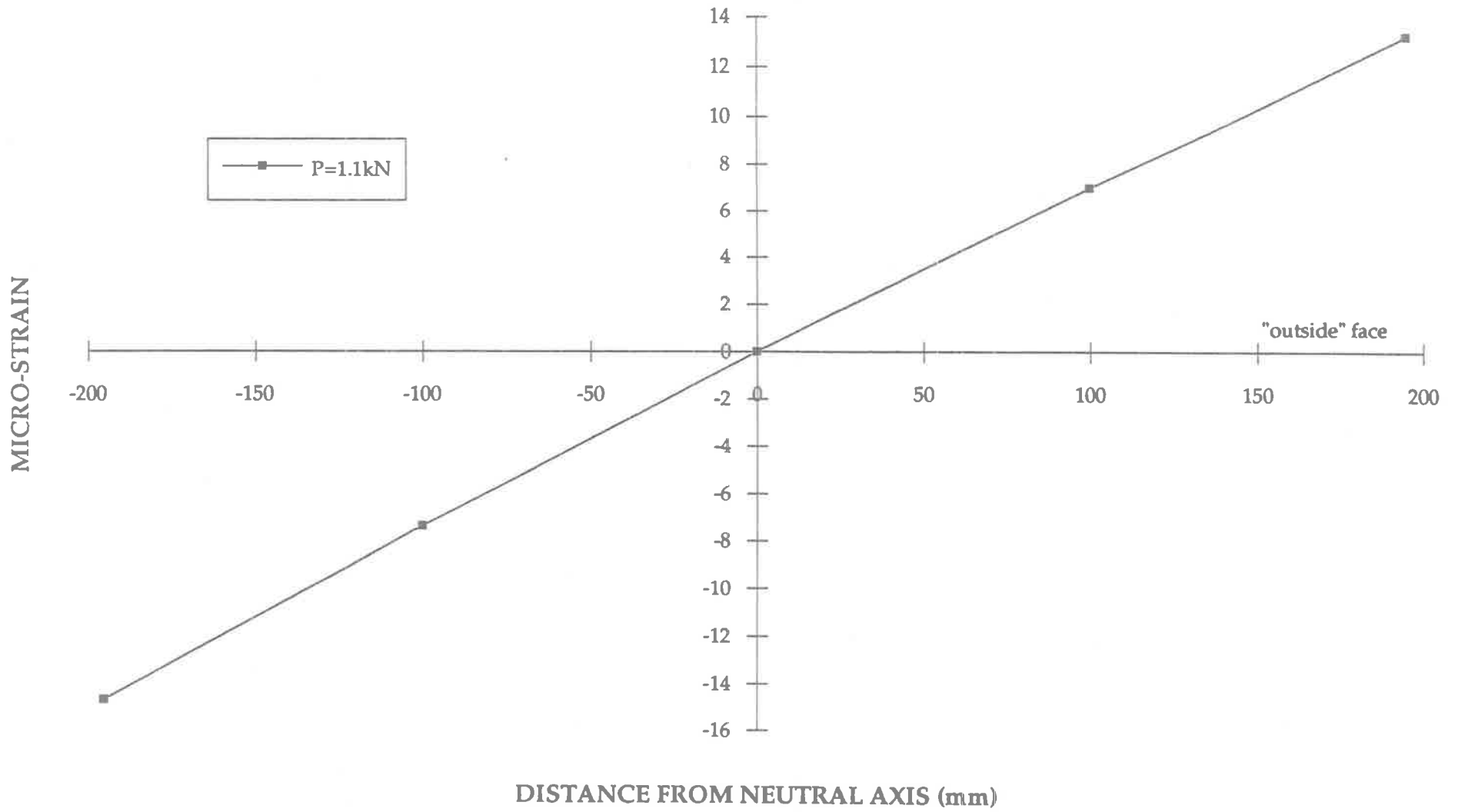
Advice from the manufacturers of the LVL used in this structure³, through reference to their own material testing, indicated that the assumption of linear elastic response would be wholly justifiable, for the LVL material itself. The results of Batchelar and Cavanagh confirmed the deep beam theory prediction of a non-linear stress distribution in the gusset plate region of the joint. However, for cross-sections in the parent members sufficiently remote from the gusset plate, a linear distribution would be expected. The simple (two strain gauge) method used in this study relied on the assumption of a linear distribution, suggesting the instrumentation of a cross-section remote from the gusset plate. However, to maximize the strain amplitudes measured, and to minimize the error involved in extrapolating the 'measured' bending moment to a 'node' moment, a section close to the plate was needed. As a compromise, an offset distance of 170mm was chosen, about half the depth of the (tapered) rafter member in this region.

The assumption of linear strain distribution was later confirmed during the laboratory tests (Lee, 1993), for both 'static' and 'cyclic' loads (in 'opening' joint mode), over the range of strain amplitudes encountered during this investigation. Five strain gauges, glued directly to the side face of the LVL rafter (at the same cross-section as used in this study), provided the rafter strain profile. Tests 1 and 5 were both 'static' tests, where a slowly increasing load was applied by the hydraulic ram, until failure of the half scale specimen. Tests 2 to 4 cycled the specimen at a controlled ram load of 25 ± 9 kN, for 1/2, 3/4 and 1 million cycles respectively, prior to 'static' testing to failure. Data was also collected at intermediate numbers of cycles, by 'statically' applying a selection of ram loads from zero up to the maximum ram load (34 kN). Tests 6 and 7 were cycled at higher stress ranges, of 25 ± 20 kN (failure at $N = 6182$) and 25 ± 15 kN ($N = 15,000$ prior to static test) respectively. A base ram load of 25 kN in the half scale specimens corresponded to a full scale bending moment of $4 \times 25 \text{ kN} \times 1.785 \text{ m} = 178.5 \text{ kNm}$, greatly above the maximum recorded moment in the Wingfield joint of 8.4 kNm.

In the two static tests, Test 1 returned a classic 'deep beam' non-linear strain profile, while Test 5 saw a highly linear strain distribution, at all loads up to failure. Of the three tests at 25 ± 9 kN, Tests 2 and 4 produced linear profiles, while in Test 3, the tensile face gauge gave non-sensical output in an otherwise curvi-linear profile. In all tests, the shape of the profile remained unchanged throughout the loading range being applied. The lowest ram load for which results are available was $P = 1.1$ kN during Test 5: corresponding to a full scale joint moment of 7.85 kNm. At this load level, highly linear strain behaviour was seen: see graph overleaf. No clear explanation was offered by Lee for these results, but for the purposes of this study, a linear distribution may be safely assumed. Serious errors would not be made in the estimate for section moment from the measured extreme fibre strains, even if strictly linear behaviour was not seen. A slightly non-linear strain profile would result in the *over-estimation* of the internal compressive and tensile forces, but this would largely be counteracted by the *under-estimation* of the lever arm between this internal force couple.

³ personal communication with Mr. Bruce Hutchings PEng, TIMBERBUILT Pty. Ltd. (Timber Engineering Consultants), on behalf of IPL (International Panel & Lumber), Boronia, Victoria.

RAFTER STRAIN in TEST 5 (STATIC LOAD)



5.2.4. THE STRAIN MEASUREMENT SYSTEM

Firstly, steel pins were embedded in the top and bottom faces of the beam, one pair on each face. Their diameter was chosen to minimize bending in these reference 'posts', and their embedment deep enough to achieve a rigid base connection, thereby minimizing local wood deformation. Being very stiff relative to the wood fibres, each post effectively 'averaged out' the different responses of the individual, neighbouring fibres, thus truly reflecting the performance of the cross-section at which it was placed. Thin (1.6mm) PVC plastic strips ($E_t \approx 3500$ MPa) were attached to the pins, with a nominal gap to the timber, and the strain gauges were in turn glued to these strips. To achieve a uniform tension across the plastic cross-section, 3mm steel clamping plates were glued to the strip, full width, at the connection to the posts. To avoid any eccentricity of loading in this connection, clamping plates were attached above and below the strip. To avoid the possibility of compression and hence buckling occurring in the strips, a pre-tension was applied, of greater magnitude than the predicted maximum compressive strain. Wind load rafter strains were predicted using the IMAGES-3D™ structural analysis package, in which a linear rotational spring was used to model the nailed joint behaviour.⁴

Conveniently, dead load strains were not measured, as they were already present in the structural elements prior to the installation and zeroing of the instrumentation. Live load was not possible because of the lack of access to the roof area, and temperature effects were largely negated (see 5.2.6.). No overhead cranes/lifting devices are connected to the interior of the structural frame, only some lightweight exhaust ducting.

KYOWA "KFW-5-C1-11L100" 'water-proof' type strain gauges were used throughout, to cope with the extremely dust-laden air within the timber joinery/workshop environment. Specifications were: Gauge Length 5mm, Gauge Resistance $120.0 \pm 0.3 \Omega$, Gauge Factor $2.10 \pm 1\%$, Adoptable Thermal Expansion 10.8PPM/°C, Thermal Output $\approx 1.8 \mu\epsilon/^\circ\text{C}$.

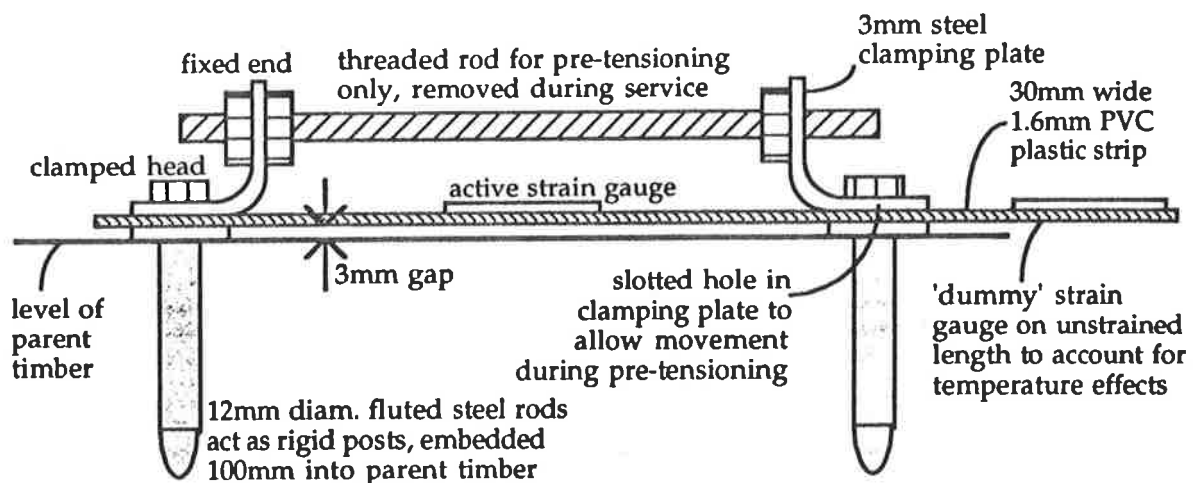


Figure 5.2.2. Strain measuring apparatus as attached to the top and bottom edges of the LVL rafter

The longitudinal axis of each embedded steel post reflects the vertical normal to the longitudinal axis of the rafter at its respective cross-section. For the "no load" case, the 'normals' associated with the pair of posts on each face will be parallel. During lateral loading of the structural frame, the rafter centreline becomes curved due to the bending moment acting upon it. Hence, the post angles change to reflect the curvature of the rafter, so changes in length occur in the plastic strips fixed between adjacent posts. Should the "suction" wind case apply to the rafter, causing an "upward" curvature in it, the 'normals' associated with two posts embedded on the top face of the rafter will diverge. This is seen as an extension of the plastic strip joining them, reflecting the

⁴ see Chapter 6: "Prediction of Frame Deformations and Strains".

tension in the extreme top fibre of the rafter. As such, the total strains in the rafter extreme fibres are indirectly measured as strains in the respective plastic strips. Since linear elastic behaviour has been assumed, their strain levels may be calculated using simple geometry.

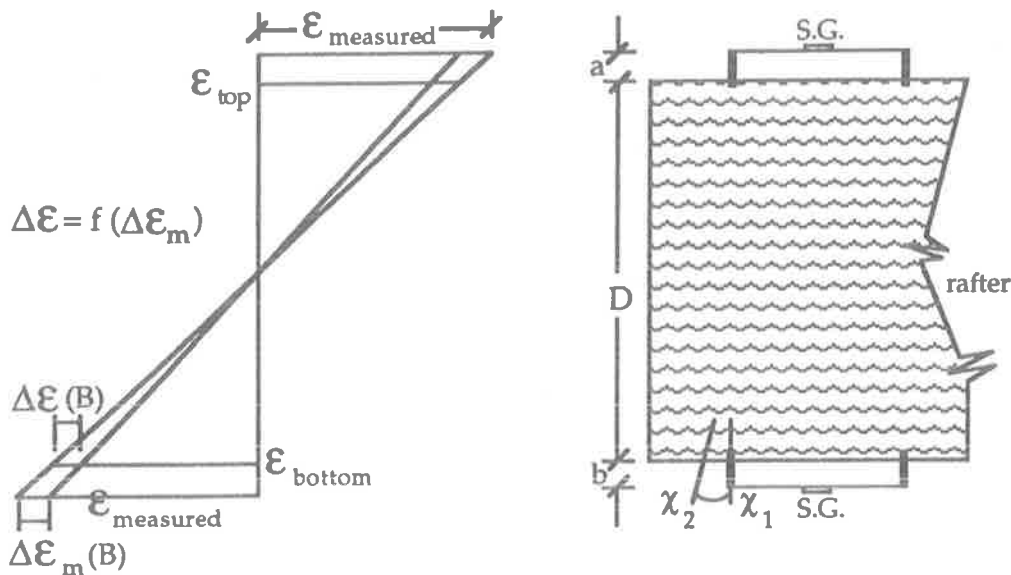


Figure 5.2.3. The indirect method of extreme fibre strain measurement.

From Figure 5.2.3., it may be shown that the true changes in strain in the two extreme fibres ($\Delta\epsilon$) are geometrically related to the concurrent changes measured (remotely) in the plastic strips ($\Delta\epsilon_m$).

$$\Delta\epsilon(B) = \left(\frac{D+a}{D+a+b} \right) \Delta\epsilon_m(B) + \left(\frac{D+a}{D+a+b} - 1 \right) \Delta\epsilon_m(T)$$

$$\Delta\epsilon(T) = \left(\frac{a}{D+a+b} \right) \Delta\epsilon_m(B) + \left(\frac{a}{D+a+b} - 1 \right) \Delta\epsilon_m(T)$$

Since 'a' and 'b' are very small (4.5mm) compared to 'D' (the overall beam depth, $\approx 760\text{mm}$), the remote measured term becomes insignificant for approximately equal $\Delta\epsilon_m(T)$ and $\Delta\epsilon_m(B)$. For example, $\Delta\epsilon(B) = +0.99\Delta\epsilon_m(B) - 0.01\Delta\epsilon_m(T)$, so is dominated by the closer measured strain change.

The above expressions assume linear elastic behaviour, and apply to the general case where the measured changes in strain at the top (T) and bottom (B) of the rafter are unequal. They were developed for a positive change (increase) in strain, a 'positive' strain in the lower portion of the rafter, and by assuming depths measured relative to the top strain gauge position. But with careful application of signs, they remain valid for any loading event. As such, there is no reliance on the absolute values of strain. The reasons for this are now explained.

5.2.5. COUNTERACTING STRAIN DRIFT

The emphasis on recording *changes* in strain (and hence timber stress) was forced by the combination of the practical difficulty in achieving a long term "absolute zero" value during strain measurements and the small magnitudes anticipated in this study, rather than from a theoretical consideration. However, recent research at the University of Adelaide (Oehlers, 1992) indicated that the stress *magnitude* at which strain cycles occur was equally important from a fatigue standpoint. The emphasis in this study was on ambient wind events, and all stress changes were well within the order of serviceability levels. The maximum *change in bending moment* measured by this study of 8.4 kNm was well below the typical laboratory-tested ultimate capacity of $4 \times 55 \text{ kN} \times 1.785\text{m} = 394 \text{ kNm}$ (1/2 scale models of Lee, 1993). The *absolute* stress levels in this study were almost certainly of this low serviceability magnitude also.

Invariably, the amplified signal of a "zeroed" strain gauge (SG) will drift steadily. Because of access limitations to the building and the desire to minimize noise and vibration from the machinery, recording sessions were usually overnight or over a weekend. Typical values of drift over 15 hours were between 40 and 60 mV for both strain gauges. For all but the most severe of wind events, this strain shift would introduce unacceptable errors into any measured strains due to the wind loading (60kph wind was expected to produce 100mV strain output, while a 10kph flutter meant only a 3mV change in SG output).

It was proposed to obviate this problem by applying a correction function to the recorded data, during the post analysis stage. By also recording the time of the recorded phenomena relative to the time when instruments were zeroed, a "true" corrected value could be obtained assuming a *linear* drift rate. Naturally, it was necessary to obtain the "on-site" values for this drift. Several overnight drift tests were conducted, recording both 'zeroed' and 'after drift' values. Because wind loading could not be isolated from the instrumentation system, the 'after' results also included this component, so the tests were only carried out in conditions of minimum wind. However, preliminary attempts to determine this drift rate were not satisfactorily conclusive.

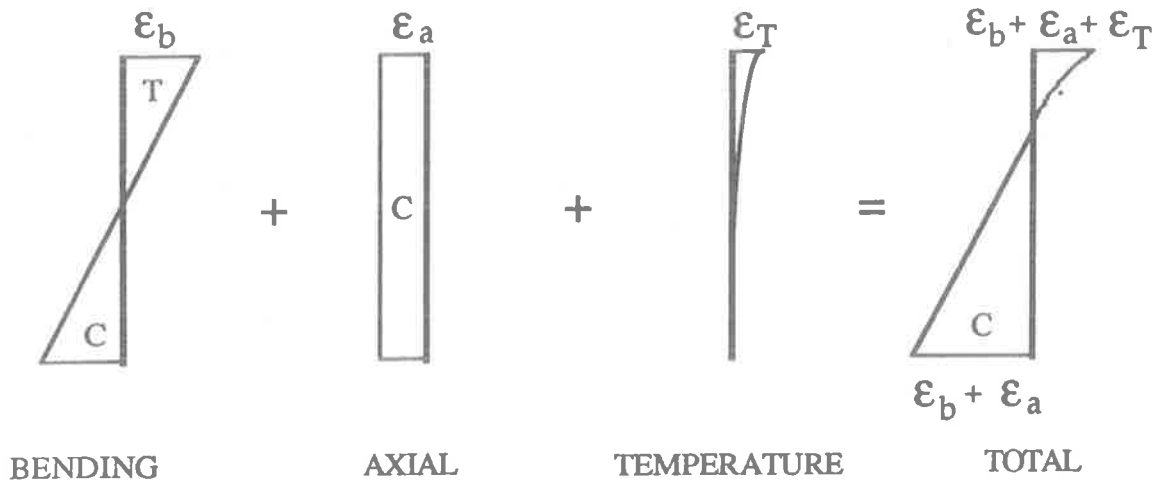
As a result of the first of these tests however, the 12V battery power supply for the two channel strain gauge amplifier was replaced by a DC supply. A closer inspection of the amplifier circuit diagram revealed that the output voltage would be proportional to the input voltage, and with the slight but steady voltage drop of the battery, a significant drift was detected over the 15 to 18 hour overnight recording period. Nevertheless, total drifts of 40 to 50 mV remained. In addition, drifts were not uniform between tests; that is, a relatively reliable *rate* could not be derived. The postulated "linear" rate of the drift could not be verified.

In subsequent overnight tests though, the instrumentation 'trigger' was set so that rafter strains were logged at short intervals (of about 10 minutes), rather than just the two 'before' and 'after' values. These tests revealed the true nature of the changing strains: they were dominated by a *cyclic temperature variation*, exactly mirroring the daily sunshine pattern (period = 1 day). The process of eliminating these strains from the final "axial + bending only" strain output are now discussed.

5.2.6. DIFFERENTIAL TEMPERATURE EFFECTS

Temperature effects on the rafter, sited immediately underneath the metallic roof sheeting of the building, influenced rafter strain in two ways. Firstly, as the temperature of the environment immediately surrounding the measuring site fluctuated during the day, the *thermal cycling of the strain gauge* and plastic mounting strip apparatus produced a length change in the strain gauge, independent of the bending curvature of the rafter. In addition, the temperature differential between the top and bottom of the rafter produced an additional, *non-linear strain distribution* in the cross-section, and a corresponding bending moment in the frame. Both of these phenomena, if ignored,

would have produced errors in the proposed method of obtaining the bending and axial strains by indirectly measuring the two extreme fibre strains.



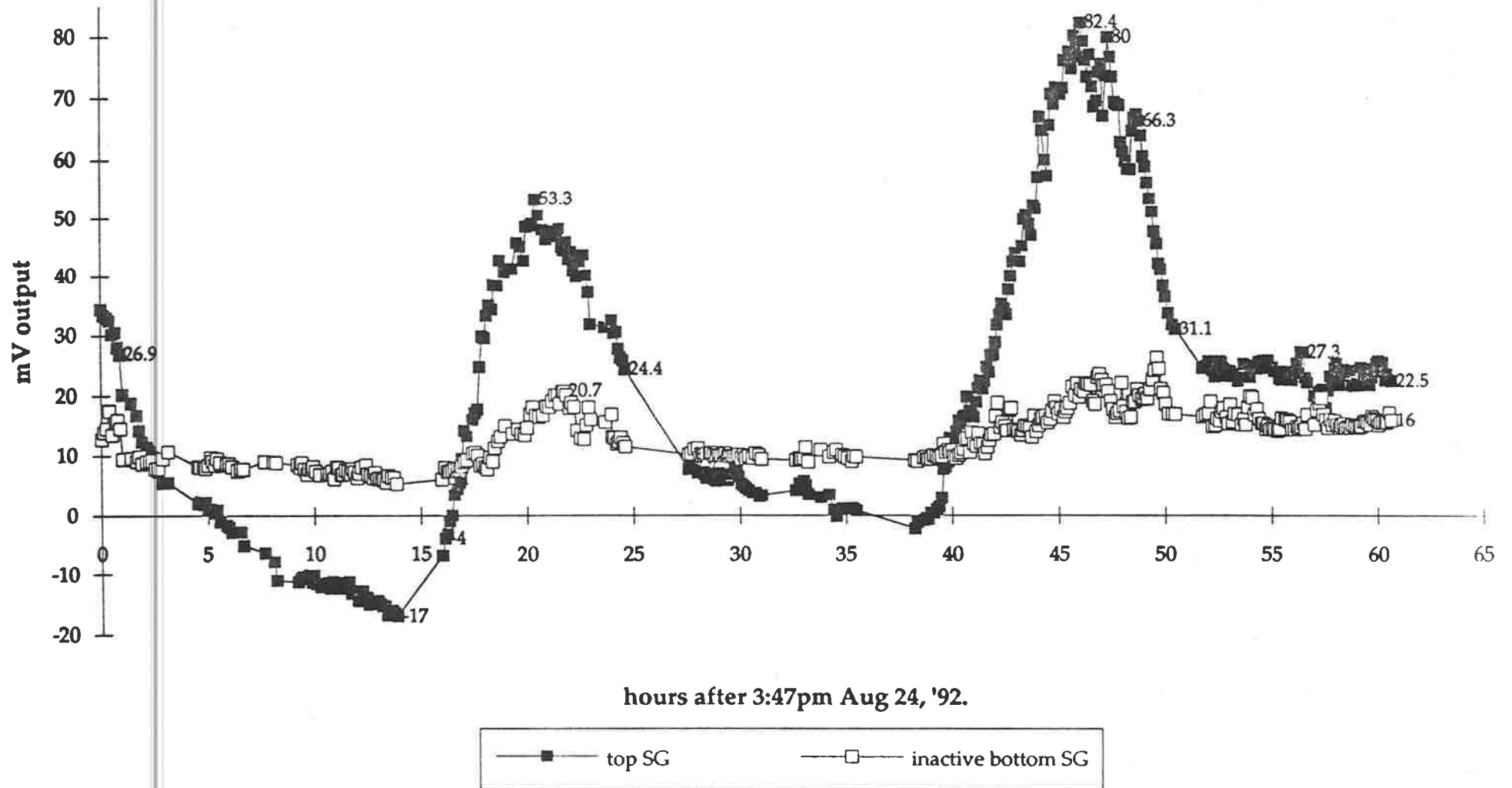
To remove the effect of fluctuating local temperature from each of the top and bottom strain measuring arrangements, 'dummy' and 'active' strain gauges were glued to the plastic mounting strips. One 'active gauge' was sited within the 'strained' length of plastic between the two reference 'posts', the other 'dummy' on an 'unstrained' length beyond one of them. This way, by assuming the two gauges were both affected equally, subtracting the 'unstrained length' strain from that of the 'strained length' gave a strain unaffected by the thermal cycling of the measuring apparatus. This was achieved using the "Wheatstone Bridge" method (see Appendix A). To ensure that the 'dummy' gauge was not affected by local material deformation or Poisson's ratio effects beyond the post, it was sited a strip width beyond the remote edge of the clamping plates at the connection.⁵

The temperature fluctuations mentioned in Section 5.2.5. were applied to both the roof cladding and LVL rafter *and* to all components of the measuring system 'below' the gauges: the strain gauge leads, amplifier and data logger. (The above 'dummy' gauge precaution only removed temperature effects on the gauges and plastic mounting strips themselves). To isolate the source of the fluctuating strain output signal, the bottom of rafter 'active' strain gauge was disconnected from its steel mounting posts, rendering it "inactive". The top of rafter gauge then provided a "rafter + temperature effect" signal, in comparison with the bottom gauge, *without* the "rafter" strains. The signal from the bottom gauge then fluctuated much less than before, while the top gauge signal remained unaffected. This effectively proved that the primary cause of the cyclic signal was 'active' temperature strains in the LVL rafter, with a minor contribution due to the effect of temperature on the measuring system itself. This may be seen from a comparison of the two graphs adjacent.

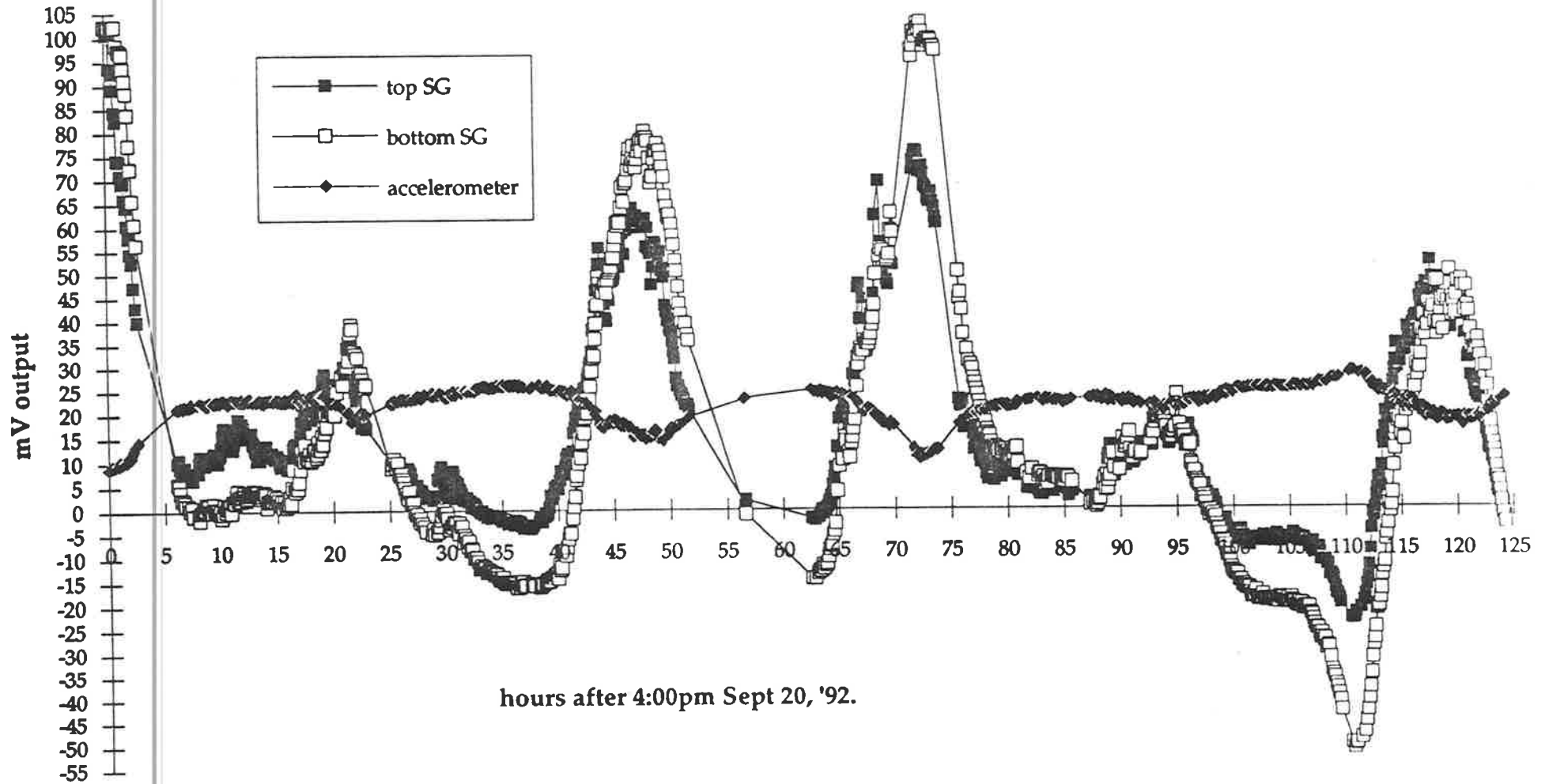
To reduce any contribution to this extraneous strain gauge (SG) signal cycling from the thermal load on the SG amplifier, it was encased in polystyrene insulation. This made no significant effect on the nature of the SG output. Temperature effects on the low pass filter box were checked by applying a thermal load directly to the internal circuitry with a hot air blower. Again, the changes to the test signal were minimal, of the order of 0.5 to 1 milliVolt. Since it was highly unlikely that the ζ MacLab data logger or ζ Macintosh computer were affected by temperature changes, the only remaining source for the 'system' contribution were the leads between the (roof level) temperature compensated gauges and SG amplifier, some 5 metres below.

⁵ personal consultation with Dr. George Sved, Honorary Visiting Research Fellow, Department of Civil Engineering, University of Adelaide.

Thermal Strain Test August 24-27, '92.



Thermal Strain Test September 20-25, '92.



The strategy for dealing with the *non-linear differential temperature strain distribution* was altered from one of 'prevention' to one of 'removal after data collection'. It was initially thought desirable to minimize the temperature differential between top and bottom of the rafter, and hence minimize the inducement of a non-linear strain distribution through the cross-section. A shade structure was proposed to achieve this, mounted over the sheeting immediately above the measuring site. However, this strain was present over the entire rafter length, so minimizing its cause at the measuring site (only) would not have removed the error it produced in the strain measurement process.

By recognizing that temperature strains were effectively 'constant' over the recording time of 10 to 12 seconds or less, compared with the highly erratic wind effects, the large difference between the frequencies of the two phenomena was exploited by employing a filtering technique to eliminate any temperature effects. The ζ MacLab Chart/8 recording package contained an "AC coupling" function, which is intended to remove signal drifts, seen as slowly changing baseline signals. Effectively operating as a 1 Hz "high pass" (HP) filter, any DC and frequency components below 1Hz may be removed before the first amplification stage. However, the value of 1 Hz was considered too close to the building natural frequency of 3-4 Hz. A HP filter value of the order of 0.1 Hz would have been acceptable in this regard, while still functioning adequately as a 'drift' remover, but this was only possible during the post-analysis phase, using the DaDisp™ data management package. Therefore, no attempt was made to remove or negate rafter temperature strains prior to data collection.

Notwithstanding the 'frequency' considerations above, it was felt⁶ that temperature strains were small enough to be neglected (during high wind events), without compensation, since:

- a) when wind speed is large, convection cooling of the roof is at its maximum,
- b) due to Adelaide's weather pattern, any significant wind gust event will most likely be associated with a *cold* front from the prevailing westerly direction, and
- c) the instrumentation had been set up on the Western side of the building, so the response to high speed, morning winds could be documented with even smaller errors.

5.2.7. CALIBRATION of the STRAIN MEASURING APPARATUS

It was originally intended to independently check the validity and reliability of the adopted strain gauge measuring arrangement using a standard tension test on the Departmental Mohr & Federhaff AG (Mannheim, Germany) loading machine. By loading an LVL specimen, instrumented with the "steel post-plastic strip" apparatus, the strain outputs could have been confirmed by the reference load and displacement information. However, as mentioned in Section 5.2.2., this confirmation was more easily achieved by directly attaching two strain gauges to the side face of the LVL rafter, midway between each of the pairs of steel posts in the original set-up. By reproducing the method used for the concurrent laboratory tests (Lee, 1993), results could also be reliably correlated.

The three graphs overleaf show the typical comparison between the two strain measuring methods for the 11.5 second wind event of 28 September 1992, 4:12:27pm. The independent outputs are perfectly in phase, with the magnitudes recorded by the "glued" gauges consistently about 80% of that provided by the "steel post-plastic strip" gauges. This "in-phase" and "proportional magnitude" result confirmed that the output of the adopted strain measuring system may be used with confidence.

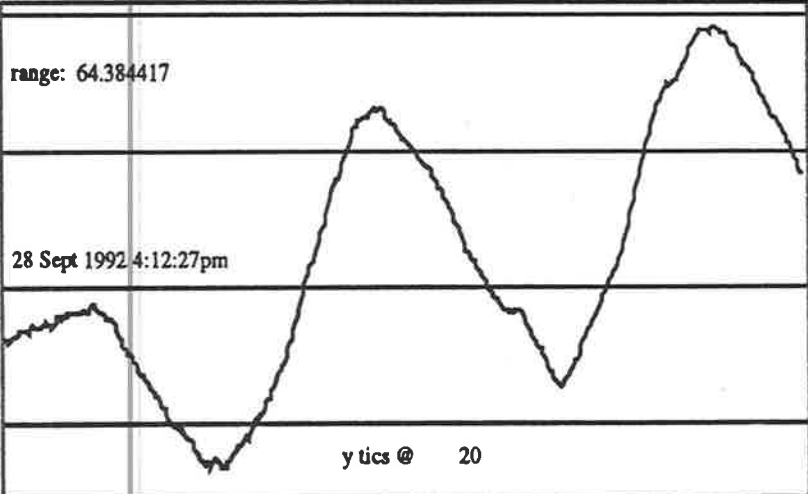
⁶ personal consultation with Dr. Malcolm Hirst, Senior Lecturer, Department of Civil Engineering, University of Adelaide. Dr. Hirst is also co-supervisor of the research project of which this Thesis is a part.

W5: plastic top microstrain

range: 64.384417

28 Sept 1992 4:12:27pm

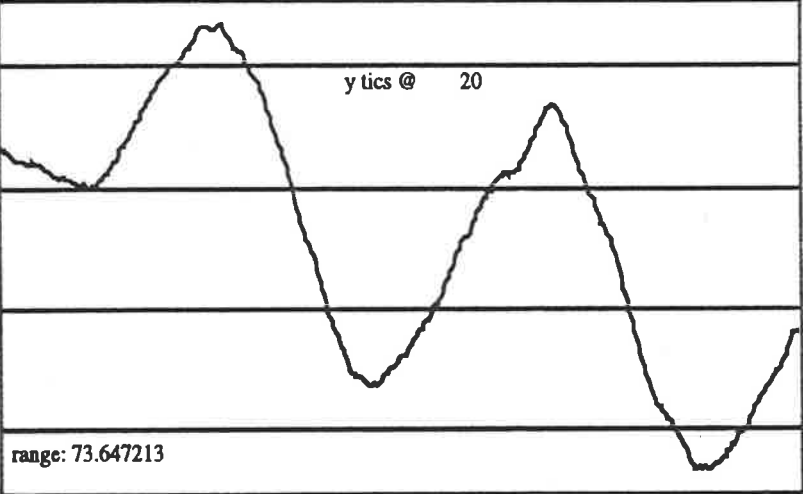
y tics @ 20



W6: plastic bott microstrain

range: 73.647213

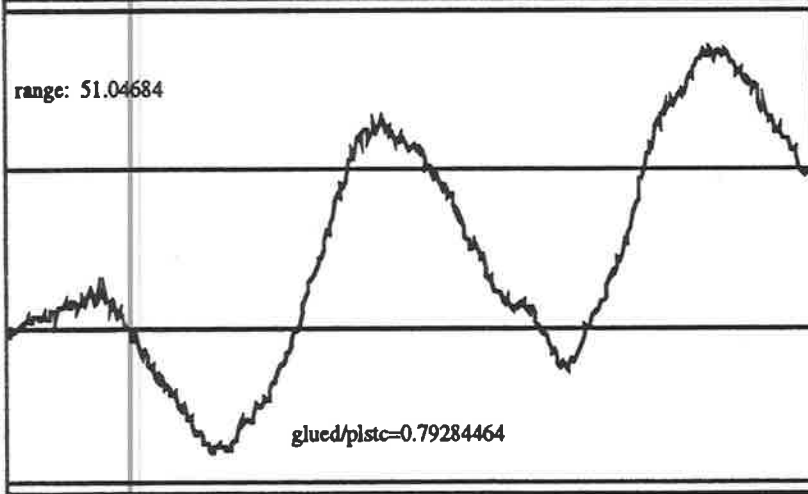
y tics @ 20



W7: glued top microstrain

range: 51.04684

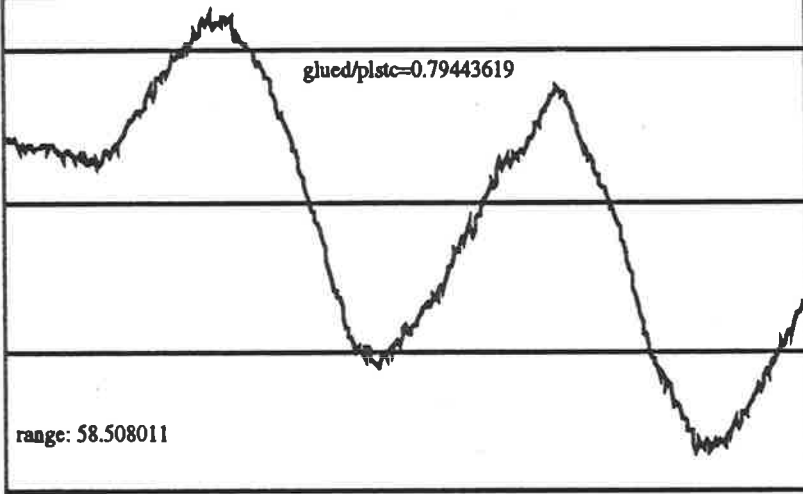
glued/plstc=0.79284464



W8: glued bott microstrain

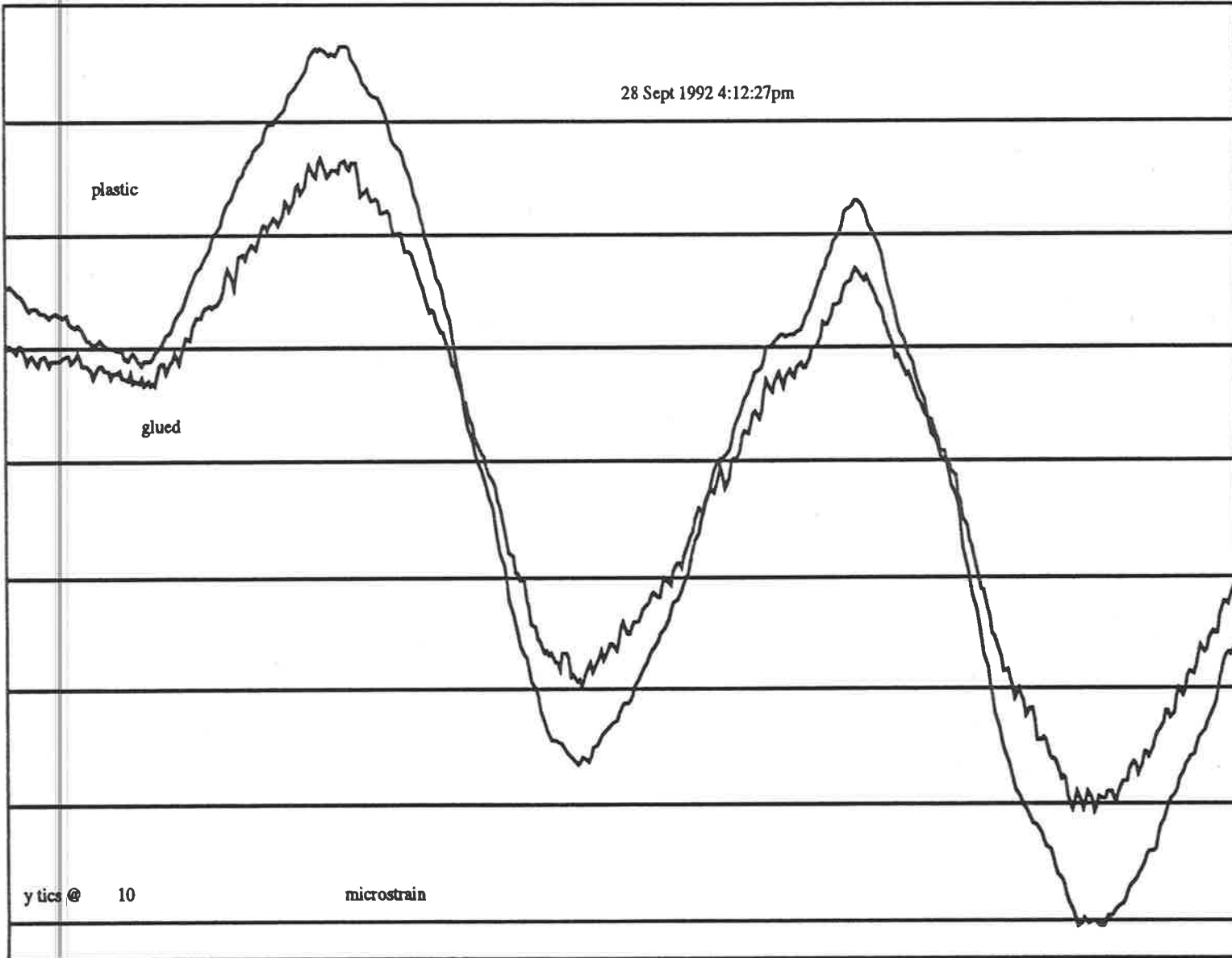
range: 58.508011

glued/plstc=0.79443619



plastic vs. glued bottom strain gauges

28 Sept 1992 4:12:27pm

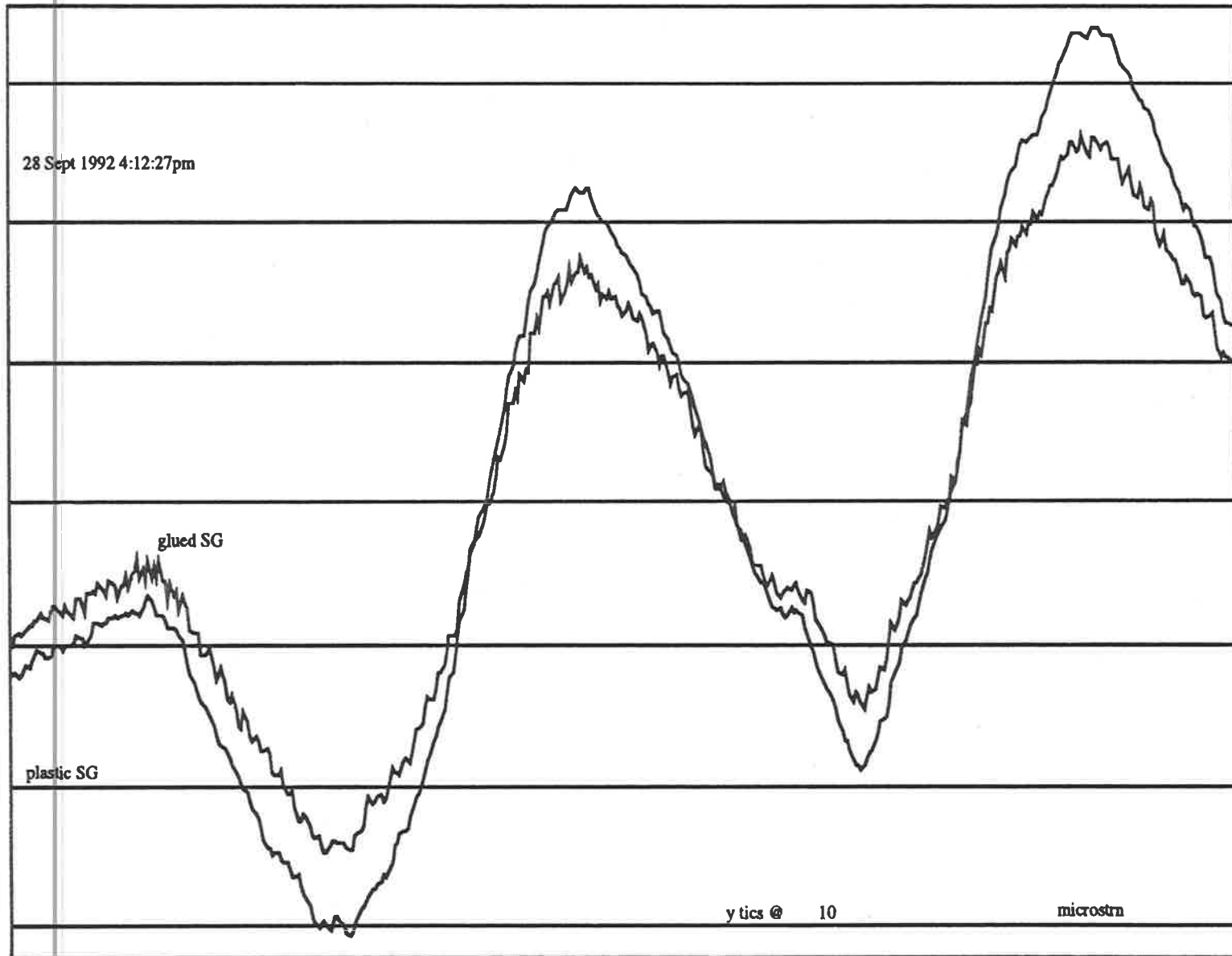


ticks @ 10

microstrain

plastic vs. glued top strain gauges

28 Sept 1992 4:12:27pm



glued SG

plastic SG

y tics @ 10

microstrn

Since the relationship between the amplitudes of the two strain measuring systems was constant, it must have been caused by their relative location on the rafter rather than being associated with their reporting of the exciting phenomena. If the two gauges had been reacting differently to the rafter deformations, a more variable relationship would have been seen. Also, both systems were identically connected to the same data logger, in the same Wheatstone Bridge arrangement, using essentially identical strain gauge amplifiers. The following reasons may explain this proportional relationship:

- (a) *errors during the two, separate calibration tests*: since 'strains' were obtained by multiplying the voltage output of the SG amplifier by a constant value, obtained from a calibration test, any errors present in these tests would have been directly passed on to the output 'strains' of the two systems.
- (b) *error in the location of the glued strain gauges* which were placed midway between the two posts used by each plastic strip. The midpoint was chosen from the assumption that at this location they would measure the same strain as averaged by the two posts. For rafter sections adjacent to the column-rafter node, the slope of the frame bending moment diagram is very steep for pressure loads such as wind. This fact would have amplified any errors due to the misalignment of the glued gauges.
- (c) *the 'damping' of strains measured off the rigid steel posts*: the reference posts, to which the plastic mounting strips are attached, are embedded in the (≈ 760 mm deep) rafter by 100mm. The common assumption that "plane sections remain plane" in flexural members implies that no bending should be experienced by the vertical post. They should remain parallel to the radius of curvature upon which bending theory is based. Any non-vertical alignment of the posts would violate this assumption, by distorting the adjacent rafter sections. Also, the drilling of 12mm holes for the embedment of the steel posts may have slightly weakened the rafter on the tension face, or distorted the original 'longitudinal strain flow' in the region. However, their effect on the above difference should have been minimal, seen equally by both strain measuring systems. Even so, this weakening or interruption to the strain profile on the tensile face would tend to accentuate (b) above.

5.3. JOINT ROTATION

A key component of this investigation was the accurate measurement of the rotation of the 'knee' joint in the plane of the frame. Initially, an arrangement was devised whereby the fluctuating lengths of a triangular model would be used to geometrically derive the instantaneous rotation at the assumed centre of rotation of the joint (see Section 5.3.4). This was rejected in favour of the more direct and precise method of using a Rotary Variable Differential Transformer, or RVDT. The device used in this study was the SCHAEVITZ ENGINEERING (Pennsauken, N.J., USA) RVDT Type R30D. This device produces a voltage whose magnitude is linearly proportional to the angular rotation of the shaft, with exceptional accuracy.

The performance of the RVDT as quoted by the manufacturer is for high linearity, over magnitudes and frequencies of rotation far in excess of the requirements of this study. The linearity for a displacement angle of ± 5 degrees is better than 0.1 percent of full scale value. This linearity decreases with displacement angle, but rotations in excess of this were not anticipated. These figures apply to cyclic loading at 2.5kHz, far greater than the expected structural response of 2-10 Hz. Even better performance can be expected at these lower frequencies.

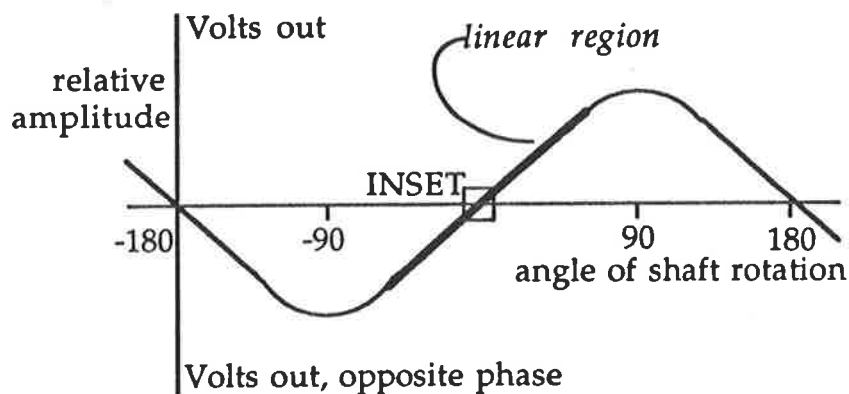


Figure 5.3.1 Output curve for the RVDT over its full operating range, showing the relevant linear range

To measure rotation, a ferromagnetic rotor (attached to the shaft) spins relative to stationary windings inside the housing and internal shielding, thereby inducing a current. Therefore, the coupling is electromagnetic only, so electrical noise is minimized, and mechanical friction is produced only by the miniature precision ball bearings supporting the operating shaft. This enables a resolution "approaching infinitely small angles", or at least, much smaller than the rotations to be measured in this study.

In order to measure the rotation of the two structural members with respect to each other, without interference from the gusset plate, 'mounting boards' were attached to the LVL members beyond the edge of the plate, as shown in Figure 5.3.2. These boards projected over the plywood gusset to allow the mounting of the RVDT at any chosen centre of rotation. A limitation of the RVDT device is that the radial load on the shaft must not exceed 3.63kg (8lbs). Accordingly, the body of the RVDT was fixed relative to the rafter, while the shaft pin reflected the relative rotation of the column. This way, no load would be transferred into the shaft due to the dead load of the mounting boards. A nominal gap was maintained between the gusset plate and each mounting board so that protruding nail heads would not foul their independent action.

NB: assumed centre of rotation is centroidal axis confluence

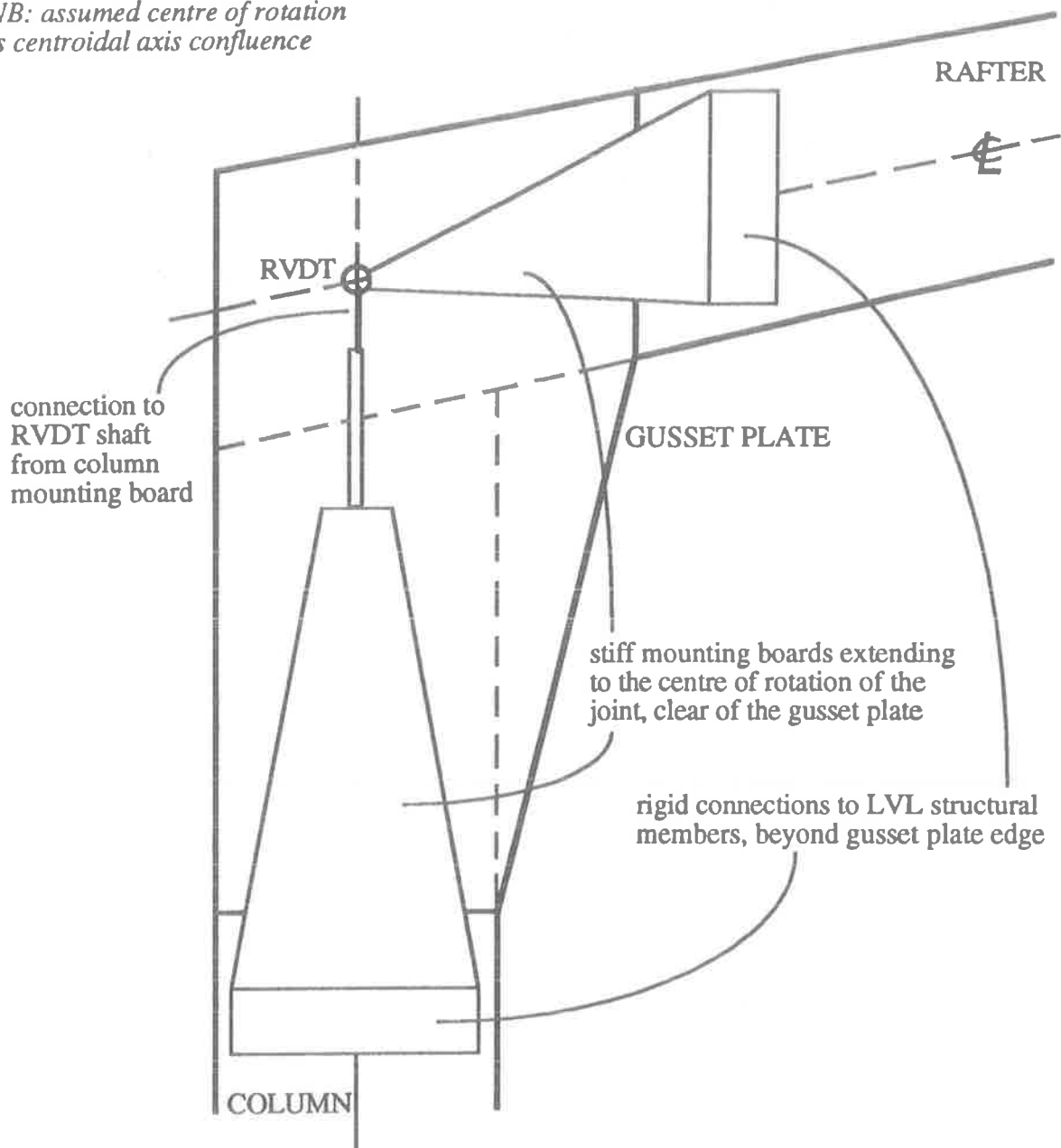


Figure 5.3.2. Elevation of the 'knee' joint showing the RVDT mounting arrangement

5.3.1. WHAT IS ROTATION?

What is the definition of "rotation" for this joint? Conventionally, rotation is based on the change in angle of a simple, two-member hinge, measured at its centre of rotation, normally considered to be the confluence of the two member centrelines, or 'node point'. This model assumes that infinitely stiff members are connected by a much weaker "rotational spring element", where the dimension of the joint is small compared with the length of the members. For moment resisting joints, a much stiffer spring element is required to provide the necessary structural integrity. In traditional steel or reinforced concrete construction, this model is still convenient because the size of the joint seldom exceeds the depth of the connected members.

The presence of the gusset plate and the two large multi-nail groups in the connection means that the Yttrup 'knee' joint also does not behave as a simple two-member hinge. In addition, there is no intuitive 'centre of rotation'. Considering the bearing of the rafter on the top of the column (as discussed in Section 3.4., "Interface Characteristics"), it was

hypothesized that the centre of rotation would most likely occur somewhere on the gusset plate near the midpoint of this contact surface. This point is a distance of half the rafter depth, or 400mm, from the conventional 'node' point.

The large (elevation) dimensions of the gusset plate relative to the column and rafter depths (and column *height!*) suggests a very stiff arrangement. The gusset plate not only controls rotation in the 'joint', but also resists bending in the connected members, as well as incorporating some 'bracing/tie' action from the gusset diagonal. As such, the stiffness (or 'degree of rigidity') of the connection will influence the rotational behaviour of the joint. If the plate were infinitely stiff, such that bending of the plate in the plane of the portal frame were negligible, no rotational change would be seen at the conventional 'node' point. In this situation, the "rigid" joint would merely translate (as a rigid body) under the application of load to the frame, and rotation would only be seen in the column and rafter members. For the more realistic "semi-rigid" joint situation, with nail slip and finite gusset plate stiffness, rotations in the members at locations adjacent to the plate edge can be expected to be greater than those seen in the plate, at the 'node' point. This was in fact observed during the concurrent laboratory tests on half-scale specimens, and became most easily noticeable at higher applied moments and rotations (Lee, 1993).

Since very small joint rotations were anticipated for the serviceability level, ambient wind events expected during the study, and in order to maximize the amplitudes to be measured, "rotation" was based on the rotations of these member sections, adjacent to the gusset plate edge. As such, 'rotation' was defined as *the difference in the slopes of the "last" two tangents to the centrelines of the connected members*. "Last" meaning "at that section closest to the node point", for which bending moment and hence rotation would be a maximum. (NB: the 'two-member hinge' model is a subset of this). Therefore, if the two centrelines were to be projected towards the 'node' point, their confluence would continually change under varying load, making the selection of a single site for the RVDT impossible. For small rotations however, the confluence would occur within a relatively small "zone". Use of a computer structural package showed that with the use of the mounting board arrangement previously described, under small rotations, damage to the RVDT shaft would be avoided. For initially straight (unloaded) column and rafter members, the confluence of their centreline tangents is the trivial case of the conventional 'node' point. The RVDT was mounted directly above this point.

One advantage of using the "mounting boards" to project the line of these 'centreline tangents' is that these projections are *independent* of that which makes the joint stiff, i.e. the gusset plate and nail groups. So the (disadvantageous) "size effect" of the gusset plate, which complicates the study of this timber moment resisting joint, is essentially countered by this rotation measuring method. The long projection length of the boards tended to increase the possibility of sideways 'wobble' and in-plane bending, so stiffeners were attached to minimize the signal noise and measuring error from these.

Due to this uncertainty regarding 'centre of rotation', the mounting arrangement for the RVDT was designed to enable adjustment of the RVDT position. Initially, the RVDT was positioned directly over the 'node point' for the joint. Subsequently however, for the purposes of uniformity and comparison of results for different wind events, this position was not altered.

5.3.2. CALIBRATION OF THE RVDT

From Departmental records, the RVDT unit was calibrated in April of 1983, when the stated linearity of 0.5% of full range, under an imposed rotation of $\pm 40^\circ$, was bettered. The quoted scale factor of 125mV/degree was re-calibrated to be 136.7 mV/deg, for a rotation range of 180° .

To confirm this finding, and to test the device's repeatability, a static calibration test was undertaken using the Departmental torque machine. It was recognized that it would have been very difficult to reproduce a reversed cyclic rotation regime within the

calibration experiment in order to gauge the device's performance under conditions similar to those produced by natural wind exciting the structure. From this 1991 calibration, the scale factor was 122.6mV/degree of rotation, for a rotation range of +5.75°-8.36°, corresponding to RVDT output voltages of +0.7V and -1.04V.

The RVDT rotation was measured against a simple hinge-board, as seen in Figure 5.3.3. This device was made up of a spirit-levelled plate, hinged to another (straight) 'datum' plate. A micrometer was mounted between the two plates, off the spirit-level plate, forming the third side of a right angled triangle.

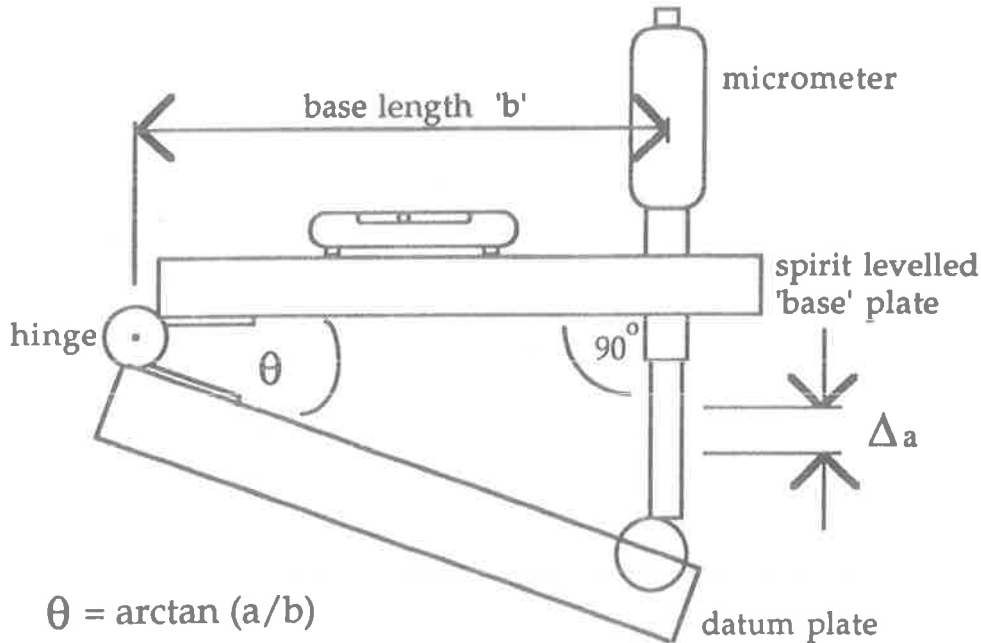


Figure 5.3.3. Hinge-Board Device used to measure the reference rotation in the calibration experiment.

The shaft of the torque machine was progressively rotated by convenient amounts, chosen from the RVDT output. Hence, the pin of the RVDT and the datum plate were rotated through equal angles. The spirit bubble was levelled using the micrometer adjustment, and the angle of both assemblies computed from the simple trigonometry of the hinge-board device. By using a micrometer accurate to 0.0015mm (including a 'user interpolation error' of a half of one division), and a base length measured to the nearest 0.02mm, error analysis¹ gave the accuracy of this 'reference rotation' to be 0.75 milli-degrees. This apparently minute error (for the unit itself) is not deceptive, as this 'exact' mathematical figure may be easily confirmed by applying the errors to the respective lengths of the right angle triangle. (1 milli-degree = 0.02 milli-radians).

A highly linear calibration was achieved, with a correlation factor negligibly below unity, as is evidenced in Figure 5.3.4. The relationship between the imposed angle of rotation and output voltage of the RVDT was:

$$\text{rotation } \theta = 8.135 \text{ Volts} + 0.033 \text{ (degrees)}$$

A stable output voltage signal for this (static) test, combined with a negligible error in the reference rotation, indicated that the measuring error associated with the RVDT itself may be ignored when considering the error of the whole rotation measuring apparatus. This error would necessarily include any "wobble" (buckling) or bending in the mounting boards, or slip in the "rigid" connections of these to the LVL members. Measuring apparatus error and noise would also contribute. The concurrent laboratory tests (Lee, 1993) helped to show that these errors were not excessive (see 5.3.3.).

¹ see Appendix B: Error Analysis in the RVDT Calibration Test.

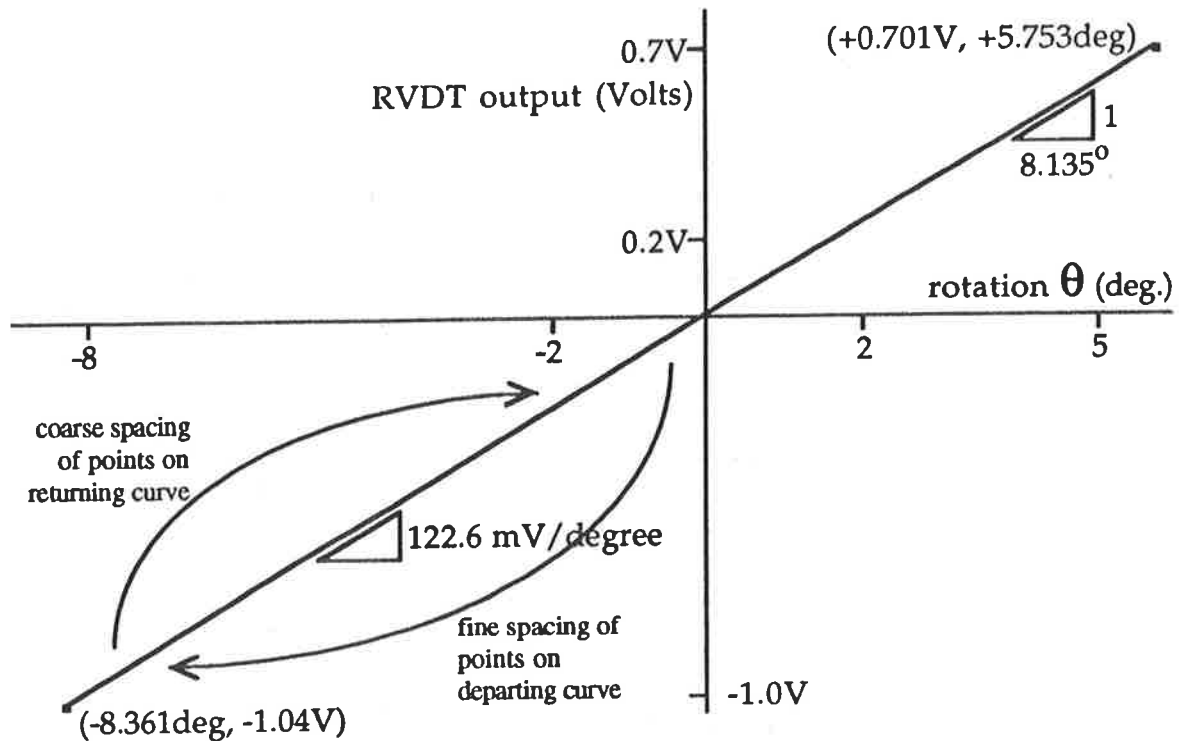


Figure 5.3.4. Plot of results from the RVDT Calibration Experiment

5.3.3. COMPARISON with ROTATIONS in LABORATORY TESTS

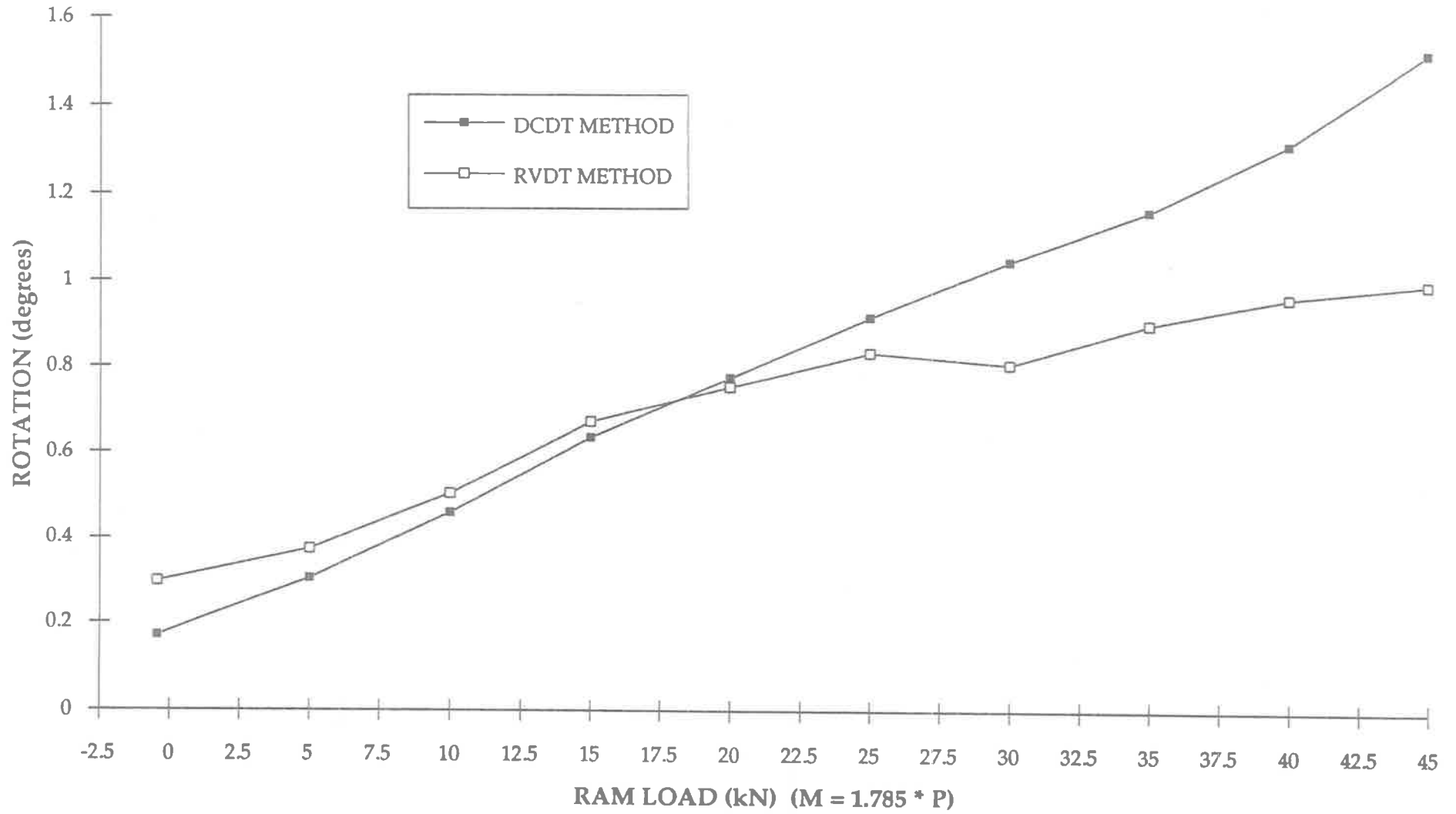
The adopted rotation measuring system was compared with three other methods during the concurrent laboratory tests (Lee, 1993). Two were impossible to recreate in the field: using information from either the Instron™ hydraulic loading ram or translations of the frame referenced from a rigid datum, as discussed in Section 5.1.5. The third is a simplification of the alternative described in the following Section 5.3.4., and was proposed by Dr. George Sved². It became the preferred method in the laboratory tests. A reference bar was attached to the rafter, adjacent to the (vertical) edge of the gusset plate, projecting to the level of the bottom (horizontal) edge of the gusset plate. A Direct Current Displacement Transducer (DCDT) was fixed in a similar way to the column member, such that its 'pointer' struck the bottom end of the 'reference bar'. This DCDT measured the variation in size of the gap between the reference bar and the column member, from which a rotation in the overall joint could be trigonometrically deduced.

Non-reversed, cyclic loads were applied to the 'V'-frame specimens, whilst recording rotations with two methods. The RVDT was placed in two possible 'centres of rotation', firstly over the midpoint of the rafter/column bearing surface, and later at the confluence of the two member centrelines, as done in this study. A special spring mount was required to prevent damage to the RVDT shaft, due to the very large rotations (several degrees) applied.

These tests conclusively showed that for the range of rotation amplitudes expected (and recorded) in this study (-0.15 to +0.25 degrees), the adopted RVDT method should provide reliable results, for either of the possible RVDT positions. A typical graph is shown overleaf, for the comparison between the 'DCDT' method and the 'RVDT' at the "midpoint of the rafter/column bearing surface" location.

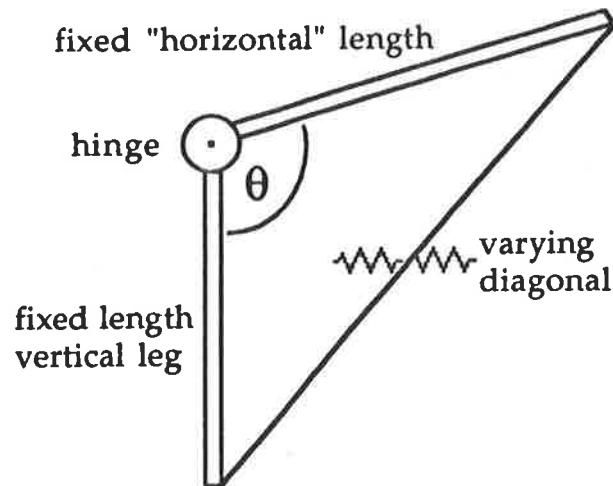
² Honorary Visiting Research Fellow, Department of Civil Engineering, University of Adelaide.

ROTATION vs MOMENT: rotation by different methods



5.3.4. AN ALTERNATIVE TECHNIQUE - NOT ADOPTED

This technique was conceived from visualizing the 'knee' joint as simply two-members hinged at their junction. To find the relative rotation at this node point, a triangle was imagined with a (near) horizontal leg (along the rafter) meeting a vertical (column) leg at the centre of rotation of the joint. For fixed lengths of these two sides of the triangle, measuring the fluctuating third (diagonal) side would provide a length from which an instantaneous angle of rotation at the node could be calculated.



The assumption of constant length holds reasonably well for the column leg, because downward vertical forces through the joint are primarily carried by bearing of the rafter on the top of the column.³ However, axial load in the rafter is carried only by shear through the upper nail group into the gusset plate, and thence into the column member. As such, a horizontal slip in the nail group is experienced relative to the rafter. In addition, the presence of axial forces in both the members infers a deformation, and hence a length change.

To overcome this deficiency, the other two legs of the triangle could be measured. The cosine rule would then provide an instantaneous joint rotation, independent of the global nodal displacement. By defining the gauge length as the distance from the node to the edge of the gusset plate, the effect of axial deformation in the member beyond the plate is negated. Changes in these lengths would then be due primarily to nail group slips only. See Figure 5.3.5. overleaf. (Alternatively, if this information was not sought, any reference length would suffice).

A second order effect which would induce a change in the horizontal gauge length, independent of joint rotation, would be bending curvature of the rafter member. This could be minimized by simply reducing the gauge length. However, the 2:1 gusset plate aspect ratio dictates that to reduce measuring errors, the horizontal gauge length should be at least that of the vertical leg. And as such, it would include not only this second order effect, but also that of rafter axial deformation. A trade-off is thus required in deciding on the horizontal gauge length, with both options leading to inevitable errors.

After a choice of gauge lengths was made, the triangle of displacement measuring devices could be installed. Linearly varying displacement transducers (LVDTs) were to be mounted between two sleeved (or "bushed") tubes, and connected as rigidly as possible at their ends to the LVL base.

³ personal consultation with Mr. Peter Ytrup, designer of the Wingfield structure.

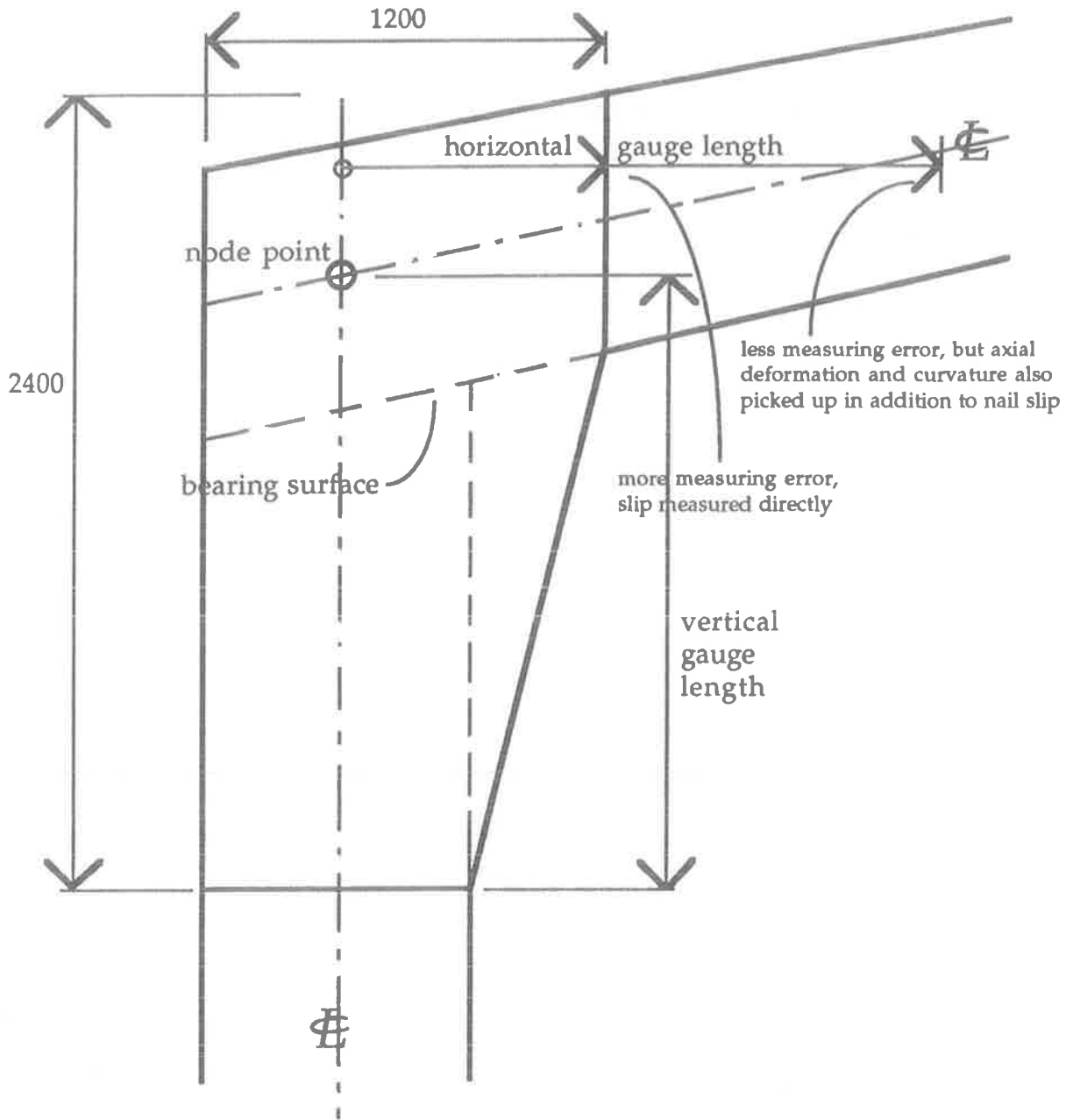


Figure 5.3.5. Elevation of the 'knee' joint showing gauge lengths for the rejected 'LVDT triangle' method.

This arrangement was rejected for two reasons: firstly, the process of measuring rotation by measuring the lengths of three sides of a triangle was much more complex than obtaining it directly from an RVDT; and secondly, its only advantage over the RVDT method was the additional information obtained about nail group slip, but as seen from the discussion above, this would contain unavoidable errors. The task of predicting this nail group slip is made difficult by the scarcity of guidance in literature or Codes, the large number of nails in the 'ring' groups, and because the combination of materials represents a 'new' technology, without the benefit of experience or reference joints. The setup as described was formulated with LVDTs in mind. From preliminary calculations however, it appeared that the slips for such large nail groups would be of a sufficiently small magnitude as to approach the resolution of the LVDT.

In addition, the problem of locating the centre of rotation of the joint, as described above, also plagues this method.

5.4. WIND MEASUREMENTS

In order to reliably relate the wind action vs. recorded structural response to the Australian Standard AS1170.2-1989, 'Wind Loads (Minimum Design Loads on Structures)', it was necessary to measure wind speed. That is, it was important to establish the range of wind loadings (from zero up to the basic design gust wind speed) in which the conclusions about joint behaviour were valid. Wind speed and direction were measured simultaneously, using a three-cup anemometer and potentiometer-type wind vane respectively. The sampling rate to measure the wind actions was the same as the rate used to measure the structural responses, since all instrumentation was recorded by the same ζ Maclab data logger.

In order to derive an estimate for the applied loads on the structure only from wind measurements, it would have been necessary to install pressure transducers over the surface of the cladding, covering the entire tributary area of at least one portal frame. Many such units would be required to minimize the extrapolation errors involved. Alternatively, key positions could be measured, and an assumed pressure profile model (e.g. AS1170.2) used to compute the loadings. Either such arrangement would be extremely time consuming, and without great accuracy, and yet still only provide the load applied to the *cladding*, not to an individual portal frame. For this reason, the applied bending moment and axial forces were inferred by measuring rafter strains directly from the frame itself.

Thus, "inexact" measurement of the wind loading of the structure was accepted. The wind speed provided by the single anemometer then acted as an 'indicator' of wind loading, since there will always be a relationship between high wind speed (at some point) adjacent a building and the wind loads acting upon it. It also became a practical way of reducing the volume of data recorded (and that which needed analysis!), as the ζ MacLab data logger would be "triggered" to record only when the wind speed rose to a predetermined value.

When measuring the wind speed impinging on a structure, it is most accurate to locate instrumentation at least five wall heights upstream of the windward wall. For locations closer than this, it is necessary to conduct wind tunnel tests to check for position error, in particular to cover other wind directions, and to determine the effect of upstream buildings.¹ Due to site constraints, the maximum distance away from the 5 metre high windward wall that the equipment could have been erected was 9-12 metres. Power supply lines occupy a one metre vertical space, 5.5 metres directly above this, adjacent the street kerb line. A proposed anemometer site, at the building eaves height of 5 metres, some 10 metres upstream of the windward wall, would have involved the above error, and a possible effect on the anemometer output signal due to the magnetic field surrounding the power lines. See Figure 5.4.1. overleaf.

The alternative was to position the anemometer much higher, at 10-20 metres, and use a wind tunnel model calibration to refer to top of building height. This option also had the advantage of being valid for a 180° range of wind directions,¹ and was less affected by shielding and flow interruption of upstream buildings. A height just over that of the ridge level of 7.225 metres was chosen for the wind measuring apparatus, so as to measure a relatively undisturbed flow. The anemometer and vane were mounted using a 7.8 metre pole, anchored by three steel cables tightened by turnbuckles. As seen in Figure 5.4.1, this was sited in line with the '5th' portal frame, the next to the North of the '4th' frame, which was instrumented for the structural deformation responses. One of these guys was attached to the gusset plate of this '5th' frame, and enabled the cables to be conveyed back to the data logger, without obstructing traffic adjacent the building.

¹ personal correspondence with Professor W. H. Melbourne, Chairman of the Department of Mechanical Engineering, Monash University, Clayton, Victoria, Australia.

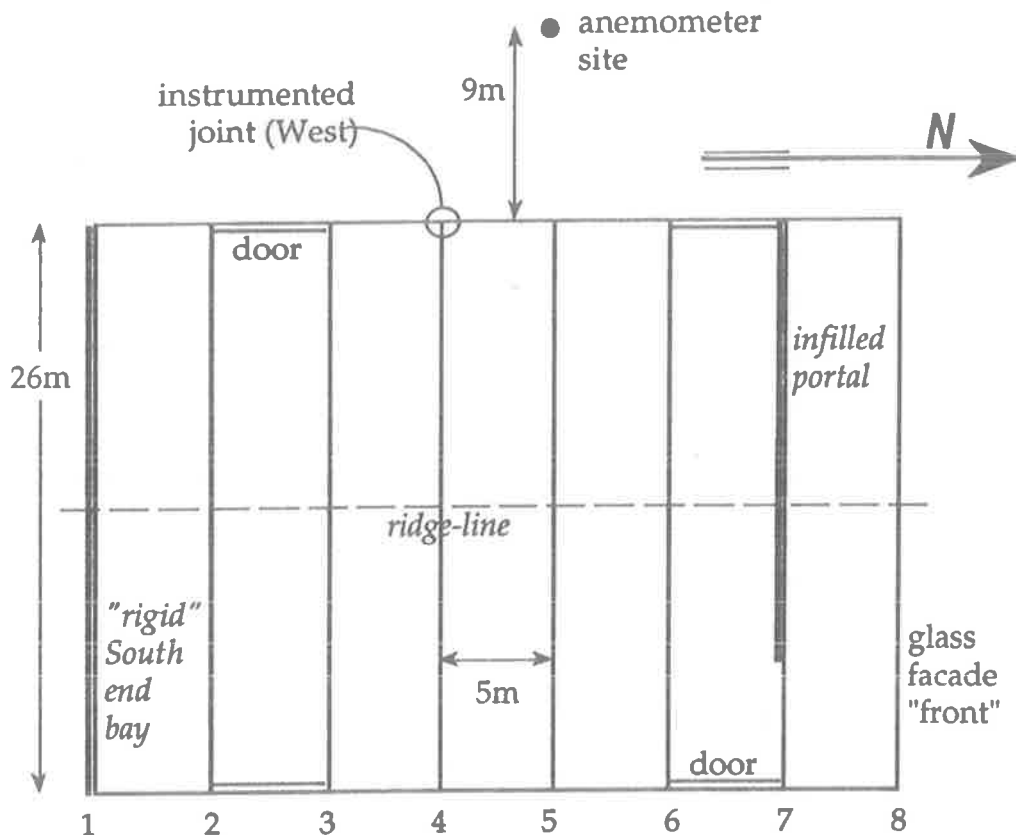


Figure 5.4.1 Building Plan showing location of wind measuring apparatus

One problem introduced by the use of only a single anemometer is that of the correlation between the instantaneous wind gust speed measured and the structural responses to it (in the form of deformations). This is particularly difficult when the angle of incidence of the wind differs greatly from the Westerly "normal" or when 'flukey' or gusty winds are experienced. In the ideal case of a predominantly Westerly wind, the anemometer positioned as shown above would give an excellent indication of the loading experienced by the instrumented "fourth" portal frame. In addition, the lag between the times at which speed was measured at the anemometer site and when this wind was acting over the majority of the frame tributary area could be readily estimated. In squally weather, wind gusts tend to be highly localized and changeable, so that pressures on the cladding vary greatly both spatially and with time.

Two extreme scenarios may be constructed whereby the correlation between anemometer wind speed and portal frame responses would be poor. Firstly, when a 'line squall' approaches from a high angle of incidence (e.g. S - SW or NW - N), recording a high velocity at the anemometer site but essentially not loading a significant portion of the instrumented frame's tributary area, and secondly, the reverse of this situation, when the same squall passes directly over the building, but records a relatively low speed at the anemometer site. The likelihood of these situations is reduced by the proximity of the anemometer to the Western wall of the building. Nevertheless, the complexity of the wind loading phenomena is such that the limitations of the adopted system are obvious. Fortunately, the high volume of data collected during each of the five most 'significant' storms (3,7,10 & 12 August, 28 September) meant that all directions of loading were measured during a variety of wind strengths and 'types'.

Due to the "large plan area, low height" building type, the rafters dominated in the total load supplied to the frame 'knee' joint. Consideration of the size of the gusset plate, being

half the column height, suggests that this would be accentuated by such a stiffened column member. Ideally then, structural responses would most likely be maximized when wind events were of sufficient duration to apply significant (negative) pressures over the length of the rafter. For a typical wind gust of 45 km/h (12.5 m/s), the time required for the 'front' of the gust to reach the far (Eastern) end of the lee rafter after registering at the anemometer site would be $(9 + 26)/12.5 = 2.8$ seconds. This is consistent with conventional frame analysis to AS1170.2, which is based on the design gust wind speed (V_z) for a 3 second gust event.

5.4.1. CALIBRATION OF THE ANEMOMETER

The three-cup anemometer, manufactured by "R.M.YOUNG COMPANY, Traverse City, Michigan, USA", supplied by Dobbie Instruments, Sandringham, Vic., had a light, free-moving head, which minimized time lag errors due to momentum on 'start-up' and cessation of loading. Its sensitivity was such that it would reliably register at walking speed, say 0.5 metres/sec. Using the Departmental (linear) wind tunnel, a very satisfactory (linear) calibration result was achieved, relating the velocity of the incident wind to the output voltage of the anemometer, according to the following equation:

$$\text{velocity of wind} = 9.64 \text{ Output Volts} + 0.30 \text{ (metres/second)}$$

This relationship is valid within the range of voltages of 0.1 to 1.8V, corresponding to velocities of 1.26 to 17.58 m/s, which was satisfactory for the purposes of this investigation. However, advice² indicated that after the slight initial non-linearity in a wind tunnel-derived expression, extrapolation beyond the upper extent of the linear range is quite valid.

The velocity of the air in the wind tunnel was derived from a pitot-tube pressure head, measured by a manometer, and adjusted for ambient atmospheric pressure, temperature and humidity ratio. The standard equation:

$$v = \sqrt{2ghR}$$

was used, where R represents a dimensionless adjustment for the ambient properties of the air in the wind tunnel described above, and h is the manometer pressure head reading. An error analysis³ showed that the maximum wind velocity derived from the tunnel, 17.5 m/s, included an error of 0.18m/s, equivalent to a linearly increasing uncertainty of 1% of the derived magnitude. By far the dominant source of error was 'R', the 'atmospheric adjuster', and not 'h'. For the conditions experienced on the day of the experiment, $R = 820 \pm 14$, effectively contributing 85% of the error in the velocity equation.

The output signal from the anemometer was far from constant, its error linearly increasing throughout the experimental range, representing an output error of about 1.5-1.8%, or ± 0.75 to 0.9% about the median observed value.

² personal consultation with Mr. Jack Ewers, Senior Lecturer (Water Engineering) in the Department of Civil Engineering, University of Adelaide.

³ see Appendix C: Error Analysis in the Anemometer Calibration Test.

5.5. LATERAL DISPLACEMENT of KNEE JOINT

As discussed previously in Section 5.1.5., limitations were imposed on the access to the joint due to the operations within the building and the necessity to leave instrumentation in place for long periods. This prevented the use of standard measuring techniques possible in the more controlled laboratory environment, and was most evident when attempting to obtain measurements for the lateral displacement (or 'sway') of the frame at the 'knee' joint (Δ_{knee}). Engineering judgement and anecdotal evidence suggested that the sideways of the frame would be in the order of several millimetres for the serviceability level wind events expected during this study. In addition, unlike the measurements of rafter strain and joint rotation, there were no comparisons to be made with the half scale model frames, and no possibility for the refinement of any proposed system during these laboratory tests.

Encouraged by the experience within the Civil Engineering Department in acceleration recordings, primarily in the field of earthquake engineering, the indirect "baseline correction" method was adopted for obtaining the frame sway. This was used in conjunction with instrumentation techniques developed for measuring ambient level vibrations in unreinforced masonry structures by Klopp and Griffith (1993).

5.5.1. BASELINE CORRECTION

"Baseline correction" (or "BLC") is a common technique used during the analysis of laboratory based earthquake simulation tests. In these tests, an acceleration record is used as the load input for the "shaking table" on which a scale model structure frame is mounted. As such, the time history records for the base acceleration (a) and displacement (s) of the model are known. Accelerometers and displacement transducers are attached to measure the frame deformations for the upper levels. Load is input for a known duration (T), at which time the base ' a ', velocity (' v ') and ' s ' become zero. Since the frame upper levels continue to oscillate harmonically after time $t=T$, measurements are continued until the response has been damped to negligible amplitudes ($t=\tau$). This gives zero final values for the acceleration and velocity of the frame $a(\tau)$ and $v(\tau)$, while final displacements for the upper levels will only be zero if the model remains elastic.

The baseline correction technique provides an independent check on the lateral displacement records for an upper level provided by the transducers, and involves the double integration of the accelerometer record for that level. The accelerometer measuring error ' e ' is very small compared with measured accelerations, and may be estimated for the purposes of this exercise. However, after double integration, the $\frac{1}{2}et^2$ term may be of significance, especially for long test records. From a knowledge of the above boundary conditions for the three functions given below, the integration errors $\frac{1}{2}et^2$, c_1 and c_2 may be removed from the derived displacement function $s(t)$.

$$\text{acceleration } \mathbf{a} = f(t) + e$$

$$\text{velocity } \mathbf{v}(t) = \int \mathbf{a} = \int f(t) + et + c_1$$

$$\text{displacement } \mathbf{s}(t) = \int \mathbf{v} = \iint f(t) + e\frac{t^2}{2} + c_1t + c_2$$

As seen in Figure 5.5.1. overleaf, the integration error ' c_1 ' appears as a constant offset in the integration-derived velocity record $v(t)$. Since it is known that final velocity $v(\tau)$ is zero, this error may be removed, prior to the next integration step. For elastic range tests,

where $s(\tau)$ is also zero, a similar correction may be applied to the derived displacement result, while in the more general inelastic case, ' c_2 ' would represent the error in the double integrated estimates for displacement.

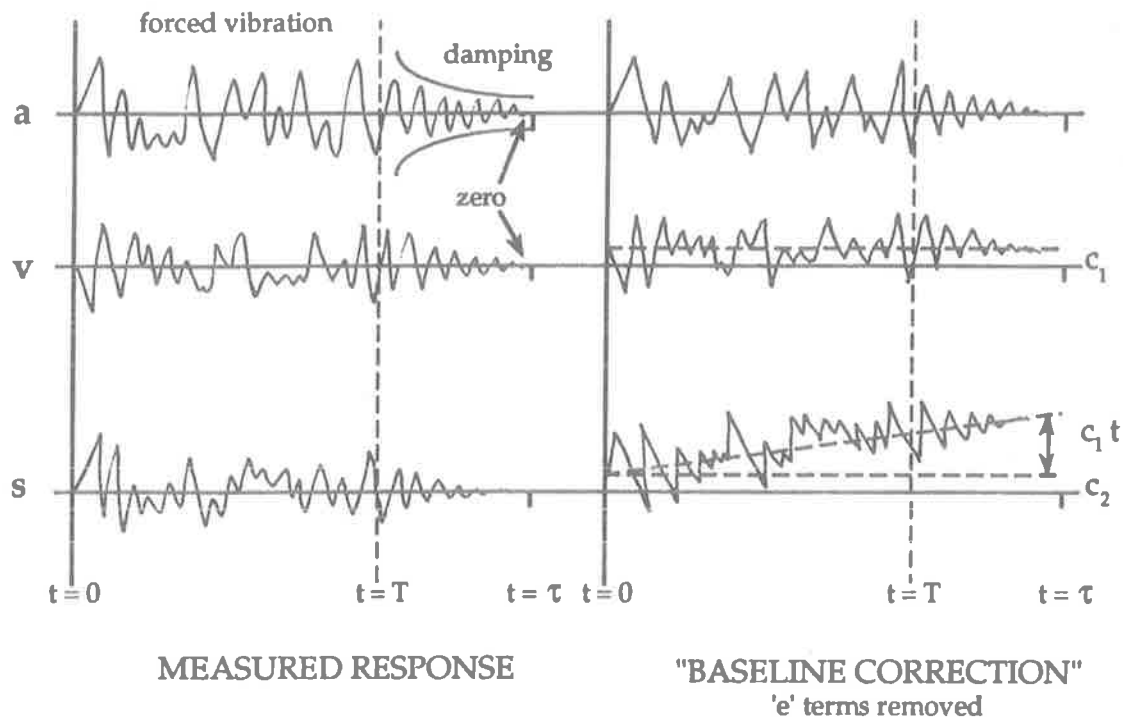


Figure 5.5.1. Upper level 'measured' and 'baseline corrected' records for elastic model case

5.5.2. ADAPTING "BLC" TO OBTAIN Δ_{knee}

It was expected that the adaptation of the above method to *this* study would produce far greater errors than normally experienced (or accepted) in earthquake simulation tests. A single accelerometer was placed at the node point of the instrumented joint, with its sensitive axis aligned horizontally. Load was not controlled in this study, and as such the boundary conditions for the accelerations and displacements at the measuring site were not known. Without knowledge of the final frame velocity value $v(t=\tau)$, the ' c_1 ' error could not be removed after the first integration. However, ' $c_1 t$ ' manifested itself as a larger and more easily recognizable feature in the derived displacement-time function $s(t)$. The error ' c_1 ' then represented the slope of the imaginary line between the final and initial displacement values in the derived $s(t)$ record.

$$\text{slope of linear error function} = \frac{c_1 \tau}{\tau} = \frac{\text{final } s(t=\tau) - \text{initial } s(t=0)}{\tau}$$

Baseline correction was the process of subtracting the linear function ' $c_1 t$ ' from the displacement record obtained from the double integration of the accelerometer record.

The selection of this 'final' value above represents the major source of error during the use of this method when calculating Δ_{knee} . During earthquake simulation tests, it is known that $a = f(t=\tau)$ is zero, so the above expression holds true after the removal of the $\frac{1}{2}et^2$ term from $s(t=\tau)$. This was not the case during this study, with its absence of (wind) load control. Therefore, some judgement had to be exercised: rather than selecting a

'final' point $s(t = \tau)$ and evaluating the function above to find this 'c₁t' line, an (inclined) baseline "equivalent" to this line was chosen from the displacement function, based on visual inspection of the acceleration and (derived) velocity records for the event. For example, during a sustained wind event, the frame would displace to a relatively consistent position, before relaxing. This response would correspond to a velocity profile of initially positively increasing, then dipping to zero, before a negatively increasing velocity. The maximum displacement would occur during this change in the sign of the frame velocity.

A series of three of these baseline selections were evaluated for each event, and the resulting maximum offsets each side of this line noted. The maxima for both positive and negative displacements from this process represented the "peak responses" for the lateral 'sway' of the frame at the 'knee' (Δ_{knee}). Although an approximation in this form, BLC provided a reliable "order of magnitude" analysis.

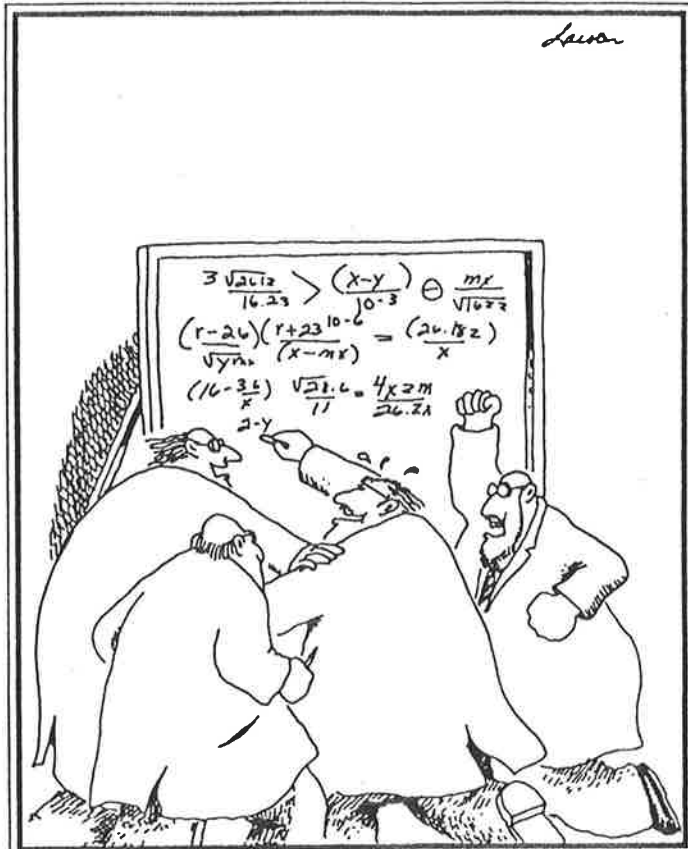
The process of numerical integration tended to obscure the constant offset error 'c₂', but it was insignificant compared to the 'c₁t' term, and no attempt was made to remove it. Also, the integration error $\frac{1}{2}et^2$ in the double integrated $s(t)$ record was expected to be significant, appearing as a distinctive 'parabolic' shape in all records. However, this did not occur, suggesting that the measuring error ('e') was well below that expected from the considerations given below. It became evident from inspection of the signal output and subsequent DaDisp™ analyses that acceleration magnitudes approaching the resolution of the instrument were measured reliably.

5.5.3. ACCELEROMETER INSTRUMENTATION

One "KISTLER 305A" accelerometer was chosen from the Department's stocks. Their quoted performance features such as ± 50 g range, 0 to 500 Hz frequency response and damping response of 0.6, were well above the requirements of this study. With a sensitivity rating of 100mV/g, it was connected to a servo-amplifier with this (minimum) signal gain.

Resolution was 500 μ g (0.0005 g), corresponding to $100 \times 0.0005 = 0.05$ mV at the above gain. As such, it was important to use a recording range for the MacLab data logger appropriate to this value: the chosen 10 mV/division range possessed a resolution of 1/4096 times its full scale range of ± 100 mV = 50 microV = 0.05 mV also. A narrower range (and higher resolution) could not be achieved due to the significant and erratic electrical noise caused by the operating machinery in the building, itself in an industrial area. DC signal shifts were also experienced after the opening of the two full-height sliding loading doors on the Western wall of the building. The measuring range had to be sufficiently wide to allow for these shifts and still 'capture' data. (see also 5.1.4.).

The results from this exercise are presented in Section 7.3. & 4 Inspection of the output signals for the accelerometer (low pass filtered at 11.5Hz) indicated that the observed resolution had been better than the 500 μ g quoted by the manufacturer. Furthermore, as detailed in Section 7.3., the "baseline corrected" values obtained for lateral frame sway at the 'knee' (Δ_{knee}) compared favorably with the form of those measured for *rotation* of the 'knee' joint. This considerably increased the confidence in both measurement techniques, since there could have been no *independent* check on their reliability to measure their respective structural phenomena.



"Go for it, Sidney! You've got it! You've got it! Good hands! Don't choke!"

Frame Response Predictions

6. PREDICTION of RAFTER STRAINS and FRAME DEFORMATIONS due to WIND LOAD

Theoretical predictions for the forces and deformations in the instrumented portal frame were required at two stages of the study:

Stage 1. During the selection and design of components of the instrumentation system detailed in Chapter 5, it was essential to estimate the expected magnitude for all the structural responses that were to be measured. Appropriate instruments could then be chosen from a knowledge of their resolutions and maximum ranges, and data logging equipment set to appropriate ranges.

Stage 2. The data recorded on-site by the instrument system was compared with the amplitudes predicted from theory. The procedure outlined below is a recreation of the accepted design procedure for determining the design forces and deformations of this structure type.

Analyses for both of these stages were made by applying design Code wind loadings to a structural model, assuming 2D portal frame action. This assumption meant that frame forces and deformations were over-estimated, since the stiffening effect on the entire structure of the external cladding and two 'rigid' end bays was not modelled. A more detailed, three dimensional structural model was proposed to theoretically investigate the effect of including these features. This would have more closely modelled the "true" behaviour of the joint as a component of the building as a whole, rather than as a feature of a single 2D frame. However, since adequate conclusions were reached using the two dimensional "upper bound" estimates, this time consuming task was not undertaken.

Wind loads only were considered, since only 'dynamic' effects were relevant in this study, and the instrumentation system had been specifically designed to eradicate the more 'static' effects of dead and thermal loads and creep (see 5.1.4. & 5.2.5.).

The Stage 2 predictions represented a refinement of the Stage 1 values, made possible by reference to the laboratory tests on half scale Yttrup Joints (Lee, 1993). The principal adjustment to the structural model was the value of spring constant K_0 used to represent the rotational behaviour of the complex joint region in the "idealized" frame (see Section 6.1.3.). The $K_0 = 20E9$ value used in Stage 1 was extrapolated from analyses of tests on *similar* joint types reported in the literature (see 6.2.1.), whereas the $3E9$ value used in Stage 2 was derived directly from the tests by Lee (see 6.2.2.), thus free of computational assumptions. By employing the "actual" K_0 , the Stage 2 structural model made more accurate deformation predictions. These were later used during comparison with the on-site measurements (Chapter 8.1.). Values for K_0 were seen to have a negligible effect on the predicted frame forces, but a significant effect on frame deformation estimates. Note that $K_0 = \text{infinity}$ would simulate a fully "rigid" joint experiencing no angle change.

- Structure Analyzed: "Signature Joinery" premises (formerly "Kent Town Gate Centre" until early 1992), Dundee Street, Wingfield (Adelaide), SA, 5013. Constructed 1989. Designed by P.J.Yttrup & Associates, 112B Mount Pleasant Road, Belmont, Vic, 3126.
- Loading Model: AS1170.2-1989 "Minimum Design Loads on Structures (known as the SAA Loading Code) Part 2: Wind Loads", Section 3. 'Detailed Procedure: Static Analysis', and Appendix E.
- Computer Analysis Package: IMAGES 3-D™ Version 2.0. A general structural analysis package, also containing modal analysis facility.
- Design Code: AS1720.1-1988 "Timber Structures (known as SAA Timber Structures Code) Part 1: Design Methods".

6.1. STRUCTURAL MODEL FEATURES

6.1.1. Material and Section Properties of Members:

1. Rafter and Column: IPL "Hyspan" LVL (laminated veneer lumber).
 Column 800 x 63 mm, Rafter tapered from 400 (ridge) to 800 (knee) x 63 mm.
 Young's Modulus (E) 13,200 MPa, Density (ρ) 620kg/m³. Shear Modulus (G) of 878 MPa
 (taken from AS1720) is artificially achieved by setting Poisson's Ratio (ν) to 6.517 in the
 IMAGES-3D™ model; derived from $\nu = \frac{E}{2G} - 1 = \frac{13,200}{2 \times 878} - 1 = 6.517$.
2. Plywood Gusset Plates: 'Knee' 2 No. (1 each side) 19-32-7 (F17), ex 2400 x 1200 sheet,
 'Ridge' 2 No. 17-25-7 (F14), ex 1800 x 900 sheet.
 Young's Modulus (E): for F14 ply 'ridge' plate is 12,000 MPa, for F17 ply 'knee' plate is
 14,000 MPa.....(AS1720 Table 5.1.)

6.1.2. ELEMENT MODELLING

Twenty elements were used in total. Each of the column and tapered rafter members were represented by four and six "beam" type elements respectively, with section properties taken at the segment mid-length. The gusset plate connection overlapped the upper three wall (column) and 'first' roof (rafter) beam segments. Modular ratio theory was used to transform plywood components to equivalent LVL areas. As an approximation, the full plywood cross-section was used to determine section properties. Figure 6.1. below represents the view looking South, with a 'Northerly' global Z direction.

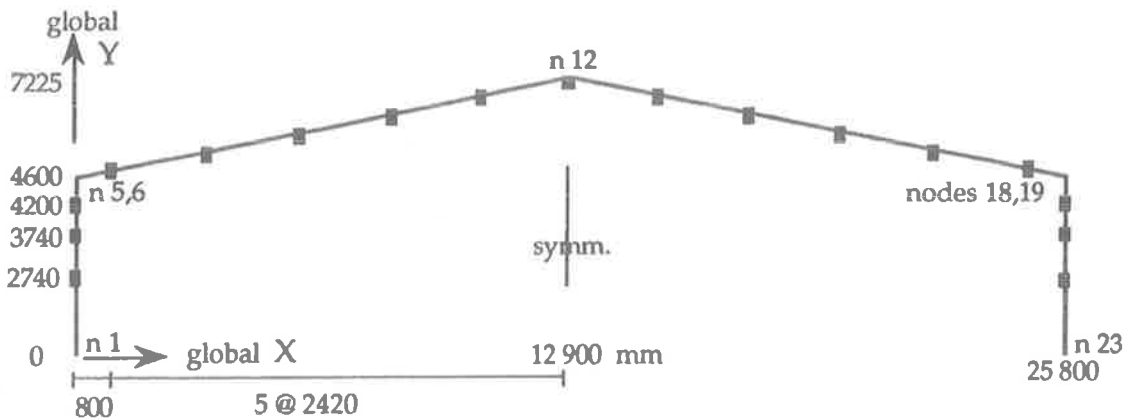


Figure 6.1.a. Geometry of idealized 2D frame - nodes.

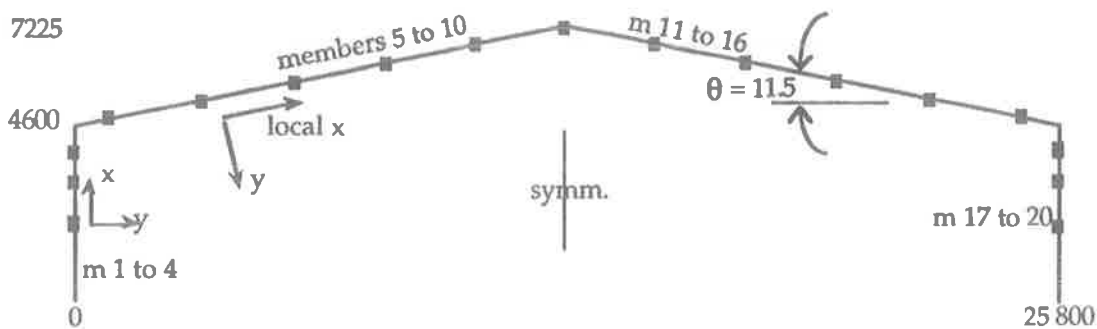


Figure 6.1.b. Geometry of idealized 2D frame - members.

6.1.3. 'KNEE' JOINT MODELLING

Being the primary focus of this study, the 'knee' joint was modelled as a linear *rotational spring* between two coincident nodes at the ends of the rafter and column members (nodes 5 & 6 and 18 & 19), of stiffness K_{θ} . The spring was assumed to be 'linear' because of the linear moment-rotation relationships reported by both Batchelar (1984) and Batchelar-Cavanagh (1984), for bending moments up to at least twice the (static) design value for joints similar to the 'Yttrup Joint'. Their quoted load-displacement traces equated to rotational stiffness values of 3.0E9 and 13.5E9 Nmm/radian respectively, and extrapolating from these values gave a (Stage 1) estimate of $K_{\theta} = 20E9$ for the 'Yttrup Joint' (see 6.2.1.). The $K_{\theta} = 3E9$ value for Stage 2 is derived in Section 6.2.2. below.

For the sake of uniformity, in all the theoretical computations, those portions of each frame 'leg' which formed the connection with the plywood gusset plate were assumed to perform rigidly. To achieve this, the rafter and column 'elements' immediately incident to the 'node' point had a rigid portion defined of 400mm length (being the half depth). This meant that the bending, axial and shear deformations of these beam lengths were set to zero and that slips in the moment resisting nail 'rings' were assumed to contribute only to the *rotation* of the joint.

6.2. DERIVATION of the ROTATIONAL SPRING CONSTANT K_{θ} .

Prior to the availability of results from the laboratory tests (late 1992), the estimate for the rotational spring constant K_{θ} was based on the research conducted in New Zealand on very similar nailed timber joints. The emphasis of their tests was on (large amplitude) 'earthquake' type loading, and provided joint rotations of sufficient magnitude to permit the approximate analysis described below. Although the frame geometry, section properties and P- Δ results for these tests were known, an error of ± 20 to 30% was associated with the value for the elastic modulus of the main timber members.

Batchelar (1984) and Batchelar-Cavanagh (1984) both tested two-member 'V-frames' possessing nailed, plywood gusset plate joints very similar to the Yttrup Joint. Their reported "ram load-deflection" traces referred to the total deflection at the base of one of the two members, in the direction of the applied ram load. Since the frames were statically determinate, it was possible to derive the moment-rotation relationships for the joints from consideration of the ram forces and component deflections. Knowing the timber material and section properties, estimates were made for the deflections due to the bending, shear and axial forces in each member. Then, by subtracting these from the quoted 'total' deflection, the component due to rotation of the joint was obtained for a given ram load:

$$\begin{aligned}\Delta_{\theta} &= \Delta_{\text{tot}} - (\Delta_{\text{b}} + \Delta_{\text{s}} + \Delta_{\text{ax}}) \\ &= \Delta_{\text{tot}} - \Delta_{\text{b,s,ax}}\end{aligned}$$

The example computations for the Batchelar-Cavanagh (1984) "Specimen II.1" 'V-frame' are given overleaf.

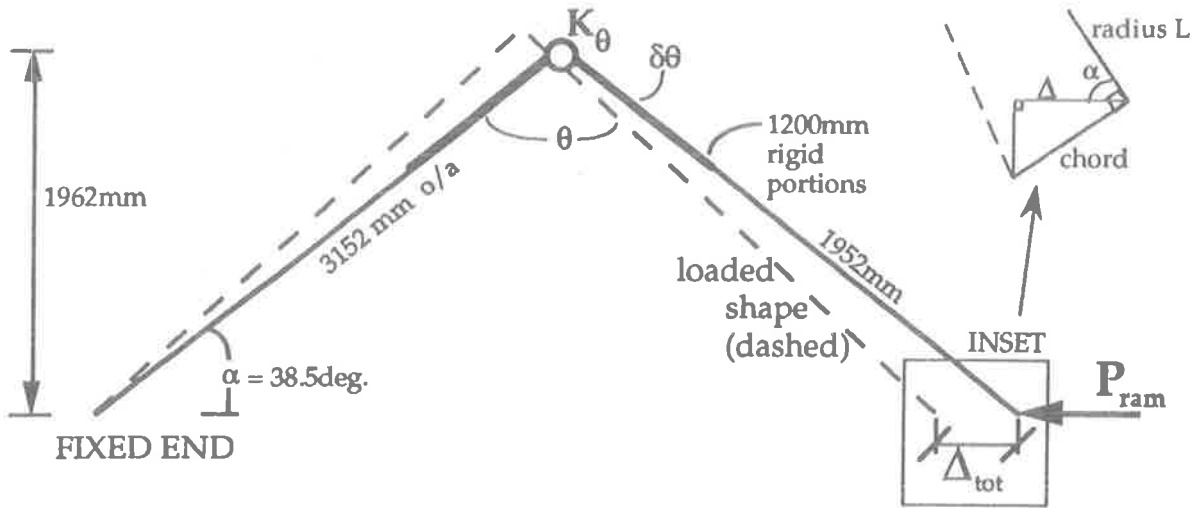


Figure 6.2. "V-frame" test setup, giving Batchelar-Cavanagh (1984) example dimensions.

For the purposes of this exercise, only the member length clear of the gusset plate was used, viz. $3152 - 1200 = 1952\text{mm}$. Deformations were also caused within the joint area by nail slips and gusset plate bending. It was assumed that all these deformations could be accounted for by a rigid body rotation of the two members, seen at the (ram) measuring site as Δ_θ , the (ram) "deflection due to rotation". This was modelled by representing the portions of the members joined by the gusset plate as "rigid", connected by a rotational spring of stiffness K_θ at the node point.

Components of the ram load P_{ram} were computed for the local x and y directions (axial P_x and shear P_y , respectively) using the initial angle between the horizontal line of ram load and the member axis of $\alpha = 38.5^\circ$: $P_x = P_{\text{ram}} \cos \alpha$ and $P_y = P_{\text{ram}} \sin \alpha$.

The parent timber size was $570 \times 115\text{mm}$ LVL, assumed to have the following material properties: Young's Modulus (E) = $11,000\text{ MPa}$, bending strength $F_b \approx 11\text{ MPa}$, and shear modulus (G) (from AS1720) as 730 MPa . Unfortunately, for both the New Zealand testing programmes, Young's Modulus of the LVL specimens was not measured, but other NZ testing on the same species and grade indicates "moduli ranging from 8 to 14 GPa".¹ As a convenient value, $E = 11 \pm 3\text{ GPa}$ was assumed. A value of 9 GPa is quoted in the New Zealand Timber Design Code NZ3603:1990 for "dry, No. 1 framing grade glue laminated timber".

From the geometry of the frame in Figure 6.2., the change in the angle enclosed by the two legs ($\delta\theta$) was related to the (known) total ram displacement (Δ_{tot}). Although one leg end was fixed and all movement recorded at the other, in the case of a symmetrical test the node point would remain equi-distant between these two ends during loading. Therefore, total ram deformations (Δ_{tot}) and change in enclosed angle θ may be attributed to the legs equally. By considering each leg as rotating about the 'node' point, the arc length 'scribed' by the end of each leg (of unchanged length ' L ') was $\frac{1}{2} \delta\theta L$. It was assumed that the length of the 'chord' between the initial and final positions of the leg end was equal to this arc length, and that this chord was perpendicular to the *initial* 'radius'. Thus, the displacement of each leg end $\frac{1}{2} \Delta_{\text{tot}} = \text{chord} \times \sin \alpha$. Therefore, $\frac{1}{2} \Delta_{\text{tot}} = \frac{1}{2} \delta\theta L \times \sin \alpha$, giving the simple expression for the change in the joint enclosed angle:

$$\delta\theta = \frac{\Delta_\theta}{L \sin \alpha}$$

¹ personal communication with Dr Richard Hunt, Timber Engineering Research Fellow, University of Auckland. In the Hunt-Bryant (1988,89) papers, Dr Hunt referenced and summarized the results of Batchelar (1984) and Batchelar-Cavanagh (1984), all of which were conducted at the University of Auckland.

Movements of each leg end due to the three elastic member displacements may be transformed into *the direction of the ram* as follows (Δ in mm, P_{ram} in kN):

Bending:

$$\Delta_b = \Delta_{b,y} \sin\alpha = \left(\frac{P_y L^3}{3 E I_z} \right) \sin\alpha = \frac{1952^3}{3 \times 11000 \times 1.7748E9} P_{ram} (\sin 38.5^\circ)^2 = 0.0492 P_{ram}$$

Shear:

$$\Delta_s = \Delta_{s,y} \sin\alpha = \left(\frac{6 P_y L}{5 A G} \right) \sin\alpha = \frac{6 \times 1952}{5 \times 65550 \times 730} P_{ram} (\sin 38.5^\circ)^2 = 0.019 P_{ram}$$

Axial:

$$\Delta_{ax} = \Delta_{ax,x} \cos\alpha = \left(\frac{P_x L}{A E} \right) \cos\alpha = \frac{1952}{65550 \times 11000} P_{ram} (\cos 38.5^\circ)^2 = 0.00166 P_{ram}$$

Thus, the total elastic deflection in the member at its base was $\Delta_{b,s,ax} = 0.0699 P_{ram}$. A total deflection of 34mm was quoted by Cavanagh for the extreme case of a ram load of 80kN. At this load, the above equates to $\Delta_{b,s,ax} = 5.59$ mm. Due to symmetry, this is equally present in both (identical) members, so the rotation component is $\Delta_\theta = 34 - 2(5.59) = 22.82$ mm. Over a radius R of 3152mm, the change in enclosed angle is:

$$\delta\theta = \frac{\text{arc}}{R} = \frac{\Delta_\theta}{\sin\alpha L} \approx \frac{22.82}{\sin 38.5^\circ \times 3152} = 0.01163^\circ = 0.6664 \text{ degrees.}$$

$$\text{Thus } K_\theta = \frac{M}{\theta} = \frac{80E3 \times 1962}{0.01163^\circ} = 13.49E9 \text{ Nmm/radian.}$$

This calculation confirmed the IMAGES-3D™ analysis of the same problem, which gave a K_θ of 13.5E9 Nmm/radian. A similar exercise for the "Specimen 6" described by Batchelar (1984) yielded a K_θ of 3.0E9 Nmm/radian. LVL members of 360 x 90 mm Radiata Pine were connected by 18mm ply gusset plates at an enclosed angle of 102.5°.

6.2.1. EXTRAPOLATION to YTRUP JOINT

The two values derived from the New Zealand tests above were then extrapolated to obtain a reliable estimate for the rotational joint stiffness K_θ of the Yttrup Joint. Various geometrical parameters were chosen, as detailed below. Refer to Figure 6.3.

However, this procedure was only approximate, due to the complexity of the joint geometries. For example, both the NZ researchers installed a gap between the connected rafter and column members. The Yttrup Joint, without such a gap, could be expected to be slightly stiffer as a result. The joints constructed by Batchelar-Cavanagh featured a 'mitre' type joint between the two members, in contrast to the 'bearing' arrangement of Batchelar and Yttrup. Also, the results quoted by Batchelar relate to his "Specimen 6", a joint stiffened by a thin steel 'reinforcing' strap on the 'outside' edge, especially effective during the closing mode when the strap would have been in tension. Because of these differences, two approaches were considered for extrapolation of the NZ results to the Yttrup Joint. The first approach assumed that the main proportioning influence on joint stiffness was the sizes of the component members, while the second also considered the nail group geometry.

(a) by Member Sizes

Three "member size" extrapolations were used, two based on section moduli (Z) and the third on moment of inertia about the major bending axis (I_{zz}). Section moduli were taken through the LVL parent member and also, the plywood "critical section", which is

defined as the plane representing the discontinuity between the joined members: where the plywood acts alone to transmit the joint bending moment between the two nail groups. An elastic frame analysis using a K_θ value derived from a 'Z' extrapolation could be expected to provide reliable results concerning frame bending moments ('M'), since M and Z are both strength terms. On the other hand, a similar exercise using 'I' might be used to predict frame deflections, so the third method of extrapolation was based on the moment of inertia of the LVL members.

	Z (LVL) [E6 mm ³]	Z (ply crit. secn.) [E6 mm ³]	I _{zz} (LVL) [E9 mm ³]	K _θ [Nmm/radian]
Batchelar	1.944 (.289)	1.574 (.166)	0.350 (.13)	3.0E9
Batchelar-Cavanagh	6.227 (.927)	8.64 (.91)	1.775 (.66)	13.5E9
Yttrup	6.72 (1.0)	9.5 (1.0)	2.688 (1.0)	< 14.7 or 20.2E9 >

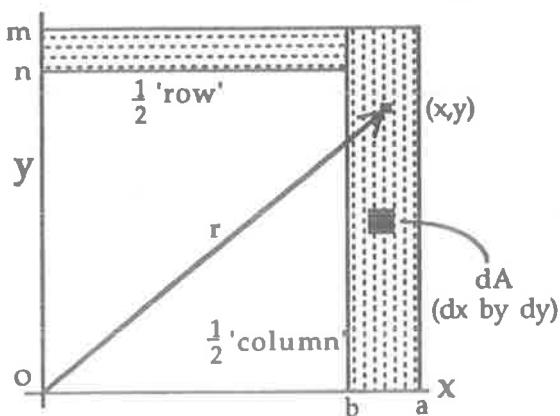
As seen in Figure 6.3., both the Section Modulus ('Z') extrapolations conveniently gave (approximately) the same rotational stiffness of $K_\theta = 14.7E9$ Nmm/rad. The Moment of Inertia ('I_{zz}') comparison yielded a K_θ value of $20.02E9$ Nmm/rad.

(b) by Nail Group Geometry

As will be seen in Appendix D, many geometrical functions exist to account for the effect of nail group size, shape and nail pattern on joint strength. The Mitchell Method (1979) was used here, as it has been shown by Walford (1988) to be an accurate approximation over a wide range of nail group aspect ratios (1 to 3), and is valid for the pre-ultimate loading range within which the linear elastic IMAGES-3D™ model was used.

The geometric term employed was "I", a polar moment of inertia: $I = \frac{s(A + B)^3}{6}$ where 's' is the transverse thickness of the ring and 'A' and 'B' are its centreline dimensions.

The two nail groups in both the Yttrup and Batchelar (1984) "Specimen 6" joints were easily evaluated, being slightly skewed 'rectangular hollow sections' in elevation. The nail groups of the Batchelar-Cavanagh (1984) 'mitred' joint however, did not conform to the constant thickness 'ring' form required by the above equation. Its polar moment of inertia was instead evaluated from first principles, using a double integral over the 'ring' area. [These 'exact' equations (seen below) were checked using the Batchelar Joint, and compared very well with the 'approximate' Mitchell 'I' above]. In addition, some assumptions regarding nail spacings and end/side distances were made for the Batchelar-Cavanagh joint (consistent with other NZ joints) since they were not included in the journal article.



$$I_o = \int r^2 dA = \int_n^m \int_b^a (x^2 + y^2) dx dy$$

comprises:

$$1/2 I_{col} = \left(\frac{a - b}{3}\right) m^3 + \left(\frac{a^3 - b^3}{3}\right) m$$

$$1/2 I_{row} = \left(\frac{m - n}{3}\right) b^3 + \left(\frac{m^3 - n^3}{3}\right) b$$

For the upper 'row', bounded by two parallel lines $y=mx+c$ (c_1 or c_2):

$$I_o = \int_b^a \int_{c_2}^{c_1} (m^2 + 1)x^2 + 2mcx + c^2 dx dc$$

	I (UPPER) [E9 mm ⁴]	I (LOWER) [E9 mm ⁴]	K _θ [Nmm/radian]
Batchelar	4.557 (.053)	5.504 (.057)	3.0E9
Batchelar-Cavanagh	36.583 (.422)	36.583 (.377)	13.5E9
Yttrup	86.714 (1.0)	97.156 (1.0)	<30 - 34E9>

Extrapolation of these results yielded a prediction of K_θ for the Yttrup Joint of ~~30E9~~ Nmm/radian using the 'upper' nail groups, and ~~34E9~~ with the 'lower'.

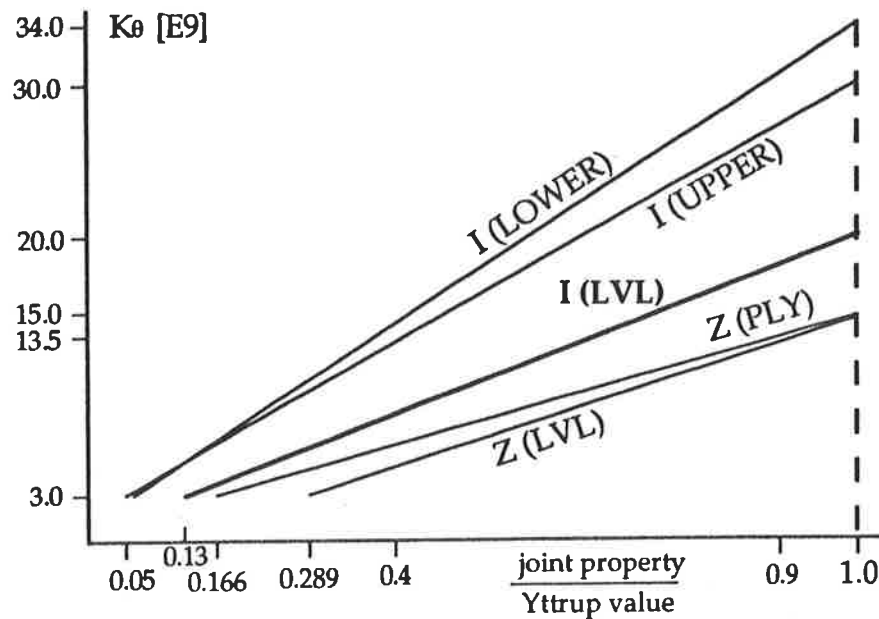


Figure 6.3. Extrapolations for Yttrup Joint K_θ based on five geometric indicators.

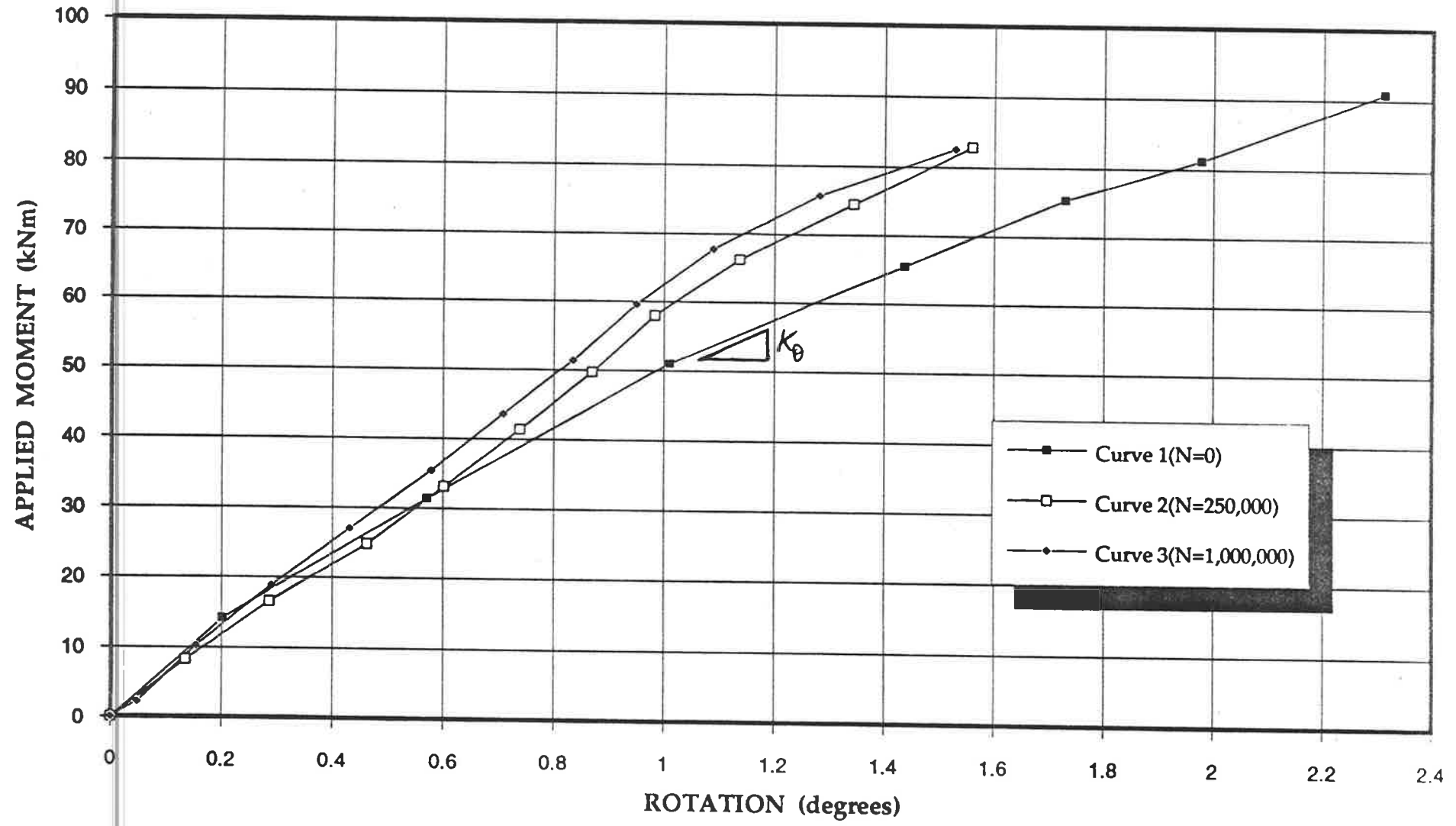
As mentioned above, the differences between the three joints prevented a convincing argument in favour of either of the five methods used above. For example, aside from all of the geometrical differences, each joint possessed a unique "over-design" factor, which distorted the extrapolations further. Furthermore, there is no valid basis for assuming that the extrapolations above should be 'linear'.

However, the process did achieve the objective of providing an "order of magnitude" estimate for the rotational stiffness of the Yttrup Joint, for input into an elastic frame analysis. Of importance here is the fact that the frame bending moments did not change significantly over the practical range of K_θ values derived. Since the primary use of the model was to predict frame *deformations* (and in turn to design instrumentation), the "I (LVL)" extrapolation value of 20E9 Nmm/radian was adopted.

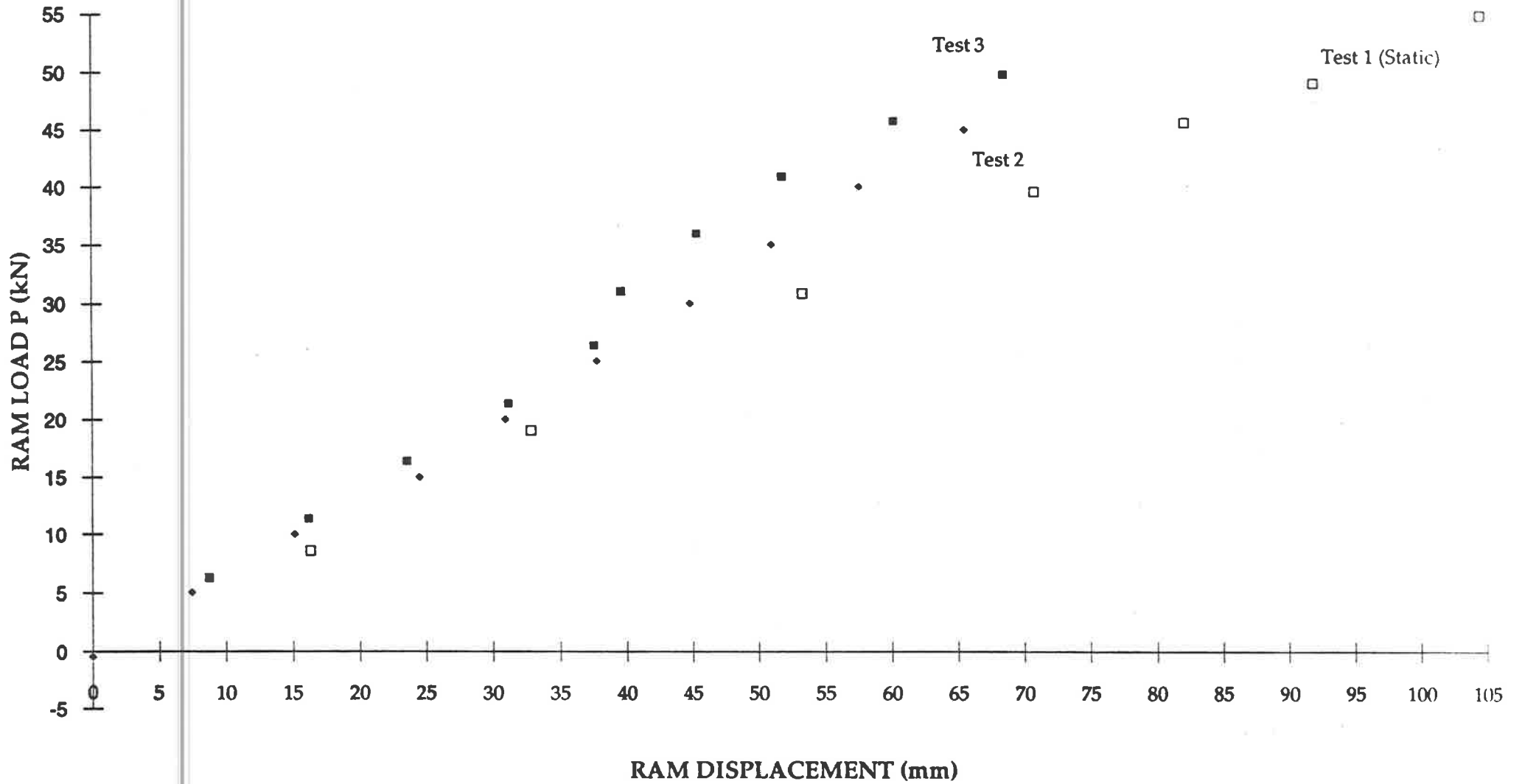
6.2.2. K_θ from the LABORATORY TESTS

An identical analysis to the one described above was conducted on the half scale Yttrup Joint test specimens, and yielded a K_θ of 7.3E9 Nmm/radian. An IMAGES-3D™ check of this calculation gave a smaller value of about 5E9, due to the asymmetry of the 'V-frame'. These were based on the P-Δ results of Tests 2 and 3 (see Section 5.2.3.), shown overleaf. However, since additional M-θ data was available for these tests (see graph overleaf from Griffith et al, 1992), the K_θ derived from these was used in the refined predictions of frame forces and deformations (Stage 2). The linear moment-curvature test results gave an *initial* joint stiffness of about 3E9 Nmm/radian (see also 6.6.).

MOMENT - ROTATION PLOTS for LABORATORY TESTS 1 to 3.



RAM LOAD vs DISPLACEMENT (Tests 1 to 3)



===== I M A G E S 3 D =====
 = Copyright (c) 1984 Celestial Software Inc. =
 =====

half scale model Yttrup Joint (Lee, 1993) laboratory test specimen
 $K_{\theta} = 5 E9 \text{ Nmm/radian}$

rigid end offsets: BEAM NO. 1: node 1 = 350 mm, node 2 = 930 mm
 BEAM NO. 2: node 3 = 410 mm, node 4 = 450 mm

LOAD CASE 1
 TENSILE RAM LOAD $P = 45 \text{ kN}$ TO NODE 1 (-ve X direction)

DISPLACEMENTS (mm, radians)

Node	Translations			/	Rotations		
	X	Y	Z		X	Y	Z
1	-.6300E+02	.0000E+00	.0000E+00	/	.0000E+00	.0000E+00	-.2299E-01
2	-.3153E+02	-.4000E+02	.0000E+00	/	.0000E+00	.0000E+00	-.1125E-01
3	-.3153E+02	-.4000E+02	.0000E+00	/	.0000E+00	.0000E+00	.5486E-02
4	.0000E+00	.0000E+00	.0000E+00	/	.0000E+00	.0000E+00	.2422E-01 (fixed in global X and Y dirn)

BEAM LOADS AND/OR STRESSES (N, Nmm)

GLoads	Node	Fx	Fy	Fz	Mx	My	Mz
BEAM NO. 1 (node 1 to 2)							
GLoads	1	-.4500E+05	.5346E-02	.0000E+00	.0000E+00	.0000E+00	.3354E-07
GLoads	2	.4500E+05	-.5346E-02	.0000E+00	.0000E+00	.0000E+00	.8035E+08
BEAM NO. 2 (node 3 to 4)							
GLoads	3	-.4500E+05	-.5370E-02	.0000E+00	.0000E+00	.0000E+00	-.8035E+08
GLoads	4	.4500E+05	.5370E-02	.0000E+00	.0000E+00	.0000E+00	-.8469E-08

SPRING LOADS between nodes 2 and 3 (N, Nmm)

Type	Node	Fx	Fy	Fz	Mx	My	Mz
SPRG NO. 1 (axial)							
GLoads	2	-.4500E+05	.0000E+00	.0000E+00	.0000E+00	.0000E+00	.0000E+00
GLoads	3	.4500E+05	.0000E+00	.0000E+00	.0000E+00	.0000E+00	.0000E+00
SPRG NO. 2 (shear)							
GLoads	2	.0000E+00	.7105E-02	.0000E+00	.0000E+00	.0000E+00	.0000E+00
GLoads	3	.0000E+00	-.7105E-02	.0000E+00	.0000E+00	.0000E+00	.0000E+00
SPRG NO. 3 (moment) $K = K_{\theta}$							
GLoads	2	.0000E+00	.0000E+00	.0000E+00	.0000E+00	.0000E+00	-.8035E+08
GLoads	3	.0000E+00	.0000E+00	.0000E+00	.0000E+00	.0000E+00	.8035E+08

REACTIONS (N, Nmm)

Node	Fx	Fy	Fz	Mx	My	Mz
1	.0000E+00	.5346E-02	.0000E+00	.0000E+00	.0000E+00	.0000E+00
4	.4500E+05	.5370E-02	.0000E+00	.0000E+00	.0000E+00	.0000E+00

6.3. WIND LOADING

Being orientated on a N-S axis and bisymmetrical in plan, the structure is analyzed for wind loads in the two orthogonal directions of North and West. Easterly winds in Adelaide are not generally critical, nor as frequent, and the consequent decision to site the single anemometer adjacent the Westerly wall of the building meant that only loadings from the Westerly 180° sector from North around to South could be measured reliably. For computational convenience, the General Case to be considered was: transverse tributary width of frame (b) of one metre, gust dynamic wind pressure (q_z) of one kiloPascal (1 kPa) and internal pressure set to zero (sealed building). Thereafter, the results from the IMAGES-3D™ analysis were scaled appropriately.

Hence from AS1170.2 Clause 3.4.2. (with K_p , K_1 and $q_z = 1.0$), $p_e = K_a C_{p,e}$ is the external pressure applied to each of the four individual faces of the building: W, U, D and L. (Building dimensions: $h_e = 5\text{m}$ (eaves height), $h_t = 7.425\text{m}$ (ridge height), b (N-W) = 40m, d (E-W) = 26.6m).

Case 1. $\theta = 0^\circ$ (Wind from West)

face	K_a	$C_{p,e}$	p_e
W.	1.0 for 25m ² walls	+0.7 (using $q_z = q_h$, $h < 25.0\text{ m}$)	Table 3.4.3.1(A) +0.7
U.	0.857 for 68m ² walls	-0.64 ($h/d = 5/26.6 = 0.188$, $\alpha = 11.5^\circ$)	Table 3.4.3.2(B) -0.549
D.	as for U.	-0.36 ($\alpha = 11.5^\circ$)	Table 3.4.3.2(C) -0.309
L.	as for W.	-0.3 ($10^\circ < \alpha < 15^\circ$)	Table 3.4.3.1(B) -0.3

Case 2. $\theta = 90^\circ$ (Wind from N or S)

face	K_a	$C_{p,e}$	p_e
S.	1.0 for 25m ² walls	-0.4 $h/d = 7.425/40 = 0.186$ as 2h (15.25m) approximately coincides with the '4th frame' (15m from leading (S) edge).	Table 3.4.3.1(C) -0.4
U., D.	0.857 for 68m ² walls	-0.4 similar to 'S' above	Table 3.4.3.2(A) -0.343

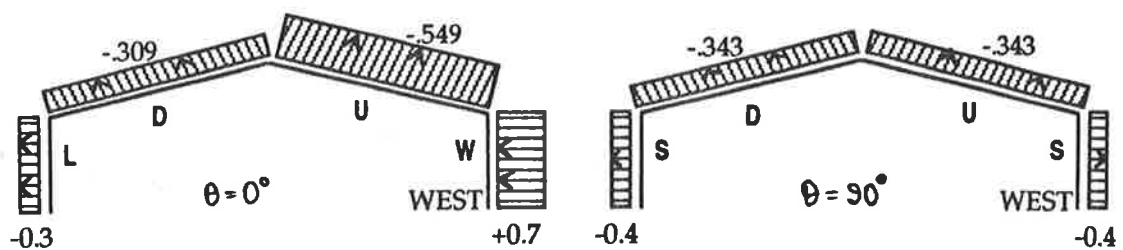


Figure 6.4. Showing W, U, D, L, S and $p_e = K_a \times C_{p,e}$ for each face for $\theta = 0$ and 90 deg. directions.

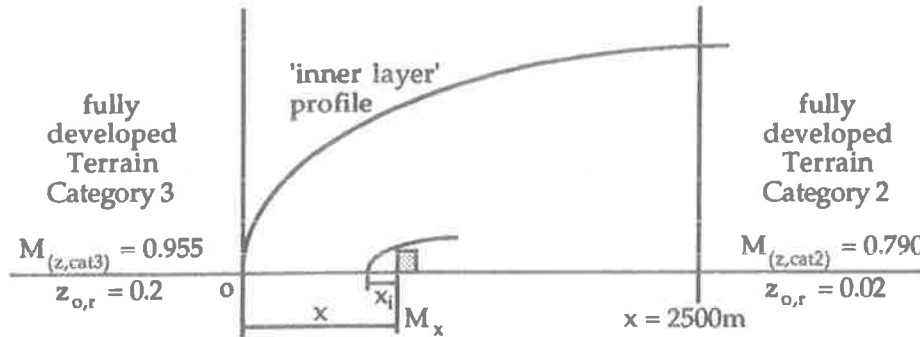
6.3.1. DERIVATION of DYNAMIC WIND PRESSURE (q_z)

By Clause 3.3, the gust dynamic wind pressure $q_z = 0.6 V_z^2 \times 10^{-3}$, where V_z is the design gust wind speed at height z . V_z is defined in Clause 3.2.2 as a function of the basic wind speed (V) and various multipliers, of which only the terrain category term $M_{(z,cat)}$ is relevant to this structure. The shielding multiplier M_s was not significant for the sparsely developed areas surrounding the site to the West and North. Also, it was decided to not use a topographic multiplier M_t to account for the effect of the Wingfield Waste Disposal Depot, representing a smooth sloped, trapezoidal hill to the WNW.

The design gust wind speed V_z may be computed for either of the limit states (ultimate strength or serviceability) or permissible ('working') case. (The permissible stress gust wind speed V_p is obtained by dividing V_u by $\sqrt{1.5}$). To predict the maximum response of the structure, the ultimate limit state gust wind speed (V_u) was used.

V_u is 50m/s for both the orthogonal directions of S and W (Table 3.2.3), but since $M_{(z,cat)}$ was assumed as fully developed Terrain Category 2 for North, this direction governed over the South, which was assumed as standard residential TC3. [$V_z = V \times M_{(z,cat)} = 48 \times 0.955 = 45.84\text{m/s}$ for N cf. $50 \times 0.79 = 39.5$ for S (both at height 7.5m)].

Westerly terrain category is *partially* developed TC2, with the South West 45° sector being fully developed TC2. The method described in AS1170.2 Clause 3.6.3 was used to derive an interpolated value for the Westerly direction terrain category multiplier, as follows:



The horizontal distance required for the 'inner layer' to develop to the average height of the upwind roof slope ('U') of 6.21m is:

$$x_i = z_{o,r} \left(\frac{h}{0.3 \times z_{o,r}} \right)^{1.5} = 0.2 \left(\frac{6.21}{0.3 \times 0.2} \right)^{1.5} = 210\text{m}.$$

The terrain category multiplier $M_{(z,cat)}$ is a function of the distance downstream of the commencement of the TC2 region ('x'). A distance $x = 900\text{m}$ was assumed for the site, thus the site $M_{(z,cat)}$ was derived from Eq. 3.2.6 (3):

$$M_x = M_o + \frac{x - x_i}{2500} (M_{(z,cat)} - M_o) = 0.955 + \frac{900 - 210}{2500} (0.79 - 0.955) = 0.909.$$

Thus for Westerly ($\theta = 0^\circ$) loading, $V_z = V \times M_{(z,cat)} = 50 \times 0.909 = 45.45 \text{ m/s}$, hence q_z became 1.239 kPa. From above, for Northerly ($\theta = 90^\circ$) loading, $V_z = 45.84 \text{ m/s}$ and $q_z = 1.261 \text{ kPa}$. Thus, the use of a 1 kPa loading in the IMAGES-3D™ model was convenient.

6.3.2. ANALYSIS at LOWER WIND LOADING LEVELS:

The probability that V_u will occur at least once in a single year is about 1 in 975, and for the 'permissible stress' design wind speed, 1 in 20. The ambient, 'serviceability level' wind loading levels measured in this investigation act on the structure virtually continually. For these wind loading levels less severe than the 'ultimate level' "worst case scenarios", the procedure following was used to analyze the structure. This method involved assuming a (shorter) return period for the chosen wind loading level in order to derive an intermediate value of q_z . Thereafter, for any known value of q_z , the output of the IMAGES-3D™ analysis for the General Case loading was simply scaled. In this way, the structural responses measured at a known wind speed could be compared to the theoretical predictions of the structural model. This is done in Chapter 8.

The ultimate limit state gust wind speed (V_u) and serviceability state wind speed (V_s) have a 5% probability of being exceeded in a 50 year and 1 year period respectively. Consequently, they have return periods of 975 and 20 years respectively. The general

formula giving basic wind speed V for an arbitrary return period R is $V = 29.2 + 3.0 \log_e R$ in Region A. (Formula E3.2.2(1)). A range of wind speeds were calculated using this method, and are given below in Table 6.A. For example, the basic wind speed for a return period of 100 years is 43m/s, compared to 50 and 38m/s for the 1000 and 20 year events of V_u and V_s respectively. Thus V_p is 40.7m/s in Region A, equivalent to a 1 in 46 year event. These are maxima for a particular location, and for Adelaide, apply to the dominant two (Westerly and South Westerly) 45° direction sectors. Thus, a basic wind speed may be obtained for any assumed return period for these two sectors.

R (years)	1	20	46.2	100	975	(1000)
V (m/s)	29.2	38	40.7	43	49.8	49.9
V (km/hr)	105.1	136.8	146.5	154.8	179.3	179.6
	-	V_s	V_p	-	V_u	(V_u)

Table 6.A. Basic Wind Speed (V) for selected return periods R for the W and SW sectors in Adelaide.

6.4. STRUCTURAL MODEL ESTIMATES

The output from the IMAGES-3D™ structural model for the two AS1170.2 wind load cases of West ($\theta = 0^\circ$) and North ($\theta = 90^\circ$) is given in Appendix F. They represent the General Case of a 1 kPa dynamic wind pressure and tributary frame width of one metre. In Table 6.B. overleaf, these figures are converted for the five metre frame width of the Wingfield building and the "ultimate" wind event pressures of 1.239 and 1.261 kPa for the Westerly and Northerly wind directions respectively. The notations used in this table for the frame bending moments and lateral deflections are shown in Figure 6.5. overleaf.

To use this information during the selection and design of the instrumentation system (Stage 1), a more realistic wind event was chosen. Table 6.A. above indicates that a good estimate for the annual maximum event is 105 km/hr. On this basis, an arbitrary value of 100 km/hr was used for V_z , giving a dynamic wind pressure of 0.463 kPa. This value was used to scale the model output to estimate expected values for the structural responses measured in the study: frame bending moment (M), joint rotation (θ) and the lateral frame displacement at the 'knee' (Δ_{knee}). As seen in Table 6.B., the Westerly wind event can be expected to provide the maximum response in all three for a given wind pressure, with all three maxima occurring in the instrumented Western 'knee' joint (subscript 'R'). The maximum Western joint responses were:

$$M_R = 23.90 \text{ kNm} \times 5 \text{ m} \times 0.463 \text{ kPa} = 55.3 \text{ kNm}$$

$$\Delta_{knee} = -5.0 \text{ mm} \times 5 \times 0.463 = -11.6 \text{ mm (to East)}$$

$$\theta_R = 1.195 \times 5 \times 0.463 = 2.766 \text{ milliradians ('opening')}$$

		$K_{\theta} = 20 \text{ E9 Nmm/radian}$	
		WEST WIND	NORTH WIND
joint 'node' bending moment	M_L	$17.85 \times 5 \times 1.239 = 110.6 \text{ kNm}$	$15.35 \times 5 \times 1.261 = 96.8 \text{ kNm}$
	M_C	$-2.5 \text{ " " " } = -15.5$	$-1.28 \text{ " " " } = -8.1$
	M_R	$23.90 \text{ " " " } = 148.1 \text{ kNm}$	$15.35 \text{ " " " } = 96.8$
lateral frame displacement	Δ_L	$3.72 \text{ " " " } = 23.0 \text{ mm}$	$3.0 \text{ " " " } = 4.8 \text{ mm}$
	Δ_R	$-5.0 \text{ " " " } = -31.0 \text{ mm}$	as above
rotation at joint centroid	θ_L	$(0.497 + 0.395 = 0.892) \times 5 \times 1.239 = 5.528 \text{ milliradians}$	$(0.460 + 0.307 = 0.767) \times 5 \times 1.261 = 4.844 \text{ milliradians}$
	θ_R	$(0.443 + 0.752 = 1.195) \times 5 \times 1.239 = 7.403 \text{ milliradians}$	as above due to symmetry

* subscripts 'R' and 'L' represent 'right' (West) and 'left' (East) sides of the frame respectively

Table 6.B. IMAGES-3D™ structural model results for "ultimate" wind events (West and North)

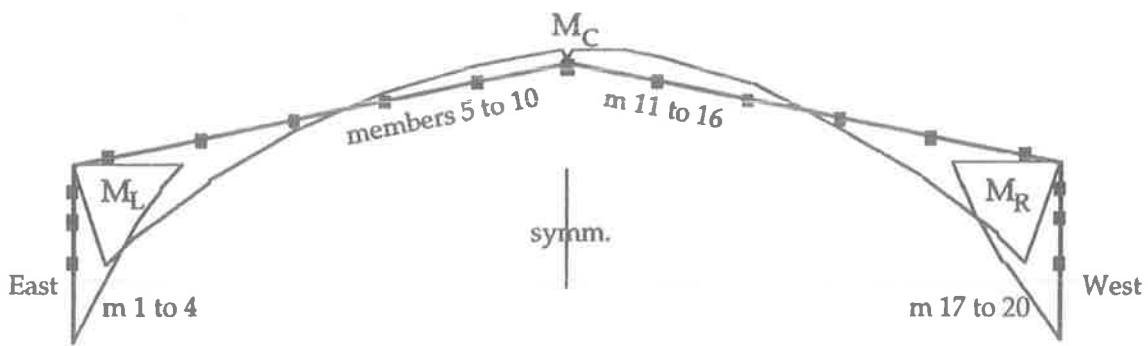


Figure 6.5a. Notation used for frame bending moments (West case shown)

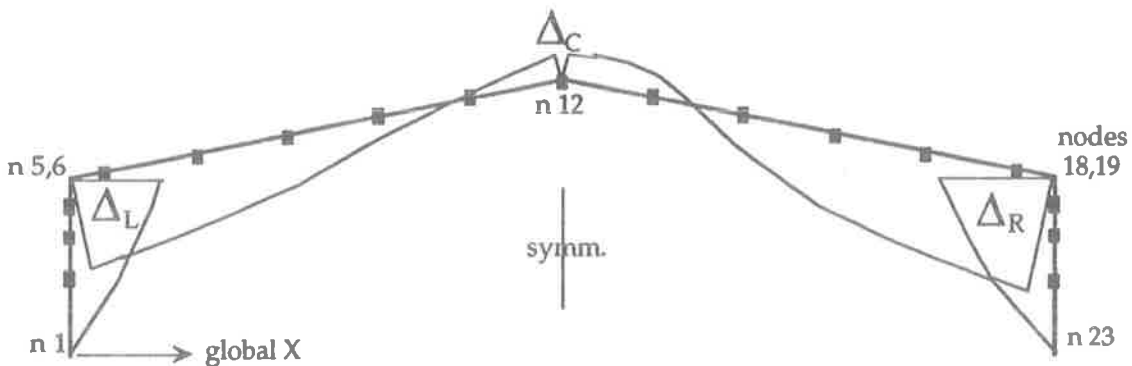


Figure 6.5b. Notation used for frame lateral deflections (West case shown)

A minor adjustment was now made to the estimate for frame moment (M_R), since it was the *rafter* bending moment (M) that was actually measured in this study. As described in Section 5.2., it was possible to obtain an estimate for the bending moment at the 'node' point of the frame by extrapolation of the value measured at the neighbouring "rafter" site, and vice versa. This involved the assumption of a relationship between them, typically given by the bending moment diagram for the frame. Since the two sites were only 864 mm apart, the error introduced by using the moment diagram produced by the assumed AS1170.2 wind loading model, as seen in Figure 6.5a, would have been minimal. Therefore, the expected frame moment M_R was adjusted as follows:

$$\begin{aligned}
 M_{\text{rafter site}} &= M_{\text{node 18,19}} + (M_{\text{node 17}} - M_{\text{node 18,19}}) \times \frac{864}{800/\cos\theta} \\
 &= 23.90 + (19.54 - 23.90) \times \frac{864}{816.4} \\
 &= 19.29 \text{ kNm/m/kPa}
 \end{aligned}$$

For the chosen 100 km/hr event, $M = M_{\text{rafter site}} = 19.29 \times 5 \text{ m} \times 0.463 \text{ kPa} = 44.65 \text{ kNm}$

Note that this simple extrapolation was far more efficient than converting all measured rafter moments back to 'node' moments, for comparison with the model estimate.

Also, the model estimate for the rafter moment (*and* deformations Δ and θ) could have been easily evaluated at *any* wind speed, since the expression above was proportional to the dynamic wind pressure q_z . Because $q_z = 0.6 V_z^2 \times 10^{-3}$, for any speed wind event V_z :

$$M = \frac{V_z^2}{100^2} \times 44.65 \text{ kNm}$$

6.5. ESTIMATES for RAFTER STRAINS

An estimate was then made for the maximum expected bending strains at the rafter site. A linear strain distribution was assumed (5.2.3.). Section modulus (Z) for the 764 x 63 mm cross-section was 6.129 E6 mm³, with Young's Modulus (E) for the LVL 13,200 MPa. Thus for the 100 km/hr wind event, bending strain (ϵ_b) became:

$$\text{maximum expected response } \epsilon_b = \frac{M}{Z E} = \frac{44.65 \text{ E6}}{6.129 \text{ E6 } 13,200} = 552 \text{ microstrain } (\mu\epsilon)$$

Since 100 km/hr was considered to be the "peak event", recording ranges were set within the Chart/8 data logging package so that these strain amplitudes would be 'captured'. Also, since a compressive strain of this amplitude would be experienced in the plastic strip attached to the rafter extreme fibres (see 5.2.4.), a 'pre-strain' of 600 $\mu\epsilon$ was applied to prevent buckling of the strip. Using the "velocity squared" relationship introduced above for the more common 60 km/hr event gave:

$$\text{typical expected response } \epsilon_b = \frac{60^2}{100^2} \times 552 = 199 \text{ microstrain } (\mu\epsilon)$$

As a guide to the required sensitivity of the strain measuring system, a wind speed change (or "flutter") of 10 km/hr was considered:

$$\text{smallest expected response } \epsilon_b = \frac{10^2}{100^2} \times 552 = 5.5 \text{ microstrain } (\mu\epsilon)$$

Converting these expected strains to voltage output using the calibration test derived equation of " $\mu\epsilon \approx 4 \text{ mV}$ " gave voltage outputs of 138, 50 and 1.4 milliVolts respectively. Due to the expected measuring system errors and signal noise, a "best case" resolution of about 1 to 2 mV (4 to 8 $\mu\epsilon$) was anticipated, equivalent to a 6 to 12 km/hr event.

However, as discussed in the opening remarks to this chapter, the simplifying assumption of 2D portal frame action meant that all of the above would have represented over-estimates of the true situation. To allow for this, for example, a "significance level" of 20 $\mu\epsilon$ (or about 5 mV) was set for the strain gauges. This equated to a Westerly wind event of 19 km/hr by the calculations above. So, even if the frame response had been over-estimated by a factor of two say, rafter strains were still significant at 17 km/hr.

(i.e. if ϵ_b actually = $\frac{V_z^2}{100^2} \cdot \frac{552}{2}$, then resolution of 2mV \equiv 8 $\mu\epsilon$ \equiv 17 km/hr)

6.6. ESTIMATES BASED ON REFINED K_{θ}

From the analysis detailed in Section 6.2.2., the “refined” value for $K = 3E9$ was obtained, and input into the structural model. The revised estimates portal frame responses are shown in the Table below, for the two “ultimate” level wind events.

		$K_{\theta} = 3E9$ Nmm/radian	
		WEST WIND	NORTH WIND
joint 'node' bending moment	M_L	$15.47 \times 5 \times 1.239 = 95.8$ kNm	$13.60 \times 5 \times 1.261 = 85.8$ kNm
	M_C	-6.23 “ “ = -38.6	-4.02 “ “ = -25.3
	M_R	21.52 “ “ = 133.3 kNm	13.60 “ “ = 85.8
lateral frame displacement	Δ_L	6.40 “ “ = 39.6 mm	7.868 “ “ = 49.6 mm
	Δ_R	-15.57 “ “ = -96.5 mm	as above
rotation at joint centroid	θ_L	$(4.121 + 1.036 = 5.157) \times 5 \times 1.239 = 31.948$ milliradians	$(3.124 + 1.409 = 4.533) \times 5 \times 1.261 = 28.581$ milliradians
	θ_R	$(2.799 + 4.376 = 7.175) \times 5 \times 1.239 = 44.449$ milliradians	as above due to symmetry

* subscripts 'R' and 'L' represent 'right' (West) and 'left' (East) sides of the frame respectively

Table 6.C. Revised structural model results for “ultimate” wind events (West and North)

A comparison between Tables 6.B. and 6.C. shows the effect on frame responses of the rotational spring stiffness K_{θ} used to model the behaviour of the 'knee' joint. A reduction in this stiffness saw an expected redistribution of frame moments from the 'knee' to the 'ridge' joints, and greatly increased deformations Δ and θ . This change from 20 to 3E9 Nmm/radian saw lateral sway (Δ_{knee}) increase by 2 to 3 times, while rotations (θ) increased by about 6 times, approximately equal to the rotational stiffness reduction.

To compare the *rafter site* bending moments predicted by the two models for the 100 km/hr storm (in the governing Westerly direction), the analysis described in Section 6.4. gave:

$$\begin{aligned} M_{\text{rafter site}} &= M_{\text{node 18,19}} + (M_{\text{node 17}} - M_{\text{node 18,19}}) \times \frac{864}{800/\cos\theta} \\ &= 21.52 + (17.08 - 21.52) \times \frac{864}{816.4} \\ &= 16.82 \text{ kNm/m/kPa} \end{aligned}$$

which converts to $M = M_{\text{rafter site}} = 16.82 \times 5 \text{ m} \times 0.463 \text{ kPa} = 38.94 \text{ kNm}$ ($V_z = 100 \text{ km/hr}$)

A similar conversion of the frame deformation predictions for the 100 km/hr event gave:

$$\begin{aligned} \Delta_R &= -15.57 \times 5 \times 0.463 = -36.0 \text{ mm (to East)} \\ \theta_R &= 7.175 \times 5 \times 0.463 = 16.61 \text{ milliradians ('opening')} \end{aligned}$$

These estimates may be evaluated for any wind event of gust speed V_z (km/hr) using the expression (shown for 'rafter site' moment):

$$M_v = \frac{V_z^2}{100^2} \times 38.94 \text{ kNm}$$

or several departments to be examined. ... had set up his own tourism consultancy, to sit on committees for TSA. ... 37 consultancies. ... PAGE 13: Libs repeat tort claim

'Mini tornado' hits State

By JENNY TURNER

Insurance companies are preparing for a flood of claims after a "mini tornado" ripped through South Australia yesterday, causing widespread damage.

Early estimates put the damage bill at more than \$500,000, but it is expected to climb much higher as more insurance claims are lodged.

Violent squalls, rain and hail swept north through Adelaide from about 6.30am, bringing down trees and powerlines and damaging property.

The storm, described by emergency workers as one of the worst for several years, appeared to strike in four main areas.

The worst hit was Salisbury where nine Housing Trust homes in two streets had parts of their roofs ripped off. Homes at Hackham, Tea Tree Gully and along the coast were also damaged by winds gusting up to 130km/h.

Falling trees caused blackouts, crashed through houses and smashed cars while many carports and garages were damaged.

The conditions also forced the cancellation of several major sporting events in SA, including the Corporate Cup running competition and horse racing at Strathalbyn.

Roads in the Far North which were cut by floodwaters left entrants in the Sydney to Darwin Australian Safari rally stranded in the Simpson Desert, near Mt Dare on the SA-Northern Territory border.

The Bureau of Meteorology said the storm was caused by a "deep intense low front" which formed south of Kangaroo Island on Tuesday night.

It moved rapidly across the State — taking only seven minutes to cross the city.

The first report of trouble was at 6.40am at Adelaide Airport when winds of 91km/h were recorded. By 6.47am, the front had reached Edinburgh Air Base at speeds of 102km/h.

By late afternoon, Edinburgh had reported winds up to 119km/h, with 130km/h winds at Cape Borda and Neptune Island. The highest overnight rainfall was recorded at Mt Compass at 39mm and Port Lincoln at 19mm. Adelaide had 4mm during the day.

City workers faced near-freezing conditions throughout the day, having to contend with driving rain and hail.

Part of a veranda ceiling crashed 15m to the ground when the high winds struck Shell House at a corner of Grenfell St and Hindmarsh Square just after 3pm.

Several sheets of gyprock and steel girders landed on the footpath. No one was injured.

SES officer said "quite a cause many". He said seven continued to be on a cutting a one-street-wide of damage," Mr Lane. "It's one of the worst ever had out here, in a city."



Results and Discussion

will

TV's

Mel-

und-

deral

grees

March

It is

ipped

ir and

places

olitics,

ature-

itback

ars to

rtinary

quired

1995

Open

d.

ie trial

Febru-

stralia,

n Vic-

d and

Durbin

terring

s will

earn-

Friday.

atched

often

Aus-

d TV

than

exam

cent

opus

lder

ont,

are

to

nth

east
pors
mar;
critic
Pr
imp
-3
like
men
been
avoid
when
victim
-1
e'

7.1. JOINT MOMENT - ROTATION

In this study, the structural response of primary interest was the moment-rotation relationship for the 'full scale' joint. Rafter strains and joint rotations were measured for ambient, 'serviceability level' wind events, as described in Chapter 5. The validity and limitations of the instrumentation techniques adopted for both of these were detailed in Sections 5.2.7. and 5.3.3. respectively. Moments were obtained from the two remotely measured extreme fibre strains by assuming a linear strain distribution across the section, as justified in 5.2.3. All joint rotation data was provided directly by the calibrated RVDT output, as detailed in Section 5.3.

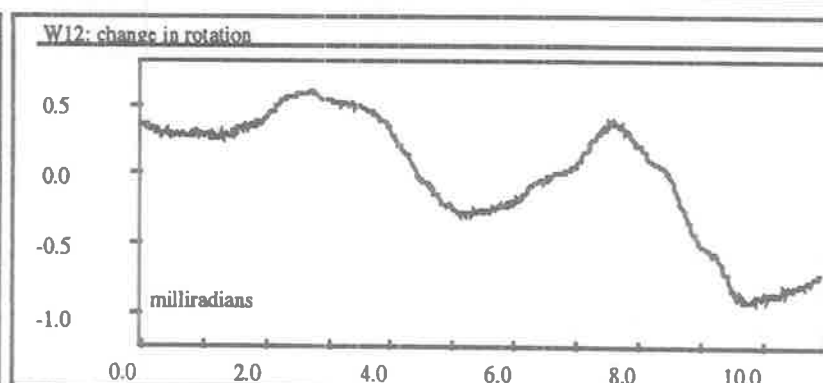
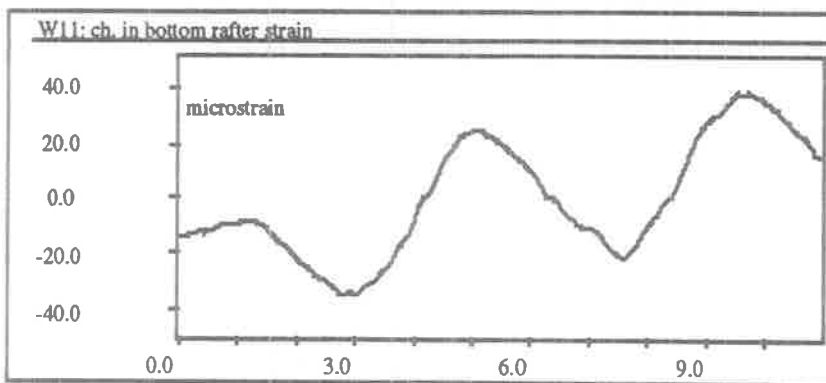
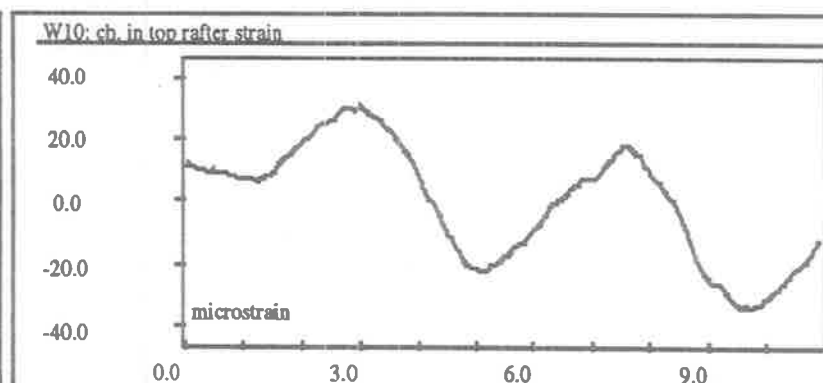
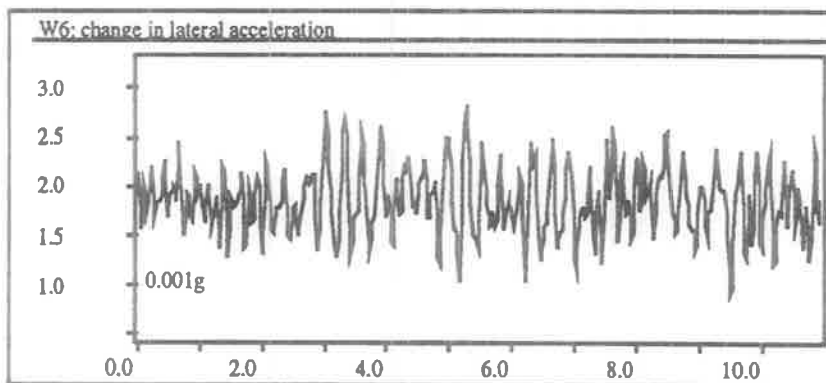
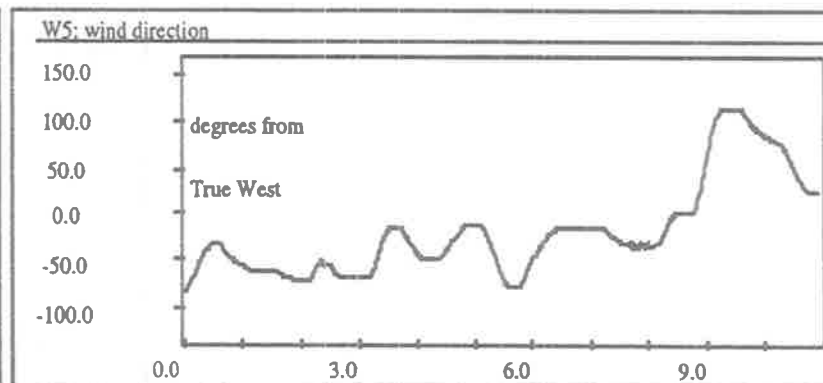
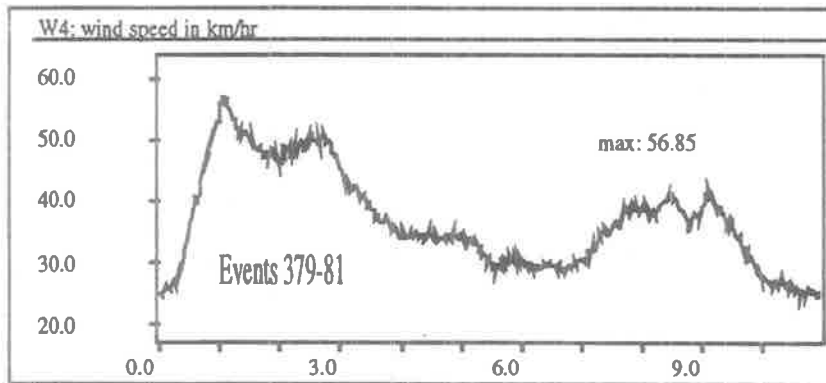
In Chapter 8, results are compared to (a) theoretical predictions, based on conventional structural analysis of portal frame structures (Chapter 6), and (b) the results from the laboratory tests on half scale model joints (Lee, 1993). For convenience, all references to "moment" in this investigation concern the bending moment at the rafter section approximately 170 millimetres from the (vertical) edge of the gusset plate, as seen in Figure 5.2.1. Conventionally, the moment at the joint 'node' point is used, since it is here that the theoretical maximum occurs. However, all data in both the laboratory and field studies was taken at the "same" rafter site, and as discussed in Section 6.4., conversion between the 'node' and this neighbouring position in the frame was possible. Therefore, the theoretical predictions were extrapolated across to the "rafter site", for comparison with the 'test' and 'field' derived bending moments. A typical 'conversion' value between the 'node' and 'rafter' moments was 1.23, based on the portal frame bending moment diagram derived from the AS1170.2 wind loading model ("rigid" knee joint, Westerly wind).

From the continuously output signals for rafter strain and joint rotation, only "excerpts" of a nominal ten second length (called wind "events") were collected, captured using the data logger's internal 'trigger', based on a nominal wind velocity. Data files containing hundreds of these response records were obtained for each windy day during June to September 1992. From these files, only the most 'significant' events were used for subsequent analysis.

During data analysis, the "significance" level was based on the magnitude of the *change in strain* in the bottom rafter fibre, not wind speed. The adopted level of $\pm 20\mu\epsilon$ (microstrain) was derived from a consideration of the measuring error and the theoretical predictions explained in Section 6.5. For the most severe days of August 10th and 12th 1992, when wind speeds of up to 80 km/hr were measured, this "cut-off" level was raised to 30 microstrain, in order to reduce the volume of data requiring analysis. The $\pm 20\mu\epsilon$ "cut-off" level corresponded to a change in bending moment (δM) of approximately ± 1.5 kNm in the rafter (hence ≈ 1.9 kNm at the 'node'). This data selection procedure is shown overleaf.

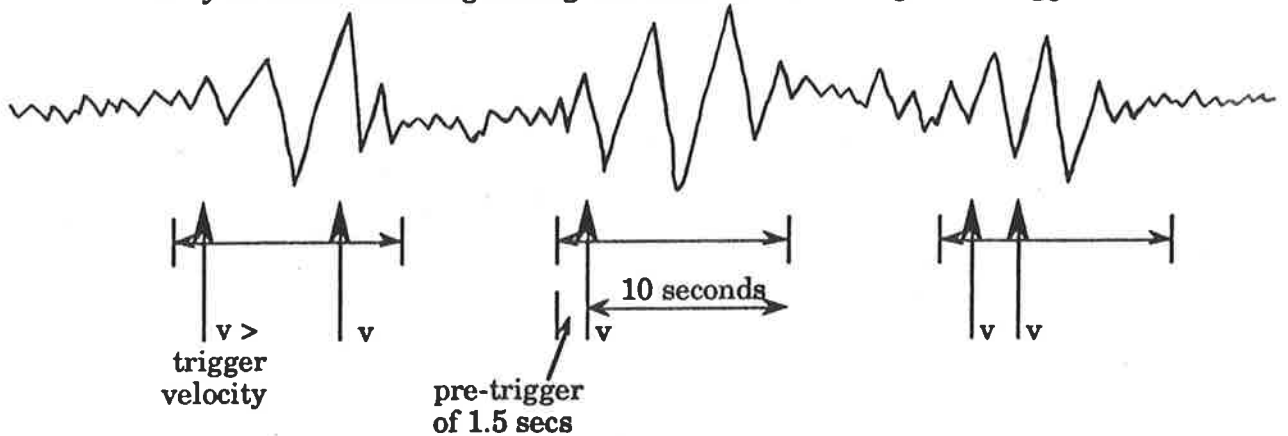
396 wind events¹ were selected on this basis, ten of which were included despite narrowly failing the "20 $\mu\epsilon$ cut". These have been listed chronologically in the Excel 3.0TM spreadsheet output of Appendix G., showing the calculation of rafter bending moment (M), joint rotation (θ) and their quotient, secant stiffness (K). Hereafter, each event is referred to numerically, with the event number corresponding to its position in the spreadsheet. An additional eleven records were included (for a total of 407) as examples where unexpectedly high rotation output was noticed, despite low (or by definition 'insignificant') strains. In particular, six events were seen to return stiffnesses as low as $1E9$ Nmm/radian or less, in comparison with the average secant stiffness of $4E9$ Nmm/radian (see Figure 7.1.1.), and featured in Stevens et al (1993).

¹ The term wind "event" is used interchangeably to refer to "ten second data collection period" and "example of significant response". Inspection of the spreadsheet reveals that some 93 of these "10 second periods" contain multiple examples of significant (5mV or greater) strain response.

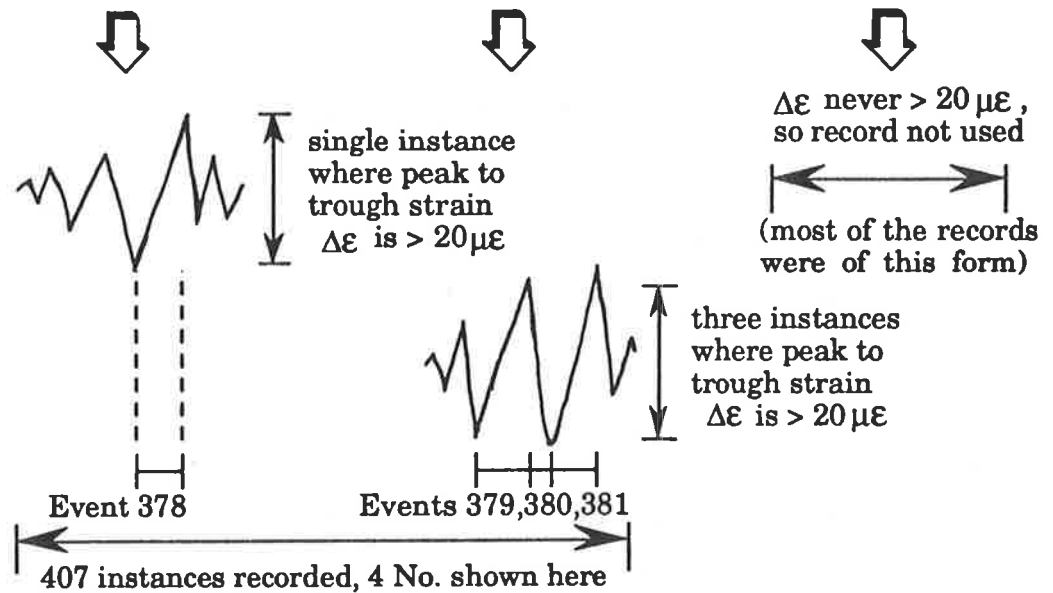


DATA SELECTION PROCEDURE:

Data is monitored continuously by the instrumentation system, but only that data occurring during the more severe wind gusts is logged:



A series of 11.5 second duration data "windows" are captured, in which a velocity exceeding that of the trigger velocity has been experienced. All instrument output is logged for 10 seconds after the *initial* gust.



poor correlation in either shape or phase between strain and rotation records, so not used in graphical analyses such as "stiffness" (7.2.): see 7.1.1.

excellent shape and phase correlation between strain and rotation records, so used in all analyses

All these 407 "events" were recorded in the spreadsheet given in Appendix G. An example of the raw data record (after unit conversion), giving the six channels of data, is shown at left (for Events 379-381, 28 September 1992). (Two more channels were added later, for the "glued strain gauges" described in Section 5.2.7.). The data shown at left was processed using the "peak analysis" method to give the moment-rotation curve shown in Figure 7.1.9.

∂ Moment vs Δ rotation :407 wind events

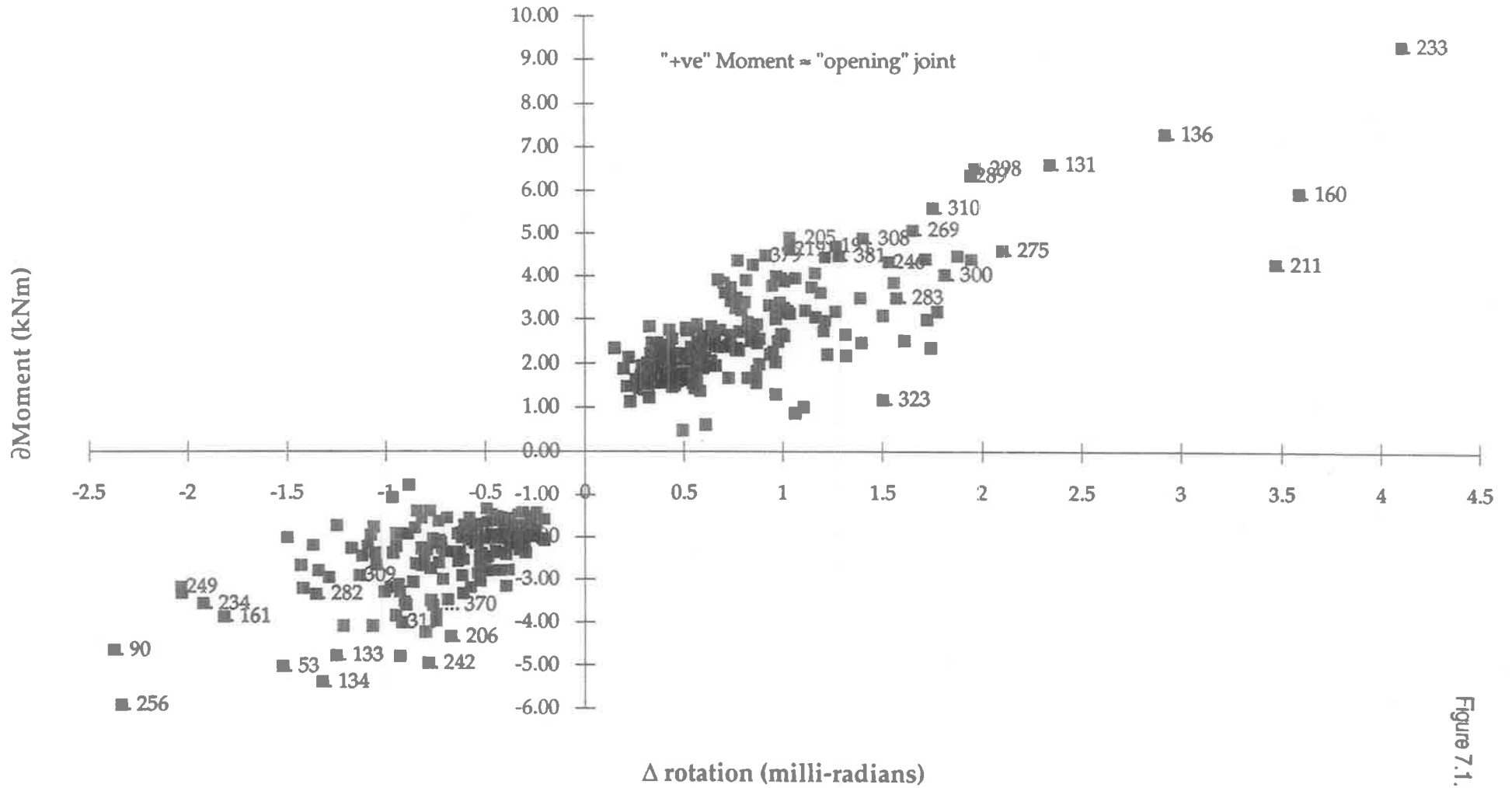


Figure 7.1.1.

Data was taken manually from the $\text{Chart/8}^{\text{TM}}$ datafile records using the “peak analysis” method for the three signals of top and bottom strain and rotation, where the *difference* between immediately adjacent peaks and troughs in output signals was recorded. Each individual “wind event” represented a single ‘rise’ or ‘fall’ in the fluctuating records of the structural responses. Therefore, as discussed in Section 5.1.4. and 5.2.5., the dynamic *changes* in the structural responses were measured. As such, the “zero point” in any analysis is effectively arbitrary, since the position of the changes relative to the datum “absolute zero” strain or rotation was not known. An example portion of the spreadsheet is shown overleaf, showing the calculations for the most significant events, which are discussed in more detail in the following text.

A strict correlation between the shape and phase of the concurrent strain and rotation signals was required by this method, but was not always seen. Moment-rotation plots could not be assembled reliably in these cases. However, when distinctive features were common to both the (slightly ‘out of phase’) strain and rotation records, it was considered reliable to concentrate only on the largest changes or steepest parts (most significant) of the signal records, despite an error in their phase correlation. This is considered further in Section 7.1.3.

Figure 7.1.1. is shown at left, showing the maximum recorded changes in moment and rotation (“ Δ Moment vs Δ rotation”) for all of the 407 ‘significant’ wind events. The largest events are labelled with their respective ‘event numbers’. A large congregation of data is seen at or above the ‘cut-off’ moments of ± 1.5 kNm. The eleven records mentioned earlier, where high rotation but low strain was noted, appear well below this distinct “bunch” of records. [Five of these in the “closing joint” quadrant appear to form a straight line to the example shown of ‘Event 323’, all having a stiffness of slightly below $1000E6$ Nmm/radian]. The maximum recorded strain response occurred during ‘Event 233’, recorded at 2:10:02pm on August 12th, 1992. Rafter moment was seen to change by 9.28 kNm in the “opening” mode, and joint rotation by 4.11 milliradians, or 0.236 degrees. The greatest changes in the “closing” mode were -5.94 kNm and -2.33 milliradians (0.134 degrees) for the 2:10:57pm Event 256 of the same day.

Figure 7.1.1. shows the “envelope” effect, suggesting that the number of records (407) was sufficient to truly represent the behaviour of the joint for this range of responses of 1 to 10 kNm and 0.2 to 4 milliradians. This data corresponded to a range of incident wind speeds between 30 and 70 km/hr, over all Westerly directions from South around to North.

7.1.1. INDIVIDUAL EVENT $\Delta M - \Delta$ rotrn PLOTS

The form of Figure 7.1.1. (at left) suggests a non-linear moment-rotation behaviour at this (serviceability) level of loading. In order to confirm this, detailed M- θ plots were made for individual events, derived from their time-history records. The larger strain events were focused on to minimize the effects of measurement errors. Moment-rotation curves appear as ‘time-history’ plots since every data point was separated by a time interval of $1/40^{\text{th}} = 0.025$ seconds. Because of this, excellent correlation between the shape and phase of the strain and rotation output signals was required to produce reliable M- θ plots.

However, several of the largest strain events were found to have *unsuitable* strain to rotation phase correlations, and had to be excluded from these graphical considerations. One example was Event 256 (-2.333 millirads, -5.94kNm), the most significant of all the recorded “closing” mode events. Other quite large events were *less* suitable because their signals were affected by excessive noise (e.g. Events 190-1, 246-7) or electrical interference spikes (Events 175-6, 206-7, 275, 369-70), or simply where signal outputs went “off scale”, as was the case during the record of Events 131-3. Noise or spikes in the signals did not affect the “peak analyses”, since they were of only a very short duration. Their presence in the signal could have been removed using a low pass filter, to allow further analysis, but since a sufficient number of “clean” examples were available, this was not done. A discussion of some of the reasons for these examples of *unsuitable* correlation is to be found in Section 7.1.3.

1	A	B	C	D	E	F	G	H	I	J	K	L	M	N
2	EVENT No.	EVENT	Δ RVDT	Δ rotation	Δ top SG	Δ bot SG	Δ top SG	Δ bot SG	Δ top extm	Δ bot extm	Δ bend strn	Δ axial strn	ΔM = Δσ Z	stiffness
3			mV	millirad	mV	mV	μ	μ	fibre strain	fibre strain	μ	μ	kNm	kNm/rad
3	53	2:16:18	10.7	-1.5194	-14.4	17.1	59.89	-67.67	59.15	-66.93	-63.04	-3.89	-5.05	3.321
4	89	3:56:41	-12.3	1.7466	6.3	-8.4	-26.20	33.24	-25.86	32.89	29.37	3.52	2.35	1.346
5	90		16.7	-2.3714	-13.4	15.7	55.73	-62.13	55.04	-61.44	-58.24	-3.20	-4.66	1.966
6	134	12:58:55	9.3	-1.3206	-15.56	18.15	64.72	-71.83	63.92	-71.03	-67.47	-3.55	-5.40	4.090
7	136	12:59:53	-20.6	2.9252	22.14	-23.23	-92.08	91.93	-91.01	90.85	90.93	-0.08	7.28	2.489
8	160	1:16:01	-25.3	3.5926	18.09	-18.87	-75.24	74.68	-74.36	73.80	74.08	-0.28	5.93	1.651
9	181		12.8	-1.8176	-11.7	12.58	48.66	-49.78	48.09	-49.21	-48.65	-0.56	-3.89	2.143
10	175	1:18:14	-8.2	1.1644	11.25	-14.07	-46.79	55.68	-46.19	55.08	50.64	4.44	4.06	3.481
11	176		6.4	-0.9088	-9.9	12.18	41.18	-48.20	40.65	-47.68	-44.17	-3.51	-3.54	3.891
12	190	1:25:23	4.05	-0.5751	-9.04	10.99	37.60	-43.49	37.12	-43.02	-40.07	-2.95	-3.21	5.578
13	191		-8.95	1.2709	13.38	-15.91	-55.65	62.96	-54.96	62.27	58.61	3.66	4.69	3.692
14	204	1:52:50	6.7	-0.9514	-10.9	13.2	45.34	-52.24	44.76	-51.67	-48.22	-3.45	-3.86	4.057
15	205		-7.3	1.0366	14.1	-16.4	-58.64	64.90	-57.92	64.18	61.05	3.13	4.89	4.715
16	206		4.73	-0.6717	-12.3	14.8	51.16	-58.57	50.52	-57.93	-54.22	-3.71	-4.34	6.463
17	207		6.53	-0.9273	-13.5	16.5	56.15	-65.30	55.44	-64.59	-60.01	-4.57	-4.80	5.181
18	208		-7.23	1.0267	9.2	-10.6	-38.26	41.95	-37.80	41.48	39.64	1.84	3.17	3.091
19	211	1:54:52	-24.45	3.4719	11.8	-14.9	-49.08	58.97	-48.45	58.33	53.39	4.94	4.27	1.231
20	212		10	-1.42	-8.8	11.4	36.60	-45.11	36.12	-44.64	-40.38	-4.26	-3.23	2.276
21	213		14.3	-2.0306	-8.8	12.1	36.60	-47.88	36.11	-47.39	-41.75	-5.64	-3.34	1.646
22	218	1:57:45	3.48	-0.4942	-7.8	9.8	32.44	-38.78	32.03	-38.37	-35.20	-3.17	-2.82	5.702
23	219		-7.3	1.0366	13.2	-15.6	-54.90	61.74	-54.22	61.05	57.64	3.42	4.61	4.451
24	232	2:10:02	7.7	-1.0934	-6.2	7.8	25.79	-30.87	25.48	-30.54	-28.00	-2.54	-2.24	2.050
25	233		-28.95	4.1109	26.7	-31.2	-111.05	123.47	-109.68	122.10	115.89	6.21	9.28	2.257
26	234		13.55	-1.9241	-10.3	12.1	42.84	-47.88	42.31	-47.35	-44.83	-2.52	-3.59	1.865
27	235		5.28	-0.7498	-11.8	12.3	49.08	-48.68	48.51	-48.10	-48.31	0.20	-3.87	5.158
28	236		8.58	-1.2184	-12.6	13	52.41	-51.45	51.80	-50.84	-51.32	0.48	-4.11	3.372
29	241	2:10:14,25	-8.55	1.2141	12.6	-15.1	-52.41	59.78	-51.75	59.10	55.43	3.68	4.44	3.655
30	242	2:10:25	5.53	-0.7853	-14.1	16.9	58.64	-66.88	57.91	-66.15	-62.03	-4.12	-4.97	6.324
31	243		-1.55	0.2201	6	-7.3	-24.96	28.89	-24.64	28.57	26.61	1.97	2.13	0.678
32	244		-6.88	0.977	7.2	-8.3	-29.95	32.85	-29.58	32.48	31.03	1.45	2.48	2.543
33	245		5.95	-0.8449	-4	4.7	16.64	-18.60	16.43	-18.39	-17.41	-0.98	-1.39	1.650
34	246		-10.8	1.5336	11.8	-15.2	-49.08	60.15	-48.44	60.51	53.98	5.54	4.32	2.818
35	247		5.45	-0.7739	-10	11.9	41.59	-47.09	41.07	-46.57	-43.82	-2.75	-3.51	4.533
36	249	2:10:37	14.33	-2.0349	-8.7	11.3	36.19	-44.72	35.71	-44.25	-39.98	-4.27	-3.20	1.573
37	250		-7.3	1.0366	9	-10.5	-37.43	41.55	-36.97	41.09	39.03	2.06	3.12	3.014
38	251		-12.5	1.775	9	-10.8	-37.43	42.74	-36.96	42.27	39.62	2.65	3.17	1.787
39	252	2:10:57	-6.23	0.8847	7.4	-8.5	-30.78	33.64	-30.40	33.26	31.83	1.43	2.55	2.880
40	253		5.48	-0.7782	-8	9.2	33.27	-36.41	32.87	-36.00	-34.43	-1.57	-2.76	3.542
41	254		-5.75	0.8165	11.2	-13.1	-46.58	51.84	-46.01	51.27	48.64	2.63	3.89	4.769
42	255		4.55	-0.6461	-6.9	7.9	28.70	-31.26	28.35	-30.91	-29.63	-1.28	-2.37	3.671
43	256		16.43	-2.3331	-16.7	20.4	69.46	-80.73	68.58	-79.85	-74.22	-5.64	-5.94	2.547
44	257		-10.6	1.5052	8.6	-10.6	-35.77	41.95	-35.31	41.49	38.40	3.09	3.07	2.043
45	259	2:11:52	6.23	-0.8847	-2.2	2.6	9.15	-10.29	9.04	-10.18	-9.61	-0.57	-0.77	869
46	269	2:18:04	-11.65	1.6543	14.4	-17.2	-59.89	68.07	-59.14	67.32	63.23	4.09	5.06	3.060
47	270		-7	0.994	7.4	-9.2	-30.78	36.41	-30.39	36.02	33.20	2.82	2.66	2.674
48	274	2:20:27	-8.5	1.207	7.8	-9.2	-32.44	36.41	-32.04	36.01	34.02	1.98	2.72	2.257
49	275		-14.8	2.1016	12.5	-16.2	-51.99	64.11	-51.31	63.43	57.37	6.06	4.59	2.185
50	282	2:22:00	9.55	-1.3561	-9.4	11.6	39.10	-45.91	38.60	-45.41	-42.00	-3.40	-3.36	2.480
51	283		-11.08	1.5734	10.2	-11.5	-42.42	45.51	-41.91	45.00	43.45	1.54	3.48	2.211
52	284		-13.23	1.8787	12.9	-14.9	-53.65	58.97	-52.99	58.31	55.65	2.66	4.46	2.371
53	287	3:03:39	3	-0.426	-5.7	7	23.71	-27.70	23.41	-27.40	-25.40	-2.00	-2.03	4.774
54	288		-5.45	0.7739	12.6	-14.6	-52.41	57.78	-51.76	57.13	54.45	2.69	4.36	5.632
55	289		-13.7	1.9454	18.3	-21.2	-76.11	83.90	-75.18	82.96	79.07	3.89	6.33	3.254
56	290		2.7	-0.3834	-8.2	9.2	34.11	-36.41	33.69	-36.00	-34.84	-1.15	-2.79	7.276
57	296	5:15:27	-5.58	0.7924	9.2	-10.7	-38.26	42.34	-37.79	41.87	39.83	2.04	3.19	4.024
58	297		5.03	-0.7143	-8.6	10.2	35.77	-40.37	35.32	-39.92	-37.62	-2.30	-3.01	4.217
59	298		-13.85	1.9667	18.7	-21.8	-77.78	86.27	-76.82	85.31	81.06	4.25	6.49	3.300
60	300	5:26:26	-12.78	1.8148	11.1	-14	-46.17	55.40	-45.57	54.81	50.19	4.62	4.02	2.214
61	301		5.33	-0.7569	-6.7	6.9	27.87	-27.31	27.54	-26.98	-27.26	0.28	-2.19	2.884
62	302		7.9	-1.1218	-6.8	8.6	28.28	-34.03	27.92	-33.67	-30.79	-2.88	-2.47	2.198
63	307	6:34:58	7.45	-1.0579	-7.1	7.8	29.53	-30.87	29.18	-30.51	-29.85	-0.67	-2.39	2.259
64	308		-9.9	1.4058	14.1	-16.3	-58.64	64.51	-57.92	63.79	60.85	2.93	4.87	3.465
65	309	6:40:19	8	-1.136	-8.2	10.1	34.11	-39.97	33.67	-39.54	-36.60	-2.93	-2.93	2.580
66	310		-12.38	1.758	15.9	-19	-66.13	75.19	-65.30	74.36	69.83	4.53	5.59	3.180
67	311		6.35	-0.9017	-10.5	12.1	43.67	-47.88	43.14	-47.35	-45.24	-2.11	-3.82	4.017
68	314	6:48:59	-6.98	0.9912	11.2	-13.4	-46.58	53.03	-46.00	52.46	49.22	3.22	3.94	3.976
69	315		6.48	-0.9202	-11.5	13.6	47.83	-53.82	47.24	-53.23	-50.23	-2.99	-4.02	4.370
70	323	7:04:23	-10.6	1.5052	3.7	-3.6	-15.39	14.25	-15.22	14.07	14.64	-0.57	1.17	779
71	324		8.8	-1.2496	-4.8	6.3	19.13	-24.93	18.87	-24.67	-21.77	-2.90	-1.74	1.395
72	325		8.28	-1.1758	-6.9	7.3	28.70	-28.89	28.36	-28.55	-28.46	-0.10	-2.28	1.938
73	369	4:10:10	-6.83	0.9699	11.4	-13.5	-47.41	53.42	-46.82	52.83	49.83	3.01	3.99	4.113
74	370		5.38	-0.764	-10.01	12.6	41.63	-49.86	41.10	-49.33	-45.21	-4.11	-3.62	4.738
75	378	4:12:27	2.48	-0.3522	-5.69	6.71	23.67	-26.55	23.37	-26.26	-24.82	-1.44	-1.99	5.641
76	379		-6.45	0.9159	12.78	-15.12	-53.16	59.84	-52.49	59.17	55.93	3.94	4.47	4.880
77	380		4.85	-0.6887	-9.96	11.88	41.43	-47.01	40.91	-46.50	-43.70	-2.79	-3.50	5.080
78	381		-9.05	1.2851	12.65	-15.22	-52.61	60.23	-51.95	59.57	55.76	3.81	4.46	3.474

A total of 23 of the largest events having excellent strain-rotation correlation were chosen for further detailed analysis. This total included 12 "joint closing" mode and 11 "opening" mode events.

Graphs are seen overleaf in the following order:

- Fig. 7.1.2. "opening" mode quadrant *excerpt* of Figure 7.1.1., $\delta M-\Delta \text{rotn}$ "407 wind event" plot, labelled with the numbers for significant wind events
3. the 4 largest "opening" mode events' individual moment-rotation curves.
 4. 8 more "opening" mode events' individual M-rotn curves.
 5. "closing" mode quadrant *excerpt* of Figure 7.1.1., $\delta M-\Delta \text{rotn}$ "407 wind event" plot
 6. all 11 "closing" mode events' individual moment-rotation curves.
 7. the 3 largest "closing" mode events' individual M-rotn curves.
 8. 8 more "closing" mode events' individual M-rotn curves.

With only three exceptions, the 23 chosen events displayed Moment-rotation curves of the curvilinear form suggested by the envelope of points on the plot of all "407 events" in Figure 7.1.1. The two closing joint examples of Events 53 and 309 (of 11) and the solitary opening Event 160 (of 12) displayed slightly "concave" curves [where δMoment was seen to increase more rapidly than $\Delta \text{rotation}$], in contrast to the "convex" curves of the other 20 chosen events.

The 'concave' Event 160 differed from the similar magnitude Event 211, as seen on Figure 7.1.3. Closer inspection of the individual $\delta M-\Delta \text{rotn}$ plots revealed many examples of vertical 'step changes', which are explained in Section 7.1.3. as due to the momentary "sticking" of the RVDT rotor arm inside its housing. The removal of these vertical steps (seen at $\Delta \text{rotations}$ of 1.95, 2.7 and 3.0 millirads) also negated the contradictory "concave" $\delta M-\Delta \text{rotn}$ curve shape, leaving a 'corrected' form that was much more linear, similar to the plots of the other 11 opening events. However, the "concave" nature of the two other examples (Events 53 and 309) was not exaggerated in this manner, but no conclusion was drawn from them.

∂ Moment vs Δ rotation :407 wind events ("opening")

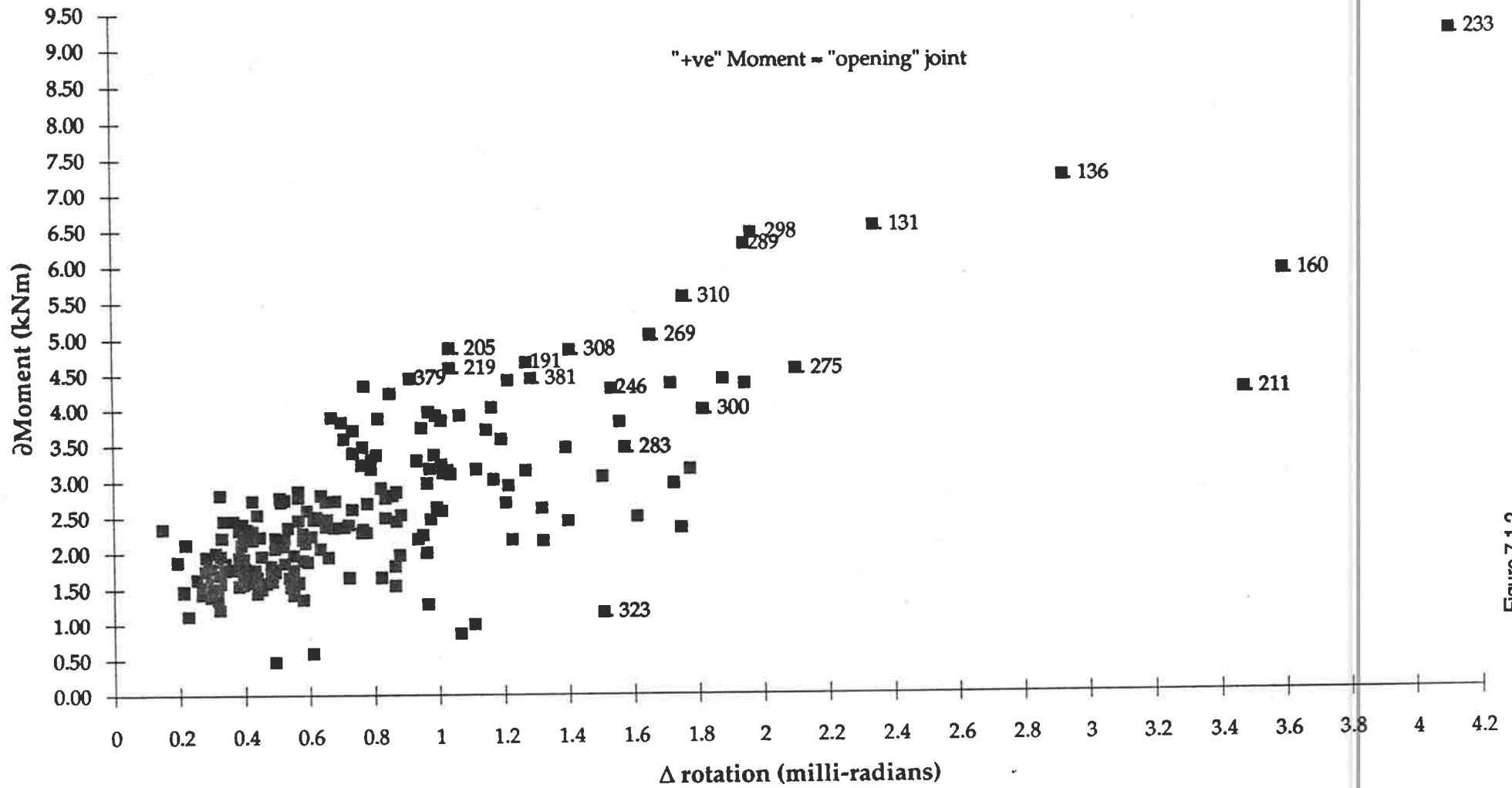


Figure 7.1.2.

4 Extreme Wind Events: Aug-Sept '92.

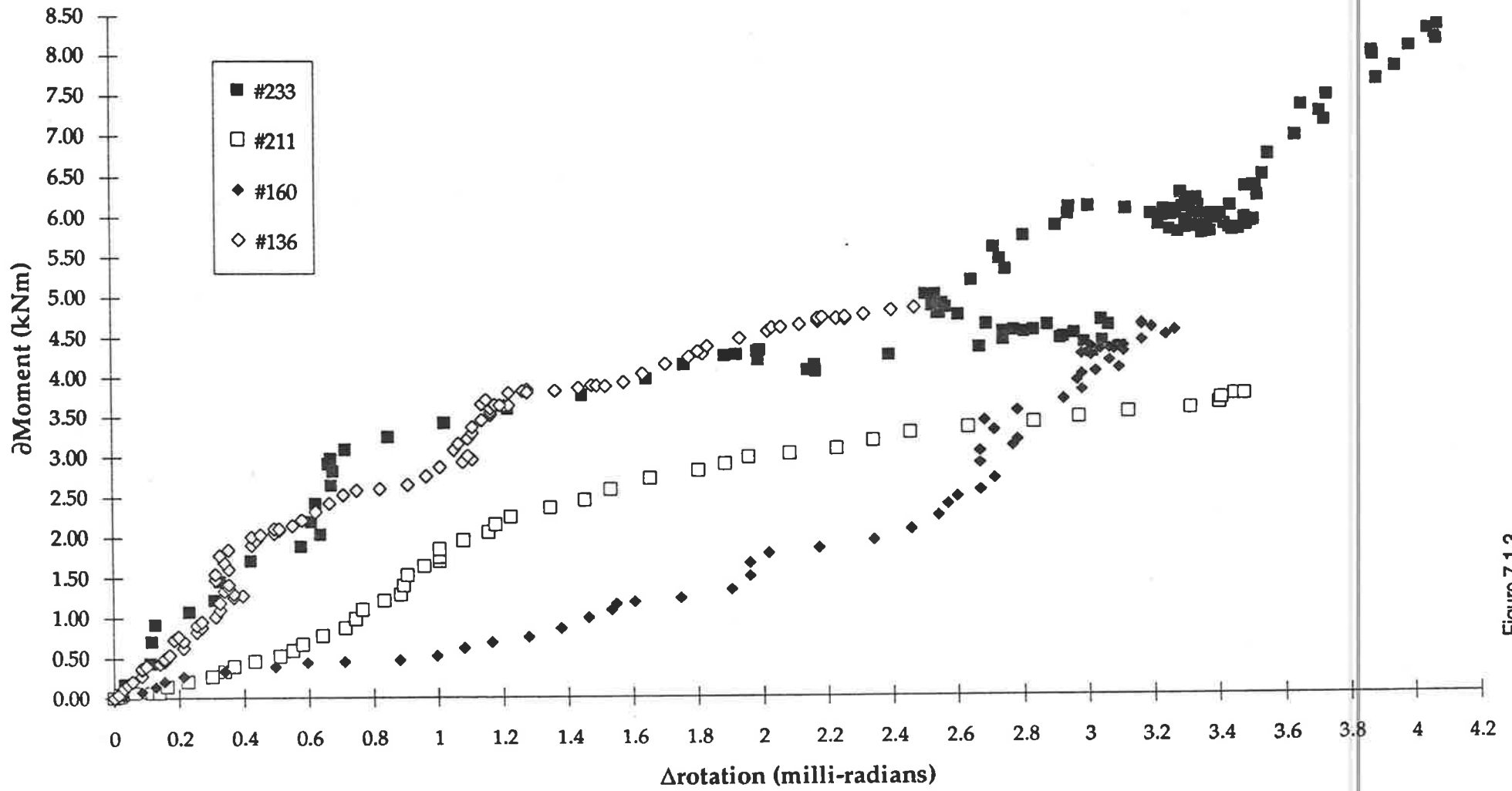


Figure 7.1.3.

8 Extreme Wind Events: Aug-Sept '92.

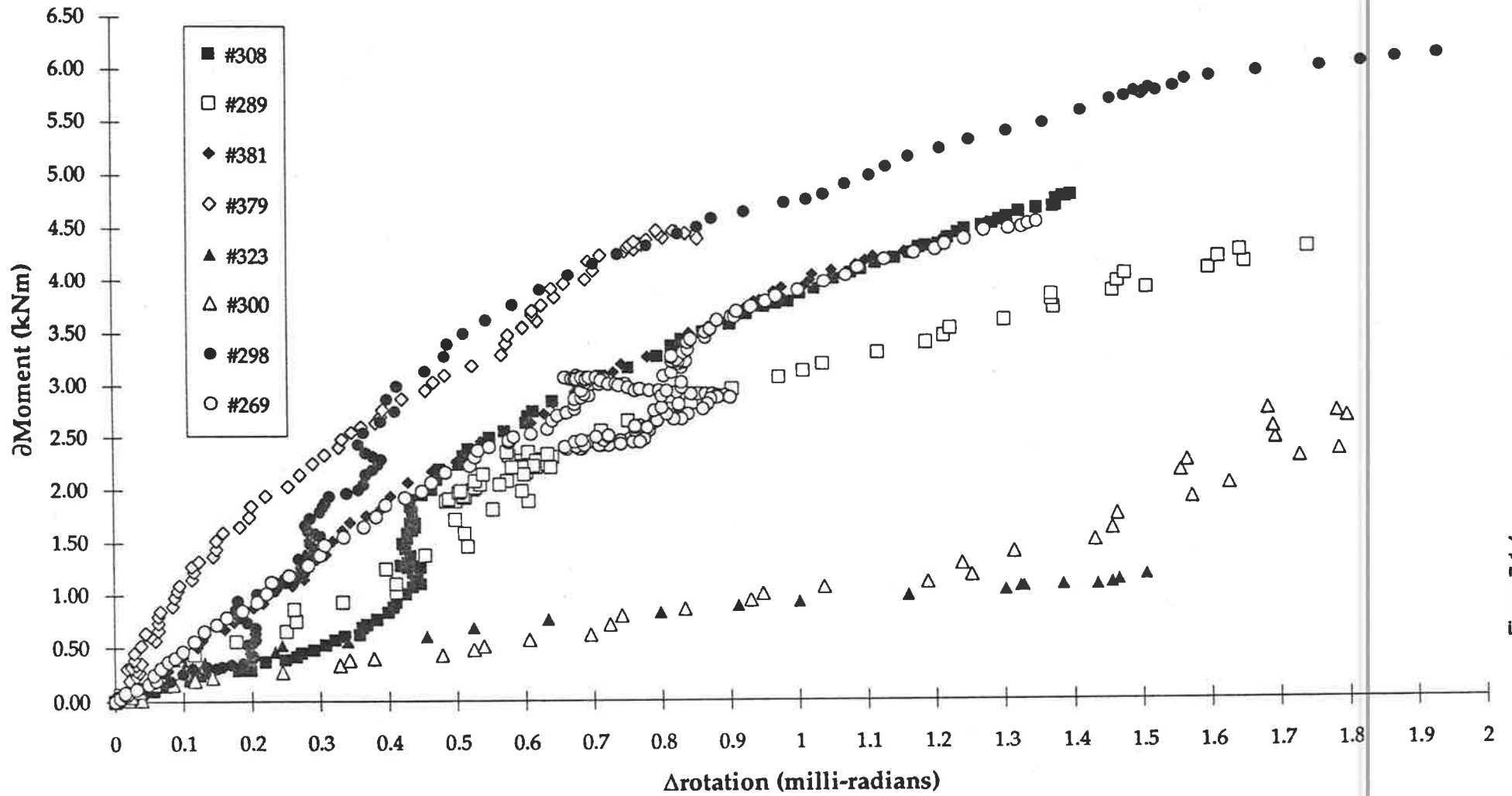


Figure 7.1.4.

∂ Moment vs Δ rotation :407 wind events ("closing")

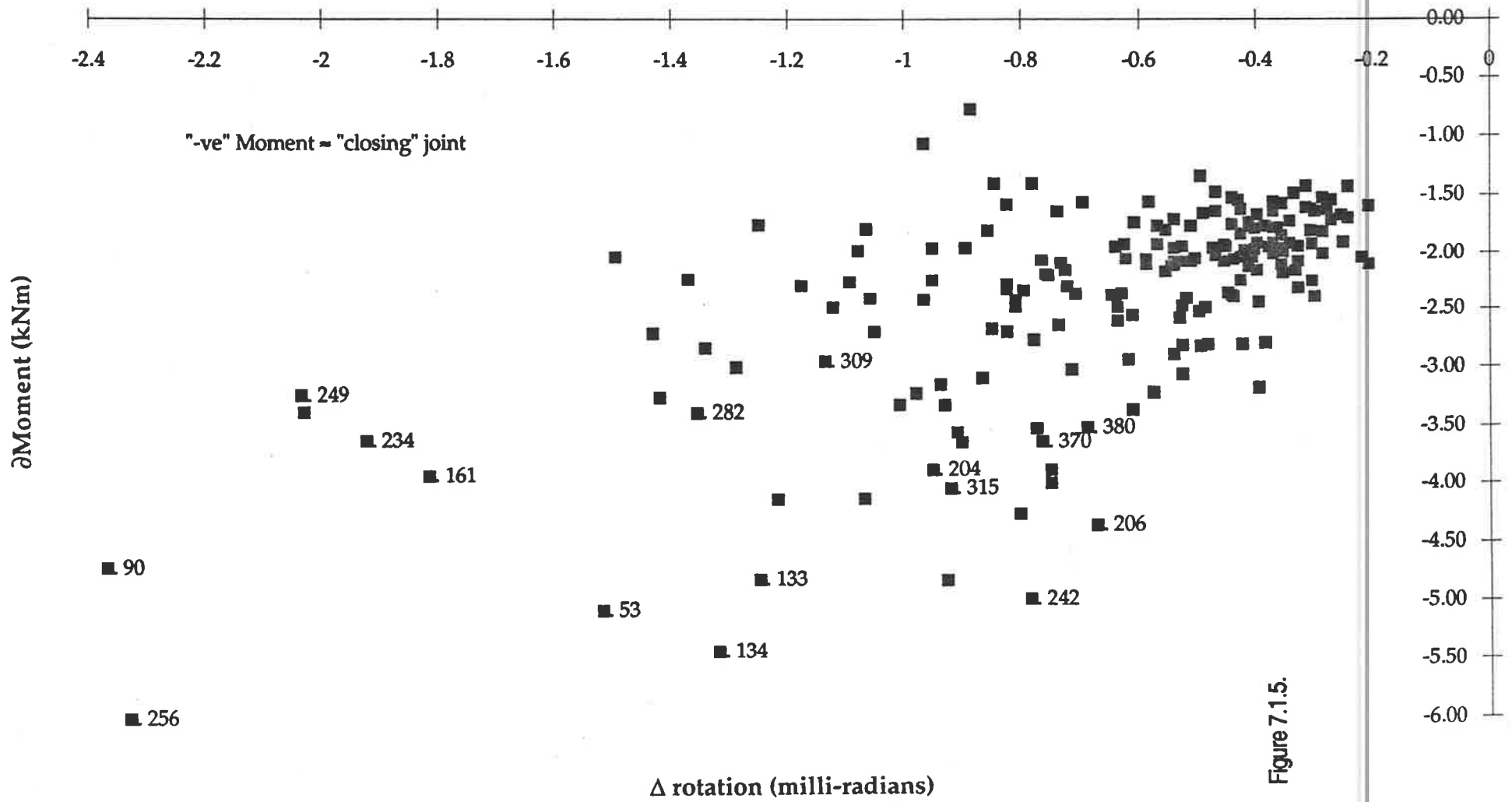


Figure 7.1.5.

11 Extreme Wind Events: Aug-Sept '92.

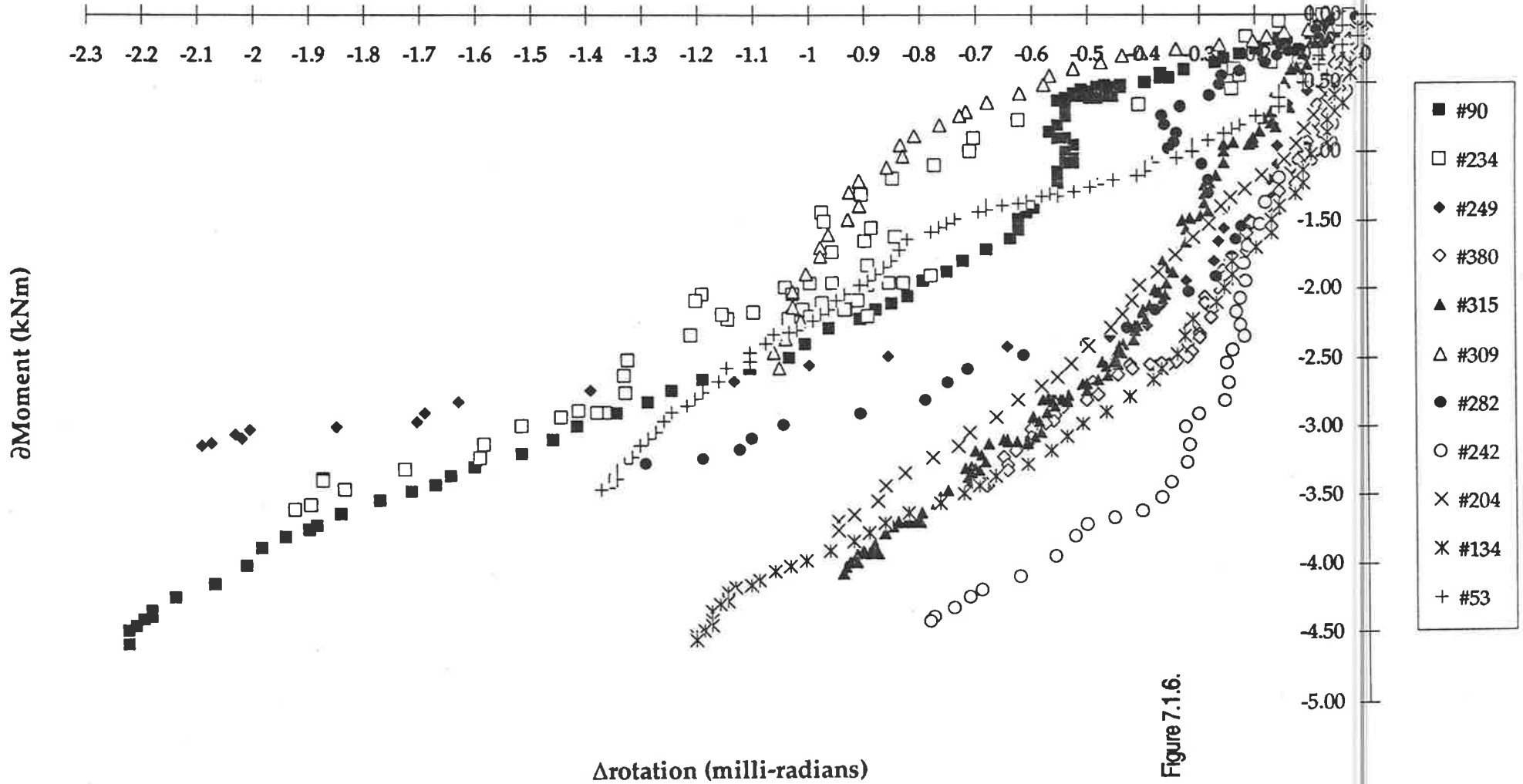


Figure 7.1.6.

3 Extreme Wind Events: Aug-Sept '92.

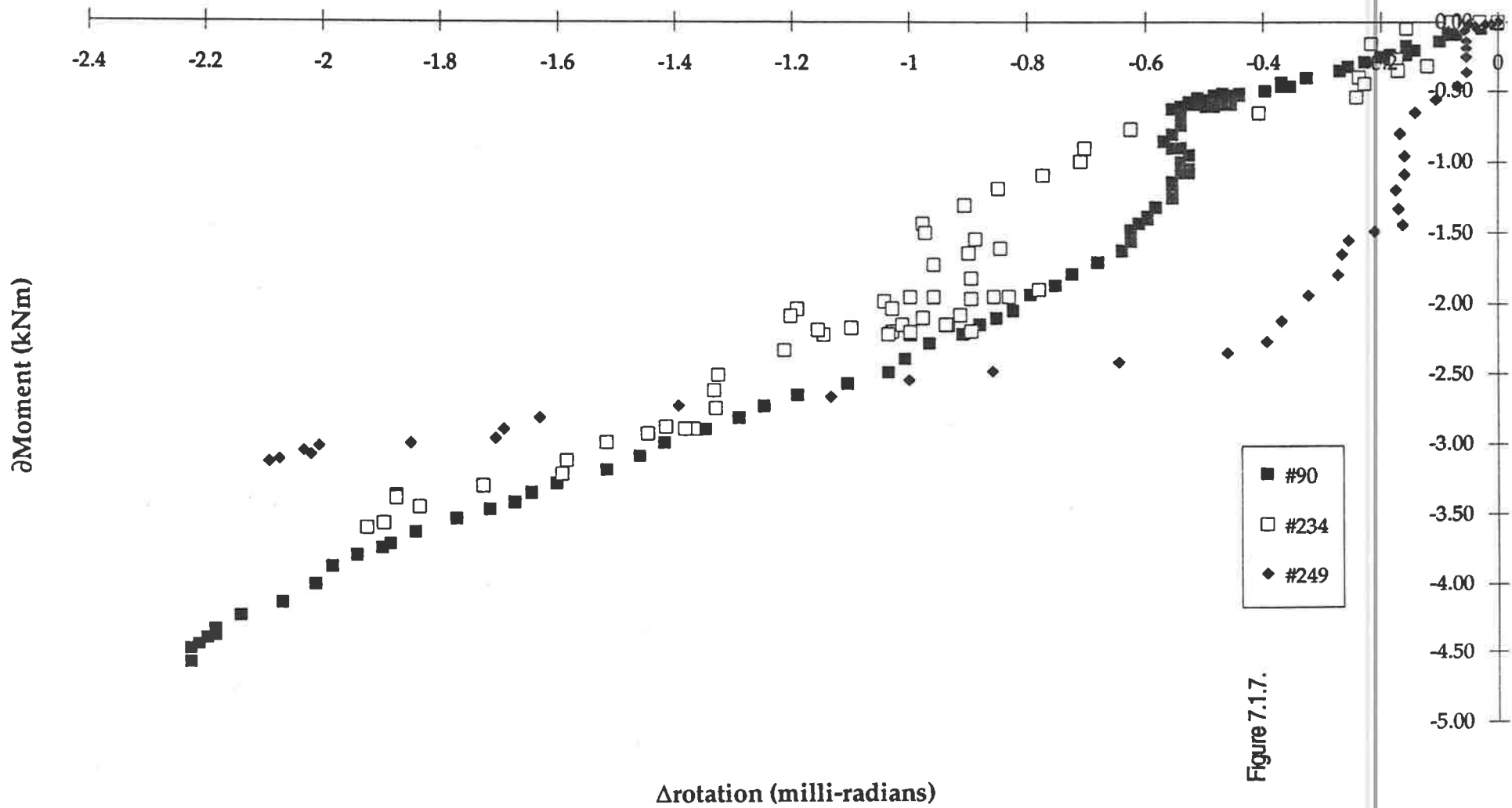


Figure 7.1.7.

8 Extreme Wind Events: Aug-Sept '92.

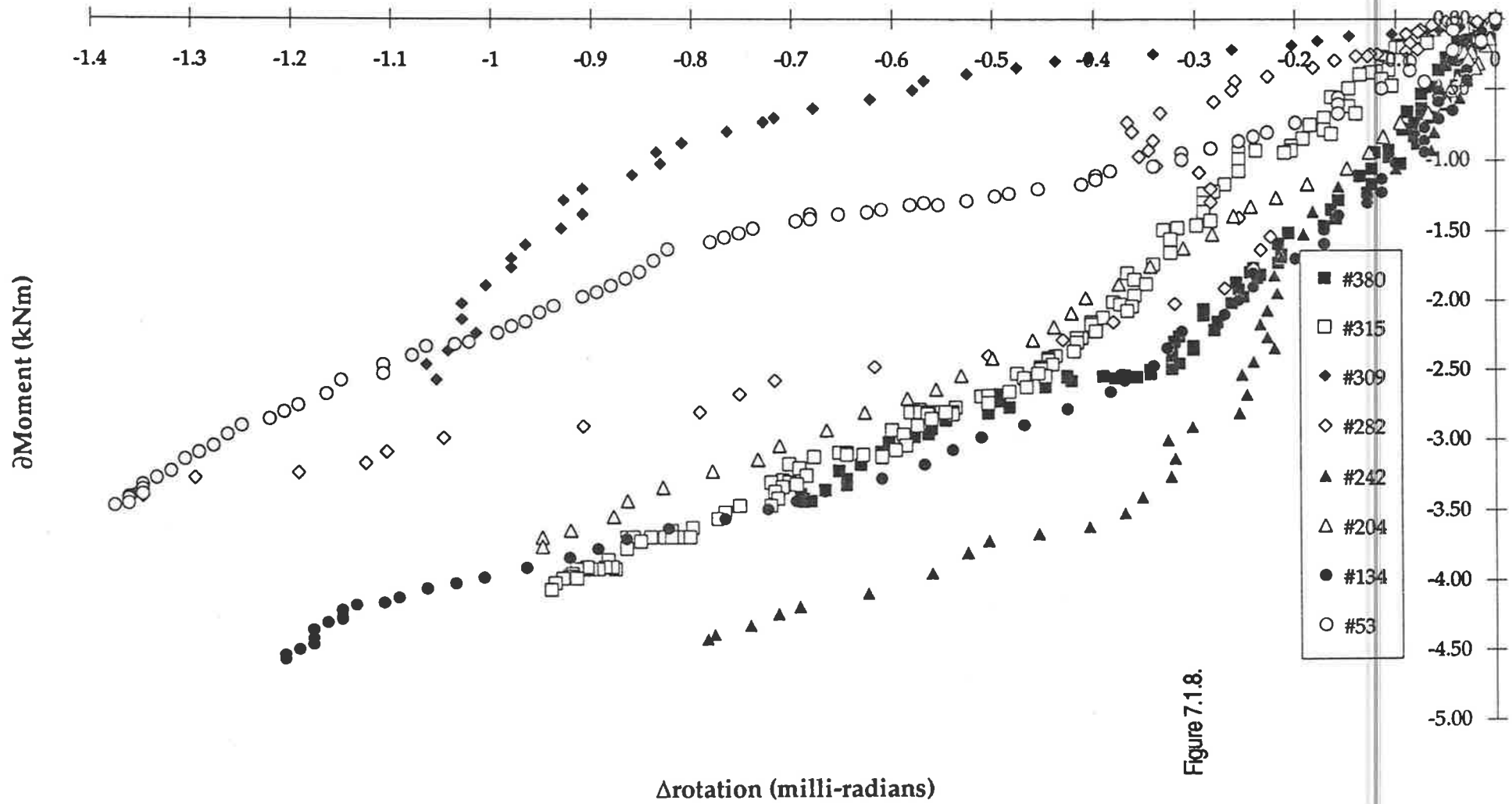


Figure 7.1.8.

7.1.2. The INFLUENCE of WIND ACTION

“Opening” mode responses were defined as positive δ Moments. A tensile bottom rafter strain represents an “opening” event, equivalent to a positive change in the bottom rafter strain (“ Δ bot extrem fibre strain”), or a negative voltage change (“ Δ bott SG”). This was known from calibration tests on the strain gauge measuring system (Appendix A). An example is ‘Event 136’ in the preceding spreadsheet.

Opening mode responses would have been caused by *increases* in wind velocity, whereas the joint “closing” represents the ‘relaxation’ after this initial loading, during the drop in wind velocity following the initial gust. Because of this, the magnitude of the dynamic opening joint responses could be expected to exceed closing ones. It is interesting to note that Figure 7.1.1. revealed a dominance of dynamic “opening” responses, of greater magnitude than their associated “closing” responses. The imbalance in numbers could be explained from this difference in magnitude, since for every dynamic “opening” event just above the ‘cut-off’ value of (positive) 1.5kNm, its subsequent closing or ‘relaxation’ mode response would have failed to exceed the “significance” level of (negative) 1.5kNm. The strategy of ‘triggering’ data collection on a “rising” wind velocity (and hence an emphasis on opening joints) should have been counteracted by the relatively long recording period of ten seconds after the initial gust.

This difference in magnitude between the two modes of dynamic response appears to suggest that either the joint is progressively opened during prolonged spells of high wind, or that “closing mode” recovery is slower than the more dynamic “opening mode” response. Since no long term datum was maintained in the instrumentation system (e.g. for a period of several hours or one day), the progressive effects of a storm of that period could not be examined.

“Double” events 204-5, 233-4 (seen in earlier plots, Section 7.1.1.) were two recorded examples where both the opening *and* the immediately following closing mode responses were of significance, and where the opening mode response exceeded that of the ‘relaxation’. An example of this may be seen in the δM - Δ rotn curve for the “triple” Event 379/380/381 shown overleaf. This plot demonstrates the joint behaviour when subjected to three successive cycles of ‘significant’ strain change. The superimposition of these three curvilinear responses produces the classic “hysteresis loop” phenomena. Also, through repeatability, these multi-event records confirm the reliability of the instrumentation system.

The phase correlation (over time) between the rafter bending moment and the instantaneous wind speed recorded at the anemometer site was not expected to be good, as explained in Section 5.4. Continuous, erratic fluctuations in wind speed and direction over time belie the simplicity implied by the design based guidelines of the AS1170.2 Wind Loading Code. Even for the simple case of a Westerly wind, parallel to the plane of the portal frames of the building, allowance for the time lag between speed measurements at the anemometer and the structural responses of the fully loaded frame did not fully account for the phase discrepancies seen between the time history records for wind speed and strain/rotation.

No simple correlation coefficient between wind speed and recorded joint moment can be deduced from the collected data. Peak structural responses did not necessarily occur during wind events having the highest instantaneous wind speeds. Rather, the expected general trend between wind speed and δ Moment was noticed. Certainly, the highest wind speeds (60 to 70 km/hr) seen in this study were recorded during the periods on August 12th between 12:58-1:20pm and 1:53-2:22pm, when the bulk of the ‘significant’ response data was collected. Event 233 saw the greatest change in Moment of +9.28kNm, at 2:10:02pm, for a wind speed of 65km/hr. But, high instantaneous wind speeds quite often produced a low strain response. For example, the second highest instantaneous wind speed recorded in the study, of 70.3km/hr (Aug 12th, 3:07:22pm), registered strains only slightly above the chosen ‘significance’ level of 30 $\mu\epsilon$, giving a change in Moment of +2.36kNm. Also, the top speed of 71km/hr (Events 249-51, Aug 12th, 2:10:37pm), produced opening and closing responses of only ± 3.2 kNm.

Extreme Wind Event: 28 September 4:12:27 pm

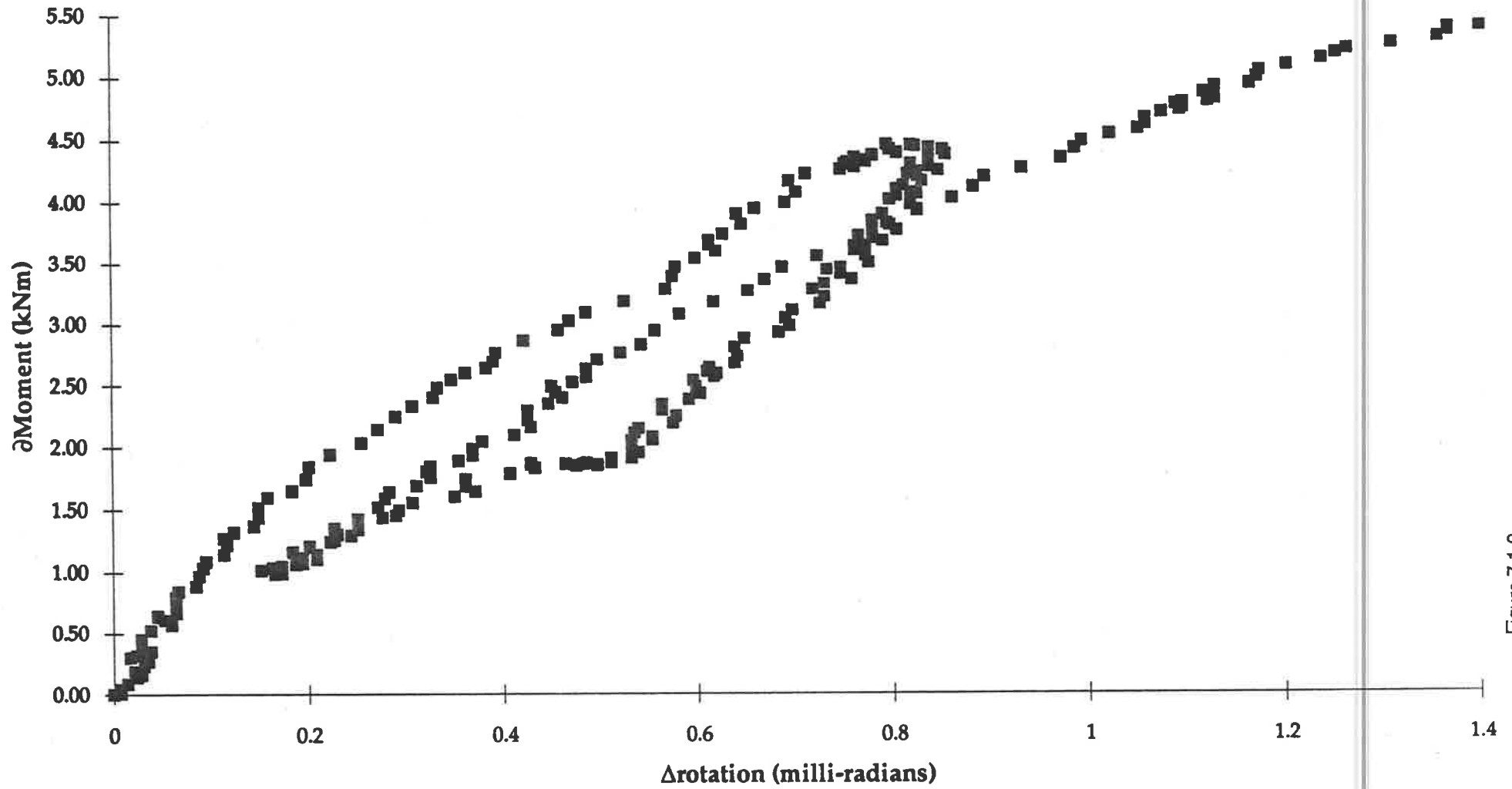


Figure 7.1.9.

It was noticed that a sharp 'spike' in the wind speed record did not produce a response as great as a more consistent gust, of a lower average speed. For the typical wind speed of between 45 and 60 km/hr, it would take between 1.5 and 2.0 seconds to completely cover or 'load' the 26 metre roof span. Therefore, extreme gusts representing spikes on the wind speed record would have caused more localized effects, without producing a high frame moment. This suggests that the roof structure acted to "average out" the effects of wind loading, and confirms the use of a "2 to 3 second design gust" for the ultimate limit state considerations of AS1170.2.

7.1.3. RVDT PERFORMANCE and its INFLUENCE on the δM - Δ rotn PLOT

Rotation measurements were seen to be the "weak link" in the instrumentation system developed for this investigation, easily representing the greatest source of uncertainty. Inspection of the datafiles revealed that in general, the shape and phase correlations between the two ('plastic strip') strain gauges were excellent, while the correlation between the RVDT and strain outputs was of variable quality. The strain signals were commonly slightly 'out of phase' with the rotation signal. The correlation seemed to improve with the magnitude of the outputs. The reason for an imperfect phase relationship between the strain and rotation responses is unclear. Fortunately, this problem was mitigated by concentrating on the larger structural responses and by adopting a "peak analysis", which was unaffected by local anomalies in the output signals.

Several comparisons between the strain and rotation records are provided overleaf, for two "good" and three "bad" phase correlation examples. In these, a perfect correlation (in both shape and phase) between two superimposed signals would have appeared as a single line.

"Window 9", in the bottom right hand corner of each DaDispTM output, shows the superimposition of the rotation (RVDT) and bottom strain gauge signals. [For the ease of comparison, the magnitude of the RVDT signal has been adjusted so that the *range* between the maximum and minimum values is equal to that present in the strain signal. The shape and time function of the signal were unaffected by this.] Collectively, the five comparisons show the variable and 'imperfect' nature of the correlation between the raw signals, which led to the adoption of the "peak analysis" method.

In all these records, the excellent shape and phase correlations between the top and bottom strain gauges can be seen in "Windows" 7 and 8 on the lower row.

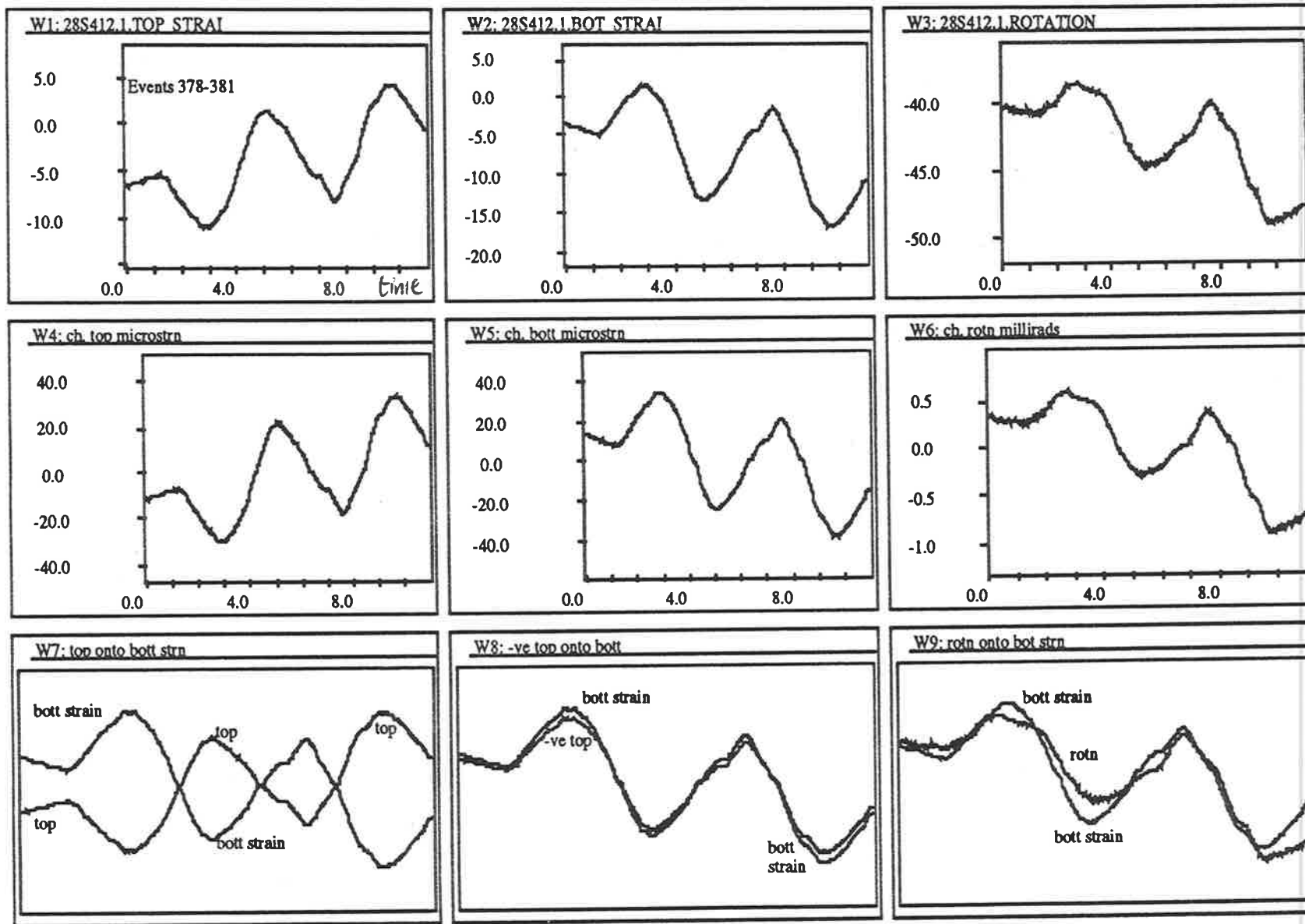


Figure 7.1.10.

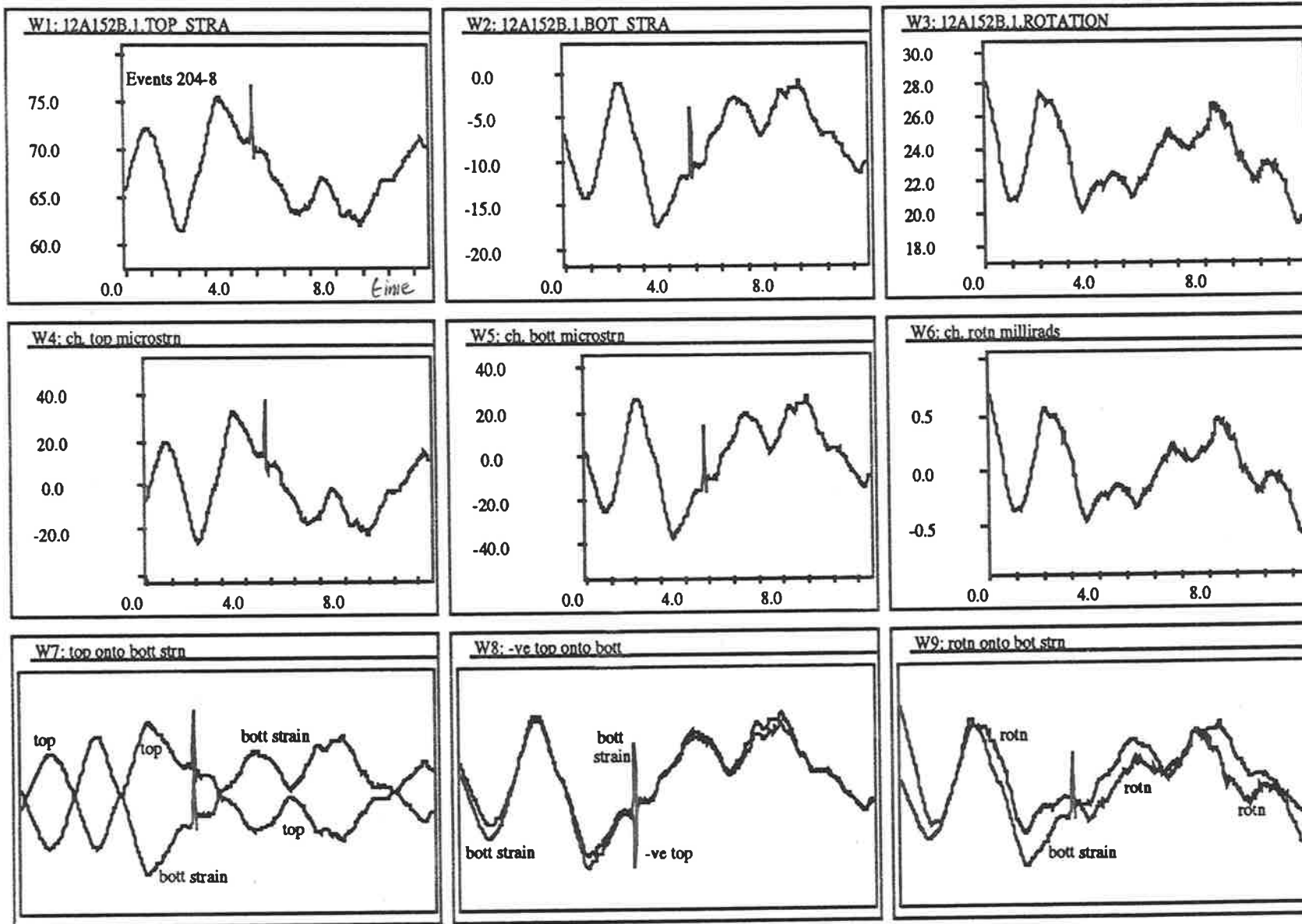


Figure 7.1.11.

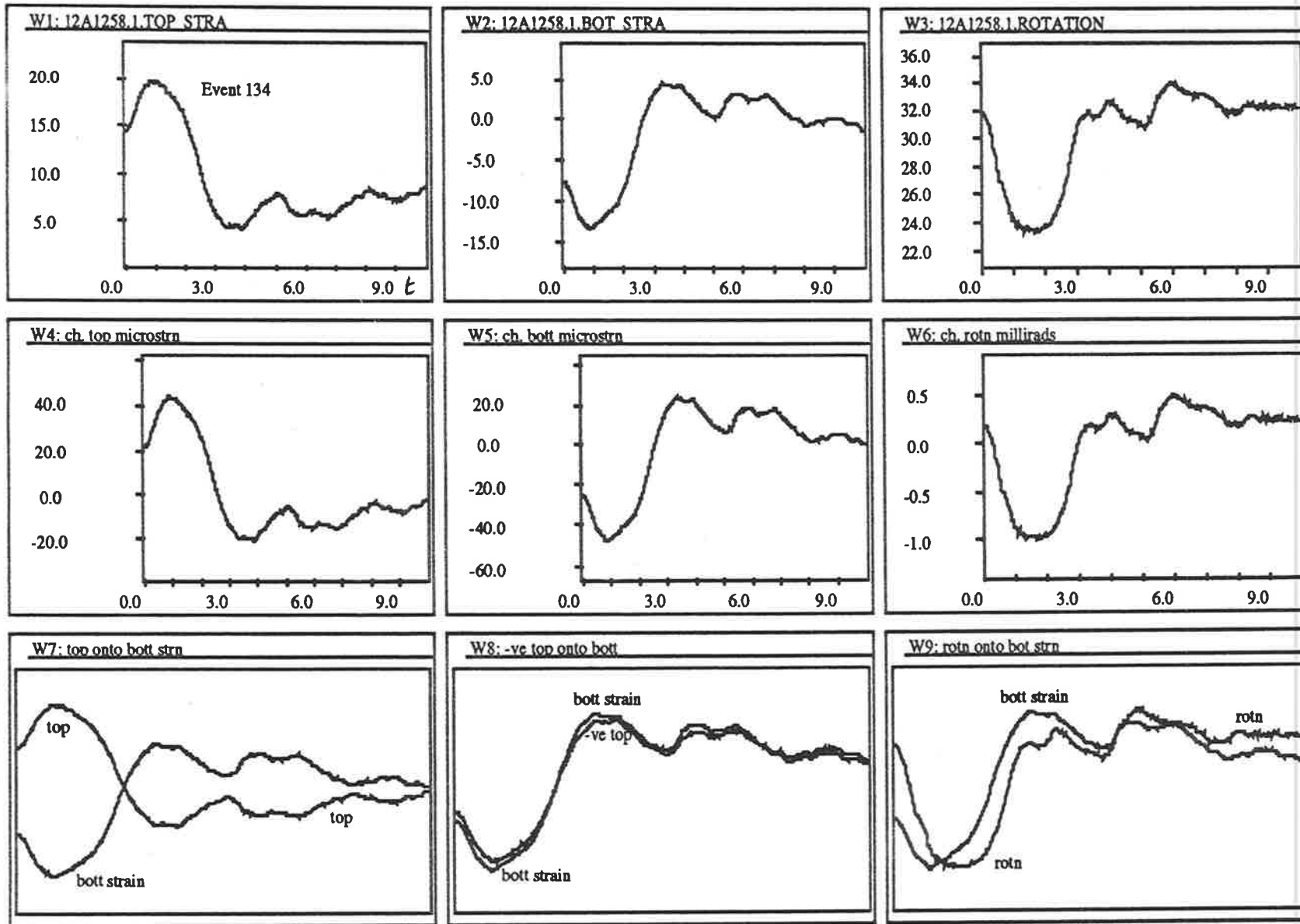


Figure 7.1.12.

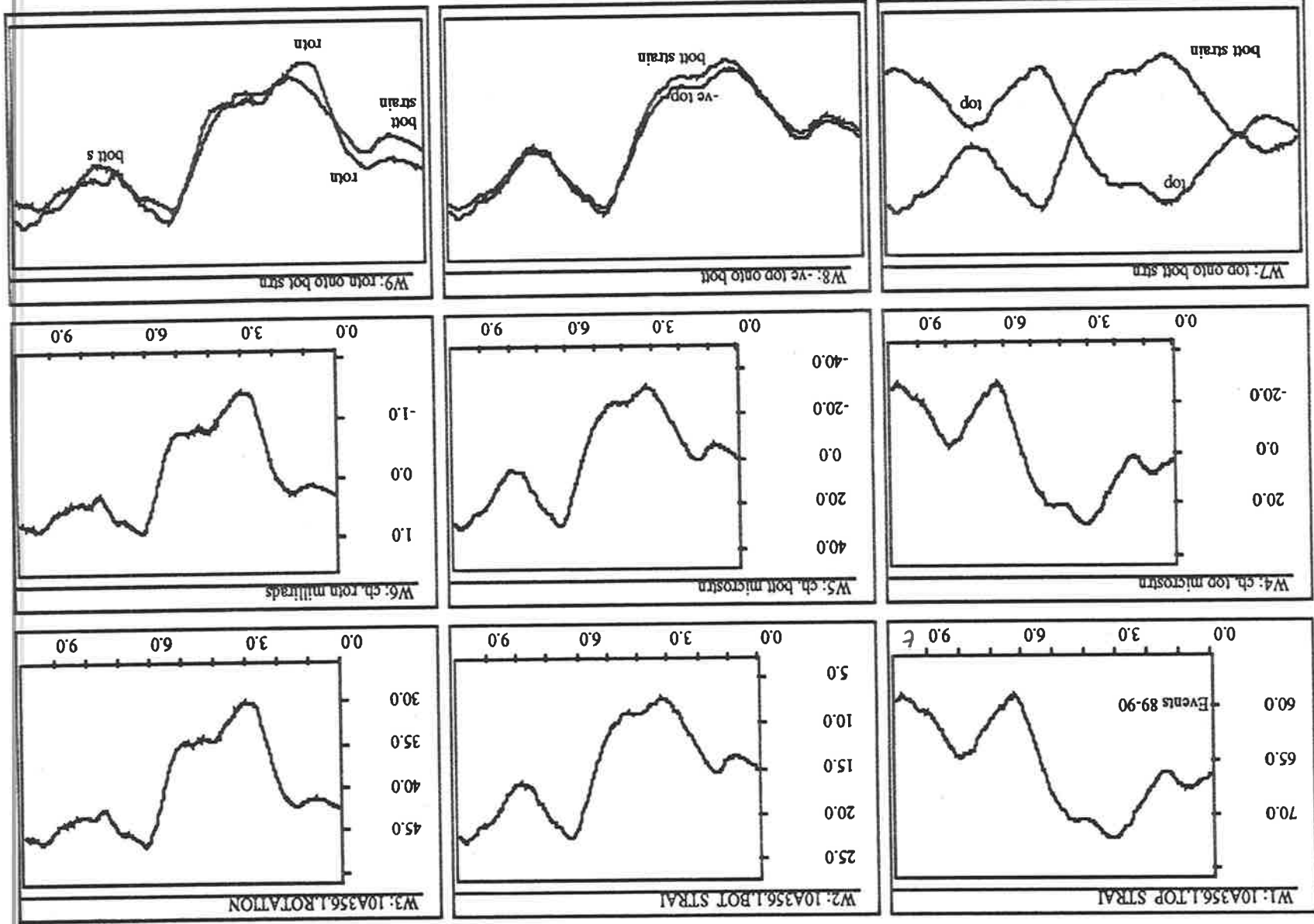


Figure 7.1.13.

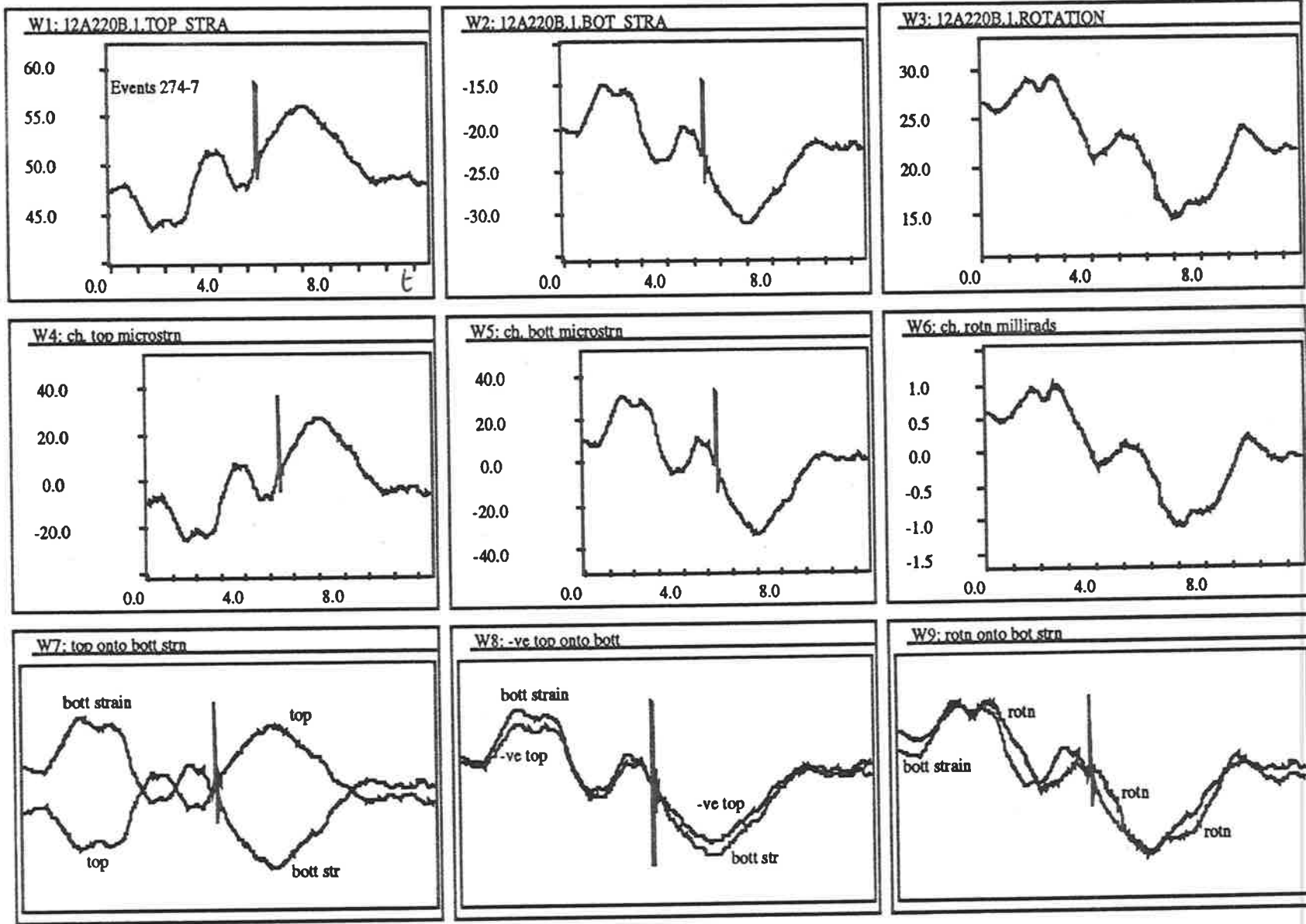


Figure 7.1.14.

Unfortunately, after the calibration, installation and refinement of the adopted RVDT arrangement described in Section 5.3., the fragile instrument was damaged during the first laboratory test by Lee (late July, 1992). Failure of the connection between the hydraulic loading ram and test specimen led to a sudden, high amplitude lateral load to the sensitive RVDT rotor arm. Following this, the previously smooth, low friction 'spin' of the rotor could be felt to "stick" or "grab" at regular intervals around a full revolution. A recalibration of the unit confirmed the calibration factor derived previously, using the same method outlined in Section 5.3.2. However, since this involved the controlled rotation of the central rotor arm relative to the housing, this could not detect the effect of any increase in friction or "stick" in the instrument. Since the use of the instrument was similar to the loading conditions seen in the calibration test, and since the very small rotations to be measured were much less than the "stick" interval of approximately ten degrees, the RVDT was retained for use in all data collection reported in this study.

This was unlikely to have influenced the aforementioned phase relationship with strain records, but other observations necessitated a more careful application of the rotation data:

- a) frequent minor differences between the *shape* of the strain and rotation records, such as:
- (i) the 'flattening' out of peaks in some RVDT outputs,
 - (ii) differences in 'emphasis' on neighbouring peaks between strain and RVDT,
- and (iii) occasional 'extra spikes' in the RVDT output.

Two examples of both (i) and (ii) are shown in the graphs overleaf: Events 252-7 and 160-1 for (i), 282-4 and 232-6 for (ii). An example of (b) below, Event 308, follows these.

- b) inspection of the δ Moment- Δ rotation plots for individual events revealed examples of vertical 'steps' during the curve, indicating an increasing strain for no change in rotation. It was postulated that this may have been caused by internal "stick" at much lower ('micro') level rotations than the originally detected 'macro' level effect. Examples of this can be seen in the earlier plots of Events 90, 160 and 308: Figures 7.1.7., 7.1.3. and 7.1.4. respectively.

This should not be confused with a similar feature found on some of the curves, where many points were seen to represent approximately the same position on the plot (i.e. a "pause"). This corresponded to a momentary 'zero change' in *both* Moment and rotation: since points are shown for each time step of 0.025 seconds, when no change occurred, multiple points were plotted. The source of this was identical 'flat spots' in the output signals for *both* strain and rotation, in contrast to the "sticking" phenomena, where only the rotation output exhibited the 'flat spot'. Examples of the "pause" feature were seen in the δ M- Δ rotrn plots of Events 233, 234 and 289 (Figures 7.1.3., 7.1.7. and 7.1.4.).

A final note on the "time history" nature of the δ M- Δ rotrn plots of individual events concerns the curve of Event 282 (closing). The arbitrary nature of the assumed 'zero point' used in these analyses is evidenced during the Event 282 δ M- Δ rotrn plot seen in Figure 7.1.6., which featured a section where δ Moment increased, but Δ rotation *decreased*, over about 12 data points, or 0.3 seconds. A momentarily poor correlation between strain and rotation was the cause. This can be seen on Figure 7.1.17., showing superimposed rotation and bottom strain signals: Event 282 represents the first rising curve, during which the rotation output features a small "spike" not present in the strain signal. Setting the 'zero point' after this spike would have avoided the problem, but reduced the maximum δ Moment recorded.

August 12, 2:10-57pm Events 252-7

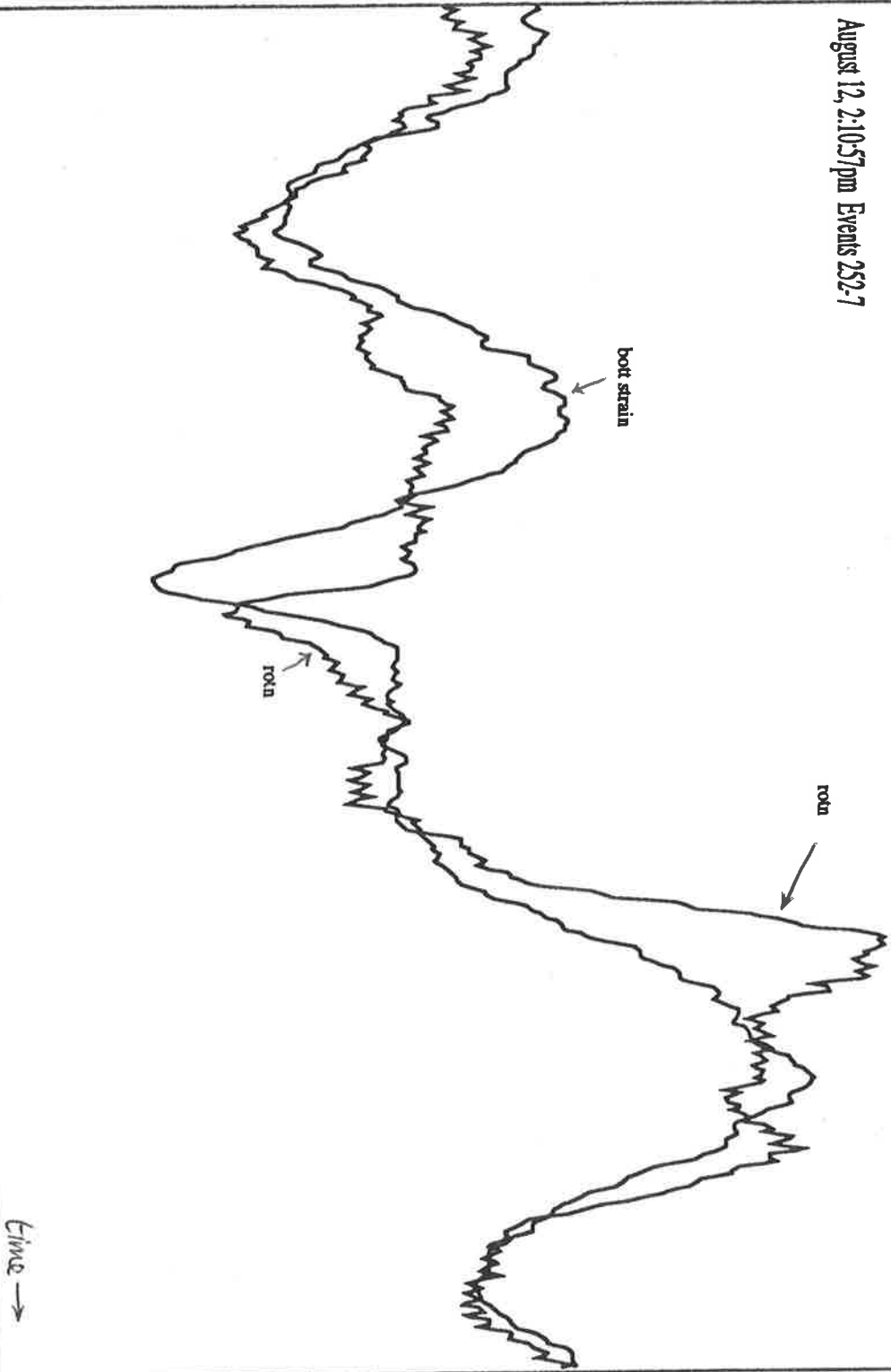


Figure 7.1.15.

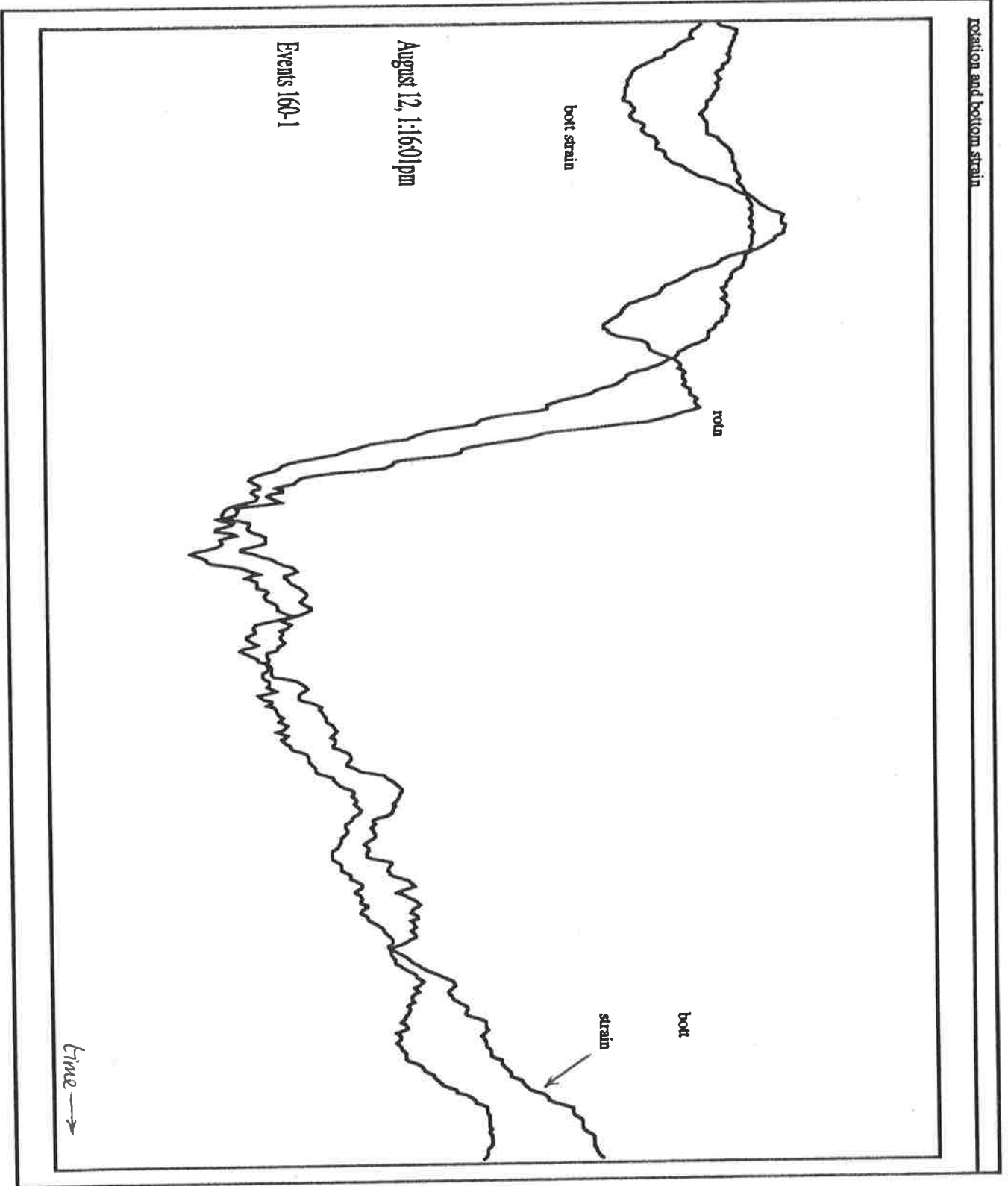


Figure 7.1.16.

rotation and bottom strain

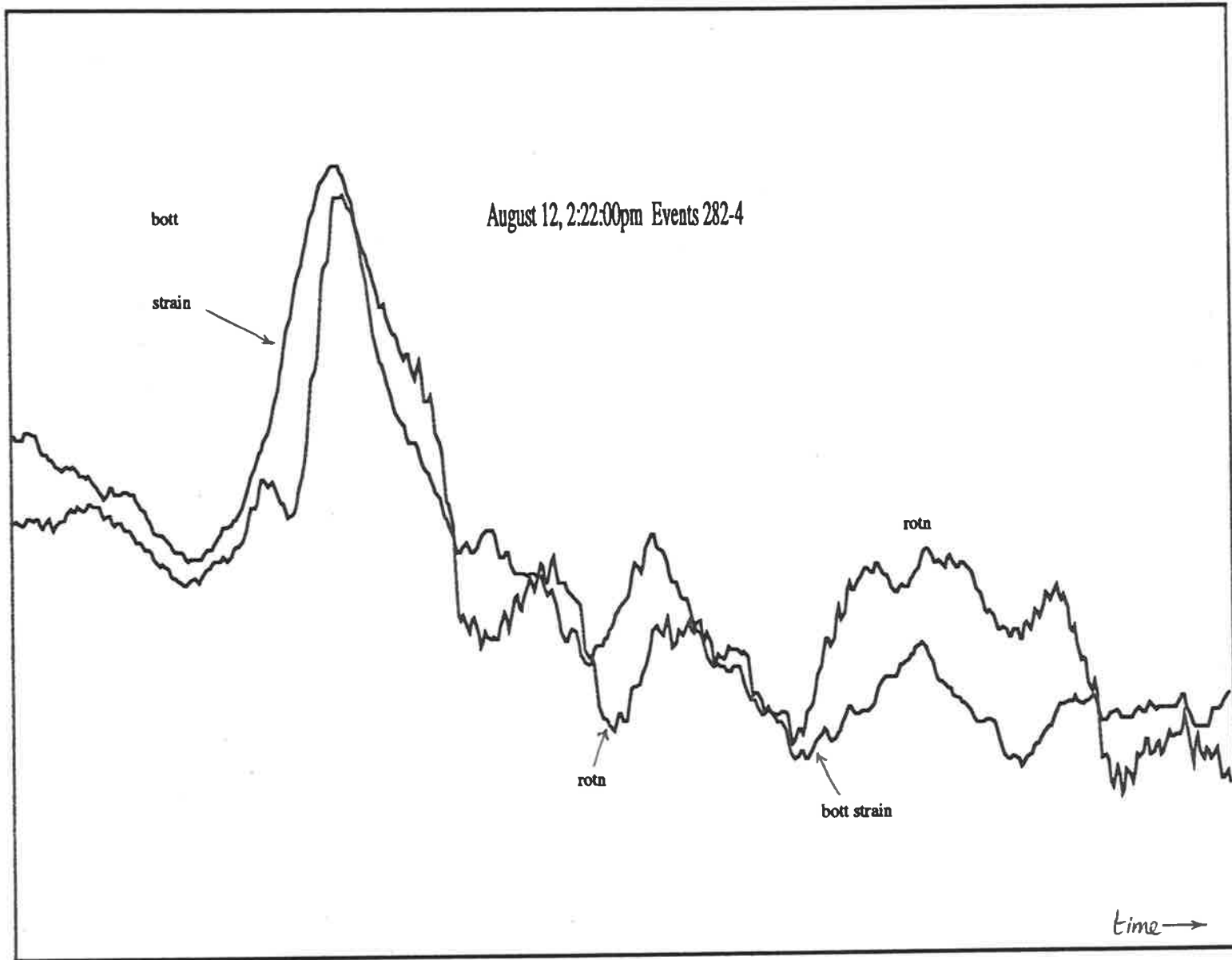


Figure 7.1.17.

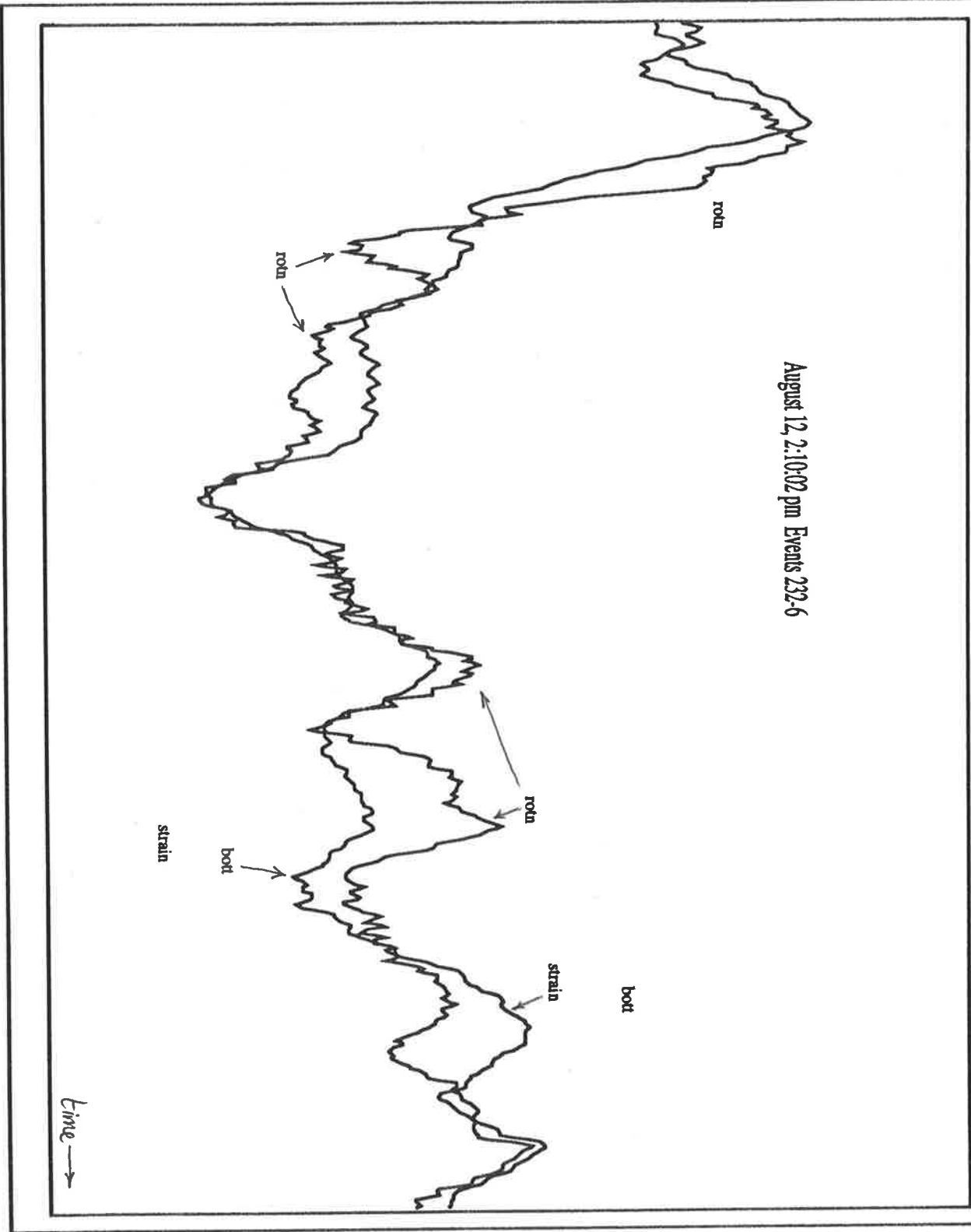


Figure 7.1.18.

rotation and bottom strain

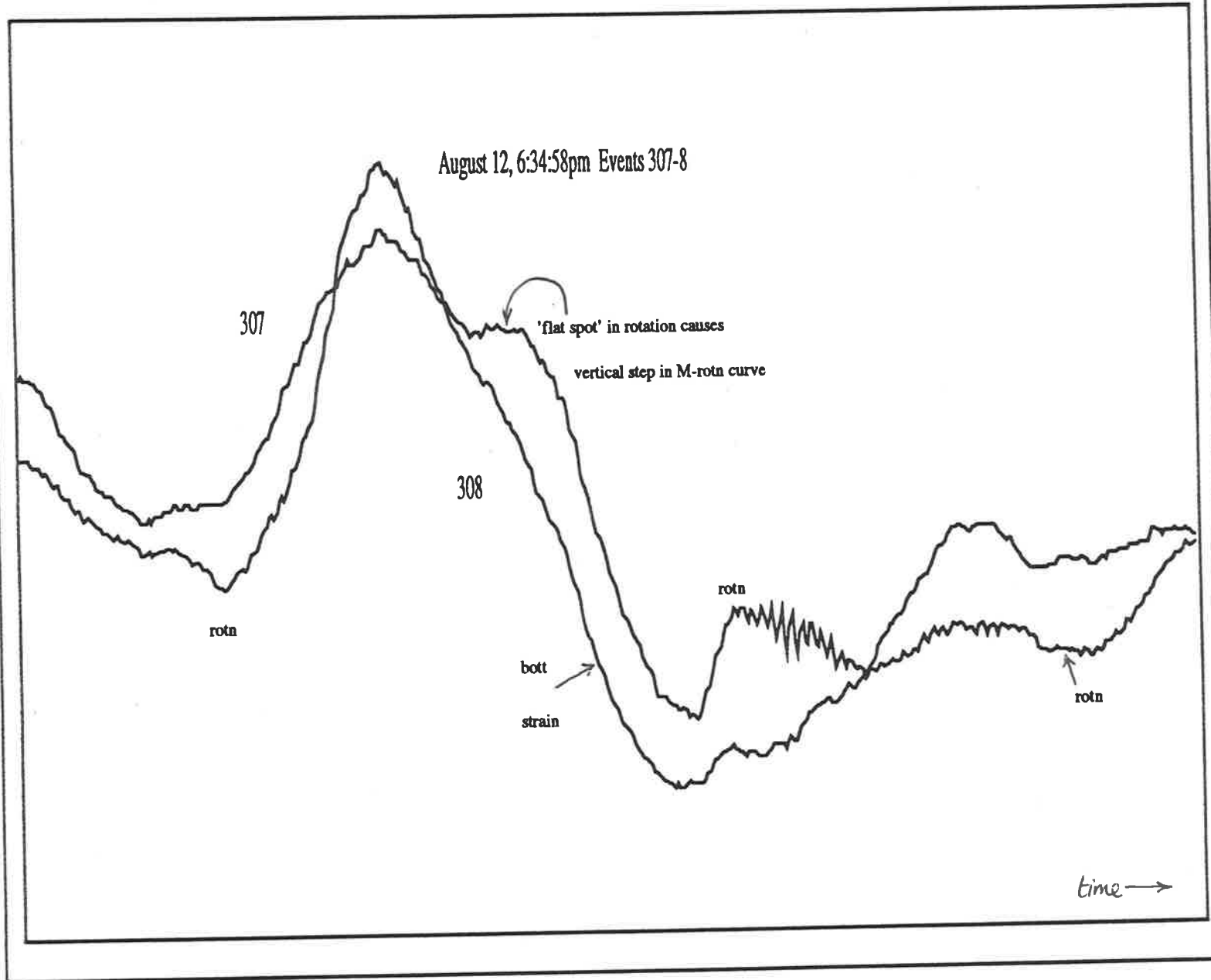
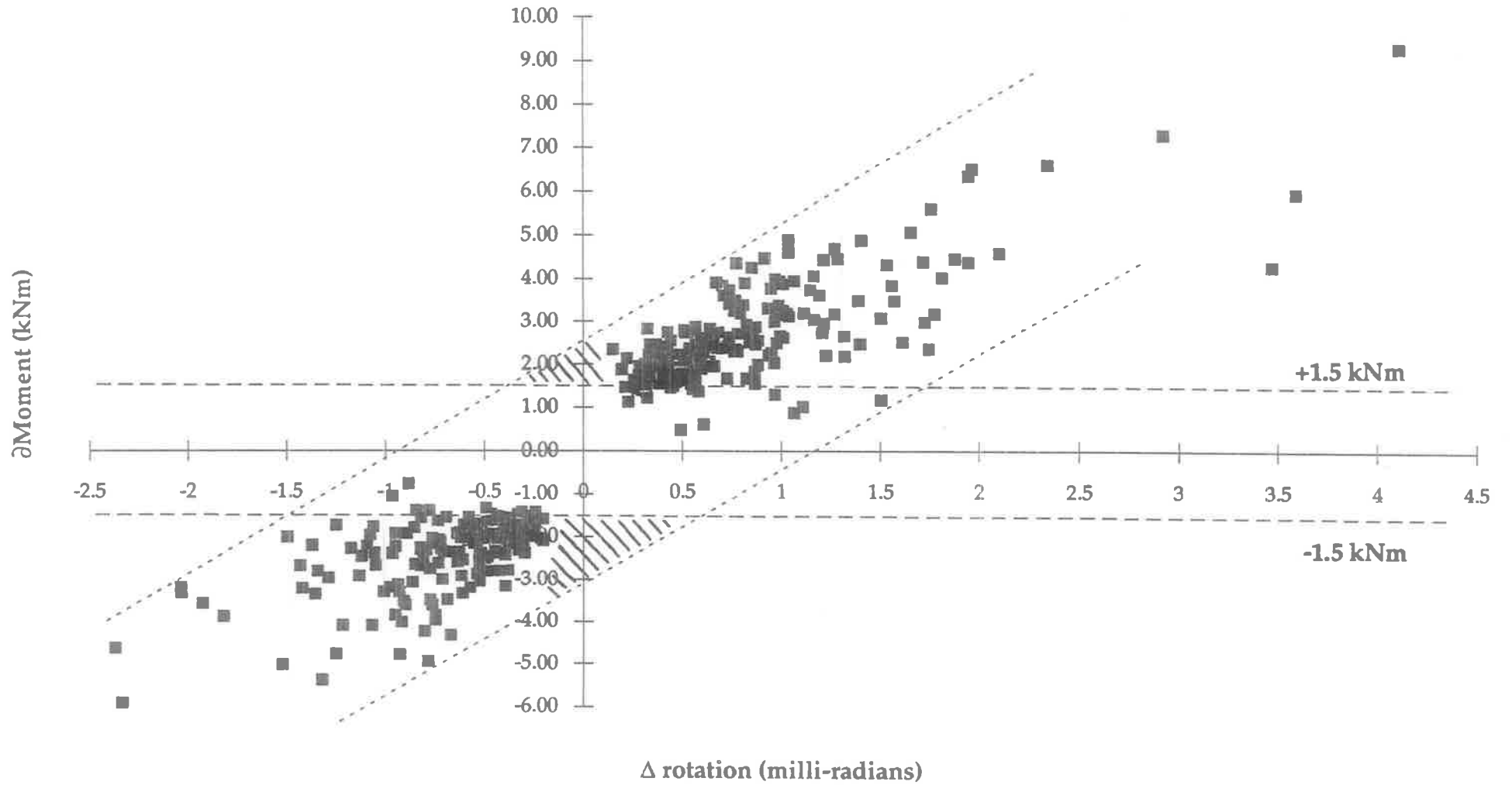


Figure 7.1.19.

Δ Moment vs Δ rotation :407 wind events



7.1.4. SAMPLING ERROR during DATA SELECTION

Originally, the overall δ Moment- Δ rotation plot of Figure 7.1.1. had been constructed by selecting only the 'best' 100 events. It was suggested that the possibly subjective manual extraction of this 'significant' data may have caused some event responses to be omitted. A "worst case" scenario was constructed whereby a wind event with a "significant" strain ($>20\mu\epsilon$) but a very poor or negative correlation between strain and rotation may have been rejected, thus artificially "improving" the δ M- Δ rotn plot. Events following this scenario would have possessed low rotation values, and would have fallen into either of the areas shaded on the figure at left. These areas are bounded by the 1.5kNm ($20\mu\epsilon$) 'significance' levels and the dashed diagonal lines, which indicate the hypothetical bounds for the loci of horizontal δ M- Δ rotn error bars, as explained in Figure 7.1.20. These bounds relied on the (pessimistic) assumption of a "constant value" error type in the RVDT rotation signal.

Note that regression theory is based on the assumption that all error occurs in the 'y' axis variable, measured against an 'x' axis quantity of zero error. The converse was true in the case of this moment-rotation plot, where the 'y'-axis strains (and hence moments) were known to a high accuracy, and the 'x'-axis rotations contained the greater measuring error. Regression theory error bars are vertical for both "constant" value and "proportional" type error, as represented in Figure 7.1.20. below.

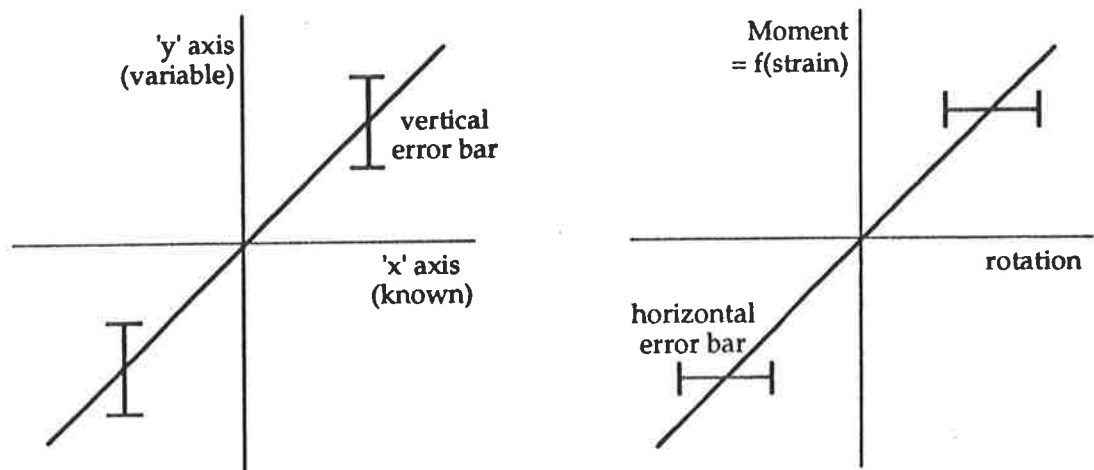


Figure 7.1.20. Error bars for (left) conventional regression theory, and (right) strain vs RVDT in this study

The selection criteria of events was thereafter changed from one of "best correlation" to a process of first selecting *all* 'significant' strain responses, and recording their corresponding rotations, regardless of correlation. In this way, the total number of events was raised to 407, with no change in the overall shape of the imaginary 'envelope' bounding them. This suggested that the analysis technique of peak analysis (through manual extraction) had *not* artificially improved the results. The (continued) absence of data points from the shaded area confirms that errors in the rotation measurement system were *proportional* to the signal amplitude, and not a *constant* value, a far more favorable situation.

7.2. JOINT STIFFNESS

Three different definitions for “stiffness” are commonly used: ‘initial’, ‘tangential’ and ‘secant’. These generally apply to different parts of the moment-rotation or load-slip curve, and are shown in Figure E.3. ‘Initial stiffness’ (K_i) could only be calculated for the 23 chosen events of Section 7.1.1., using the individual event moment-rotation plots. Due to computational convenience, secant stiffness was evaluated for all 407 events, as seen in the spreadsheet of Appendix G. ‘Secant stiffness’ (K_{sec}) was defined in this study as the quotient of the maximum changes in moment and rotation for each event, representing the slope from the origin to the “last” point in the individual δM - Δ rotrn plots (Figures 7.1.2.-8.). As seen from Figure 7.1.1., initial stiffness could be expected to be greater than secant stiffness.

The results are shown in Table 7.2.A. below. Due to the variable correlation between strain and rotation discussed earlier, the stiffnesses of many events were actually greater for the secant definition ($K_{sec} > K_i$). For those $K_{sec} > K_i$ examples not explained by the presence of either a “concave” curve” or “vertical step” in the δM - Δ rotrn plot (see 7.1.3.), the difference between the two stiffnesses was seen to be generally small. Initial stiffnesses ranged from 1.0 to 10.2 (± 0.1) E9 Nmm/radian, and were more variable than secant stiffness, with values from 0.779 to 6.324 E9 Nmm/radian. Averages for the ‘initial’ value was 3.93, and a similar 3.033 for ‘secant’. The 12 chosen “opening” joint responses varied little from the 11 “closing” ones, having average initial stiffnesses of 3.8 and 4.1 respectively.

wind event number	joint mode	initial stiffness E9 Nmm/radian	secant stiffness E9 Nmm/radian
53	close	1.6	3.321 **
90	close	1.2	1.966 *
134	close	7.7	4.090
136	open	3.4	2.489
160	open	1.4	1.651 *,**
204	close	7.5	4.057
211	open	1.0	1.231
233	open	6.3	2.257
234	close	1.5	1.865
242	close	7.8	6.324
249	close	2.9	1.573 *
269	open	4.7	3.060
282	close	2.2	2.480
289	open	3.0	3.254
298	open	5.7	3.300
300	open	1.2	2.214
308	open	1.4	3.465 *
309	close	1.0	2.580 **
315	close	4.3	4.370
323	open	1.9	0.779
379	open	10.2	4.880
380	close	7.7	5.080
381	open	4.8	3.474

* “sticking” RVDt produced vertical step in δM - Δ rotrn plot

** example of slightly “concave” δM - Δ rotrn curve

Table 7.2.A. Initial and secant stiffnesses for the 23 chosen events

Analysis of the 23 chosen events suggested that average 'initial' and 'secant' stiffnesses were not greatly different, and that no distinction was necessary between "opening" and "closing" joint responses. Consideration of the RVDT reliability (7.1.3. & 4.) deemed the "average" method to be the most appropriate during these stiffness calculations. From the spreadsheet for all 407 events, secant stiffness varied from 0.779 to 15.694 E9Nmm/radian, with a mean value of 4.082E9.

It should be remembered that each wind event's *change in Moment vs. rotation* curve has a unique origin point, which was not recorded due to the emphasis on 'dynamic' $\delta M - \Delta \theta$ measurements. These "local" $\delta M - \Delta \theta$ plots can be considered to lie on a "global" $M - \theta$ curve for the joint, their position defined by their individual origin points. As such, the 'initial' and 'secant' stiffnesses for each wind event response depend on the position of the local curve along this global curve. Since these origin points are unknown, and since the average values for 'initial' and 'secant' stiffnesses were similar, it might be deduced that the shape of the global $M - \theta$ curve is also slightly curvilinear (at the serviceability level), but less curved than the Figure 7.1.1. might suggest.

These calculations showed that a reliable estimate for the stiffness of the full scale, on-site joint, in both "opening" and "closing" modes, was 4E9 Nmm/radian. Comparisons are made with the results of the laboratory tests (Lee, 1993) in Section 8.2.

7.3. LATERAL DISPLACEMENT of KNEE JOINT

The lateral "sidesway" of the frame (Δ_{knee}) was derived by applying the "baseline correction" ('BLC') method to the acceleration record of a single accelerometer mounted horizontally on the knee joint (Section 5.5). Twenty four of the "ten second records" were analysed, and the results are seen in Table 7.3.A. below. These contained a total of 67 'significant' wind events, and were chosen from the largest and "best correlated" events, and included those 23 used in the previous δM - Δ rotn and stiffness analyses (Sections 7.1. and 7.2.).

The application of the 'BLC' method for the purposes of this study was approximate, and some judgement was used in choosing the "baselines" used to correct errors introduced during the double integration of the acceleration record. Three choices were made for the position of this baseline, based on inspection of the "raw" curves of frame displacement and velocity. The greatest positive and negative offsets from each of the baselines were recorded, which represented estimates for the "peak responses" of the lateral frame displacement at the knee (Δ_{knee}). The "range" of values was the difference between these extreme values. The maximum values over the three BLC analyses were then recorded for each of the 'max. +ve', 'max. -ve' and 'max. range' of frame sways. (Note that the "maximum range" is always exceeded by the difference between the two maxima with this approach).

The "range" of Δ_{knee} varied the least of these three, and was least affected by the subjective choice of baseline, as it remained relatively unaffected by 'flat' or very steep sections of the raw displacement-time function. These features tended to exaggerate some estimates for the peak positive or negative Δ_{knee} values, and were rejected.

event numbers	date/time (filename)	max +ve Δ_{knee} (mm)	max range of Δ_{knee}	max -ve Δ_{knee} (mm)	form of raw 's' curve	δ Moment (kNm)
89-90	10a356	3.1	5.8	-3.5	steady drop	-4.66
134	12a1258*	0.8	1.4	-0.7	steady rise	-5.40
136	12a1259	5.5	7.2	-4.0	rising	7.28
160-1	12a116	5.8	10.1	-4.3	rising	5.93,-3.89
194-5	12a140	3.0	4.0	-1.5	rising	-3.17,3.05
201	12a151	1.8	3.7	-2.7	"U"-curve	3.60
204-8	12a152	1.5	2.0	-1.3	drop	4.89,-4.80
222-5	12a204	4.7	5.4	-1.1	drop	2.98,-3.30
232-6	12a210*	7.0	10.7	-5.0	drop	9.28
242-7	12a210c	3.4	4.7	-4.4	rising	-4.97,4.32
252-7	12a210b	1.7	4.8	-4.0	drop	3.87,-5.94
269	12a218	1.2	2.0	-1.6	rising	5.06
274-5	12a220	4.1	5.4	-2.0	inverted "U"	4.59
282-4	12a222	3.4	4.4	-2.4	rising	-3.36,4.46
287-90	12a303	2.4	3.2	-2.0	rising	6.33
296-8	12a515*	3.6	4.6	-2.7	"U"-curve	6.49
307-8	12a634*	1.4	3.5	-3.0	rising	4.87
309-11	12a640	2.5	3.0	-1.0	rising	5.59
352-3	28s357	2.0	2.7	-2.1	rising	-1.97,2.24
355-7	28s401	1.3	1.8	-0.6	drop	2.61,-2.63
376-7	28s411	1.6	2.1	-0.9	drop	2.36
378-381	28s412	1.3	2.8	-2.0	rising	4.47
382	28s412b	1.8	3.0	-2.4	rising	2.52
398-9	28s435	1.4	3.4	-2.8	rising	2.23,-2.57

"filename": first three characters give date, others give time in 'pm'. e.g. '10a356' = 10 August, 3:56pm event.

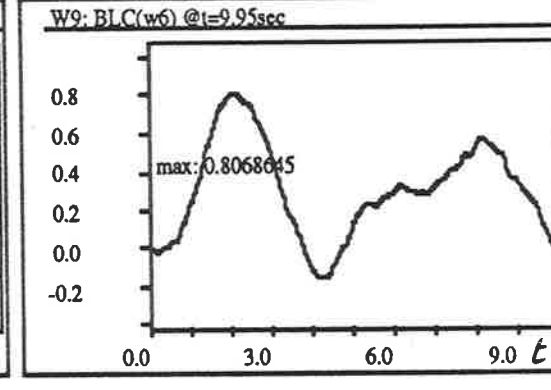
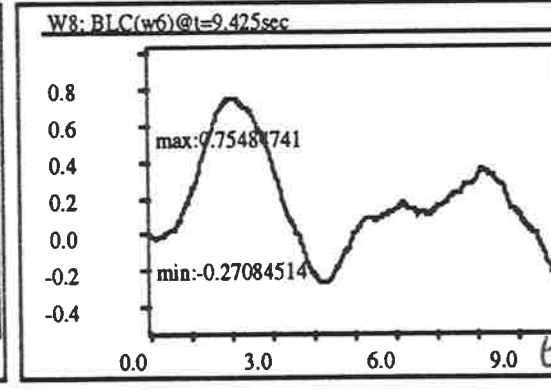
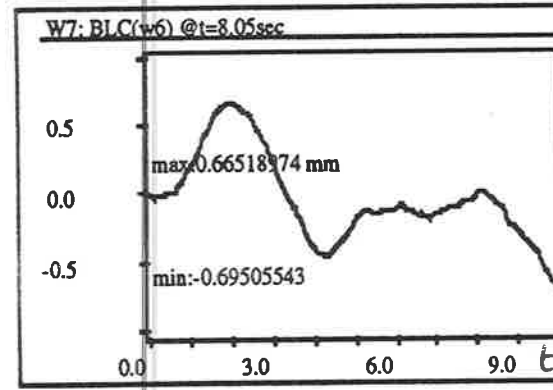
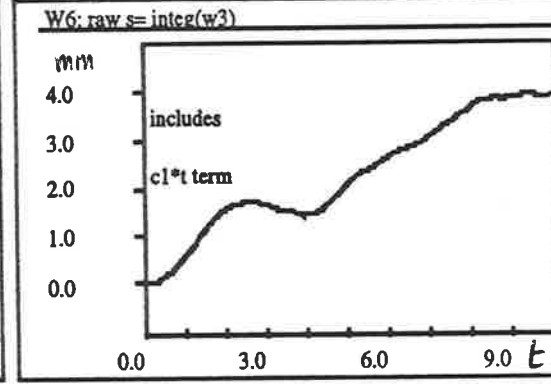
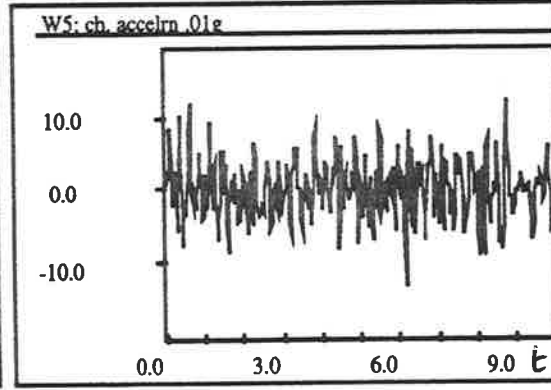
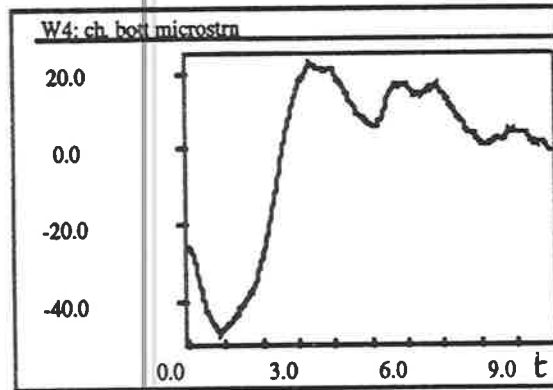
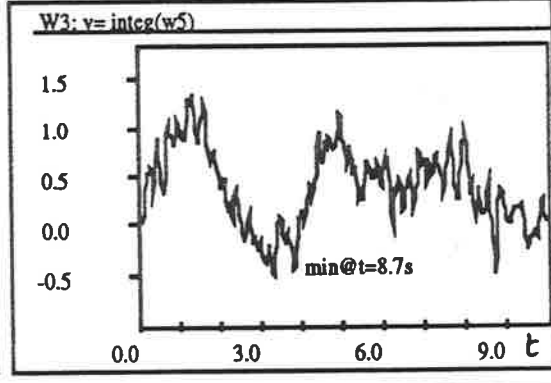
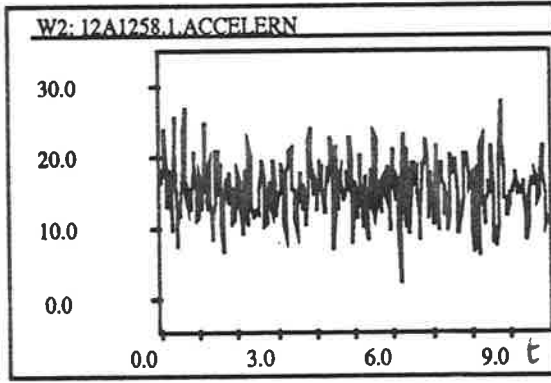
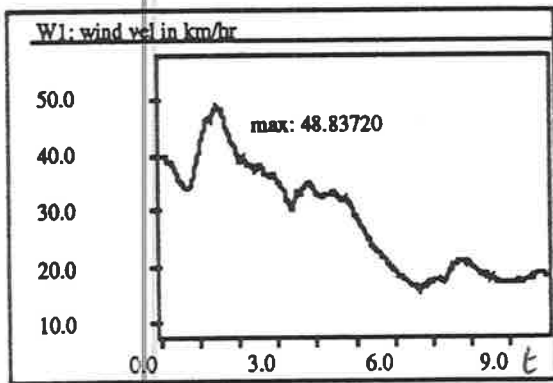
Table 7.3.A. Lateral displacements for selected events using the BLC method.

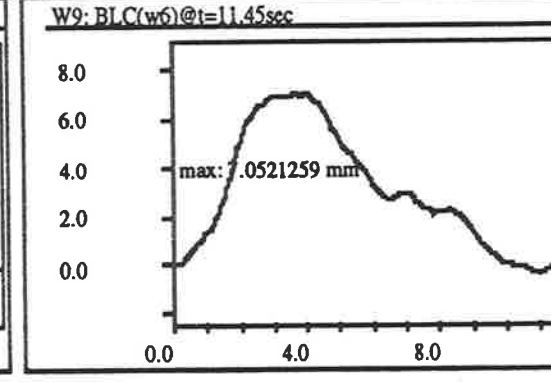
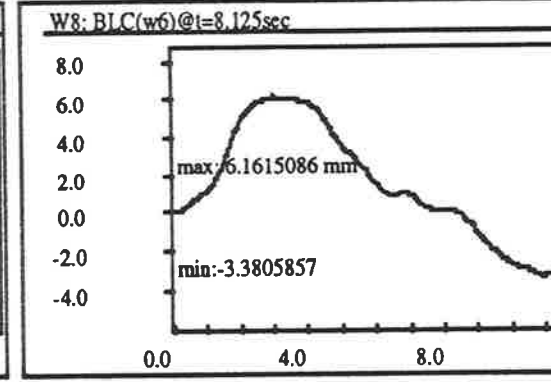
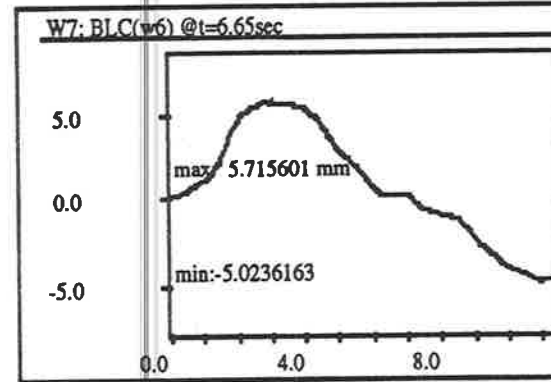
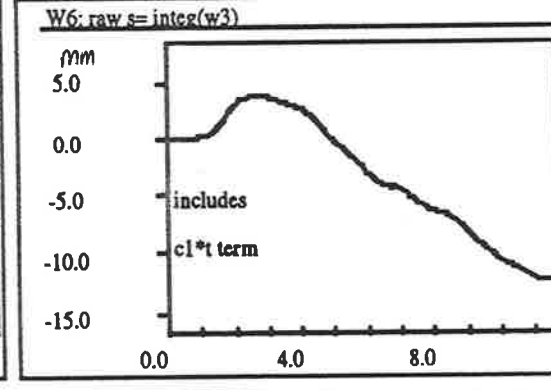
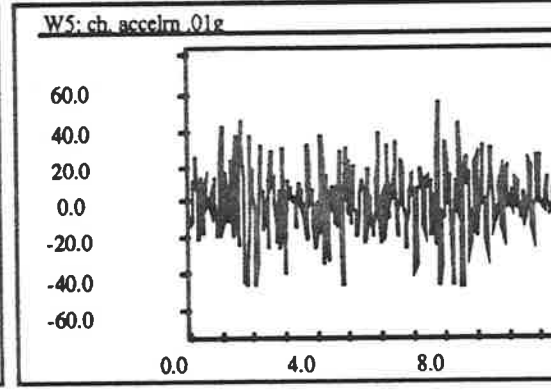
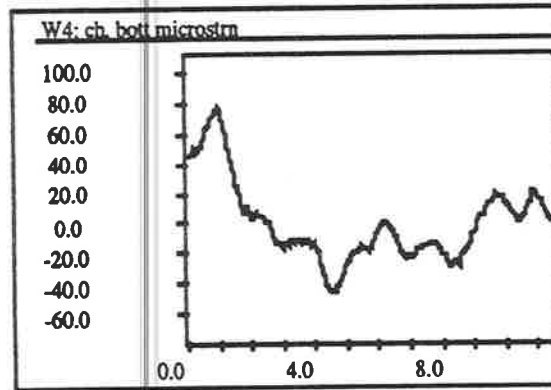
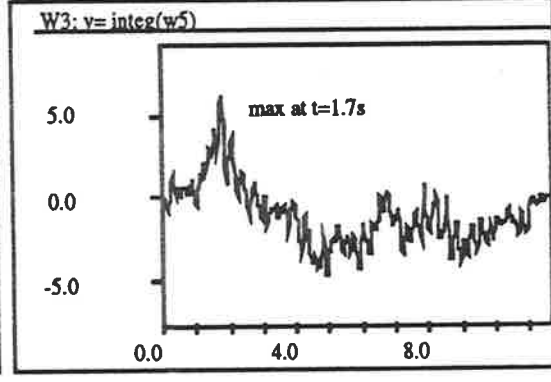
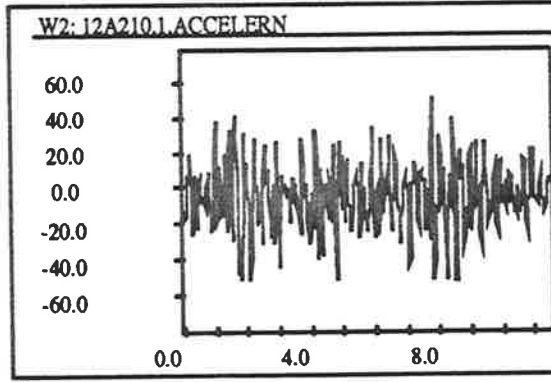
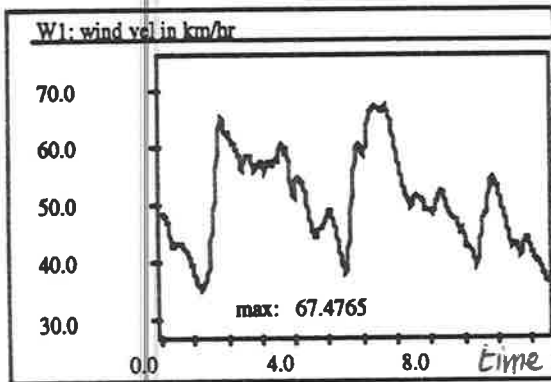
The accelerometer record contained an arbitrary DC offset, which was 'zeroed out' at the start of each recording session, but due to signal drift and electrical noise etc., this was invariably non-zero. Subtracting the mean of the "raw" signal provided an initial zero baseline for the integration process, and was seen as a reasonable assumption for a ten second period acceleration record. This was confirmed by the integration of this record (i.e. "velocity"), which returned to near zero at the end of all 24 data records.

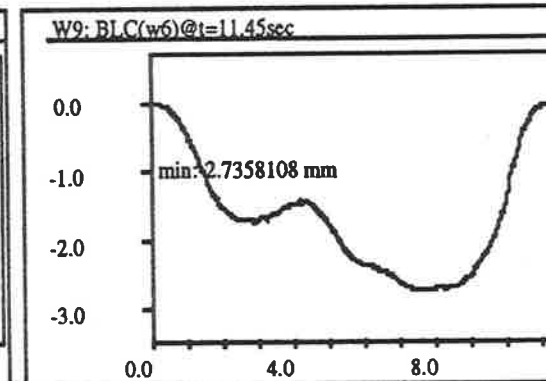
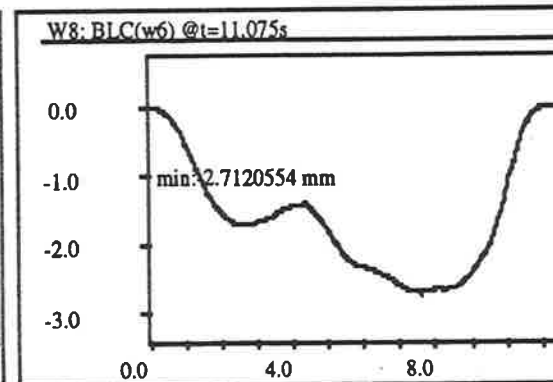
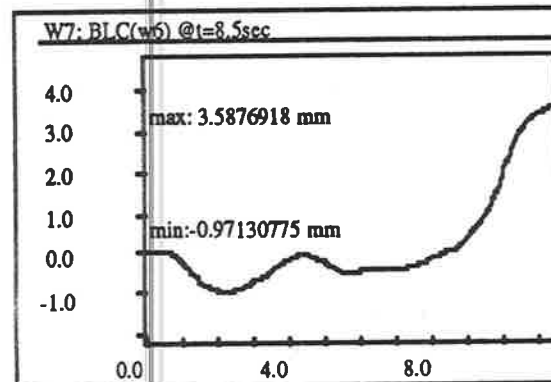
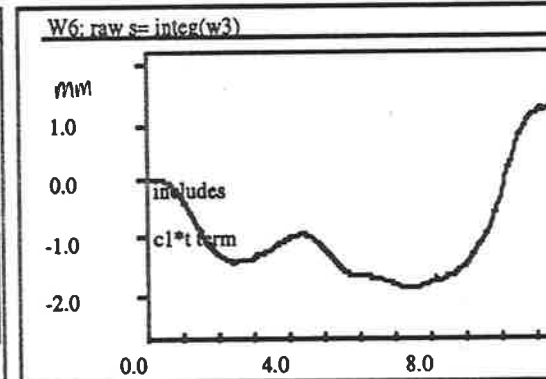
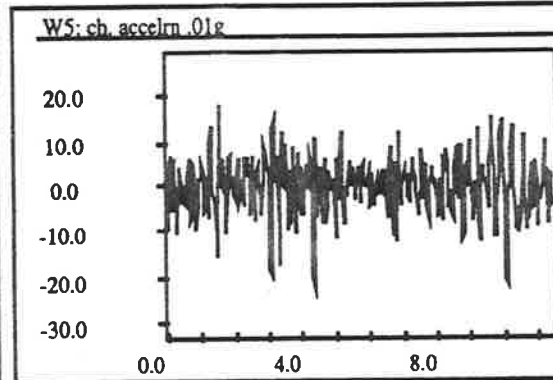
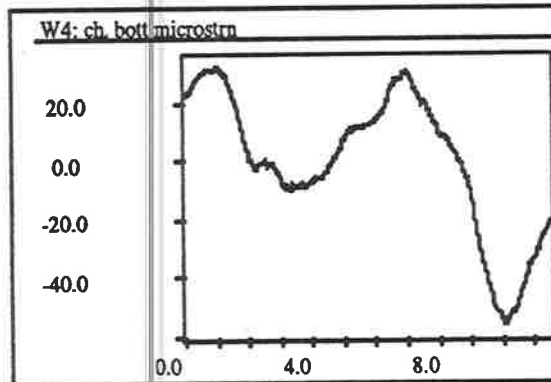
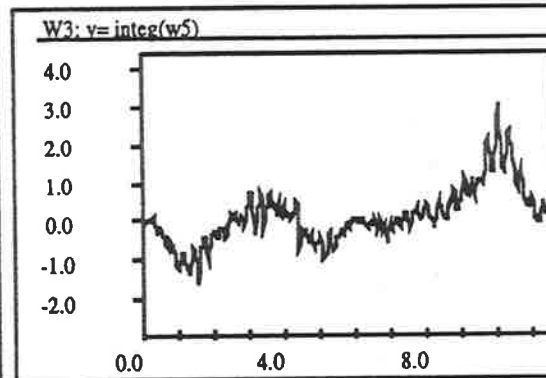
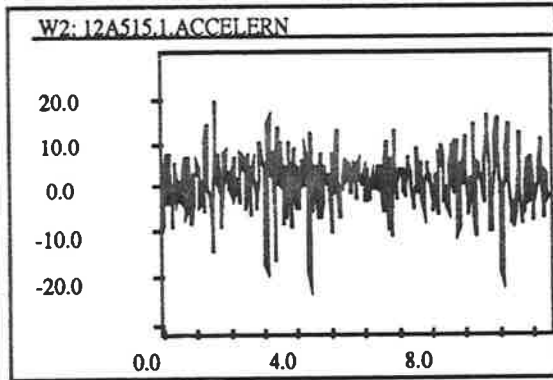
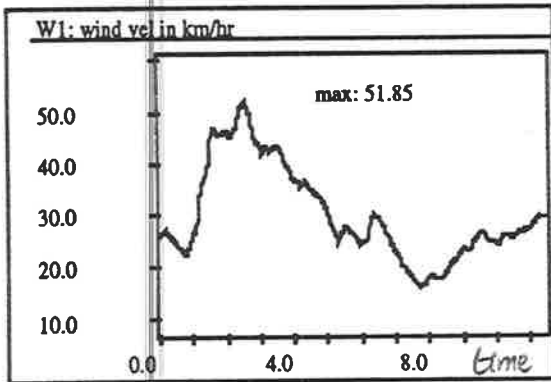
A zero velocity could be expected to indicate a reversal (and peak) of frame oscillation, and the selection of this time point as the 'end point' for the corrective baseline helped to reduce integration errors and provided a good result.

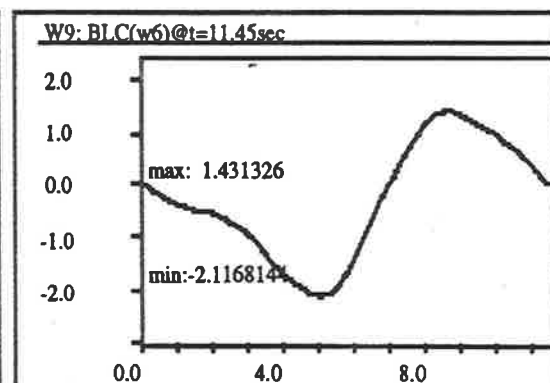
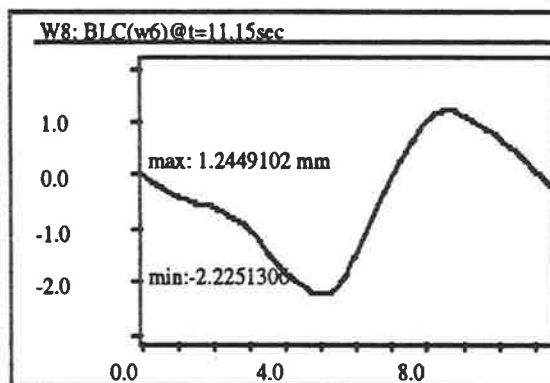
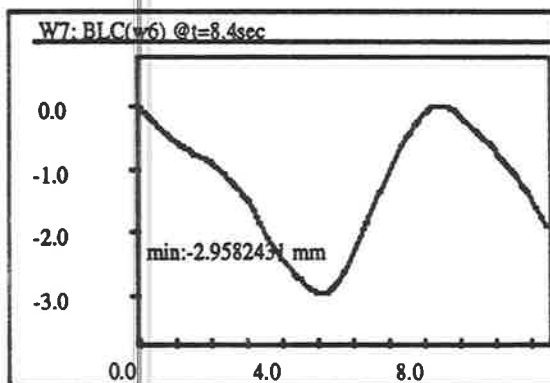
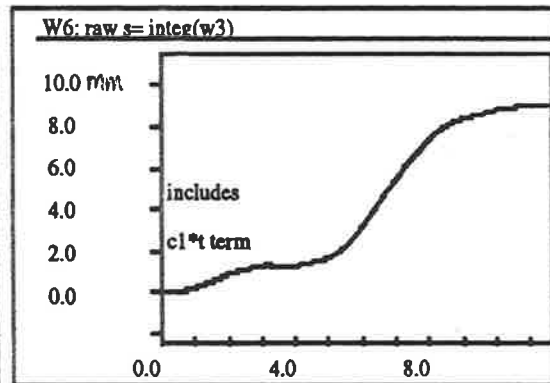
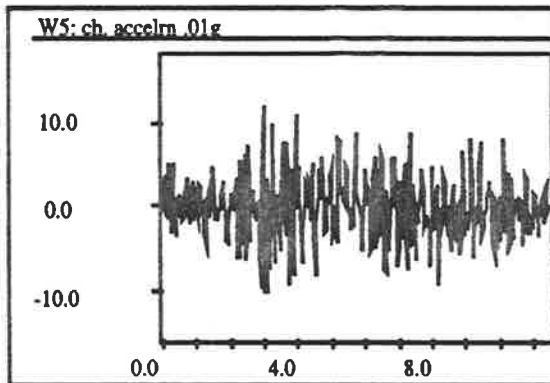
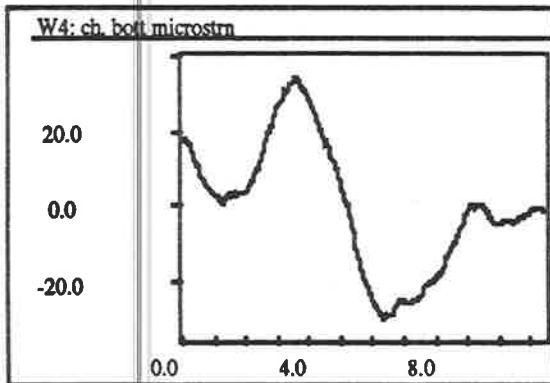
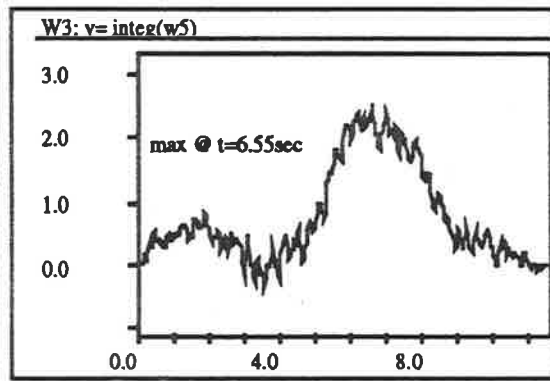
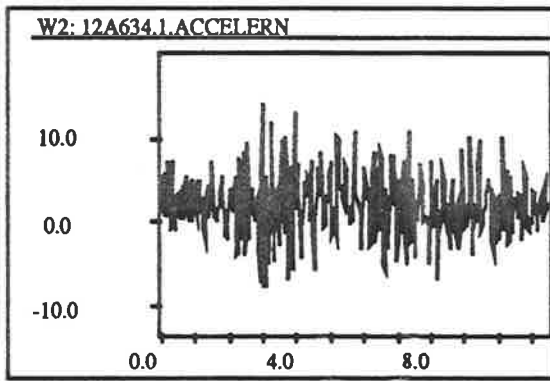
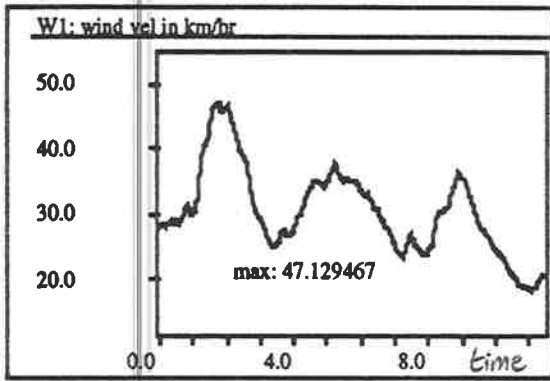
The results presented in the Table 7.3.A. were generated using the DaDisp™ data analysis package. Four printouts are shown overleaf, as examples of the "baseline correction" method. Nine 'windows' of data are shown, as outlined below:

W1: wind speed (km/hr) converted from the anemometer record.	W2: raw acceleration record, with filename (derived from the date and time of event)	W3: raw velocity, found by integrating the W5 "change in acceleration" record once
W4: "change in bottom rafter strain" (microstrain), used to calculate δ Moment	W5: "change in acceleration" found by subtracting the mean from the W2 record	W6: "raw" displacement (s) record, found by integrating the W3 'velocity' record
W7-9: three baseline corrections applied to the raw 's' record, the "c ₁ t" linear function defined from the origin to a point selected from inspection of the raw displacement and velocity records. "BLC(w6) @t=11.45s" means that this BLC line passed through the raw displacement record at the time point of 11.45 seconds. Maximum '+ve' and '-ve' Δ_{knee} values were measured from this "corrected" baseline, labelled on the W7-9 plots.		









7.3.1. An INDEPENDENT CHECK on the BLC METHOD.

As an attempt to verify the "baseline corrected" results above, the values for "maximum range" of lateral frame sway (from Table 7.3.A.) were plotted against the associated "maximum change in Moment" for the 24 nominal ten second data periods. A correlation might be expected since both structural responses share the same cause and occurred concurrently. A reliable body of data had been collected for the rafter strains (and hence moments), and the accuracy of the resultant moment-rotation plot had not been unduly affected by the variable correlation of the RVDT signal to that of the strains (Section 7.1.). Therefore, the more reliable strain data was used as a basis for comparison.

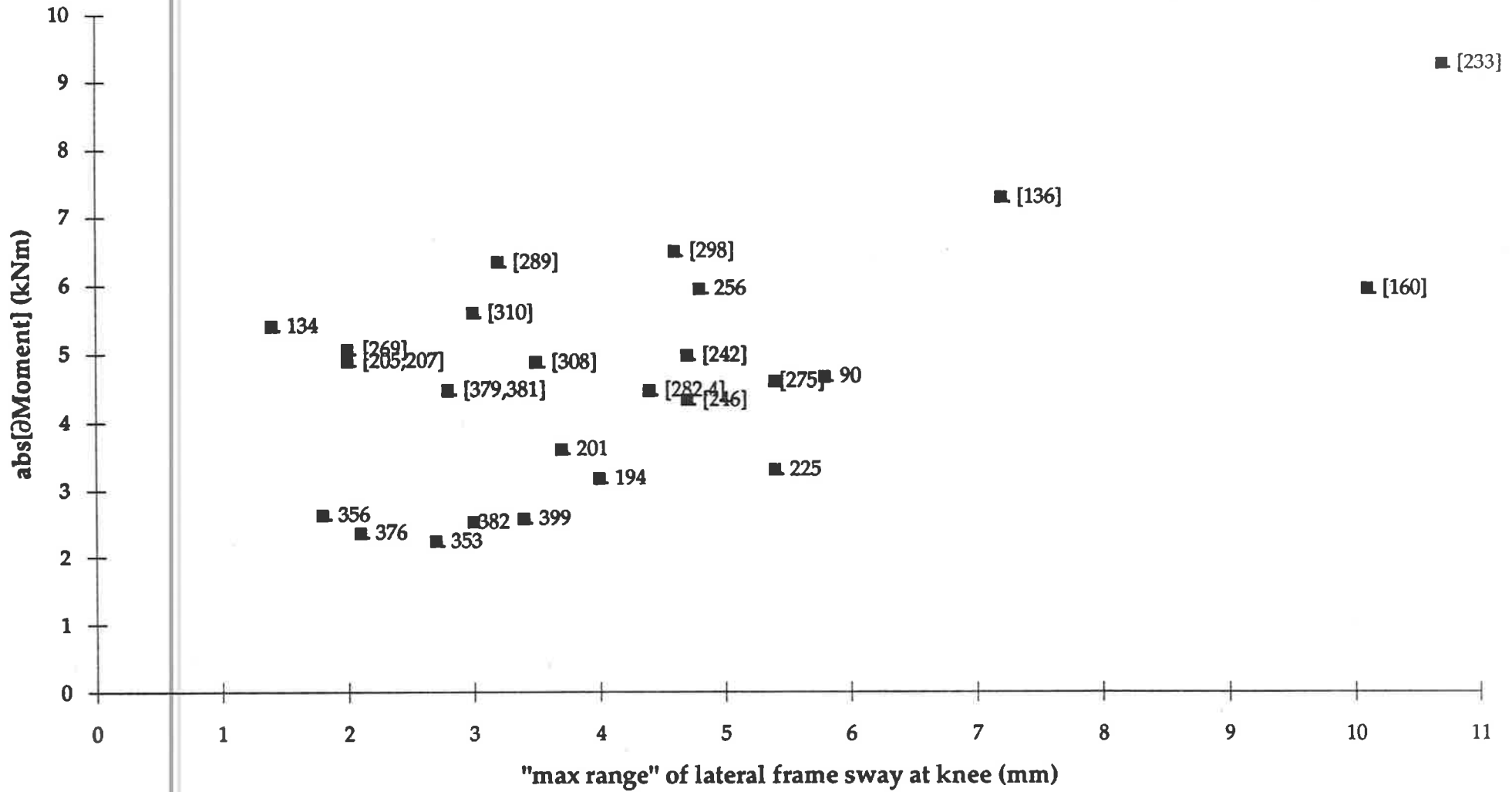
"Change in Moment" was plotted against both "lateral frame sway at knee" and " Δ rotation" for the 24 selected data records, and are shown overleaf. Since the "maximum range" values were not 'sign-specific', both δ Moment and Δ rotation were converted to absolute values for the purposes of this comparison. All event numbers are labelled on the 'frame sway' graph, with bracketed event numbers also shown on the 'rotation' plot. All of these 67 events also appeared on the overall δM - Δ rotrn plot of all 407 events (Figure 7.1.1.), while the bracketed event numbers were also labelled on the "opening" joint (positive quadrant) excerpt of this plot (Fig. 7.1.2.).

This comparison provided very similar results, with the general form of the δM - Δ rotrn plots repeated in the " δ Moment- Δ_{knee} " graph. Correlation between the two graphs was very good for the largest events, of about 4.4 kNm (\approx 55 microstrain) or more. It showed that ± 1 mm would be a good estimate for the Δ_{knee} error. Also, since the moment-rotation plot was merely an excerpt from the overall "407 events" plot, this correlation for the larger events suggests that an expanded Δ_{knee} analysis would produce a similar correlation for *all* events. This led to an increased confidence in the "baseline" corrected results, and inferred greater reliability in the rotation data, since a poor performance by both the accelerometer and RVDT instruments would not have provided as good a comparison.

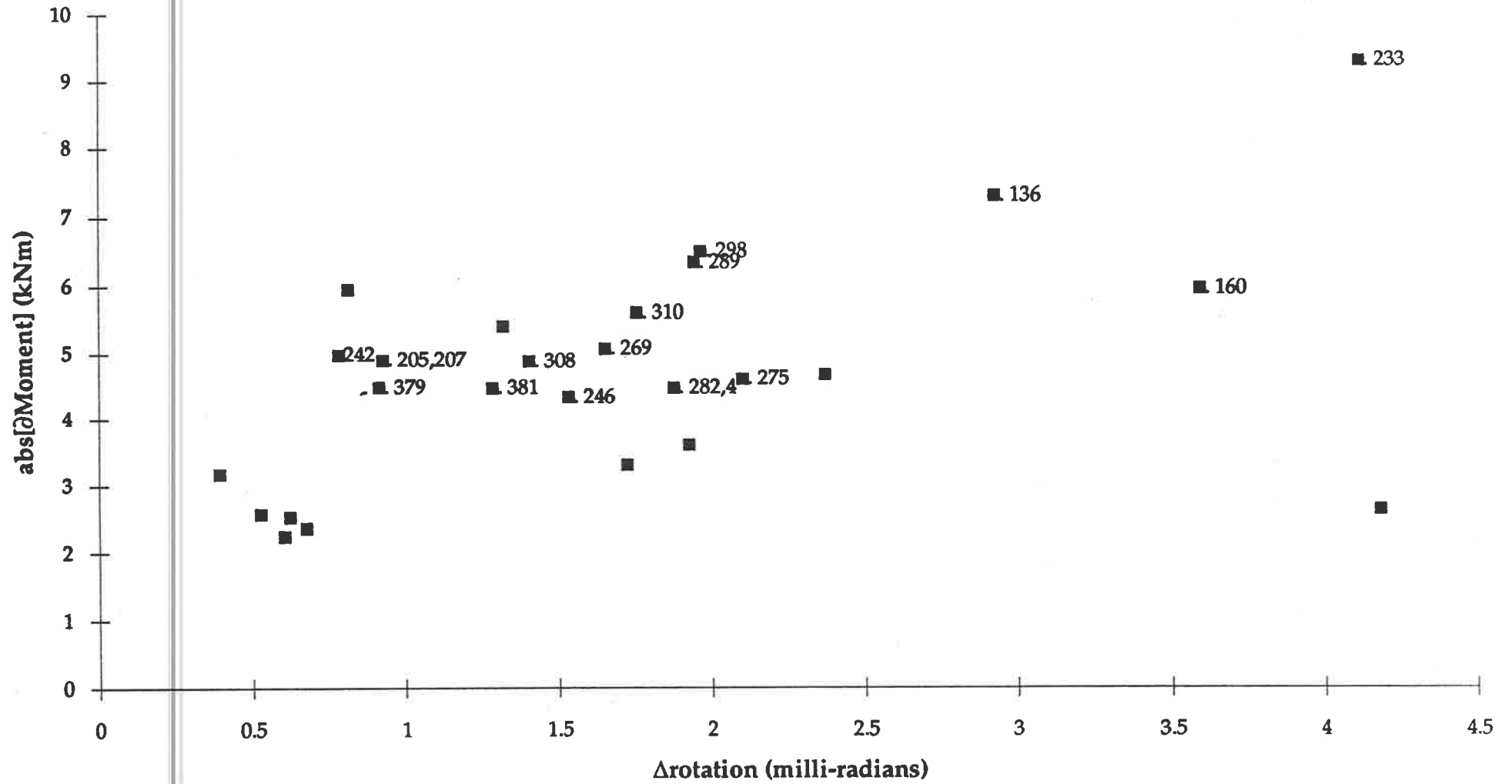
Note that the above was not an argument of syllogism, since all three structural responses used in the comparison (strain, rotation and acceleration) were measured with independent instruments and occurred simultaneously (with a shared driving action -wind).

A maximum lateral frame displacement of approximately 10 millimetres was recorded for two events, and many in the order of 5 to 6 mm, for average ("two second gust") wind speeds predominantly in the range of 42 to 60 km/hr.

abs[∂Moment] vs max range of frame sway



abs[∂Moment] vs Δrotation



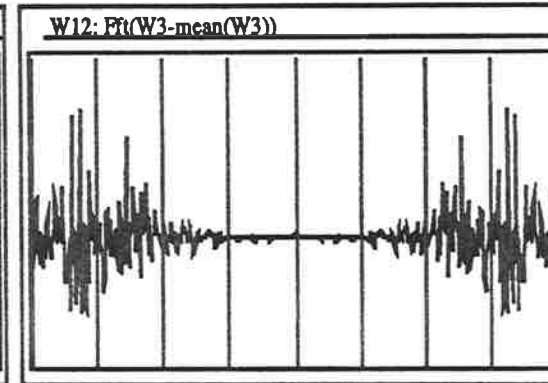
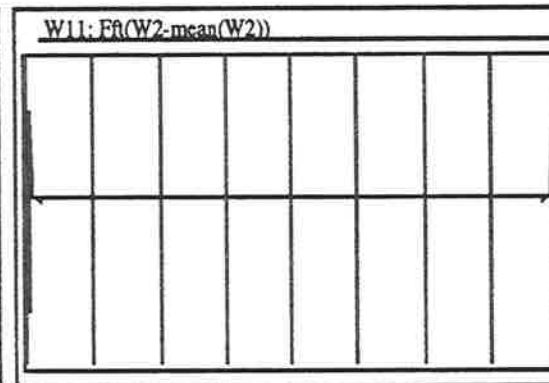
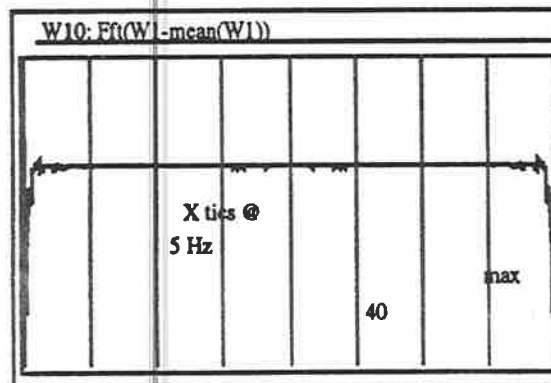
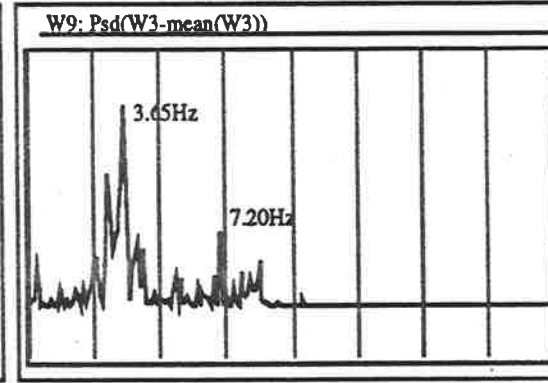
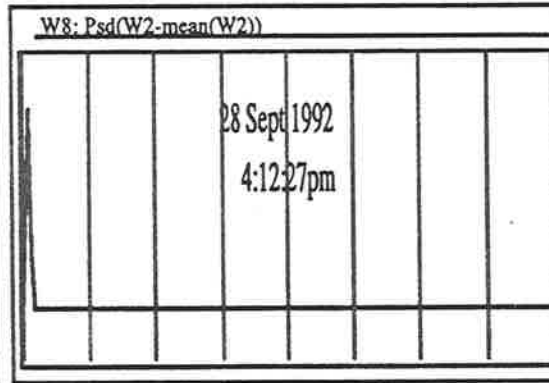
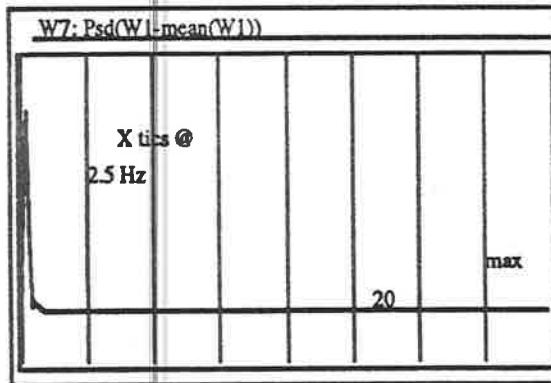
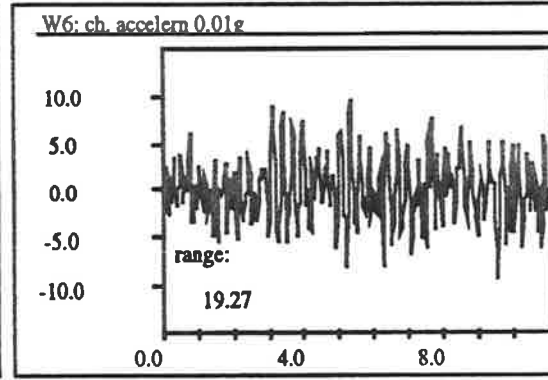
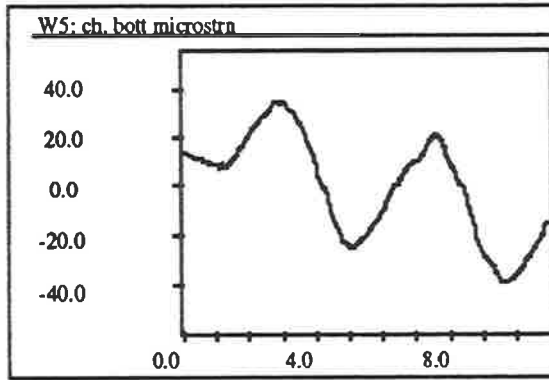
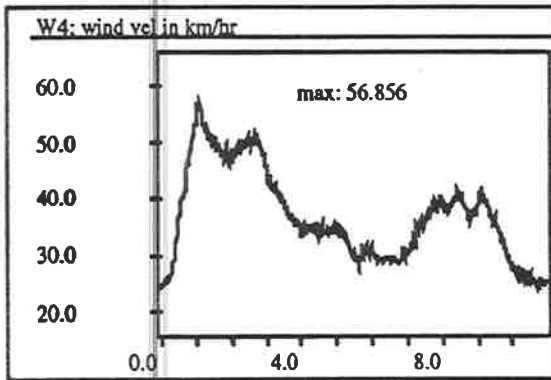
7.4. FREQUENCY of RESPONSE

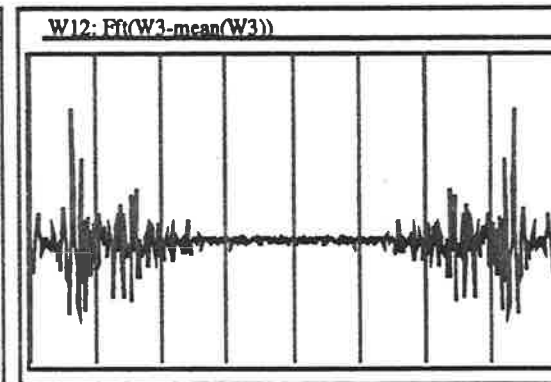
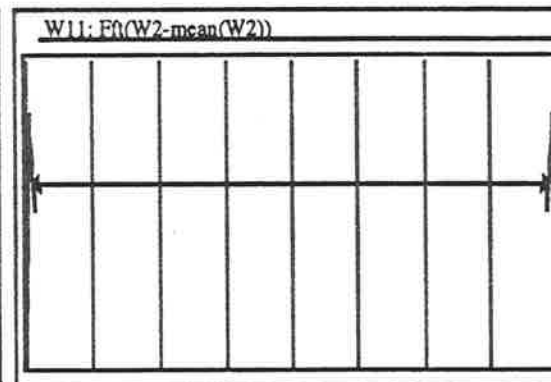
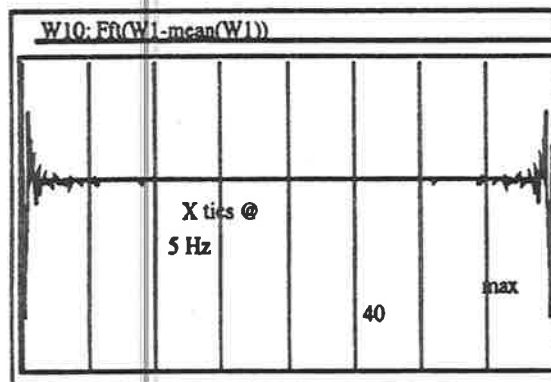
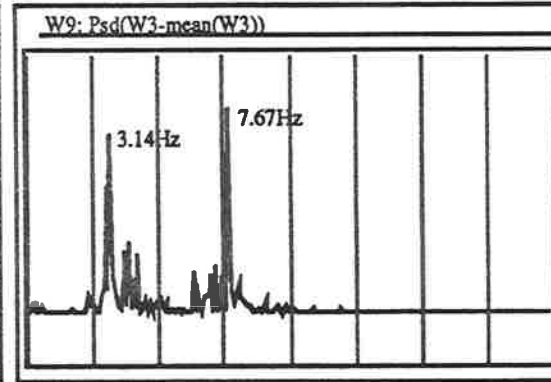
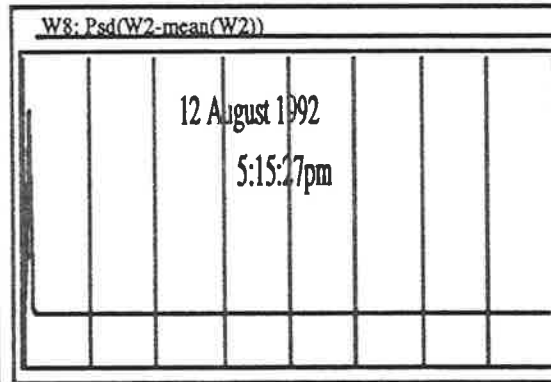
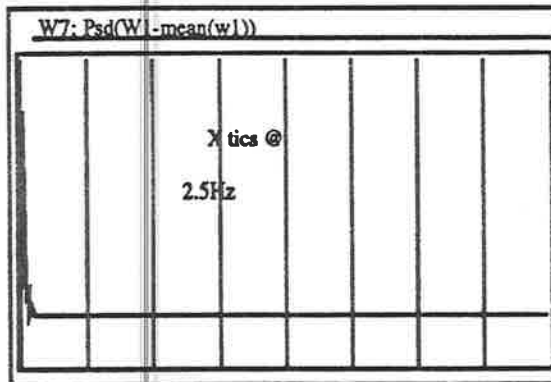
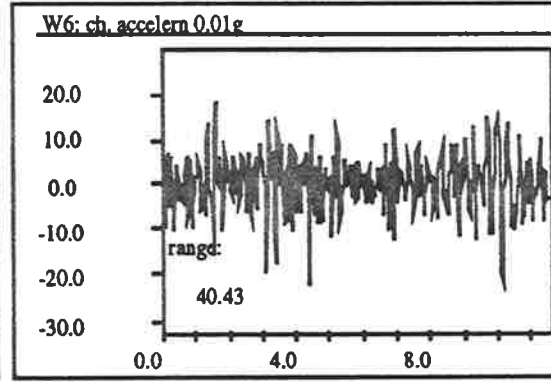
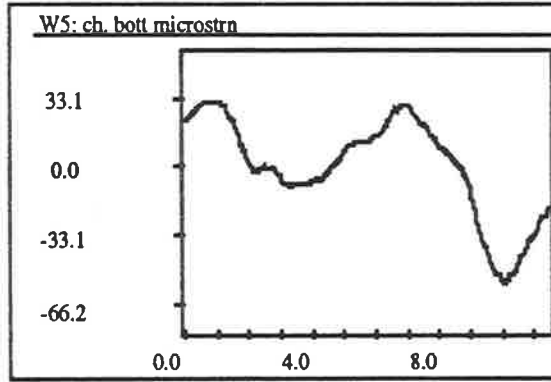
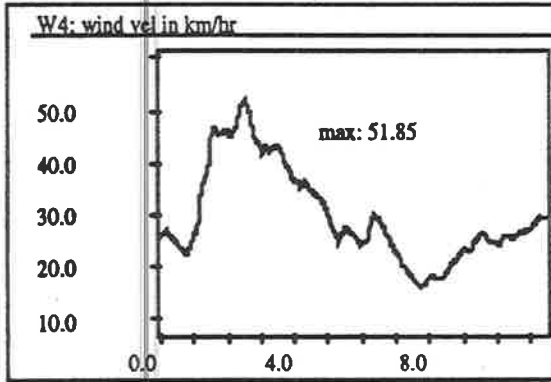
Klopp and Griffith (1992) developed a method for obtaining the modal frequencies of response for low rise structures utilizing only ambient vibrations, as part of their investigation into the earthquake effects on unreinforced masonry buildings. They showed that large scale events such as earthquakes and high level wind were not required, and that building oscillations due to traffic and ambient wind were sufficient. Fast Fourier Transforms (FFT) of accelerometer records at each storey level provided reliable frequencies for each oscillatory mode of response. This analysis method was adapted for the 'single-storey' structure in this study.

Power spectrum distributions (PSD) and Fast Fourier Transforms (FFT) were carried out on the wind action and two responses, bottom rafter strain and joint lateral acceleration. For the latter, the signal from the single horizontal accelerometer was used, as described in the preceding Section 7.3. PSD's were seen to correctly approximate the positive values for the lower frequency half of the FFT analyses. Several examples are given overleaf, with FFT's covering the range 0 to 40 Hz, and PSD's from 0 to 20 Hz.

The analyses of the acceleration output show that the first two modal frequencies of the building fall in the ranges 3.2 to 4.2 Hertz and 7.2 to 7.6 Hz. This result was not reflected in the similar analyses of the wind action or strain response signals. Curtailment of all the signals occurred at the 11.5Hz "filter" frequency, preventing the reliable measurement of the third mode frequency.

Section 7.4 is deleted





FEATURES

Reeling from nature's fury

By LEANNE WEIR

It was a rocky, sorry year for South Africa in 1992 but, while we lament the loss of life, property and agricultural earnings induced by the big war, spare a thought for those who endured even greater suffering nature's hands.

Much of the bizarre and severe weather experienced all over the globe in the past two years has been attributed to an drought-causing El Niño effect - an unpredictable, cyclic phenomenon occurring about every 10 years, caused by changes in air and sea surface temperatures in the Pacific ocean.

During the 1991-92 El Niño, Pacific surface temperatures rose by 7C to 10, 3C. This increase weakened the trade winds which normally carry moisture to eastern Australia and south east Asia, resulting in widespread droughts and heatwaves early last year. Global weather patterns which led to drought in Africa and floods throughout the American continent also have been linked to El Niño.

When El Niño abates, as it is doing now, there is a 50 per cent chance it will be followed by La Niña, the opposite swing of the cycle. When ocean surface temperatures cool, trade winds carrying moisture increase, resulting in wet conditions in eastern Australia, southeast Asia and Africa and drier conditions in the American continent.

Some say the effects of El Niño and La Niña have been compounded by human interference with the earth's natural balance. In particular, the release of greenhouse gases into the atmosphere, believed to cause global warming.

Other natural events are adding to our woes. In the northern hemisphere, volcanoes in the northern hemisphere of Mt. Pinatubo, which soared high into the atmosphere, was blamed for some of the coldest and wettest winters on record in the northern hemisphere - a trend expected to continue this year.

Another less-conventional theory on our crazy climate is that the

Puerto Rico, claiming at least 20 lives. On the other side of the Atlantic, South Africa and its neighbouring nations lamented their driest January in 30 years, with more than 15 per cent of maize harvests lost.

FEBRUARY

Drought continued to plague the African continent. The Kenyan capital, Nairobi, suffered its biggest water short- age.

MARCH

The US reported its warmest winter in Zimbabwe, the prolonged droughts were declared a national disaster. The drought was last declared the worst in recorded history.

APRIL

Wild winds and waters ripped through south-east China, resulting in 18 Good deaths and about 600 injuries. A later thunderstorm which lashed Hunan in southern China caused almost 100 deaths. The weather pattern was duplicated in the United States when floods in North Carolina and parts of Virginia killed 21 people.

MAY

Alarming records were set. England suffered its worst drought since 1749, forcing officials to ration water to 45 million people. Parts of the north-western US also were in the grip of their worst water shortage. Hong Kong, on the other hand, had its worst floods in 34 years. In the southern Brazilian State of Paraná, eight people were killed by a tsunami.

JUNE

The climatic nightmare became more complicated with a combination of flood, drought, cyclones and heatwaves. The onset of the south-west monsoon in Sri Lanka brought the worst Dombro, forcing 250,000 people from their homes. About 250,000 people endured more rain than at any other time this century. In contrast, Thailand endured its hottest six months on record through the first half of 1992. Due to the El Niño effect, an unprecedented drought swept the south Pacific and South-East Asia dried up New Zealand's lakes, leaving residents with months of water cuts. The southern hemisphere was not spared. Northern

Hurricane Az south Florida's 10 people. With a of 123 billion dollars disaster, the northern hemisphere's coldest floods in Venezuela.



Explanations range from scientific theories and educated guesses to bizarre hunches -

Comparisons of Results

8.1 COMPARISON with STRUCTURAL MODEL

Any attempt to compare the measured and predicted responses for a particular wind gust must assume the level of wind loading responsible for any measured response. Throughout the study, building responses were seen to be dynamic, and the result of the constantly fluctuating 'driving' frequency and magnitude of the wind loading. The uniqueness of the profile of each 10 second wind gust foiled any attempt to identify and compare similar gusts, and the frame responses they caused. In this way, establishing a link between wind action and building response was hampered by the "approximate" method employed to record the wind effects (5.4), and to a certain extent the "triggering" of data collection relative to high velocity winds. The latter tended to optimize the recording of responses, but it was not until late in the study (September 1992) that sufficient 'pre-triggering' was used to record the wind and response "before" scenario, prior to the loading of the frame by each wind gust (5.1.4).

No simple correlation between the measurements for wind action and structural responses was found (7.1.2., 7.4.). Since the 'wind speed-structural response' link was not the primary focus of the study, and as no correlation was easily found, only the following preliminary analysis was undertaken.

Predictions for the structural responses were calculated in Chapter 6 by applying the Australian Wind Loading Code design loads to a structural model developed using a conventional computer analysis package, IMAGES-3D™. The moment resisting joint was modelled as a linear rotational spring of stiffness K_{θ} . Responses were calculated for two values of this spring constant, the second of these using the "refined" estimate of $3E9$ Nmm/radian, derived during the laboratory tests (Lee, 1993).

The frame loads and deformations output by the computer model corresponded to a constant stream with a 1 kPa dynamic pressure q_z . Responses for a reference 100 km/hr ($q_z = 0.463$ kPa) event are shown in Table 8.1A below, from which predicted responses for lower velocities are obtained using the ratio of squared velocities (from Chapter 6).

Wind Events 233 and 160 were identified in Chapter 7 as examples of the typical "large event" recorded during the field measurements of the study, and were associated with average "2 second gust" wind speeds of 58 and 53 km/hr respectively. From an inspection of the data records, a measured change in rafter moment (δM_{rafter}) of approximately 6 kNm might be expected for a similar Westerly 55 km/hr event. The scaled IMAGES-3D™ model output (for $K_{\theta} = 3 E9$ Nmm/rad) gave an estimate of $M_{\text{lot}} = 11.8$ kNm for this wind speed.

	IMAGES-3D™ analysis for $K_{\theta} = 3E9$ Nmm/rad		field measurements	
	West	West	Event 233	Event 160
	100 km/hr	55 km/hr	WNW	W
opening M_{rafter}	38.9 kNm	11.8 kNm	9.28 kNm	5.93kNm
opening θ rotation	16.610 millirads	5.025 millirads	4.111 millirads	3.593 millirads
opening Δ_{knee}	36.0 mm	10.9 mm	$\Delta = 10.7$ mm +7.0,-5.0	$\Delta = 10.1$ mm +5.8,-4.3

Table 8.1A. Comparison of structural model estimates and measured changes in structural responses

However, the instrumentation system used in the full scale field measurements recorded *changes* in structural responses due to wind loading only. As such, they were associated with the *changes* in wind speed, whereas the model estimates were based on *absolute* wind speed, thus providing a "total" wind load response".

An approximate extrapolation method was used in Griffith et al (1992) to estimate the "total wind load moment" from the measured "change in moment due to wind load". This indicated that the estimated "total wind load moment" would generally be about twice the measured *change* in rafter moment (Table 8.1.B.), giving a total moment of 12 kNm for the typical Westerly 55 km/hr event above. This estimate compared favourably with the "55 km/hr" total moment predicted by the computer model of 11.8 kNm.

From Griffith et al (1992), the estimation function was:

$$\text{total } M = \text{"base wind" Moment} + \text{measured change in Moment}$$

It was assumed that this "base wind" Moment was caused by the "base" level of wind above which the change in wind speed (and hence moment) occurred, and that it could be estimated from the ratio of base wind speed and change in wind speed:

$$M_{\text{total}} = M_{\text{basewind}} + M_{\text{change}} = \frac{V_{\text{base}}}{V_{\text{change}}} M_{\text{change}} + M_{\text{change}}$$

This was calculated for six wind events of high δ Moment in Table 8.1B. below. However, no simple correlation was found between frame moment and any of the wind speed characteristics, of peak gust speed, average "2 second gust" speed or change in wind speed.

	12a210	12a116	12a515	12a1258	12a634	12a303
	Event 233	160	298*	134	308	298
δ Moment	9.28 kNm	5.93	6.49	-5.40	4.87	6.33
(1) "base" speed	42 km/hr	40	25	18	27	25
(2) pre-lull speed	40 km/hr	37	24	38	28	25
(3) "peak" speed	65 km/hr	56	52	49	47	48
(4) "2s ave gust"	58 km/hr	53	46	46	45	47
(5) post-lull speed	42 km/hr	48	18	18	26	37
(6) $\delta v_{\text{pre}} = (4) - (2)$	18 km/hr	16	22	11	17	22
(7) $\delta v_{\text{post}} = (4) - (5)$	16 km/hr	5	28	28	19	10
(8) $\delta v = \max(6,7)$	18/km/hr	16	28	28	19	22
$M_{\text{base}} = \delta M \frac{(1)}{(8)}$	24.4 kNm	14.8	5.8	3.5	6.9	7.2
M_{total}	33.6 kNm	20.4	11.3	-1.9	11.8	11.6

* seen in Griffith et al (1992) as "Figure 2".

Table 8.1.B. Estimates for "total" Moment due to wind load.

For the relevant wind gust, a "2 second" average (4) was calculated and changes in wind speed were measured relative to this level. δv_{pre} (6) and δv_{post} (7) were calculated using the average speed of the pre-gust "lull" in wind loading (2) and post-gust "lull" (5) respectively. The maximum of these two became δv (8), used as v_{change} in the expression above. The magnitude of the change in wind speed (δv) rarely exceeded the "base" level wind speed, so even *total* moments due to wind loading were measured at 12 kNm or less in this study, with an estimated maximum of 34 kNm.

The maximum "total wind" moment of about 20 kNm was significant in comparison with the AS1170 'ultimate' wind load moment of 133 kNm. The fatigue effects of the repeated application

of this common load (say several thousand times per year) are discussed in detail in the companion work of Lee (1993), whose loading regimes are illustrated in Figure 8.2.1. Fatigue performance of the Yttrup Joint was excellent under (non-reversed)cyclic loading up to three times "ultimate wind load" levels. Therefore, the effects of these serviceability level wind events was expected to be insignificant.

Overall, the larger events recorded in this study may be summarised as a typical wind event having a "2 second gust" speed of 50-60 km/hr, and a change in wind speed of 20-25 km/hr, producing a change in moment of 6kNm within a total wind load moment of 12 kNm. The "total wind" moment was seen to be between two and three times that of the *change* in moment.

However, the model predictions for the total joint rotation and lateral frame sway correlated less well. To have corresponded well with the average measured values, the model should have predicted a total rotation of $2 \times 3.85 = 7.7$ m/rads and a total sway of $2 \times 6.4 = 12.8$ mm. Nevertheless, the model 55 km/hr predictions of 5.03 m/rads and 10.9 mm did compare well with the doubled values for Event 160 (7.2 and 11.6 respectively). Given the approximate nature of this exercise, it may be concluded that the 2-D computer model possessing a "true" rotational spring stiffness provided reasonable predictions for the "total" joint responses.

Nevertheless, the scaled computer model predictions *under-estimated* the *changes in* responses measured in this study. For instance, both the example wind events used above featured changes in wind speed of about 20 km/hr, but the scaled model predictions at this speed (derived from Table 8.1.A.) fell well short of the measured *changes* in responses. For this reason, it appeared more reliable to compare the "total wind load" responses of the structural model and recordings.

The 'near' or *under-estimation* of building response by the 2-D model was the converse of the expected result, because the considerable stiffening effects provided by the exterior cladding, rigid end bays and bracing were not present in the model. For single story, brick veneer (internal timber frame) structures, it was reported by Reardon (1989) that:

"... conventional^{al} cladding materials, fixed according to the manufacturers' specifications for normal use, play a significant role in resisting lateral wind forces."

Normal internal walls were found to approach the bracing capacity of similarly clad, 'engineered' bracing walls, while *internal lining materials provided a much stiffer bracing mechanism than conventional steel or timber diagonal bracing*". The roof and ceiling were found to act as a stiff horizontal diaphragm, significantly reducing the lateral response. In more lightweight structures such as the conventional "warehouse" (portal frame) building in this study, a similar contribution from the cladding is generally accepted.

The scaling of computer output would not have introduced further error into the estimates since it was based on the AS1170.2 Wind Load Code definition where dynamic pressure (q_2) is proportional to the square of the free stream velocity (Clause 3.3). However, the design Code considerations assume an uninterrupted "free" stream of constant velocity and pressure. The static, "two second gust" implicit in the Code would have been of sufficient duration to load the entire building frame, but the constantly varying nature of the measured wind made the selection of representative gust wind speeds and directions difficult. In addition, the measuring error for all wind speeds recorded in this study would have been amplified by the use of a single anemometer, and its associated "position error" discussed in section 5.4. Nevertheless, errors of nor more than ± 5 km/hr would have resulted from these two influences.

Certainly, a more refined and detailed computer model would have provided more accurate estimates. However, it was felt more relevant to limit the complexity of the model to that level practical during the design of these buildings. Portal frame structures are considered relatively simple by designers and models incorporating the three dimensional effects of cladding, end bays and building length are rarely used. Responses output by these 3D models would have been lower again than those obtained from the two dimensional analysis above.

Quantifying the relationship between the wind loading characteristics in Table 8.1.B and the structural responses of lightweight building would be an obvious extension of this research. It

would be of particular importance, since the design of the Wingfield building was governed by 'serviceability' limit state criteria (e.g. creep deflection under dead load), which were not reliably predicted by the simple computer models typically used during their design (as re-created above).

8.1.1. The EFFECT of K_{θ} VALUES

Portal frame design is typically conducted using the "rigid" joint assumption inherently contained by structural analysis packages. This corresponds to an 'infinite' spring stiffness, and theoretically results in no angle change at the joint. This assumption was used for the non-critical 'ridge' joint in all previous computer models. To test the validity of a "rigid" knee joint, IMAGES 3D™ output for a high value of rotational spring stiffness (1 E12 Nmm/radian) was compared with the previous analyses. This value had been used successfully for the axial and shear "spring" stiffnesses in all the structural models.

$K_{\theta} = 1 \text{ E12}$ gave net rotations at the frame node points approximately 290 times smaller than the "3E9" results, as expected from the K_{θ} ratio of 333. Lateral frame sway (Δ_{knee}) at the 'East' and 'West' nodes were seen to approach equality for increasing "rigidity" of the joint. For K values of 3E9, 20E9 and 1E12 Nmm/radian, the (critical) Western joint deflections were 15.57, 5.0 and 3.0 mm/kPa/m width respectively, for the General Loading Case of a 1kPa Westerly wind stream applied to a unit frame width. For the full 5m frame width, the three models predicted sways of 36.0, 11.6 and 6.9 mm for a nominal 100 km/hr Westerly event. Output for the "rigid" joint case is tabulated below, showing the 1kPa output converted to a nominal 100 km/hr (0.463 kPa) event:

		$K_{\theta} = 1 \text{ E12 Nmm/radian}$	
		WEST WIND	NORTH WIND
joint 'node'	M_L	18.32 x 5 x 0.463 kPa = 42.41 kNm	
	M_C	-1.753	-0.73 (-1.68) kNm
bending moment	M_R	24.37	15.70 (36.35)
	Δ_L	3.083	2.03 (4.69) mm
lateral frame displacement	Δ_R	-2.996	-2.03 (-4.69)
	θ_L	0.0183	0.0157 (0.0363)
rotation at joint centroid	θ_R	0.0244	0.0157 millirads

* subscripts "R" and "L" represent 'right' (West) and 'left' (East) sides of the frame respectively

Table 8.1.b. IMAGES-3D™ "rigid knee joint" case output converted to the 100 km/hr event

For the Westerly 55 km/hr event discussed in Section 8.1., the "rigid" model predicted responses of $M_{tot}(\text{node}) = 17.07 \text{ kNm}$ ($M_{rafter} = 13.9$), $\Delta_{knee} = 2.1 \text{ mm}$ and $\Delta\theta = 0.0074$ milliradians (essentially zero). These were obtained from the 'ratio of the squared velocities' relationship inherent in AS1170.2, explained in Section 6.4. Typical measured values were $\delta M = 6 \text{ kNm}$, $M_{tot} = 12 \text{ kNm}$, $\Delta_{knee} = +6.4 \text{ mm}$ and $\Delta\theta = 3.85$ milliradians. Reliable predictions were obtained for bending moments, but the low lateral frame sway for the "rigid" case gave unacceptably inaccurate estimates. A comparison of the rotations is not valid, since the model value is theoretically zero. the slight over-estimation of total moment due to the use of a "rigid" knee joint confirmed the design philosophy of ignoring the beneficial effects of the cladding. However, frame deformations due to wind loading estimated using this "rigid joint" method should be regarded as *unconservative*.

Also of interest is the stability of the frame moments predicted by the model, despite alterations to the joint stiffness. Using the General Loading Case again for comparison, the three models

predicted the bending moment in the Western joint to be 21.52, 23.9 and 24.37 kNm/kPa/m width for $K_{\theta}=3E9$, $20E9$ and $1E12$ respectively. That is, a change of only 13% in Moment for a change in stiffness of 333 times. The bending moment profile of symmetrical portal frames is independent of the joint stiffness for symmetrical loading, although an ideal (fully developed) Westerly wind (as assumed by AS1170.2) produced a slightly asymmetrical moment profile.

8.1.2 CONCLUSION

The selection of a value for the rotational stiffness of the 'knee' joint to be used in the computer aided design of these portal frames may be guided by the following comments:

- a) *frame bending moments* may be predicted accurately for any value of K_{θ} within the range used in the preceding theoretical considerations. A lower bound would be the stiffness of the joint only, without cladding (possibly derived from a 'bare frame' test as for this study). The "rigid" joint assumption ($K_{\theta} = \text{infinity}$) is convenient and accurate.
- b) *lateral frame sway* at the 'knee' (Δ_{knee}) was greatly under-estimated with the use of the "rigid" joint assumption, but only slightly under-estimated with the use of the $K_{\theta} = \text{'bare frame'}$ value. A more accurate stiffness value, incorporating the three dimensional stiffening effects of the building as a whole (such as the $20E9$ Nmm/rad value used in Section 6.5.) would provide sways somewhere between these bounds.
- c) predictions for the *joint rotations* are rarely required during design and could only be accurately "predicted" if the exact K_{θ} value were already known (!), according to the stiffness method definition incorporated into computer structural analysis packages.

A refinement of the choice for joint stiffness is available from the data presented in this Thesis. Using model analysis, values of K_{θ} might be trialed until the frequencies of the two dimensional structural model iterate to the (measured) modal frequencies reported in Section 7.4. This additional task was not undertaken during this project.

The results of this procedure would be more accurate for a three dimensional model. In this exercise, the "true" K_{θ} (from tests, e.g. $3E9$ Nmm/rad) could be input, and the iteration made with the section properties of the plate elements used to model the exterior cladding (since frame members and properties are known accurately). However, as argued in Chapter 6, such a 3D model would be impractical during the design process for the simple portal frame, so all theoretical simulations were made with a two dimensional model.

6

8.2. COMPARISON WITH LABORATORY TESTS

One of the original intentions of the overall research project was to incorporate the magnitudes of wind load responses measured in the full scale building into the loading regime of the half scale laboratory tests. It was soon discovered that the changes in rafter bending moment were too small for this to be practical. However, the measurements obtained during the two tests provided a record of the Yttrup Joint performance at both serviceability and ultimate level loading levels.

The largest recorded dynamic (wind) component of rafter moment was +9.3 kNm in this study, for a wind speed less than that of the "one year event". This value is far smaller than the maximum moment simulated in the laboratory of +321 kNm, or the AS1170.2 'ultimate' wind moment of +1.5 kNm.

8.2.1 RAFTER MOMENT

In order to avoid "scale effects" in the laboratory test specimens, the lateral load per nail (P/n), timber stresses (σ_b and σ_{ax}) and nail spacings were held to the values present in the full scale joint. To achieve this for a half depth (D) and length (L) timber members, the number of nails (n) and lateral loads (P) were halved, but the timber member width (b) was *not*. For these scale factors, the boundary conditions are checked below:

$$\text{load per nail} = \frac{P}{n} = \frac{1/2}{1/2} = 1$$

$$\text{Timber axial stress} = \frac{P}{A} = \frac{P}{bD} = \frac{1/2}{1 \cdot 1/2} = 1$$

$$\text{timber bending stress} = \frac{M}{Z} = \frac{PL}{bD^2} = \frac{1/2 \cdot 1/2}{1 \cdot (1/2)^2} = 1$$

Thus, bending moments recorded in the laboratory tests are equivalent to moments four times greater in the full scale joint.

These laboratory tests involved the application of a *non-reversed*, cyclic ram load (P) to the half scale "V"-frame specimen, simulating a single M/V ratio. The column was set at half full scale length, while the choice of the rafter 'half length' was based on the position of the contraflexure point in the frame under *dead* load.

A loading regime of $P = 25 \pm 9$ kN was used for the first three cyclic tests with variations of ± 20 and ± 15 kN used later. All loads were applied in the "*opening*" joint mode. The base ram load of 25 kN represented the constant "dead load", and the changes in ram load simulated "wind load" effects. these regimes represented half scale node point moments of $44.6 \pm 16.1 / \pm 35.7 / \pm 26.8$ kNm, corresponding to full scale moments of four times these, of $178.6 \pm 64.3 / 142.8 / 107.1$ kNm. These are plotted in Figure 8.2.1. overleaf.

Frame analysis indicated that dead load for the full scale building would have caused a theoretical '*closing*' bending moment of -32 kNm at both node points in the frame, and the AS1170.2 ultimate wind load event an "*opening*" moment of $21.52 \times 5\text{m} \times 1.239 \text{ kPa} = 133.3$ kNm (West wind) or 85.8 kNm (North). This gave a maximum theoretical opening node moment of $-28.6 + 133.3 \text{ kNm} = 104.7 \text{ kNm}$.

To accurately simulate this 133.3 kNm loading range (38.0 ± 66.7 kNm) in the half scale model (@ 9.5 ± 16.76 kNm), a ram load profile of $P = 5.3 \pm 9.3$ kN would have been required, rather than the 25 ± 9 kN used.

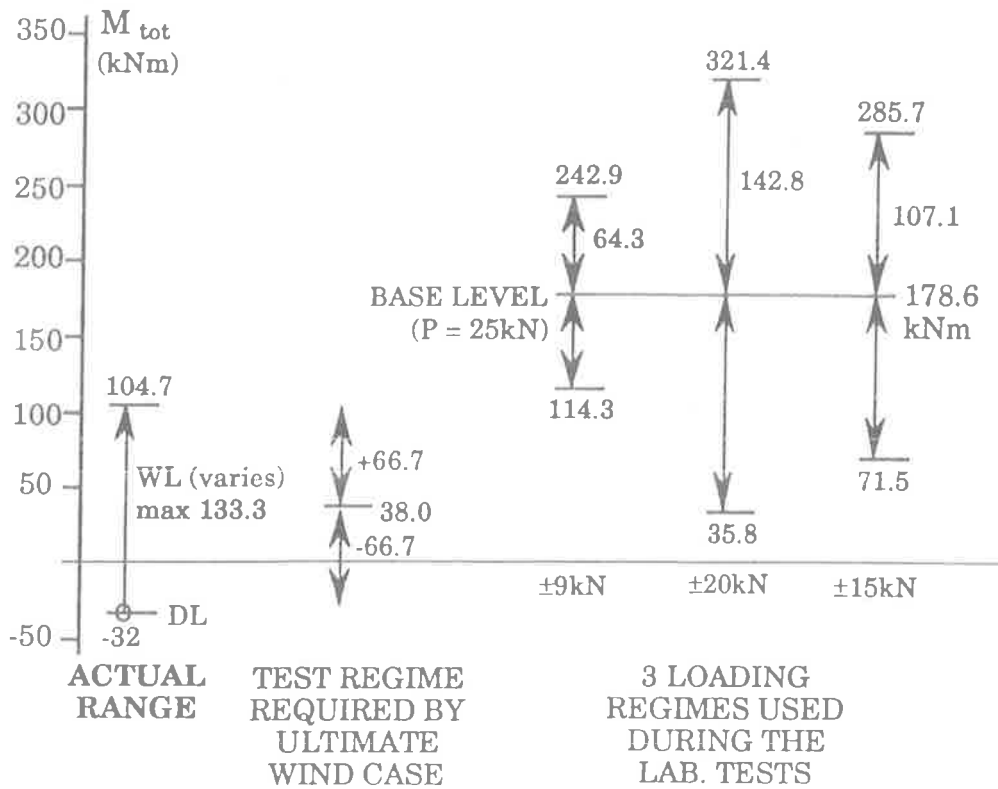


Figure 8.2.1. Comparison of AS1170 "ultimate" wind loads and loading regime used in laboratory tests

As may be seen in the Figure 8.2.1, the loading regimes used throughout the concurrent laboratory tests by Lee (1993) simulated consistently higher "opening" moments. The decision to not simulate cyclic load reversal meant that the "closing" mode behaviour of the joint was not modelled.

However, after considering the magnitude of these moments and the very low probability of their occurrence, the testing load regime concentrated on a "percentage of capacity" approach in preference to the "recreation" of the wind load moments above. The 25 ± 9 kN ram load (full scale moment 178.6 ± 64.3 kNm) was repeated for one million cycles during Test 3, for no discernible fatigue effect on ultimate strength or stiffness (Griffith et al, 1992). This range of $2 \times 64.3 = 128.6$ kNm approximated the ultimate wind event "range" of 133.3 kNm. The ultimate event wind load is based on a 5% probability of being exceeded in a 50 year period of 975 years, so the one million cycles at this load level effectively simulated 975 million years of wind loading.

As discussed in the preceding Section 8.1., measured "total" moments due to serviceability level winds were seen to be similar to those predicted by the computer model for the full scale building. Overall, the larger wind events recorded in this study may be summarized as a typical "2 second gust" wind speed of 60 km/hr, producing a change in moment of 6 kNm within a total

wind load moment of 12 kNm. Extrapolating this to the ultimate level wind event of 179.3 km/hr (Table 6.A.) gave an approximate total moment of:

$$M_u = \frac{v_u^2}{v^2} \times M_{\text{tot.v}} = \frac{179.3^2}{60^2} \times 12 = 107 \text{ kNm.}$$

This is in line with the wind load moment of 133.3 kNm predicted by the IMAGES-3D™ package and the 128.6 kNm range of loadings simulated by the ± 9 kN ram load during the laboratory tests. Therefore, the extrapolation above would suggest that a full scale rafter moment "range" equivalent to the "ultimate wind event", might have been successfully recreated during the laboratory test results with the ± 9 kN load cycle.

8.2.2 MOMENT- ROTATION

The moment-rotation plot of all the data collected in this study (deemed to have passed a 'significance test') was presented in Figure 7.1.1. This plot suggested a slightly curvilinear form, which was later confirmed by the time-history moment-rotation plots for individual events seen in Section 7.1.1. Analysis of the laboratory tests revealed a linear relationship for the half scale specimens. During these tests, insufficient data was collected at the serviceability level of loading, nor could the cladding be modelled, preventing a direct comparison of these conclusions. In addition, larger magnitude events captured during further recording by the file instrumentation may have helped verify the extent of the curvilinear trend.

Inherent in the method of inferring a rafter bending moment from the measurement of the two extreme fibre strains, as used in this study, is the assumption of a linear strain profile. This was justified in Section 5.2.3. Slight non-linearity of this profile within the rafter section would not have caused large errors in the calculated moment, since any increase in the internal forces due to this non-linearity is to an extent offset by the commensurate reduction in the lever arm between this force couple. Both linear and non-linear strain profiles were measured during the laboratory tests, with the strain profile remaining constant throughout the cyclic load test, regardless of load magnitude. No explanation has been offered by Lee for this anomaly.

8.2.3. JOINT STIFFNESS

Calculations for the half scale model specimens (Lee, 1993) shown previously in Section 6.2.2., returned an 'initial' stiffness values of 3E9 Nmm/radian. The 'initial' stiffness definition was considered most appropriate for the comparison of the ultimate level laboratory tests with the serviceability level data from this study. A value of 4E9 was derived for the instrumented 'field' joint in Section 7.2. Direct comparison was made possible by the placement of strain measuring gauges at the same rafter cross section in both field and laboratory tests. True "node point" moments (and hence stiffnesses) may be obtained by the method described in Section 6.4.

Both these values are of an appropriate order of magnitude, from the comparisons with the New Zealand research on similar joint types discussed in Section 6.2.

However, the close similarity between the 'field' and 'laboratory' values does not reflect the scale factor present in the half scale model tests. For any equivalent loading scenario, bending moments found in the test specimens were a factor of four smaller than corresponding moments in the full scale joint. Rotations and angle changes are independent of scale effects, so stiffnesses in the half scale models should have been one quarter of those found in the full scale joint. When corrected for scale effects, the laboratory specimen figure is equivalent to a 'full-scale' value of 12E9 Nmm/radian.

In addition, as discussed in the preceding Section 8.1., account must be taken of the additional stiffening effects of the exterior cladding and rigid end bays in the building. As such, the stiffness of the portal frame test joint was expected to return the approximate result:

$$K_{(\text{test, portal})} = \frac{1}{4} K_{(\text{full scale, portal})} \approx \frac{1}{4} \times \frac{1}{2} \times K_{(\text{full scale, building})}$$

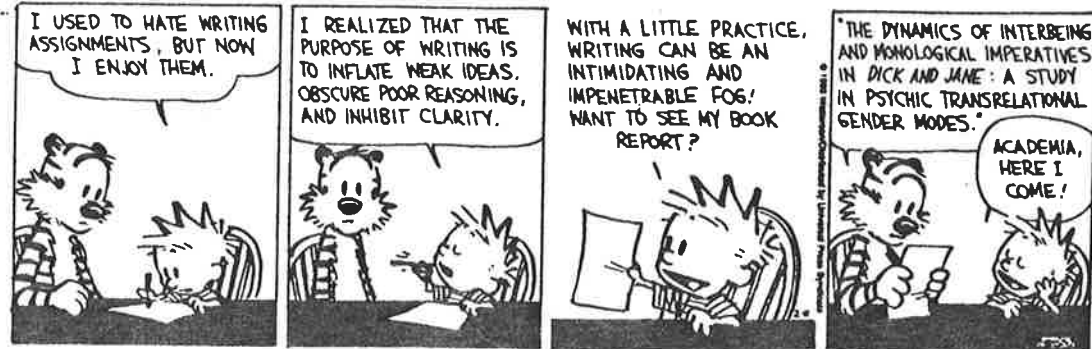
Therefore, up to one order of magnitude might be expected between the field and laboratory stiffness results.

An additional factor would be an allowance for the degree of 'softening' which had occurred in the field joint prior to instrumentation. As the laboratory specimens were constructed as "new" joints, no prior loading had been applied. However, the tests indicated only a 10% reduction in joint stiffness after 1 million cycles of loading equivalent to the AS1170.2 "ultimate wind load" on the real structure (see Fig. 8.2.1). Therefore, no allowance was made for the three years of ambient wind loading of the field joint.

A closer examination of this result revealed the two different methods for rotation measurements as the possible source of the difference. These were correlated during the preliminary laboratory tests for the range of rotations seen in this study (5.3.3.), but each contained an inherent "definition of rotation". The total joint rotation is a combination of rigid body rotation of the gusset plate, flexure at the ends of the incident structural members and opening of the rafter/column interface. Measurements taken in the field assumed that the member flexure would dominate at serviceability level loads. The anticipated high 'rigidity' of the nailed connections was expected to dominate over plate rotation, usually seen as nail slips or localized crushing of the timber side plate. On the other hand, during laboratory measurements a variety of methods were used (Lee, 1993). The adopted method captured all three components.

It is unknown whether this difference could completely account for the discrepancy of one order of magnitude. No explanation for the absence of the above relationship between 'field' and 'half scale model' measurements was formulated.

Calvin and Hobbes



Conclusions

9.1 SUMMARY

The major contribution of this work has been the first ever documentation of the true behaviour of a typical, 'as constructed' "Yttrup Joint", a common type of moment resisting, multi-nailed joint used in portal frame structures. Since the chosen building had been "in service" for several years prior to mid-1992, the joint had been "softened" from its initial tight construction by ambient wind buffeting.

The frame responses to the action of ambient, "serviceability" level wind events were recorded during the period June - September 1992. The responses measured were:

- rafter bending moment (adjacent the gusset plate);
- joint rotation; and
- lateral displacement (sway) of the frame.

The latter two were measured at the frame "node" point, taken as being the intersection of the frame member centrelines.

Wind events of up to 70 km/hr were logged. The larger (10 second) wind events recorded in this study may be summarised as a typical event having a "2 second gust" speed of 50-60 km/hr, and a change in wind speed of 20-25 km/hr, producing a change in rafter moment of 6 kNm within a total wind load moment of 12 kNm. The "total wind moment", consisting of both the static and dynamic components, was seen to be between two and three times that of the (dynamic) "change in moment". This same typical event caused an opening joint rotation of 4 milliradians and a lateral frame sway of 10 mm.

The focus of wind measurement in the study was not to attempt a quantitative link between wind action and structural response (5.4). Rather, the single anemometer wind speed records were used to identify the range of wind loadings experienced. These showed that 'serviceability' level loadings equivalent to a return interval of slightly less than one year were measured.

The successful design, installation and calibration of the instrumentation system was of critical importance, to ensure reliability of the collected data. Additional care was required since a) the recorded phenomena was an instantaneous and dynamic one; b) access restrictions prevented the adoption of standard or otherwise simpler measuring techniques; c) no independent or 'duplication' measurements were feasible; and d) no report of a similar undertaking had been found to provide expected magnitudes or guidance on instrumentation methods.

Since no previous full scale field testing had been carried out on a fully clad portal frame building, a two dimensional theoretical model based on the stiffness method was used to predict frame responses. This required an assumption for the beam - column joint stiffness modelled as a rotational spring. Initially a spring stiffness of $20E9$ Nmm/radian was estimated based on earlier laboratory tests of similar joints in New Zealand. Later, tests by Lee (1993) revealed the newly constructed "joint only" stiffness to be closer to $3E9$. This figure was subsequently used in the 2D model to compare with field results.

Overall, it was seen that this 2D approach was too simplified to predict the responses of a complex 3D structure to a randomly fluctuating pressure load. The 2D model ignored the effects of cladding and stiff end bays of the building, and could only be loaded by static, code recommended free stream winds from a constant direction, parallel to the frame. However, the nature of portal frame design is such that 2D models are the conventional analytical tool used by designers. Frame moments required for strength design are largely independent of joint stiffness, even for assymetrical loading.

Since frame design is invariably controlled by serviceability criteria, especially frame sway, stiffness considerations assume an increased importance. The use of the laboratory-derived joint stiffness in the 2D model improved the prediction of sway and deflection responses.

These preliminary comparisons of the measured frame responses with the theoretical estimates concluded that the field recording had yielded quantities of a correct order of magnitude. In

conjunction with the results of the laboratory tests, which used loading regimes more severe than the equivalent ultimate wind levels, the measured wind actions and structural responses were confirmed as being in the "serviceability wind" range.

Rafter strain measurements were also independently confirmed using a different technique (5.2.7); that used by Lee (1993). Rotation measurements were identified as the least reliable, and the analysis procedure used to estimate lateral frame sways, an adaptation of the "baseline correction" method common in earthquake "shaking table" tests, was felt to be only approximate. But when both were plotted against the more reliable structural response of strain, and a similar result exposed (7.3.1), much greater confidence in their reliability was justified.

The final impediment to a confident analysis of the recorded data was the variable and 'imperfect' phase relationship between the strain and rotation signals. No complete explanation for this is available. Therefore, analysis focused on those larger wind events possessing excellent correlation. "Peak analysis" of the data was adopted since it was unaffected by the local anomalies in the signals (7.1.1).

407 of the largest wind "events" were selected, based on a chosen "significance level" of 20 microstrain in the rafter extreme fibre (7.1). Figure 7.1.1. shows the δ Moment vs Δ rotation plot of these 407 events. The form of the plot suggests a curvi-linear moment - rotation behaviour at this level of loading. To confirm this, detailed M- θ plots were made for individual events, derived from their time-history records. These plots, for both "opening" and "closing" joint modes, confirm the curvilinear form.

"Opening" joint responses (defined as positive δ Moments) would have been caused by increases in wind velocity, while the "closing" mode represents the 'relaxation' following the initial loading. It is for this reason that positive δ Moment events exceed in both number and magnitude the negative δ Moment events (7.1.2).

'Secant' and 'initial' stiffnesses of the full-scale joint were calculated from the δM - $\Delta\theta$ data (7.2). Values for these two, averaged over the 407 events, were similar at 3.0 and 3.9 E9 Nmm/radian respectively. Stiffnesses were not greatly different between 'opening' and 'closing' modes. This slight difference between stiffnesses is consistent with a curvilinear δM - $\Delta\theta$ graph. However, these results contrasted with the laboratory findings of Lee (1993) on half-scale specimens of a linear value of 12E9 Nmm/radian when corrected for scale effects. Since strains were measured at the same rafter site and compared well (5.2.7), the difference was attributed to the "definition of rotation" inherent to the two different methods used in the parallel studies (8.2.3).

9.2 FURTHER RESEARCH

Several avenues for possible future research arose from the work carried out during this study. Obviously, improvements could be made to the analysis and instrumentation phases of this work, but new areas of research were also suggested.

9.2.1 INSTRUMENTATION

a. Rotation

Comparisons of measured joint stiffness between various studies were hampered by the different methods used for measuring rotation. Each method was found to account differently for the various components of the overall joint rotation, e.g. plate bending and member bending. Access difficulties had forced a different "in field" method to that used in the laboratory tests of Lee (1993). Given more time, this contradiction could be resolved.

b. Snapback test

The 'Snapback Test' is a standard building investigation tool in which a known load is statically applied, then released suddenly. Building responses are measured throughout the loading and free oscillation phases. The latter phase was comprehensively measured during this study, giving adequate information on building dynamics. However, since no link was attempted between applied load and structure response during the wind loading events, a calibrated test could provide such information easily.

c. Vacated building

As detailed previously, instrumentation had to be adapted to suit the constraints of a fully operational, occupied building. Ironically, the building was vacated shortly after this study was completed. By way of example, the same rotation measuring method as used in the laboratory tests could only be installed within the vacant building, negating Item A. above.

9.2.2. ANALYSIS

Estimates for the "bare" joint stiffness were originally derived from research conducted on similar nailed, moment resisting joints in New Zealand. That estimate was used in the input of the theoretical (computer) model of the structure, but at $20E9$ Nmm/radian was greater than the final laboratory measurement of the bare joint of $4E9$. Closer modelling of all the NZ joint types, as well as the "newly constructed" laboratory 1/2 scale models (Lee, 1993) and the "in field" joint, might explain the discrepancy. This may also allow better estimates for the "in field" stiffnesses of other joints to be extrapolated from the results of this investigation in the future.

9.2.3 EXTENSIONS

a. Interlayer friction

The role of interlayer friction between joined members is usually ignored at ultimate level loading, since the gap between members will naturally increase under higher loading. At serviceability level loading however, it has a significant effect on the lateral load capacity of the timber joint. This effect is amplified in joints having a large number of nails (i.e. higher nail withdrawal capacity, therefore a greater resistance to gap widening, or "clamping"). Such a situation exists in all nailed, moment resisting joints. Lheude (1990) re-examined the load capacity of nailed timber joints at ultimate levels using modern timber industry materials such as structural plywood, LVL and hardened nails. This work should be extended to consider

behaviour in the serviceability range for these same materials. The "clamping" effect could be studied by merely varying the number of nails in the joint.

b. Optimizing joint strength

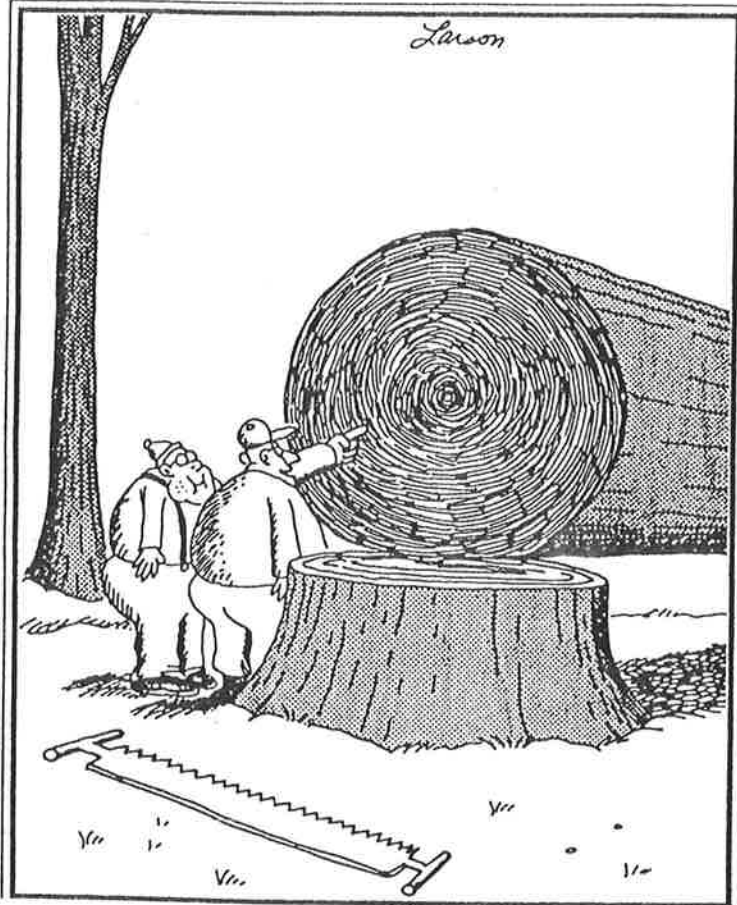
Most nailed, moment resisting joints are over-designed for strength, as serviceability considerations of the timber frame govern in the design. Boulton (1987) considered the profits and consequences of optimizing the strength capacity of joints by limiting the number of nails used. Advantages included more ductile in-service behaviour and ductile failure of the nails instead of brittle timber failure in the joint. The cost saving in nails would be negligible for the structure. Under high amplitude dynamic lateral loading, such as ultimate wind or earthquake, greater energy levels would be absorbed. However, the governing frame deflections are typically computed assuming a simple 2-D 'bare frame' (i.e. timber members only, without cladding). The true deflections would be less, and may be reduced to such an extent that strength considerations governed if the effect of cladding was known. Joint strength optimization would then be advantageous.

c. Cladding

Following on from Item above, the effect of the cladding on structural performance should be quantified in the manner of Bryant's work in the UK during the 1960's and 70's. An enhanced 3-D computer model would now be feasible to assist with this exercise. The quantification of the interaction between timber frame and thin, profiled steel cladding is a crucial extension of this investigation.

d. Moment Capacity

Contemporary prediction equations for the moment resistance of ring-nailed timber joints are empirical. They are accepted for the stability of their predictions of failure load rather than their theoretical rationale. One assumption made is that all four corners of a nail ring will rotate equally, but this was contradicted during laboratory tests (Lee, 1993). Data from the Lee tests, and the similar NZ research (c.1984) could be used to assemble and verify a new equation. In addition, a beam-column 'knee' joint in a portal frame actually employs two nail rings, joining column to gusset plate and this to rafter. The validity of employing prediction equations based on single nail rings to 'knee' joints of this form has never been investigated.



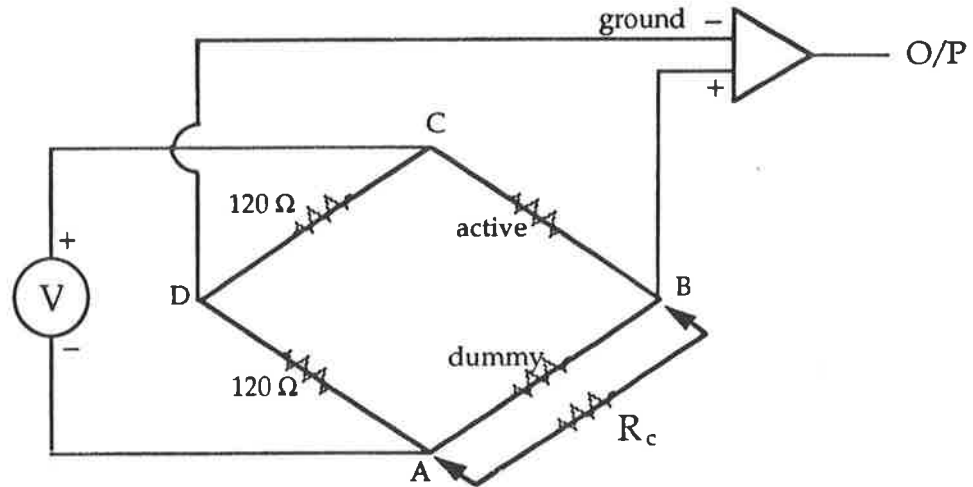
"And see this ring right here, Jimmy? ... That's another time when the old fellow miraculously survived some big forest fire."

Appendices

APPENDIX A

The Strain Gauge Calibration Tests.

The standard method of calibrating the Wheatstone Bridge of the strain gauge apparatus was used, where various resistances (R_c) are placed in parallel across the 'dummy' gauge to infer a range of known strains, whilst simultaneously measuring the output voltage. The resulting highly linear relationship between strain and voltage allowed easy conversion at any strain level.



As load is applied, strain (ϵ) is derived from the gauge, proportional to changes in gauge resistance, according to the formula:

$$\epsilon = \frac{\Delta R}{R \times GF} \quad \left(\text{where } \Delta R = \frac{-R_{\text{dummy}}^2}{R_c + R_{\text{dummy}}} \text{ during calibration} \right)$$

Results obtained from the third of three field calibrations are tabulated below for both the 'top of rafter' and 'bottom of rafter' ("plastic strip") bridges, using the quoted gauge factor $GF = 2.10 \pm 1\%$ and resistance $R_d = 120 \pm 0.3 \Omega$:

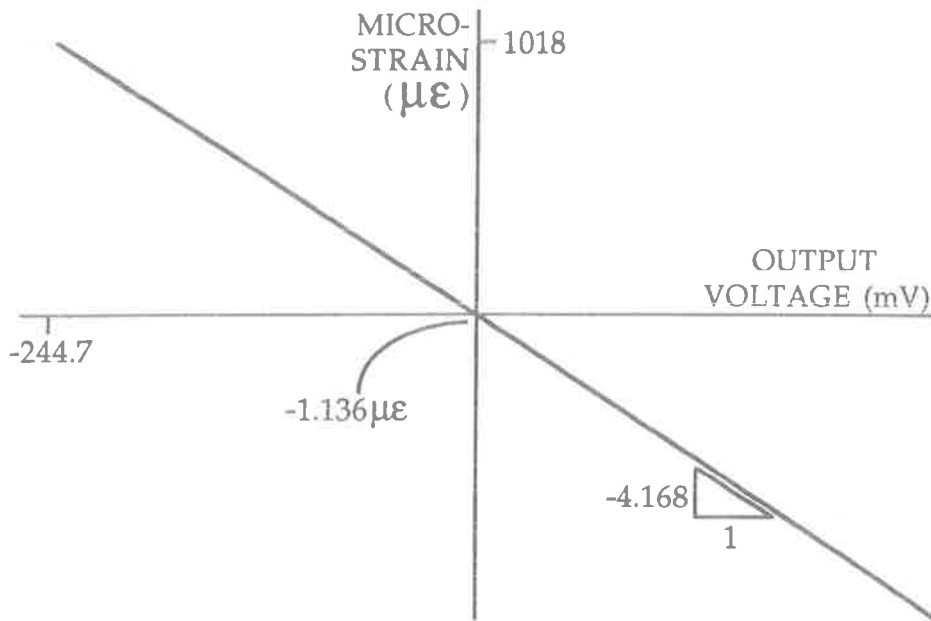
R_c	miro-strain	V top (mV)	V bot (mV)
560 k Ω	102.02	-24.9	-25.3
110 k Ω	518.91	-124.5	-131.4
56 k Ω	1018.23	-244.7	-257.5

These values (taken June 1992) compare well with the other two on-site calibrations in mid 1991 and March 1992, and from linear regression yield the highly linear relationships of:

$$\mu\epsilon = \left\{ \begin{matrix} -4.168 \\ -3.946 \end{matrix} \right\} \times \text{O/P VOLTS (mV)} + \left\{ \begin{matrix} -1.136 \\ +1.546 \end{matrix} \right\} \quad \text{for the } \left\{ \begin{matrix} \text{top} \\ \text{bottom} \end{matrix} \right\} \text{ bridges.}$$

It is considered valid to simply ignore the constant offset terms due to their insignificant size ($\sim 1\mu\epsilon$), especially since they were within the error for the calibration test (see below). But they may also be removed during the linear regression calculation.¹ Setting this vertical axis intercept to zero in the regression produced a slightly different slope, and a more logical result (i.e. zero output voltage = zero strain) as well as negating any measuring errors in the calibration test. This method was used, and yielded:

$$\mu\epsilon = \left\{ \begin{array}{l} -4.159 \\ -3.957 \end{array} \right\} \times \text{O/P VOLTS (mV)} \quad \text{for the } \left\{ \begin{array}{l} \text{top} \\ \text{bottom} \end{array} \right\} \text{ bridges.}$$



From the strain (ϵ) equation used previously, the measuring error for strain ($\xi\epsilon$) may be evaluated. (Resistors R_c used in the test were accurate to 0.5%).

$$\frac{\xi\epsilon}{\epsilon} = \frac{\xi R_c}{R_c} + 2 \frac{\xi R_d}{R_d} + \frac{\xi GF}{GF}$$

Thus, $\frac{\xi\epsilon}{1018\mu} = 0.005 + 2 \times \frac{0.3}{120} + 1\% = 0.02$

Hence $\xi\epsilon = 2\% = 2\mu\epsilon$ for an expected maximum rafter strain of $100\mu\epsilon$

Using the derived relationship between output voltage and actual strain above, this maximum error corresponds to an output voltage of approximately 0.5 mV. This was acceptable, since the "significance" level (*minimum* rafter strain) of $20\mu\epsilon$ (or 5 mV) was adopted during the data analysis phase.

As may be observed in the above linear $\mu\epsilon$ -mV relationship (and table), an increasingly negative voltage output implies an increasingly positive strain. It is essential that the sign of the measured strain (C or T) is known from a consideration of the sign of the output voltage signal.

A *tensile response* in the attached medium infers an decreased gauge cross-section and hence *decreased resistance* in the strain gauge. A tensile event is thus equivalent to the

¹ Ang, A.H.S. & Tang, W.H. "Probabilistic Concepts in Engineering and Planning Design", Chapter 7, 124

introduction of another resistor (R_c) in parallel with the gauge, since for any value of R_c , the total resistance of that leg of the Bridge will always be numerically *less* than just the gauge resistance. During all applications of R_c it was observed that output voltage *dropped*. By definition, strain is linearly proportional to the change in resistance (hence voltage) of the gauge. Therefore, this tensile event implies a *negative change in the output voltage*. ("TENSION = mV DROP") The converse is true for the compressive event:

Tensile event: c/s A ↓ ∴ ΔR ↓ R_{tot} ↓ gives mV ↓ (e.g. Temp ↑)
 Compressive event: c/s A ↑ ∴ ΔR ↑ R_{tot} ↑ gives mV ↑ (e.g. Temp ↓)

The strain gauges which were later directly adhered to the rafter surface were calibrated in the same way, giving the following results averaged from two tests (GF = $2.08 \pm 1\%$ and $R_d = 119.8 \pm 0.3 \Omega$):

R_c	miro-strain	V top (mV)	V bot (mV)
560 k Ω	102.83	-22	-22
110 k Ω	523.03	-113	-111
56 k Ω	1026.31	-222	-218

$$\mu\varepsilon = \left\{ \begin{array}{l} -4.628 \\ -4.707 \end{array} \right\} \times \text{O/P VOLTS (mV)} \quad \text{for the } \left\{ \begin{array}{l} \text{top} \\ \text{bottom} \end{array} \right\} \text{ (glued SG) bridges.}$$

Using the previous method, error analysis for these gauges also yielded a result of $\xi \varepsilon = 2\%$, once ^{again} quite acceptable.

APPENDIX B

Error Analysis in the RVDT Calibration Test.

The reference rotation in the experiment was given by the relation:

$$\text{rotation } \theta = \arctan\left(\frac{\text{micrometer side length 'a'}}{\text{base length 'b'}}\right)$$

For a general function involving two independent variables, x_1 and x_2 , $P=f(x_1, x_2)$. Differentiation of this equation gives:

$$\Delta P = \frac{\delta f(\mathbf{x})}{\delta x_1} \cdot \Delta x_1 + \frac{\delta f(\mathbf{x})}{\delta x_2} \cdot \Delta x_2$$

To manipulate the errors (or uncertainties ξ) as percentages, this may be rewritten¹:

$$\xi_P = \frac{\delta P}{\delta x_1} \cdot \xi_{x_1} + \frac{\delta P}{\delta x_2} \cdot \xi_{x_2}$$

In the case of the hinged-plate device, $\theta = \arctan(a/b)$:

$$\begin{aligned} \frac{\delta}{\delta a} \arctan\left(\frac{a}{b}\right) &= \frac{\delta}{\delta(a/b)} \arctan\left(\frac{a}{b}\right) \cdot \frac{\delta(a/b)}{\delta a} = \frac{1}{1+(a/b)^2} \cdot \frac{1}{b} \quad \text{and} \\ \frac{\delta}{\delta b} \arctan\left(\frac{a}{b}\right) &= \frac{\delta}{\delta(a/b)} \arctan\left(\frac{a}{b}\right) \cdot \frac{\delta(a/b)}{\delta b} = \frac{1}{1+(a/b)^2} \cdot \frac{-a}{b^2} \end{aligned}$$

Using the above partial derivatives,

$$\xi_\theta = \frac{\delta}{\delta a} \arctan\left(\frac{a}{b}\right) \cdot \xi_a + \frac{\delta}{\delta b} \arctan\left(\frac{a}{b}\right) \cdot \xi_b$$

$$\xi_\theta = \frac{\xi_a}{[1+(a/b)^2]b} + \left(\frac{-a}{b^2}\right) \frac{\xi_b}{1+(a/b)^2}$$

$$\xi_\theta \cdot b [1+(a/b)^2] = \xi_a - \left(\frac{a}{b}\right) \cdot \xi_b$$

Since max. 'a' (micrometer)= 14.202 +/- .0015mm, and 'b' (base)= 100.03 +/- .02mm,

$$\text{Maximum } \xi_\theta \cdot 100.03 \left[1 + \left(\frac{14.202}{100.03}\right)^2 \right] = 0.0015 - \left(\frac{14.202}{100.03}\right) \cdot 0.02$$

Thus, $\xi_\theta = -0.0000131^\circ$ or 0.00075°

¹ RAY, M.S. (1988). "Engineering Experimentation", McGraw-Hill, London.

APPENDIX C

Error Analysis in the Anemometer Calibration Experiment

$$v = \sqrt{2ghR} \Rightarrow R = \frac{\xi \gamma_w}{\gamma_{da}} = \frac{\gamma_w}{\gamma_{da}(1+w)} \Rightarrow \gamma_{da} = \gamma_{daT} \left(\frac{\rho_{amb}}{\rho_{st.atm}} \right)$$

where: g = gravitational acceleration = 9.807 m/s^2

h = pitot tube pressure head, read by a manometer to the nearest $0.001''$

R = adjustment term for ambient atmospheric condition at the time of the experiment

γ_{wa}, γ_{da} = ambient specific gravity of wet and dry air respectively

$\gamma_{daT} = \gamma_{da}$ at a given temperature, and standard atmospheric pressure $\rho_{st.atm}$

γ_w = specific gravity of air (at a given pressure ρ_{amb} and temperature T)

w = humidity ratio, obtained from Psychrometer and chart¹

The above equations are used in the reverse order. From published values² for the specific gravity of air at standard atmospheric pressure $\rho_{st.atm}$, a value for γ_{daT} was interpolated for the Psychrometer dry bulb temperature of 18.1°C as 1.20855 kg/m^3 . This was then converted to γ_{da} at ambient pressure ρ_{amb} , which although measurable to 0.1 mbar , fluctuated during the test by about 1 bar .

Since $\gamma_{da} = \gamma_{daT} \left(\frac{\rho_{amb}}{\rho_{st.atm}} \right)$ then $\frac{\xi \gamma_{da}}{\gamma_{da}} = \frac{\xi \gamma_{daT}}{\gamma_{daT}} + \frac{\xi \rho_{amb}}{\rho_{amb}} + \frac{\xi \rho_{st.atm}}{\rho_{st.atm}}$ where ξ signifies 'error'.

$$\text{Thus } \frac{\xi \gamma_{da}}{1.2064} = \frac{0.01}{1.20855} + \frac{1}{1011.4} + \frac{0.1}{1013.2} = 0.009362$$

Therefore, $\xi \gamma_{da} = 0.0094$, so $\gamma_{da} = 1.21 \pm 0.01 \text{ kg/m}^3$

γ_{wa} is obtained from γ_{da} , which was converted to ambient conditions above, by using the humidity ratio 'w'.

Since $R = \frac{\gamma_w}{\gamma_{wa}} = \frac{\gamma_w}{\gamma_{da}(1+w)}$ then $\frac{\xi R}{R} = \frac{\xi \gamma_w}{\gamma_w} + \frac{\xi \gamma_{da}}{\gamma_{da}} + \frac{\xi w}{w}$

$$\text{Thus } \frac{\xi R}{819.2} = \frac{0.15}{999.66} + \frac{0.0094}{1.2064} + \frac{0.0001}{0.0115} = 0.016637$$

Therefore $\xi R = 13.6$, so $R = 820 \pm 14$ (dimensionless)

Now, velocity $v = \sqrt{2ghR}$ so $\frac{\xi v}{v} = \frac{1}{2} \left(\frac{\xi g}{g} + \frac{\xi h}{h} + \frac{\xi R}{R} \right)$

$$\text{Hence } \frac{\xi v}{17.51} = \frac{1}{2} \left(\frac{0.001}{9.807} + \frac{0.002}{0.750} + \frac{13.6}{819.2} \right) = 0.009685$$

Which gives $\xi v = 0.175$ and $v = 17.5 \pm 0.18 \text{ m/s}$

¹ Departmental Ashrae wet and dry bulb Psychrometer, and accompanying chart produced by the American Society of Heating, Refrigerating and Air-Conditioning Engineers, Inc. 1963. The chart relates Saturation Temperature T_s and Dry bulb temperature T_D to relative humidity and humidity ratio (w).

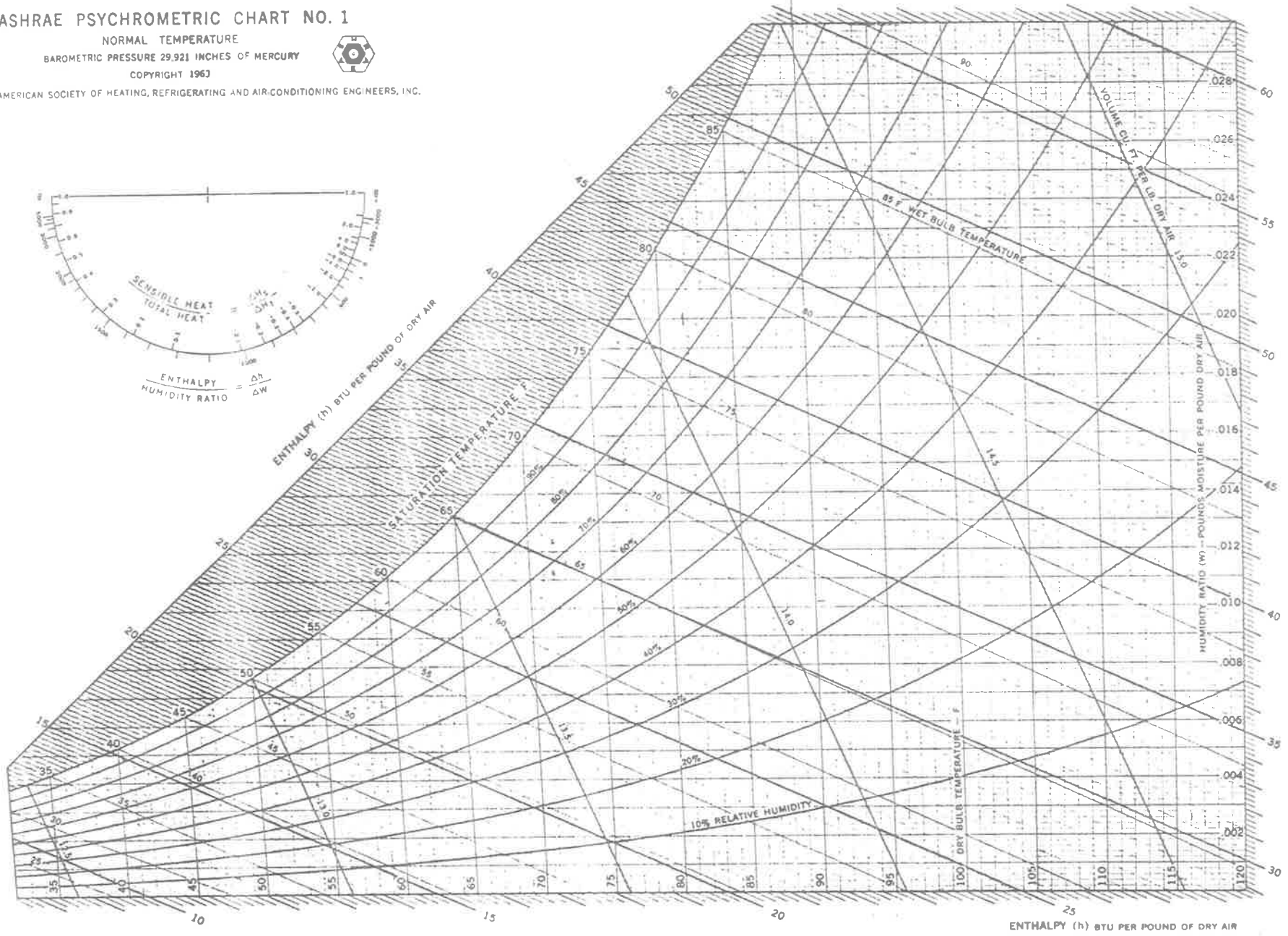
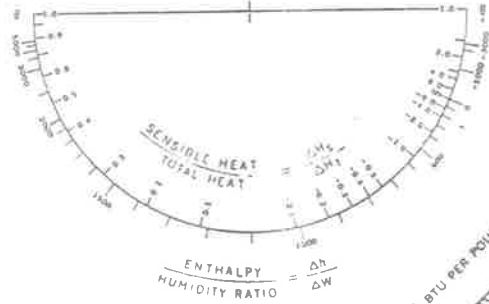
² DOUGLAS, J.F., GASIOREK, J.M., SWAFFIELD, J.A. (1979). "Fluid Mechanics". Pitman Books Ltd., London.

ASHRAE PSYCHROMETRIC CHART NO. 1

NORMAL TEMPERATURE
BAROMETRIC PRESSURE 29.921 INCHES OF MERCURY
COPYRIGHT 1963



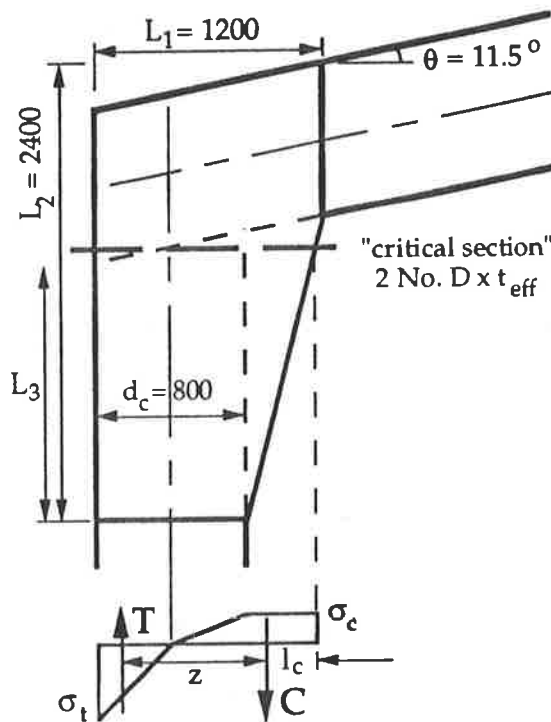
AMERICAN SOCIETY OF HEATING, REFRIGERATING AND AIR-CONDITIONING ENGINEERS, INC.



APPENDIX D.

Calculations for the Ultimate Moment Capacity of the Yttrup Joint

D.1. Plywood Failure: a) Batchelar (1984) Method.



$$L_3 = \frac{(L_2 - L_1 \tan \theta - d_r / \cos \theta)}{\cos \theta}$$

$$= 1367 \text{ mm}$$

From Batchelar (1984):

$$D = L_1 - \left[\frac{(L_1 - d_c/2) \tan \theta}{L_3 + L_1 \tan \theta} \right] (L_1 - d_c)$$

$$= 1200 - (162.76 / 1611.14) 400$$

$$= 1160 \text{ mm (locates 'critical section').}$$

$$\ln \sigma_t = \alpha \sigma_c, \alpha = 4 \left(\frac{L_1}{D} \right) - 3 = 3.0$$

$$l_c = \frac{a^2/2 + d_c/4(a + d_c/6)}{a + d_c/4} = \frac{163,238}{559.6}$$

$$= 291.7 \text{ mm}$$

$$z = D - l_c - d_c/6 = 1159.6 - 291.7 - 133.33$$

$$= 734.6 \text{ mm}$$

$$M = T z$$

$$T = \frac{1}{2} \alpha \frac{1}{2} d_c 2 t_{\text{eff}} = \frac{1}{2} \sigma_t d_c t_{\text{eff}}$$

$$\sigma_t = F'_b = 17.0 \text{ MPa}, t_{\text{eff}} = 11 \text{ mm}$$

$$M = \frac{1}{2} 17.0 \times 800 \times t_{\text{eff}} \times 734.6 = 55 \text{ kNm}$$

The strain distribution shown above was confirmed by strain gauge recordings across the "critical section", at which the plywood acts alone to transfer the applied moment between the two nail groups. The method has been somewhat modified for the purposes of this joint, due to the absence of the "gap" between rafter and column commonly found in New Zealand joints, and the slight changes in geometry of the gusset plate. Note that this method implicitly accounts for AS1720 beam depth factor k_{11} , which essentially accounts for "deep beam" effects.

It also ignores axial stress as $\sigma_{\text{ax}} = P_{\text{ax}}/A = \frac{8.6 \text{ kN}}{2 \times 1160 \times 11} = 0.34 \text{ MPa} \ll \sigma_{\text{bending}}$

D.1. b) AS1720 Method

Assumes linear elastic strain distribution (Sections 2. & 5.). Using the section of above:

$$M = k_1 k_{11} F'_b Z = 1.0 \times 0.801 \times 17.0 \times \frac{2 \times 11 \times 1160^2}{6} = 67.2 \text{ kNm}$$

D.2. LVL Section Failure: AS1720 Method

Assumes linear elastic strain distribution (Sections 2. & 7.). Section at instrumented rafter site was 764 x 63 mm.

$$M = k_1 k_{11} F'_b Z = 1.0 \times 0.858 \times 16.0 \times \frac{63 \times 764^2}{6} = 84.1 \text{ kNm}$$

D.3. "Nail Yielding" Failure

a) "Thin Walled Tube" Analogy

$$M_u = 4 f s A B \cos \theta$$

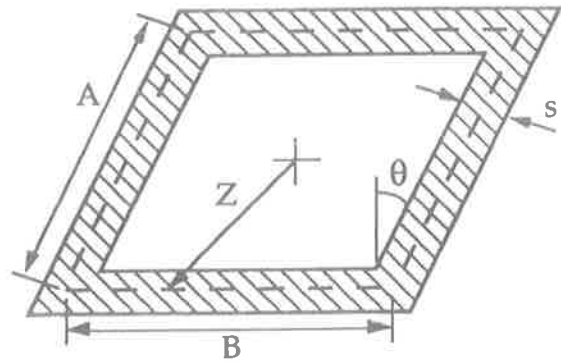
where $f = \frac{Q_o}{c p}$ and $'s' = c n$,

($'c' =$ nail row spacing, $'n' =$ no. rows)

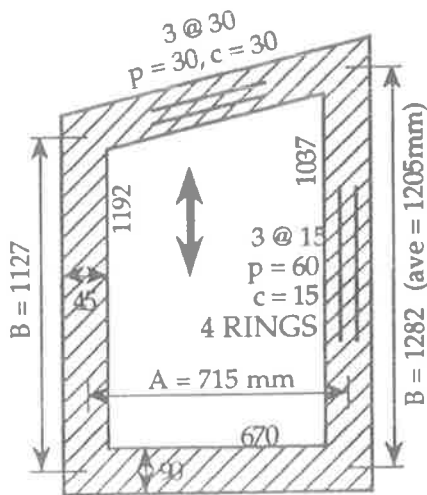
and $'Q_o' =$ "allowable nail load"

$$\text{thus } M_u = 4 \frac{n}{p} A B \cos \theta \times Q_o$$

In the thin walled tube analogy, $'f'$ is equivalent to "shear flow", $'AB' =$ "enclosed area", and $'s' =$ "tube thickness".



A. LOWER GROUP

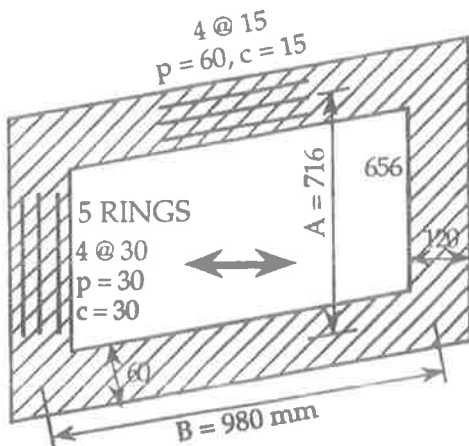


$$\begin{aligned} \text{weighted } p_{ave} &= \frac{1205 \times 60 + 715 \times 30}{1205 + 715} \\ &= 48.83 \text{ mm} \end{aligned}$$

$$\begin{aligned} \text{weighted } c_{ave} &= \frac{1205 \times 15 + 715 \times 30}{1205 + 715} \\ &= 20.59 \text{ mm} \end{aligned}$$

$$\begin{aligned} M_u &= K Q_o, \text{ so } K = \frac{4 n A B}{p} \cos 0^\circ \\ &= \frac{4 \times 4 \times 715 \times 1205}{48.83} \times 1 \\ &= 282,310 \text{ (mm)} \end{aligned}$$

B. UPPER GROUP



$$\begin{aligned} \text{weighted } p_{ave} &= \frac{980 \times 60 + 716 \times 30}{980 + 716} \\ &= 47.33 \text{ mm} \end{aligned}$$

$$\begin{aligned} \text{weighted } c_{ave} &= \frac{980 \times 15 + 716 \times 30}{980 + 716} \\ &= 21.33 \text{ mm} \end{aligned}$$

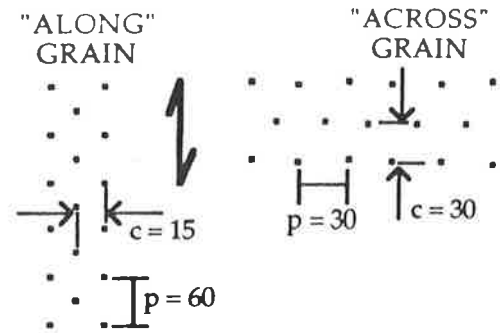
$$\begin{aligned} M_u &= K Q_o, \text{ so } K = \frac{4 n A B}{p} \cos 11.5^\circ \\ &= \frac{4 \times 5 \times 716 \times 980}{47.33} \times 0.98 \\ &= 290,553 \text{ (mm)} \end{aligned}$$

Note that the effect of using a "compressed" nail spacing, as seen in the following figure, is to concentrate the nails at their most remote possible (and hence most effective) locations. For a given outside dimension and a given total number of nails in the 'ring', an improvement could be expected in the geometric 'K' term. Using the "Thin Walled Tube" analogy, this improvement was 15 and 26% for the lower and upper groups in the Yttrup Joint respectively .

The nailing pattern in the Yttrup Joint is such that adjacent rows of nails are offset by half the nail pitch, enabling the spacing of the rows to be halved (seen at right).

For a run of nails 'across' the timber grain, $c = \frac{1}{2} 60 = 30$, and pitch $p = 30$.

For a run of nails 'along' the timber grain, $c = \frac{1}{2} 30 = 15$, and pitch $p = 60$.



b) Mitchell (1979) Method ("Shared Rivet Group" Analogy)

$$M_u = \frac{2 I_p Q_o}{c p r_{\max}} \quad \text{where } I_p = \frac{s (A+B)^3}{6}, \quad s = c n \quad \text{and } r_{\max} = \frac{1}{2} \sqrt{A^2 + B^2 + 2AB\cos\theta}$$

$$M_u = K Q_o \quad \text{so } K = \frac{2 n (A+B)^3}{3 p \sqrt{A^2 + B^2 + 2AB\cos\theta}}$$

PARAMETER	LOWER GROUP	UPPER GROUP
n	4 rings	5 rings
c_{ave}	20.59 mm	21.33 mm
$s = c n$	82.36 mm	106.65 mm
A	715 mm	716 mm
B	1205 mm	980 mm
p_{ave}	48.83 mm	47.33 mm
θ°	0	11.5
I_p	97.1558 E9 mm ⁴	86.7136 E9 mm ⁴
r_{\max}	960 mm	843.8 mm
K	201,319 (mm)	203,578 (mm)

c) "Discrete Rivet Group" Analogies

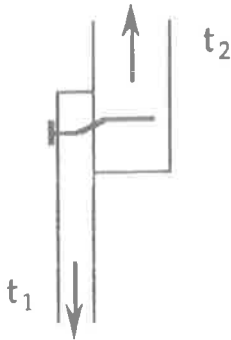
This group incorporates the final three methods introduced in Tables 4.2.A. & B., where the load on each individual nail is treated as unique, and assumed to be a function of its distance from the nail group centroid. To evaluate these methods, this distance must be known for *each* nail. To simplify calculations, a scale diagram was made, using the nail group dimensions and spacings quoted on the structural drawings (and confirmed on-site). Nail "radii" were taken from this diagram. Results are shown in Table 4.2.B.

As a check for the accuracy of this method, the geometric function 'K' was evaluated for the half scale model used in the concurrent laboratory tests (Lee, 1993). A value for 'K' of 38,227 mm was obtained for the upper nail group, which converted to full-scale value of four times this, 152,909 mm (*cf.* 185,115). However, nail positions were slightly different in these model joints: a selection of the most remote nails had not been used. This was because of the 'force' scale factor of two, which required the use of exactly half the number of nails in the model as in the full scale joint. This ensured that the lateral load on each "model" nail was the same as its equivalent "full scale" nail. Also, a "compressed" nail spacing arrangement was *not* used. The effect of neglecting the issue of nail spacings during the construction of the scale models was amplified by the scaled nature of these joints. Nails were 15mm apart in the transverse, cross-grain direction, compared with the "correct" spacing of 30 mm, the same as that used in the on-site joint. This may have caused premature "splitting" failures in some of the test specimens.

D.4. NAIL LOADS

a) Yield Theory Prediction

References: Aune and Patton-Mallory (1986, USA), whose equations were checked and found to be very similar to those of Smith and Whale et al (1988, Canada/UK) and Hilson-Whale (1990, UK).



Consider each nail as a 'two-member' joint.

$$\alpha = \frac{t_1}{t_2} \quad \beta = \frac{f_{e1}}{f_{e2}} \quad \gamma = \frac{F_y d^2}{6 f_e}$$

F_u = Yield Theory nail load capacity (N), f_e = timber embedment stress (MPa), t = member thickness (mm).

F_y = nail yield stress (MPa), d = nail diameter (mm), M_y = nail yield moment = $F_y d^3/6$ (Nmm).

i) Selection of Material Properties

The three input variables required by Yield Theory prediction equations, f_e (for ply and LVL) and F_y , were not measured during the laboratory tests (Lee, 1993). However, reliable estimates were obtained by careful examination of the reports on other tests involving similar materials. As is shown later, these assumptions did not affect the reliability of the Yield Theory estimate for nail load capacity.

Lheude (1990) conducted a similar Yield Theory comparison of AS1720 derived nail loads, for Radiata Pine solid wood joints involving high strength nails. His 'centrepoint bending' tests on 3.8mm diameter nails gave F_y values of 750 and 1750 MPa for dimensionally similar 'plain' and 'hardened' nails respectively. Allowing for the "high" 1750 value for the non-typical nail type used, a yield stress for 2.87mm diameter nails was estimated at 1200 MPa, using the findings of Smith and Whale et al (1988).

Lheude also showed (1988,90) that the embedment strength f_e is much greater than the nominal compressive strength for the timber, a finding also seen in the experimental verification of Aune and Patton-Mallory (1986 b) and Smith and Whale et al (1988). Nicholls (1990) conducted an embedment test on the same F16 LVL timber (tradename "HYSPAN") as that used in the Yttrup Joint, at moisture content 10.1% and density 620 kg/m³ using a "bearing" type test. He found a maximum embedment stress (at 5mm deformation) of 93.5 MPa and a 'limit of proportionality' stress (at 1.2mm) of 81.4 MPa for the longitudinal direction using 2.5mm nails. Aune and Patton-Mallory used the 'maximum' f_e value, defined as 3.8mm deformation for their 3.3mm diameter nails, while Lheude (1988,90) adopted the '3mm' f_e value for his 3.8mm nails. For the case of 2.87mm nails, it would seem that the 3mm deformation value of $f_e = 87.1$ MPa from Nicholls' experiment could be adopted for this study.

For an estimate of the plywood embedment strength, it was necessary to assume a ratio between ply and LVL f_e values, based on the work of Lheude (1988), with the LVL value derived above. Lheude found embedment strengths for Pinus radiata in both solid wood (F8) and plywood (F11) of 45 and 65 MPa respectively. The stronger and more uniform LVL product would be expected to possess a higher f_e than solid wood of a given nominal strength grade, perhaps 55 MPa in this case. This implies a ratio (β value) of 55/65 = 0.85. Therefore, for a "HYSPAN" LVL f_e of 87.1 MPa, plywood f_e may be about 102.9 MPa.

To allow for material variability in the LVL material and error in Nicholls' single experiment, a reduction of 10% was made to these figures. Embedment strengths of 78 MPa for LVL and 92 MPa for plywood were adopted in the following calculations.

ii) Yield Load Calculations

$$F_y = 1200 \text{ MPa}, d = 2.87 \text{ mm}\phi, \alpha = 63/19 = 3.316, \beta = 78/92 = 0.848, \gamma = 17.906 \text{ mm}^2$$

For the case of two member joints with unequal embedment strengths:

$$\text{Test Mode 3: Is } 2 - 2 \sqrt{\frac{\beta}{1+\beta}} < \frac{t_1}{\sqrt{\gamma}} < 2 + 2 \sqrt{\frac{\beta}{1+\beta}} \quad ?$$

$$0.645 < 4.490 < 3.355 \quad \text{NO}$$

$$\text{Check Mode 3A: Is } \frac{1}{\sqrt{\beta}} \left[2 - 2 \sqrt{\frac{1}{1+\beta}} \right] < \frac{t_2}{\sqrt{\gamma}} < \frac{1}{\sqrt{\beta}} \left[2 + 2 \sqrt{\frac{1}{1+\beta}} \right] \quad ?$$

$$0.574 < 14.888 < 3.770 \quad \text{NO, therefore Mode 4.}$$

The "Mode 4" failure is the strongest possible scenario, where the timber members have sufficient strength to allow two yield points (or 'hinges') to develop in the nail, so that the *nail* behaviour governs this failure. Yield Theory predicts a failure load of:

$$\begin{aligned} F_u &= \sqrt{\frac{4 \beta f_{e1} d M_y}{(1 + \beta)}} = d^2 \sqrt{\frac{2}{3} \frac{\beta}{1+\beta} f_{e1} F_y} \\ &= 1514 \text{ N} \end{aligned}$$

Both of the "Mode 3" failure types involve only one yield point in the nail, close to the interface between the two members. In Mode 3A, this hinge occurs within the t_1 (PLY) member, and as a result, the prediction for the yield load F_u is higher than that for Mode 3, in which the hinge forms within the t_2 (LVL).

To 'force' a Mode 3A failure, the right side of the inequality above must be obeyed. For the same 1200 MPa nails and $\beta = 0.85$ ratio between the embedment strengths, the very low value for f_{e1} of 5.9 MPa would be required. This shows that "Mode 4" will occur for these two conditions, for *all* practical values of member strengths.

It was evident from the case of two member joints (of *similar* thickness members) that the difference in timber member embedment strengths (f_e) was allowed for with the

function: $\sqrt{\frac{2\beta}{(1+\beta)}}$. Thus the expression $F_u = \sqrt{\frac{2\beta 2 f_{e1} d M_y}{(1+\beta)}}$ for the "Mode 4" yield

load, where the members have different embedment strengths ($\beta \neq 1$), was obtained from the general case ($\beta = 1$) of $F_u = \sqrt{2 f_{e1} d M_y}$. This function of β was 0.958 for the ($\beta = 0.7$) Yttrup Joint case. Therefore, any error caused by the estimate of β (taken from Lheude (1990) is *greatly* diminished. For example, if the approximation was made, representing an error of 15% in the LVL f_e , an error of only 4% would be seen in the F_u capacity

calculation: evaluating the $\beta = 1$ expression above gives $F_u = d^2 \sqrt{\frac{f_{e1} F_y}{3}} = 1580 \text{ N}$. Errors in F_u remain proportional to any error in the embedment strength f_e , so the reduced value of 92 (not 103) MPa was seen as prudent.

Therefore, a reliable Yield Theory estimate for the lateral load capacity of a single hardened nail of nominal yield strength 1200 MPa (within Yttrup Joint timber members) would be $F_u = 1515 \text{ N}$.

b) AS1720 Method

From Clause 4.2.1.2., the permissible lateral load on a single (low carbon steel) nail is:

$$Q = k_1 k_{13} k_{14} k_{16} k_{17} Q'$$

$$= 1.0 \times 1.0 \times 1.0 \times 1.1 \times 1.2 \times 239.3 = 316 \text{ N}$$

To account for the presence of high strength nails, Lheude (1990) suggested a factor of 1.4. This would give $Q = 1.4 \times 316 = 442.4 \text{ N}$. Even this “hardened nail” value is well below that given by “Yield Theory”. The major difference between the two methods is the treatment of the greater strengths of the plywood and LVL members. This was seen to increase nail head restraint to such an extent as to produce “Mode 4” failure. Also, Yield Theory is based on the (local) *embedding* strength of the timber members, rather than the (global) *compression* strength as used in AS1720. For the F17 plywood, the ratio between these is $92/12.8 = 7.2$ (AS1720 Table 5.1), while f_e is approximately $78/12 = 6.5$ times greater than F_c for the F16 LVL (AS1720 Table 2.3). So for the same joint, the AS1720 Design Method gives more conservative results than Yield Theory, as expected.

APPENDIX E. TESTING VARIABLES

E.1. NAILED JOINTS

The comparison of results between experimental programmes conducted by different researchers must include consideration of the testing apparatus and data analysis method used. The absence of a single, unified and widely adopted standard procedure for testing nailed timber joints prevents confident data correlation and in some cases the confirmation of specific results.

The main factors influencing the 'objective' nature of experiments fall into four broad categories: (a) specimen assembly techniques, (b) test apparatus, (c) interpretation and analysis of experimental data, and for the case of cyclic loading studies, (d) load magnitude and rate of application.

Polensek (1988) set himself the task of investigating the effects of these variables, specifically with respect to dynamic loading and response, for a chosen test apparatus. In relation to the damping and stiffness of nailed wood-to-sheathing joints, he commented that

"...the technique of constructing joint specimens profoundly affects test results," (a)
and that

"In evaluating equivalent viscous damping from experimental hysteresis traces relating load and slip, cyclic slip-work capacity has usually been based on a linear recovery trace of the slip and restoring force, which substantially underestimates actual damping of nailed joints." (c)

Both he and Pellicane-Bodig (1984) pointed out that because of the non-linearity of the nailed timber joint load-slip curve, three definitions are used for the slip modulus as an indication of stiffness in the elastic range. These are namely tangent, secant and chord moduli, and to further complicate the process, each one relies on the choice of characteristic points on the curve at which they are to be evaluated. (c)

A specific discussion of the effect of load magnitude and rate of application is provided in the Chapter 3.5. "Cyclic Loading Characteristics." (d)

In the light of the above, and since a large amount of experimental evidence is quoted in the "Literature Review" sections, a detailed review of the specimen assembly parameters of these researchers is provided in Table E.1. overleaf. The volume of data implied in this brief tabulation demands commentary, and this follows below: (a,b)

(a). TEST SPECIMEN ASSEMBLY TECHNIQUES

As discussed in Section 3.4. "Interface Characteristics", the lateral load resistance of a timber joint is directly related to the magnitude of the gap and the amount of interface friction between the connected members. Assembly techniques which influence these are:

- (1) wood drying after joint assembly and moisture pre-conditioning,
- (2) method used and extent of nail driving (local zones of high nail contact pressure),
- (3) withdrawal capacity (nail head shape, shank shape and coefficient of friction) and straightness of installation (pre-bored holes) of the fastener, and
- (4) roughness (planed or rough-sawn) of the wood prior to assembly.

Also, the magnitude of the load applied to the specimen will influence the rapidity of this gap formation, due to the 'yield' failure mode of the nail fastener.

Lheude (1990)	3-member 38mm or 45mm R.Pine or hardwood	1.6 or 4.5mm steel 30mm R.Pine or hardwood	12% M.C.	0.8mm shims used in all tests	3.14 mm d or 3.75mm plain and 3.80mm hardened	1.5mm, driven 10 d penetration throughout	flush to side plate	90 in 6 grouped combinations	two nails (4 used with 1.6mm steel side plates)	C push only, lateral static	deformation control, 2-3mm/min
Liu-Soltis	Douglas fir 1.5 x 3"	0.5" CDX plywood	10% M.C. 73 degF 50% R.H.	zero, .036, .057" shim, wax paper	degreased 8d common wire round	1/16"	flush and non-flush to wood	ASTM: 5 x 16 new test rig: 10 x 16 e@	single nail	T pull only, lateral static	deformation control 0.1 in./min
Lowe- Edwards	88 x 88 mm Radiata Pine	3mm cold rolled steel 12.5mm 5 ply	12.5% M.C.	half friction half .5mm	2.8mm '01A' Duplex	-	flush to side plate	12: 6 // grain and 6 perp as above	36 nails // grain, 18 perp.	push-pull, lateral cyclic	deformation control
Mack (1966)	3-member 4 species, Pine & jarrah	joins, incl. Radiata jarrah	-	zero, 0.028" and 0.056"	0.104 x 2", 0.144 x 3", 0.176 x 4"	80% d	flush to wood	6 of each species and nail size set	two nails, one in from each side	C push only	load control, 10 min duration
Nicholls	R. Pine LVL 100 x 39mm	2mm mild steel plate both sides	10.1% M.C.	-	2.5 d x 25mm hard steel	N.A., gun-nailed or driven	flat head flush to plate	three	3 nails, same both sides	T pull only, lateral static	load control, 0.2kN/sec.
	R. Pine LVL 240 x 63mm		-					two	28 each side, rectangular	T pull only, lateral static	load control, 0.13kN/sec.
Pellicane- Bodig	Douglas fir 38mm	Douglas fir 19mm	12% M.C. 0.42 SG	0, 0.51mm, talcum	6 and 8d c.'wire	1.8mm	flush to wood	10e@ x 6 tests x4 = 240 total	single nail	T pull only, lateral static	deformation 2.5mm/min
Pellicane	2" x 4" DF or Engelmann Spruce	11 species, varying thickness	ambient summer conditions	0.508mm shim for 0.01" gap	6d 0.113 x 2" 8d 0.131x 2.5" c.'wire	-	flush to wood	110 D fir 118 E. Spruce	single nail	C push only, lateral static	deformation 2.54mm/min 1 pre-cycle
Polensek	Douglas fir 2" x 4"	Douglas fir 10mm	12% M.C. for 24 hrs	(see text)	6d galv 2.5mm diam.	2mm, 75% of 6d nails	drive + push flush	25 each @ 9 loading rates	single nail	push-pull, lateral cyclic	def. control, load limited
Smith- Whale et al (nail tests)	7 solid woods	6 sheet materials, incl. 4 plys	20 +/- 2 degC, 65 +/-5%RH	-	2.65 to 4mm d common steel wire	80% d	flush to wood	4700 material, 420 joints	single nail	C push only, short term (15 min)	9 preloading cycles, loaded to failure
Soltis- Mtonga	Douglas fir 2" x 3.5"	Douglas fir 1.5"	15% M.C. ave,	clamped assembly	10d c.' wire 0.15"d x 3"	5/64" 53% of 10d	flush to wood	total of 100 cyclic, 34 static	single nail	push-pull, lateral T-C cyclic	deformation control, 20 cycles at 4 definn levels
	Douglas fir 1.5" x 4"	0.5", 5 ply plywood	65 degF, 74% RH		8d c.' wire 0.135"d x 2.5"	5/64" 60% of 8d	flush to wood		single nail		
Thomas- Malhotra	3-member Eastn. Spruce 0.75" x 3.5"	3-member Eastn. Spruce 1.5" x 3.5"	12% M.C. for 3 days (<1 hour)	tested joints 'with friction'	3.23mm d x 70mm c.'wire	2.64mm	flat head flush to wood buried 1.1"	material tests, 140 total joints	1 to 8 nails per row	C push only, lateral static	deformation control, 0.5mm/min
Wilkinson (1971)											
	main member	side plate material	pre- condition	interface gap	nail type	pre-bored hole size	nail head restraint	number of tests	nail group	load type static/cyclic	load control

The various methods used to achieve particular magnitudes of interface gap within two-member nailed timber joints are as follows:

- (i) placing precise thickness shims between the members before nailing (and removal prior to testing) (by Antonides 1980, Atherton 1980, Aune and Patton-Mallory 1986, Lheude 1990, Liu-Soltis 1984, Mack 1966, Pellicane-Bodig 1984, Pellicane 1991),
- (ii) drying the assembled joint before testing (Chou-Polensek 1987, Polensek 1988),
- (iii) drying an assembled joint with one pre-soaked member (Antonides 1980),
- (iv) over-driving of nails (Atherton 1980, Jenkins 1979),
- (v) incomplete driving of nails (Girhammar-Anderson 1988, Liu-Soltis 1984),
- (vi) clamping of members during loading (Liu-Soltis 1984, Soltis-Mtenga 1985),
- (vii) inserting wax paper into a zero-inch gap (Liu-Soltis 1984),
- (viii) the use of several oil-lubricated polyethylene shims (Jenkins 1979) and
- (ix) sprinkling talcum powder on one contact surface (Pellicane-Bodig 1984).

All provide different levels of contact pressure between the joined timber test pieces, at different stages of loading.

One point of interest was found in the Polensek (1988) paper, where interface gap was produced by the drying or 'curing' of the wood. They noticed that damping for "with gap" joints actually *increased* with increasing load. This observation is the reverse of their result for 'tight' joints, and contradicts the commonly accepted mechanism of increasing gap (hence reduced damping) for increasing load, which has been developed from 'shim' gap tests. His explanation, that "*the original gap partially disappears, so that the connected components come into partial contact, thus increasing interlayer friction and damping*" provides a new view of the 'gap vs. no gap' phenomena.

The ramifications of this would be seen in any test where a shim was removed after its use in joint fabrication (prior to loading), as is the customary practice, on the assumption that gap only increases during subsequent loading. Shims were removed in this way by Atherton et al (1980), who had a very similar cyclic loading regime to Polensek. However, since they include no similar 'damping ratio vs. load magnitude' conclusion, no judgement can be made. Lheude (1990), Liu-Soltis (1984) and Pellicane (1991) and others also removed their shims, but prior to static load tests, so the damping context is absent. Therefore, the validity of the Polensek mechanism cannot be confirmed.

One suggestion is that the very use of progressively cured unseasoned wood to obtain a desired interface gap provides the explanation. As the timber dries, its moisture content reduces, hence its timber volume reduces, creating a gap of a magnitude controlled by the time it is permitted to shrink. Timber being an organic material, this drying may also change the fibre spacing (and density) at the member surface, thus altering its roughness and friction properties, also in proportion to the drying time. Since the use of shims does not alter surface friction, a disparity may exist between the results of different tests for the same gap, created by the use of the two alternative means. However,

"Interlayer gaps obtained mechanically with shims have been shown to produce effects on nail stiffness (secant joint stiffness on load-slip curve) similar to those obtained by wetting and drying of the wood",

by Antonides et al (1980). Their joint preparation actually went to the extreme of wetting the main member (only), before fabricating the two-member joint, followed by the curing to achieve a chosen gap (same as equivalent shim produced gap) before testing. As such, surface fibre disturbance would have been maximized. Therefore, the above suggestion that this moisture content change accounts for additional friction effects not seen in 'shim' tests, must be discounted.

Hence, comparisons within two-member test series are only valid between results for one combination of main member and side plate size. No mention is made of test rig geometry by Luke and Edwards (1984) or Smith and Whale et al (1987), and eccentricity is present in the arrangement given in both referenced papers by Thomas-Malhotra.

The bending moment produced by the eccentricity of applied forces also has the effect of increasing the magnitude of the interface gap between the connected members. Since the failure mode of the nail fastener involves bending (which in turn instigates a 'prying' action, forcing the joined pieces apart) and subsequent yielding, any additional external moment acting on the nail due to test rig geometry will accelerate this 'yield' failure.

Many others have preferred a three-member assembly, thereby removing the eccentricity problem altogether, including Antonides et al (1980), Girhammar-Anderson (1988), Lheude (1990), Nicholls (1990) and Wilkinson (1986).

Pellicane and Bodig (1984) tested a range of joints using the three major two-member testing apparatus mentioned above (ASTM, Colorado and Oregon), along with three different three-member test setups. They compared the performance parameters secant elastic modulus, loads at 'proportional' and 'yield' slips, ultimate load and slip at ultimate load. (see Fig. E.2. overleaf). The comparison was made for the four combinations of two nail sizes and two interface gaps. They found that for slips greater than the 'yield' slip of 2.54mm, for all of the four joint arrangements, "*similar results can be obtained with any of the (six) test configurations*" for these performance parameters. However, during the initial stages of the load-slip record, for all four configurations, there was

"a considerable degree of sensitivity to the test method used."

They observed that with greater restraint against rotation of the test specimen, greater stiffness was recorded. The ASTM assembly (with an added restraining roller at the nail site) generally outperformed the three-member setups (two-nails per side) and the Colorado assembly, which in turn gave stiffer moduli than the Oregon rig. The uniformity of result in later stages of loadings indicates that "*initial misalignments in the specimens have become insignificant against the large slip.*"

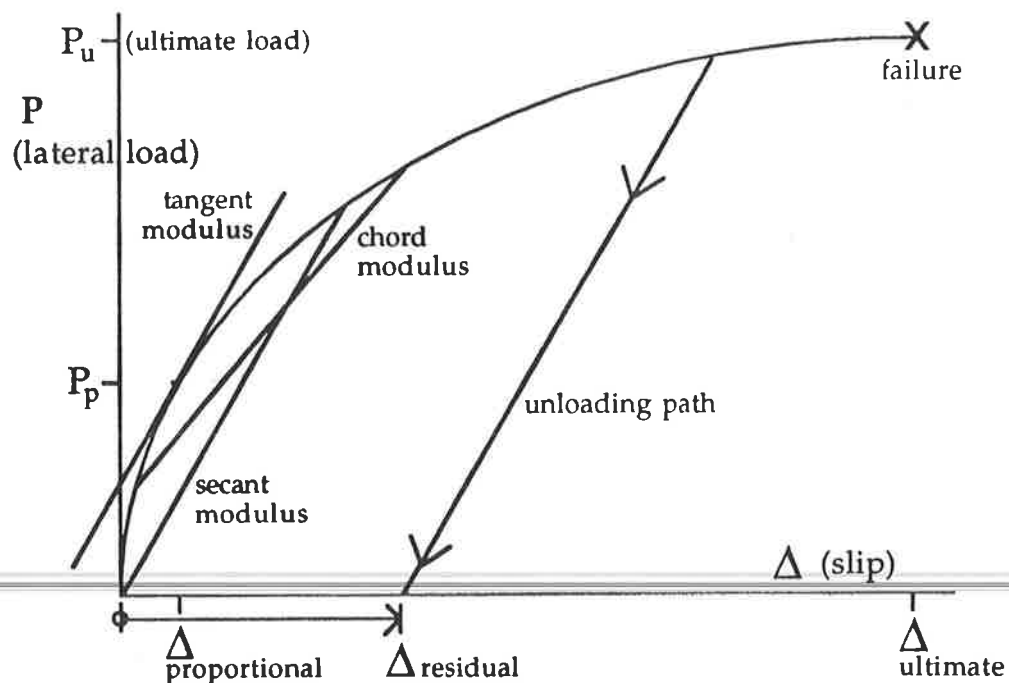


Figure E.3. An explanation of the descriptive terms for timber load-slip traces

Results from either of these two standard tests would differ from pure *tensile* yield stress values because a) bending tests neglect shear deformation effects, significant in short-span tests, b) clamps in tensile tests reduce the cross-section and cause surface indentation, affecting nail capacity at this, the failure site, c) strain hardening and applied strain rate effects and d) the definition used for 'yield' point on the stress-strain trace.

During their study to quantify the effect of static loading rate on material properties and joint performance, Girhammar-Anderson (1988) showed that F_y increased with the logarithm of the deformation rate. A 10mm/second rate gave a 10% increase in F_y over the 'static' loading case, and 14% for 100mm/sec.

b) YIELD STRESS F_y AND DIAMETER

A result of extensive nail property tests by Smith and Whale et al (1988) was the definition of nail yield strength as having a linear and negative dependency on diameter. This conclusion was supported by the work of Prof. Jurgen Ehlbeck at the Universitat Karlsruhe, Germany, and subsequently included in the current Eurocode.¹ White-McLain-Padla (1990) initially contended, then later as Loferski-McLain (1991) confirmed this finding. Even so, in 1990 they noted that :

"...the degree of work hardening during manufacture is a function of wire diameter, finished nail geometry and manufacturing technique, which are unrelated to wire chemistry."

Equations proposed for nail yield strength have been:

$$F_y = 50 (19-d) \quad (F_y \text{ in MPa, } d \text{ in mm}) \dots\dots\dots \text{Smith and Whale et al (1988, UK)}$$

$$F_y = 58 (15.5-d) \quad \dots\dots\dots \text{Loferski-McLain (1991, USA)}$$

¹ personal correspondence with Dr. Luke R. J. Whale, Technical Director, Gang Nail Systems Ltd., formerly of the Department of Civil Engineering, Brighton Polytechnic, Brighton, UK.

APPENDIX F. IMAGES-3D OUTPUT

UNIVERSITY OF ADELAIDE S/N:801903 01/02/93
 Run ID=TT14614 10:10:17
 ===== I M A G E S 3 D =====
 Copyright (c) 1984 Celestial Software Inc.
 =====

SIGNATURE JOINERY portal 4 (filename SJ23)

spring numbering: 1: left 'knee' node (5,6) "X" spring 4: right 'knee' node (18,19) "X" spring
 2: left 'knee' node (5,6) "Y" spring 5: right 'knee' node (18,19) "Y" spring
 3: left 'knee' node (5,6) "Z" spring 6: right 'knee' node (18,19) "Z" spring

frame restrained at ground level nodes 1 (East) and 23 (West) in X and Y directions only. ALL nodes restrained to zero deformation in "3-4-5" degrees of freedom: Z translation and X and Y rotations.

left column represented by members.....1 to 4 ('left' = East)

left rafter represented by members.....5 to 10 ('apex' is node 12)

right rafter represented by members.....11 to 16 ('right' = West)

right column represented by members...17 to 20

see Fig. 6.1.
 in Chapter 6

global axis sign notation: origin at node 1, X to right (West) through node 23, Y vertically through left (East) column, Z from right hand rule, out of page (North).

LOAD CASE 1 ($K_\theta = 20 \text{ E9 Nmm/radian}$)

EXTERNAL PRESSURE $p_e = C_{p,e} \times K_a (\theta = 0^\circ)$ (i.e. $q_z = 1 \text{ kPa}$, $b = 1 \text{ m}$)

GLOBAL DISPLACEMENTS (mm, radians)

Node	Translations			/	Rotations		
	X	Y	Z		X	Y	Z
1	.0000E+00	.0000E+00	.0000E+00	/	.0000E+00	.0000E+00	-.9903E-03
2	.2653E+01	.1827E-01	.0000E+00	/	.0000E+00	.0000E+00	-.6233E-03
3	.3313E+01	.2208E-01	.0000E+00	/	.0000E+00	.0000E+00	-.4604E-03
4	.3565E+01	.2369E-01	.0000E+00	/	.0000E+00	.0000E+00	-.3973E-03
5	.3723E+01	.2376E-01	.0000E+00	/	.0000E+00	.0000E+00	-.3952E-03
6	.3723E+01	.2376E-01	.0000E+00	/	.0000E+00	.0000E+00	.4972E-03
7	.3633E+01	.4759E+00	.0000E+00	/	.0000E+00	.0000E+00	.5765E-03
8	.3043E+01	.3484E+01	.0000E+00	/	.0000E+00	.0000E+00	.1618E-02
9	.2052E+01	.8472E+01	.0000E+00	/	.0000E+00	.0000E+00	.2242E-02
10	.9011E+00	.1426E+02	.0000E+00	/	.0000E+00	.0000E+00	.2326E-02
11	-.1067E+00	.1937E+02	.0000E+00	/	.0000E+00	.0000E+00	.1759E-02
12	-.6368E+00	.2215E+02	.0000E+00	/	.0000E+00	.0000E+00	.5652E-03
13	-.6760E+00	.2179E+02	.0000E+00	/	.0000E+00	.0000E+00	-.1116E-02
14	-.1519E+01	.1750E+02	.0000E+00	/	.0000E+00	.0000E+00	-.2341E-02
15	-.2793E+01	.1111E+02	.0000E+00	/	.0000E+00	.0000E+00	-.2667E-02
16	-.4042E+01	.4858E+01	.0000E+00	/	.0000E+00	.0000E+00	-.2124E-02
17	-.4864E+01	.7161E+00	.0000E+00	/	.0000E+00	.0000E+00	-.8562E-03
18	-.5001E+01	.3372E-01	.0000E+00	/	.0000E+00	.0000E+00	-.7524E-03
19	-.5001E+01	.3372E-01	.0000E+00	/	.0000E+00	.0000E+00	.4426E-03
20	-.4824E+01	.3362E-01	.0000E+00	/	.0000E+00	.0000E+00	.4455E-03
21	-.4548E+01	.3134E-01	.0000E+00	/	.0000E+00	.0000E+00	.5355E-03
22	-.3759E+01	.2593E-01	.0000E+00	/	.0000E+00	.0000E+00	.7853E-03
23	.0000E+00	.0000E+00	.0000E+00	/	.0000E+00	.0000E+00	.1436E-02

GLOBAL BEAM LOADS (N, Nmm)

GLoads	Node	Fx	Fy	Fz	Mx	My	Mz
BEAM NO. 1							
GLoads	1	.3195E+04	-.4436E+04	.0000E+00	.0000E+00	.0000E+00	-.5821E-09
GLoads	2	.4017E+04	.4436E+04	.0000E+00	.0000E+00	.0000E+00	.9880E+07
BEAM NO. 2							
GLoads	2	-.4017E+04	-.4436E+04	.0000E+00	.0000E+00	.0000E+00	-.9880E+07
GLoads	3	.4317E+04	.4436E+04	.0000E+00	.0000E+00	.0000E+00	.1405E+08
BEAM NO. 3							
GLoads	3	-.4317E+04	-.4436E+04	.0000E+00	.0000E+00	.0000E+00	-.1405E+08
GLoads	4	.4455E+04	.4436E+04	.0000E+00	.0000E+00	.0000E+00	.1606E+08
BEAM NO. 4							
GLoads	4	-.4455E+04	-.4436E+04	.0000E+00	.0000E+00	.0000E+00	-.1606E+08
GLoads	5	.4458E+04	.4436E+04	.0000E+00	.0000E+00	.0000E+00	.1785E+08
BEAM NO. 5							
GLoads	6	-.4458E+04	-.4436E+04	.0000E+00	.0000E+00	.0000E+00	-.1785E+08
GLoads	7	.4484E+04	.4310E+04	.0000E+00	.0000E+00	.0000E+00	.1505E+08
BEAM NO. 6							
GLoads	7	-.4484E+04	-.4310E+04	.0000E+00	.0000E+00	.0000E+00	-.1505E+08
GLoads	8	.4636E+04	.3562E+04	.0000E+00	.0000E+00	.0000E+00	.7773E+07
BEAM NO. 7							
GLoads	8	-.4636E+04	-.3562E+04	.0000E+00	.0000E+00	.0000E+00	-.7773E+07
GLoads	9	.4788E+04	.2814E+04	.0000E+00	.0000E+00	.0000E+00	.2378E+07
BEAM NO. 8							
GLoads	9	-.4788E+04	-.2814E+04	.0000E+00	.0000E+00	.0000E+00	-.2378E+07
GLoads	10	.4940E+04	.2066E+04	.0000E+00	.0000E+00	.0000E+00	-.1132E+07
BEAM NO. 9							
GLoads	10	-.4940E+04	-.2066E+04	.0000E+00	.0000E+00	.0000E+00	.1132E+07
GLoads	11	.5092E+04	.1319E+04	.0000E+00	.0000E+00	.0000E+00	-.2757E+07
BEAM NO. 10							
GLoads	11	-.5092E+04	-.1319E+04	.0000E+00	.0000E+00	.0000E+00	.2757E+07
GLoads	12	.5244E+04	.5707E+03	.0000E+00	.0000E+00	.0000E+00	-.2498E+07
BEAM NO. 11							
GLoads	12	-.5244E+04	-.5707E+03	.0000E+00	.0000E+00	.0000E+00	.2498E+07
GLoads	13	.4974E+04	-.7579E+03	.0000E+00	.0000E+00	.0000E+00	-.4787E+07
BEAM NO. 12							
GLoads	13	-.4974E+04	.7579E+03	.0000E+00	.0000E+00	.0000E+00	.4787E+07
GLoads	14	.4704E+04	-.2086E+04	.0000E+00	.0000E+00	.0000E+00	-.3729E+07
BEAM NO. 13							
GLoads	14	-.4704E+04	.2086E+04	.0000E+00	.0000E+00	.0000E+00	.3729E+07
GLoads	15	.4433E+04	-.3415E+04	.0000E+00	.0000E+00	.0000E+00	.6783E+06
BEAM NO. 14							
GLoads	15	-.4433E+04	.3415E+04	.0000E+00	.0000E+00	.0000E+00	-.6783E+06
GLoads	16	.4163E+04	-.4744E+04	.0000E+00	.0000E+00	.0000E+00	.8433E+07
BEAM NO. 15							
GLoads	16	-.4163E+04	.4744E+04	.0000E+00	.0000E+00	.0000E+00	-.8433E+07
GLoads	17	.3893E+04	-.6072E+04	.0000E+00	.0000E+00	.0000E+00	.1954E+08
BEAM NO. 16							
GLoads	17	-.3893E+04	.6072E+04	.0000E+00	.0000E+00	.0000E+00	-.1954E+08
GLoads	18	.3847E+04	-.6296E+04	.0000E+00	.0000E+00	.0000E+00	.2390E+08
BEAM NO. 17							
GLoads	19	-.3847E+04	.6296E+04	.0000E+00	.0000E+00	.0000E+00	-.2390E+08
GLoads	20	.3854E+04	-.6296E+04	.0000E+00	.0000E+00	.0000E+00	.2236E+08
BEAM NO. 18							
GLoads	20	-.3854E+04	.6296E+04	.0000E+00	.0000E+00	.0000E+00	-.2236E+08
GLoads	21	.4176E+04	-.6296E+04	.0000E+00	.0000E+00	.0000E+00	.2051E+08
BEAM NO. 19							
GLoads	21	-.4176E+04	.6296E+04	.0000E+00	.0000E+00	.0000E+00	-.2051E+08
GLoads	22	.4876E+04	-.6296E+04	.0000E+00	.0000E+00	.0000E+00	.1599E+08
BEAM NO. 20							
GLoads	22	-.4876E+04	.6296E+04	.0000E+00	.0000E+00	.0000E+00	-.1599E+08
GLoads	23	.6794E+04	-.6296E+04	.0000E+00	.0000E+00	.0000E+00	-.7567E-09

GLOBAL SPRING LOADS (N, Nmm)

Type	Node	Fx	Fy	Fz	Mx	My	Mz
SPRG NO. 1							
GLoads	5	-.4458E+04	.0000E+00	.0000E+00	.0000E+00	.0000E+00	.0000E+00
GLoads	6	.4458E+04	.0000E+00	.0000E+00	.0000E+00	.0000E+00	.0000E+00
SPRG NO. 2							
GLoads	5	.0000E+00	-.4436E+04	.0000E+00	.0000E+00	.0000E+00	.0000E+00
GLoads	6	.0000E+00	.4436E+04	.0000E+00	.0000E+00	.0000E+00	.0000E+00
SPRG NO. 3							
GLoads	5	.0000E+00	.0000E+00	.0000E+00	.0000E+00	.0000E+00	-.1785E+08
GLoads	6	.0000E+00	.0000E+00	.0000E+00	.0000E+00	.0000E+00	.1785E+08
SPRG NO. 4							
GLoads	18	-.3847E+04	.0000E+00	.0000E+00	.0000E+00	.0000E+00	.0000E+00
GLoads	19	.3847E+04	.0000E+00	.0000E+00	.0000E+00	.0000E+00	.0000E+00
SPRG NO. 5							
GLoads	18	.0000E+00	.6296E+04	.0000E+00	.0000E+00	.0000E+00	.0000E+00
GLoads	19	.0000E+00	-.6296E+04	.0000E+00	.0000E+00	.0000E+00	.0000E+00
SPRG NO. 6							
GLoads	18	.0000E+00	.0000E+00	.0000E+00	.0000E+00	.0000E+00	-.2390E+08
GLoads	19	.0000E+00	.0000E+00	.0000E+00	.0000E+00	.0000E+00	.2390E+08

GLOBAL REACTIONS (N, Nmm)

Node	Fx	Fy	Fz	Mx	My	Mz
1	-.3195E+04	-.4436E+04	.0000E+00	.0000E+00	.0000E+00	.0000E+00
23	.6794E+04	-.6296E+04	.0000E+00	.0000E+00	.0000E+00	.0000E+00

LOAD CASE 2 ($K_{\theta} = 20 \text{ E9 Nmm/radian}$)

EXTERNAL PRESSURE $p_e = C_{p,e} \times K_a (\theta = 90^\circ)$

GLOBAL DISPLACEMENTS (mm, radians)

Node	Translations			/	Rotations		
	X	Y	Z		X	Y	Z
1	.0000E+00	.0000E+00	.0000E+00	/	.0000E+00	.0000E+00	-.7934E-03
2	.2134E+01	.1767E-01	.0000E+00	/	.0000E+00	.0000E+00	-.4984E-03
3	.2670E+01	.2136E-01	.0000E+00	/	.0000E+00	.0000E+00	-.3624E-03
4	.2874E+01	.2291E-01	.0000E+00	/	.0000E+00	.0000E+00	-.3088E-03
5	.2997E+01	.2298E-01	.0000E+00	/	.0000E+00	.0000E+00	-.3070E-03
6	.2997E+01	.2298E-01	.0000E+00	/	.0000E+00	.0000E+00	.4603E-03
7	.2914E+01	.4421E+00	.0000E+00	/	.0000E+00	.0000E+00	.5272E-03
8	.2402E+01	.3058E+01	.0000E+00	/	.0000E+00	.0000E+00	.1356E-02
9	.1603E+01	.7094E+01	.0000E+00	/	.0000E+00	.0000E+00	.1742E-02
10	.7630E+00	.1135E+02	.0000E+00	/	.0000E+00	.0000E+00	.1601E-02
11	.1560E+00	.1447E+02	.0000E+00	/	.0000E+00	.0000E+00	.9228E-03
12	-.2588E-06	.1540E+02	.0000E+00	/	.0000E+00	.0000E+00	-.3601E-10
13	-.1560E+00	.1447E+02	.0000E+00	/	.0000E+00	.0000E+00	-.9228E-03
14	-.7630E+00	.1135E+02	.0000E+00	/	.0000E+00	.0000E+00	-.1601E-02
15	-.1603E+01	.7094E+01	.0000E+00	/	.0000E+00	.0000E+00	-.1742E-02
16	-.2402E+01	.3058E+01	.0000E+00	/	.0000E+00	.0000E+00	-.1356E-02
17	-.2914E+01	.4421E+00	.0000E+00	/	.0000E+00	.0000E+00	-.5272E-03
18	-.2997E+01	.2298E-01	.0000E+00	/	.0000E+00	.0000E+00	-.4603E-03
19	-.2997E+01	.2298E-01	.0000E+00	/	.0000E+00	.0000E+00	.3070E-03
20	-.2874E+01	.2291E-01	.0000E+00	/	.0000E+00	.0000E+00	.3088E-03
21	-.2670E+01	.2136E-01	.0000E+00	/	.0000E+00	.0000E+00	.3624E-03
22	-.2134E+01	.1767E-01	.0000E+00	/	.0000E+00	.0000E+00	.4984E-03
23	.0000E+00	.0000E+00	.0000E+00	/	.0000E+00	.0000E+00	.7934E-03

GLOBAL BEAM LOADS (N, Nmm)

GLoads	Node	Fx	Fy	Fz	Mx	My	Mz
BEAM NO. 1							
GLoads	1	-.2423E+04	-.4290E+04	.0000E+00	.0000E+00	.0000E+00	.8731E-10
GLoads	2	.3519E+04	.4290E+04	.0000E+00	.0000E+00	.0000E+00	.8140E+07
BEAM NO. 2							
GLoads	2	-.3519E+04	-.4290E+04	.0000E+00	.0000E+00	.0000E+00	-.8140E+07
GLoads	3	.3919E+04	.4290E+04	.0000E+00	.0000E+00	.0000E+00	.1186E+08
BEAM NO. 3							
GLoads	3	-.3919E+04	-.4290E+04	.0000E+00	.0000E+00	.0000E+00	-.1186E+08
GLoads	4	.4103E+04	.4290E+04	.0000E+00	.0000E+00	.0000E+00	.1370E+08
BEAM NO. 4							
GLoads	4	-.4103E+04	-.4290E+04	.0000E+00	.0000E+00	.0000E+00	-.1370E+08
GLoads	5	.4107E+04	.4290E+04	.0000E+00	.0000E+00	.0000E+00	.1535E+08
BEAM NO. 5							
GLoads	6	-.4107E+04	-.4290E+04	.0000E+00	.0000E+00	.0000E+00	-.1535E+08
GLoads	7	.4135E+04	.4150E+04	.0000E+00	.0000E+00	.0000E+00	.1261E+08
BEAM NO. 6							
GLoads	7	-.4135E+04	-.4150E+04	.0000E+00	.0000E+00	.0000E+00	-.1261E+08
GLoads	8	.4304E+04	.3320E+04	.0000E+00	.0000E+00	.0000E+00	.5651E+07
BEAM NO. 7							
GLoads	8	-.4304E+04	-.3320E+04	.0000E+00	.0000E+00	.0000E+00	-.5651E+07
GLoads	9	.4473E+04	.2490E+04	.0000E+00	.0000E+00	.0000E+00	.7822E+06
BEAM NO. 8							
GLoads	9	-.4473E+04	-.2490E+04	.0000E+00	.0000E+00	.0000E+00	-.7822E+06
GLoads	10	.4642E+04	.1660E+04	.0000E+00	.0000E+00	.0000E+00	-.1996E+07
BEAM NO. 9							
GLoads	10	-.4642E+04	-.1660E+04	.0000E+00	.0000E+00	.0000E+00	.1996E+07

```

GLoads 11 .4811E+04 .8301E+03 .0000E+00 .0000E+00 .0000E+00 -.2681E+07
***BEAM NO. 10***
GLoads 11 -.4811E+04 -.8301E+03 .0000E+00 .0000E+00 .0000E+00 .2681E+07
GLoads 12 .4980E+04 .1633E-04 .0000E+00 .0000E+00 .0000E+00 -.1275E+07
***BEAM NO. 11***
GLoads 12 -.4980E+04 .1633E-04 .0000E+00 .0000E+00 .0000E+00 .1275E+07
GLoads 13 .4811E+04 .8301E+03 .0000E+00 .0000E+00 .0000E+00 -.2681E+07
***BEAM NO. 12***
GLoads 13 -.4811E+04 .8301E+03 .0000E+00 .0000E+00 .0000E+00 .2681E+07
GLoads 14 .4642E+04 .1660E+04 .0000E+00 .0000E+00 .0000E+00 -.1996E+07
***BEAM NO. 13***
GLoads 14 -.4642E+04 .1660E+04 .0000E+00 .0000E+00 .0000E+00 .1996E+07
GLoads 15 .4473E+04 .2490E+04 .0000E+00 .0000E+00 .0000E+00 .7822E+06
***BEAM NO. 14***
GLoads 15 -.4473E+04 .2490E+04 .0000E+00 .0000E+00 .0000E+00 -.7822E+06
GLoads 16 .4304E+04 .3320E+04 .0000E+00 .0000E+00 .0000E+00 .5651E+07
***BEAM NO. 15***
GLoads 16 -.4304E+04 .3320E+04 .0000E+00 .0000E+00 .0000E+00 -.5651E+07
GLoads 17 .4135E+04 .4150E+04 .0000E+00 .0000E+00 .0000E+00 .1261E+08
***BEAM NO. 16***
GLoads 17 -.4135E+04 .4150E+04 .0000E+00 .0000E+00 .0000E+00 -.1261E+08
GLoads 18 .4107E+04 .4290E+04 .0000E+00 .0000E+00 .0000E+00 .1535E+08
***BEAM NO. 17***
GLoads 18 -.4107E+04 .4290E+04 .0000E+00 .0000E+00 .0000E+00 -.1535E+08
GLoads 19 .4103E+04 .4290E+04 .0000E+00 .0000E+00 .0000E+00 .1370E+08
***BEAM NO. 18***
GLoads 19 -.4103E+04 .4290E+04 .0000E+00 .0000E+00 .0000E+00 -.1370E+08
GLoads 20 .3919E+04 .4290E+04 .0000E+00 .0000E+00 .0000E+00 .1186E+08
***BEAM NO. 19***
GLoads 20 -.3919E+04 .4290E+04 .0000E+00 .0000E+00 .0000E+00 -.1186E+08
GLoads 21 .3519E+04 .4290E+04 .0000E+00 .0000E+00 .0000E+00 .8140E+07
***BEAM NO. 20***
GLoads 21 -.3519E+04 .4290E+04 .0000E+00 .0000E+00 .0000E+00 -.8140E+07
GLoads 22 .2423E+04 .4290E+04 .0000E+00 .0000E+00 .0000E+00 .3842E-08

```

GLOBAL SPRING LOADS (N, Nmm)

Type	Node	Fx	Fy	Fz	Mx	My	Mz
SPRG NO. 1							
GLoads	5	-.4107E+04	.0000E+00	.0000E+00	.0000E+00	.0000E+00	.0000E+00
GLoads	6	.4107E+04	.0000E+00	.0000E+00	.0000E+00	.0000E+00	.0000E+00
SPRG NO. 2							
GLoads	5	.0000E+00	-.4290E+04	.0000E+00	.0000E+00	.0000E+00	.0000E+00
GLoads	6	.0000E+00	.4290E+04	.0000E+00	.0000E+00	.0000E+00	.0000E+00
SPRG NO. 3							
GLoads	5	.0000E+00	.0000E+00	.0000E+00	.0000E+00	.0000E+00	-.1535E+08
GLoads	6	.0000E+00	.0000E+00	.0000E+00	.0000E+00	.0000E+00	.1535E+08
SPRG NO. 4							
GLoads	18	-.4107E+04	.0000E+00	.0000E+00	.0000E+00	.0000E+00	.0000E+00
GLoads	19	.4107E+04	.0000E+00	.0000E+00	.0000E+00	.0000E+00	.0000E+00
SPRG NO. 5							
GLoads	18	.0000E+00	.4290E+04	.0000E+00	.0000E+00	.0000E+00	.0000E+00
GLoads	19	.0000E+00	-.4290E+04	.0000E+00	.0000E+00	.0000E+00	.0000E+00
SPRG NO. 6							
GLoads	18	.0000E+00	.0000E+00	.0000E+00	.0000E+00	.0000E+00	-.1535E+08
GLoads	19	.0000E+00	.0000E+00	.0000E+00	.0000E+00	.0000E+00	.1535E+08

GLOBAL REACTIONS (N, Nmm)

Node	Fx	Fy	Fz	Mx	My	Mz
1	-.2423E+04	-.4290E+04	.0000E+00	.0000E+00	.0000E+00	.0000E+00
23	.2423E+04	.4290E+04	.0000E+00	.0000E+00	.0000E+00	.0000E+00

LOAD CASE 1 ($K_\theta = 3 \text{ E9 Nmm/radian}$)

EXTERNAL PRESSURE $p_e = C_{p,e} \times K_a$ ($\theta = 0^\circ$) (i.e. $q_i = 1 \text{ kPa}$, $b = 1 \text{ m}$)

GLOBAL DISPLACEMENTS (mm, radians)

Node	Translations			/	Rotations		
	X	Y	Z		X	Y	Z
1	.0000E+00	.0000E+00	.0000E+00	/	.0000E+00	.0000E+00	-.1545E-02
2	.4184E+01	.1827E-01	.0000E+00	/	.0000E+00	.0000E+00	-.1233E-02
3	.5450E+01	.2208E-01	.0000E+00	/	.0000E+00	.0000E+00	-.1093E-02
4	.5989E+01	.2369E-01	.0000E+00	/	.0000E+00	.0000E+00	-.1038E-02
5	.6404E+01	.2376E-01	.0000E+00	/	.0000E+00	.0000E+00	-.1036E-02
6	.6404E+01	.2376E-01	.0000E+00	/	.0000E+00	.0000E+00	.4121E-02
7	.5724E+01	.3373E+01	.0000E+00	/	.0000E+00	.0000E+00	.4188E-02
8	.3410E+01	.1484E+02	.0000E+00	/	.0000E+00	.0000E+00	.4989E-02
9	.8421E+00	.2757E+02	.0000E+00	/	.0000E+00	.0000E+00	.5253E-02
10	-.1660E+01	.3998E+02	.0000E+00	/	.0000E+00	.0000E+00	.4777E-02
11	-.3660E+01	.4995E+02	.0000E+00	/	.0000E+00	.0000E+00	.3305E-02
12	-.4581E+01	.5464E+02	.0000E+00	/	.0000E+00	.0000E+00	.5652E-03
13	-.5011E+01	.5237E+02	.0000E+00	/	.0000E+00	.0000E+00	-.2663E-02
14	-.6847E+01	.4322E+02	.0000E+00	/	.0000E+00	.0000E+00	-.4792E-02
15	-.9471E+01	.3021E+02	.0000E+00	/	.0000E+00	.0000E+00	-.5678E-02
16	-.1230E+02	.1622E+02	.0000E+00	/	.0000E+00	.0000E+00	-.5496E-02
17	-.1484E+02	.3613E+01	.0000E+00	/	.0000E+00	.0000E+00	-.4467E-02
18	-.1557E+02	.3372E-01	.0000E+00	/	.0000E+00	.0000E+00	-.4376E-02
19	-.1557E+02	.3372E-01	.0000E+00	/	.0000E+00	.0000E+00	.2799E-02
20	-.1445E+02	.3362E-01	.0000E+00	/	.0000E+00	.0000E+00	.2801E-02
21	-.1310E+02	.3134E-01	.0000E+00	/	.0000E+00	.0000E+00	.2883E-02
22	-.9989E+01	.2593E-01	.0000E+00	/	.0000E+00	.0000E+00	.3110E-02
23	.0000E+00	.0000E+00	.0000E+00	/	.0000E+00	.0000E+00	.3706E-02

GLOBAL BEAM LOADS (N, Nmm)

GLoads	Node	Fx	Fy	Fz	Mx	My	Mz
BEAM NO. 1							
GLoads	1	-.2678E+04	-.4436E+04	.0000E+00	.0000E+00	.0000E+00	.2707E-08
GLoads	2	.3500E+04	.4436E+04	.0000E+00	.0000E+00	.0000E+00	.8464E+07
BEAM NO. 2							
GLoads	2	-.3500E+04	-.4436E+04	.0000E+00	.0000E+00	.0000E+00	-.8464E+07
GLoads	3	.3800E+04	.4436E+04	.0000E+00	.0000E+00	.0000E+00	.1211E+08
BEAM NO. 3							
GLoads	3	-.3800E+04	-.4436E+04	.0000E+00	.0000E+00	.0000E+00	-.1211E+08
GLoads	4	.3938E+04	.4436E+04	.0000E+00	.0000E+00	.0000E+00	.1389E+08
BEAM NO. 4							
GLoads	4	-.3938E+04	-.4436E+04	.0000E+00	.0000E+00	.0000E+00	-.1389E+08
GLoads	5	.3941E+04	.4436E+04	.0000E+00	.0000E+00	.0000E+00	.1547E+08
BEAM NO. 5							
GLoads	6	-.3941E+04	-.4436E+04	.0000E+00	.0000E+00	.0000E+00	-.1547E+08
GLoads	7	.3967E+04	.4310E+04	.0000E+00	.0000E+00	.0000E+00	.1259E+08
BEAM NO. 6							
GLoads	7	-.3967E+04	-.4310E+04	.0000E+00	.0000E+00	.0000E+00	-.1259E+08
GLoads	8	.4119E+04	.3562E+04	.0000E+00	.0000E+00	.0000E+00	.5057E+07
BEAM NO. 7							
GLoads	8	-.4119E+04	-.3562E+04	.0000E+00	.0000E+00	.0000E+00	-.5057E+07
GLoads	9	.4271E+04	.2814E+04	.0000E+00	.0000E+00	.0000E+00	-.5916E+06
BEAM NO. 8							
GLoads	9	-.4271E+04	-.2814E+04	.0000E+00	.0000E+00	.0000E+00	.5916E+06
GLoads	10	.4423E+04	.2066E+04	.0000E+00	.0000E+00	.0000E+00	-.4356E+07
BEAM NO. 9							
GLoads	10	-.4423E+04	-.2066E+04	.0000E+00	.0000E+00	.0000E+00	.4356E+07

GLoads 11 .4576E+04 .1319E+04 .0000E+00 .0000E+00 .0000E+00 .6236E+07
 BEAM NO. 10
 GLoads 11 -.4576E+04 -.1319E+04 .0000E+00 .0000E+00 .0000E+00 .6236E+07
 GLoads 12 .4728E+04 .5707E+03 .0000E+00 .0000E+00 .0000E+00 .6231E+07
 BEAM NO. 11
 GLoads 12 -.4728E+04 -.5707E+03 .0000E+00 .0000E+00 .0000E+00 .6231E+07
 GLoads 13 .4457E+04 .7579E+03 .0000E+00 .0000E+00 .0000E+00 .8266E+07
 BEAM NO. 12
 GLoads 13 -.4457E+04 -.7579E+03 .0000E+00 .0000E+00 .0000E+00 .8266E+07
 GLoads 14 .4187E+04 .2086E+04 .0000E+00 .0000E+00 .0000E+00 .6953E+07
 BEAM NO. 13
 GLoads 14 -.4187E+04 -.2086E+04 .0000E+00 .0000E+00 .0000E+00 .6953E+07
 GLoads 15 .3917E+04 .3415E+04 .0000E+00 .0000E+00 .0000E+00 .2292E+07
 BEAM NO. 14
 GLoads 15 -.3917E+04 -.3415E+04 .0000E+00 .0000E+00 .0000E+00 .2292E+07
 GLoads 16 .3646E+04 .4744E+04 .0000E+00 .0000E+00 .0000E+00 .5718E+07
 BEAM NO. 15
 GLoads 16 -.3646E+04 -.4744E+04 .0000E+00 .0000E+00 .0000E+00 .5718E+07
 GLoads 17 .3376E+04 .6072E+04 .0000E+00 .0000E+00 .0000E+00 .1708E+08
 BEAM NO. 16
 GLoads 17 -.3376E+04 -.6072E+04 .0000E+00 .0000E+00 .0000E+00 .1708E+08
 GLoads 18 .3330E+04 .6296E+04 .0000E+00 .0000E+00 .0000E+00 .2152E+08
 BEAM NO. 17
 GLoads 18 -.3330E+04 -.6296E+04 .0000E+00 .0000E+00 .0000E+00 .2152E+08
 GLoads 19 .3337E+04 .6296E+04 .0000E+00 .0000E+00 .0000E+00 .2019E+08
 BEAM NO. 18
 GLoads 19 -.3337E+04 -.6296E+04 .0000E+00 .0000E+00 .0000E+00 .2019E+08
 GLoads 20 .3659E+04 .6296E+04 .0000E+00 .0000E+00 .0000E+00 .1858E+08
 BEAM NO. 19
 GLoads 20 -.3659E+04 -.6296E+04 .0000E+00 .0000E+00 .0000E+00 .1858E+08
 GLoads 21 .4359E+04 .6296E+04 .0000E+00 .0000E+00 .0000E+00 .1457E+08
 BEAM NO. 20
 GLoads 21 -.4359E+04 -.6296E+04 .0000E+00 .0000E+00 .0000E+00 .1457E+08
 GLoads 22 .6277E+04 .6296E+04 .0000E+00 .0000E+00 .0000E+00 .7858E-08
 GLoads 23 -.6277E+04 -.6296E+04 .0000E+00 .0000E+00 .0000E+00 .7858E-08

GLOBAL SPRING LOADS (N, Nmm)

Type	Node	Fx	Fy	Fz	Mx	My	Mz
SPRG NO. 1							
GLoads	5	.3941E+04	.0000E+00	.0000E+00	.0000E+00	.0000E+00	.0000E+00
GLoads	6	.3941E+04	.0000E+00	.0000E+00	.0000E+00	.0000E+00	.0000E+00
SPRG NO. 2							
GLoads	5	.0000E+00	.4436E+04	.0000E+00	.0000E+00	.0000E+00	.0000E+00
GLoads	6	.0000E+00	.4436E+04	.0000E+00	.0000E+00	.0000E+00	.0000E+00
SPRG NO. 3							
GLoads	5	.0000E+00	.0000E+00	.0000E+00	.0000E+00	.0000E+00	-.1547E+08
GLoads	6	.0000E+00	.0000E+00	.0000E+00	.0000E+00	.0000E+00	.1547E+08
SPRG NO. 4							
GLoads	18	-.3330E+04	.0000E+00	.0000E+00	.0000E+00	.0000E+00	.0000E+00
GLoads	19	.3330E+04	.0000E+00	.0000E+00	.0000E+00	.0000E+00	.0000E+00
SPRG NO. 5							
GLoads	18	.0000E+00	.6296E+04	.0000E+00	.0000E+00	.0000E+00	.0000E+00
GLoads	19	.0000E+00	-.6296E+04	.0000E+00	.0000E+00	.0000E+00	.0000E+00
SPRG NO. 6							
GLoads	18	.0000E+00	.0000E+00	.0000E+00	.0000E+00	.0000E+00	-.2152E+08
GLoads	19	.0000E+00	.0000E+00	.0000E+00	.0000E+00	.0000E+00	.2152E+08

GLOBAL REACTIONS (N, Nmm)

Node	Fx	Fy	Fz	Mx	My	Mz
1	-.2678E+04	-.4436E+04	.0000E+00	.0000E+00	.0000E+00	.0000E+00
23	.6277E+04	.6296E+04	.0000E+00	.0000E+00	.0000E+00	.0000E+00

LOAD CASE 2 ($K_{\theta} = 3 E9 \text{ Nmm/radian}$)

EXTERNAL PRESSURE $p_e = C_{p,e} \times K_a$ ($\theta = 90^\circ$)

GLOBAL DISPLACEMENTS (mm, radians)

Node	Translations			/	Rotations		
	X	Y	Z		X	Y	Z
1	.0000E+00	.0000E+00	.0000E+00	/	.0000E+00	.0000E+00	-.1832E-02
2	.4987E+01	.1767E-01	.0000E+00	/	.0000E+00	.0000E+00	-.1577E-02
3	.6599E+01	.2136E-01	.0000E+00	/	.0000E+00	.0000E+00	-.1458E-02
4	.7304E+01	.2291E-01	.0000E+00	/	.0000E+00	.0000E+00	-.1410E-02
5	.7868E+01	.2298E-01	.0000E+00	/	.0000E+00	.0000E+00	-.1409E-02
6	.7868E+01	.2298E-01	.0000E+00	/	.0000E+00	.0000E+00	.3124E-02
7	.7350E+01	.2572E+01	.0000E+00	/	.0000E+00	.0000E+00	.3182E-02
8	.5571E+01	.1141E+02	.0000E+00	/	.0000E+00	.0000E+00	.3835E-02
9	.3613E+01	.2113E+02	.0000E+00	/	.0000E+00	.0000E+00	.3956E-02
10	.1780E+01	.3026E+02	.0000E+00	/	.0000E+00	.0000E+00	.3403E-02
11	.4435E+00	.3696E+02	.0000E+00	/	.0000E+00	.0000E+00	.2060E-02
12	-.7090E-05	.3929E+02	.0000E+00	/	.0000E+00	.0000E+00	-.4760E-09
13	-.4435E+00	.3696E+02	.0000E+00	/	.0000E+00	.0000E+00	-.2060E-02
14	-.1780E+01	.3026E+02	.0000E+00	/	.0000E+00	.0000E+00	-.3403E-02
15	-.3613E+01	.2113E+02	.0000E+00	/	.0000E+00	.0000E+00	-.3956E-02
16	-.5571E+01	.1141E+02	.0000E+00	/	.0000E+00	.0000E+00	-.3835E-02
17	-.7350E+01	.2572E+01	.0000E+00	/	.0000E+00	.0000E+00	-.3182E-02
18	-.7868E+01	.2298E-01	.0000E+00	/	.0000E+00	.0000E+00	-.3124E-02
19	-.7868E+01	.2298E-01	.0000E+00	/	.0000E+00	.0000E+00	.1409E-02
20	-.7304E+01	.2291E-01	.0000E+00	/	.0000E+00	.0000E+00	.1410E-02
21	-.6599E+01	.2136E-01	.0000E+00	/	.0000E+00	.0000E+00	.1458E-02
22	-.4987E+01	.1767E-01	.0000E+00	/	.0000E+00	.0000E+00	.1577E-02
23	.0000E+00	.0000E+00	.0000E+00	/	.0000E+00	.0000E+00	.1832E-02

GLOBAL BEAM LOADS (N, Nmm)

GLoads	Node	Fx	Fy	Fz	Mx	My	Mz
BEAM NO. 1							
GLoads	1	-.2043E+04	-.4290E+04	.0000E+00	.0000E+00	.0000E+00	-.3289E-08
GLoads	2	.3139E+04	.4290E+04	.0000E+00	.0000E+00	.0000E+00	.7099E+07
BEAM NO. 2							
GLoads	2	-.3139E+04	-.4290E+04	.0000E+00	.0000E+00	.0000E+00	-.7099E+07
GLoads	3	.3539E+04	.4290E+04	.0000E+00	.0000E+00	.0000E+00	.1044E+08
BEAM NO. 3							
GLoads	3	-.3539E+04	-.4290E+04	.0000E+00	.0000E+00	.0000E+00	-.1044E+08
GLoads	4	.3723E+04	.4290E+04	.0000E+00	.0000E+00	.0000E+00	.1211E+08
BEAM NO. 4							
GLoads	4	-.3723E+04	-.4290E+04	.0000E+00	.0000E+00	.0000E+00	-.1211E+08
GLoads	5	.3727E+04	.4290E+04	.0000E+00	.0000E+00	.0000E+00	.1360E+08
BEAM NO. 5							
GLoads	6	-.3727E+04	-.4290E+04	.0000E+00	.0000E+00	.0000E+00	-.1360E+08
GLoads	7	.3755E+04	.4150E+04	.0000E+00	.0000E+00	.0000E+00	.1080E+08
BEAM NO. 6							
GLoads	7	-.3755E+04	-.4150E+04	.0000E+00	.0000E+00	.0000E+00	-.1080E+08
GLoads	8	.3924E+04	.3320E+04	.0000E+00	.0000E+00	.0000E+00	.3655E+07
BEAM NO. 7							
GLoads	8	-.3924E+04	-.3320E+04	.0000E+00	.0000E+00	.0000E+00	-.3655E+07
GLoads	9	.4093E+04	.2490E+04	.0000E+00	.0000E+00	.0000E+00	-.1401E+07
BEAM NO. 8							
GLoads	9	-.4093E+04	-.2490E+04	.0000E+00	.0000E+00	.0000E+00	.1401E+07
GLoads	10	.4262E+04	.1660E+04	.0000E+00	.0000E+00	.0000E+00	-.4366E+07
BEAM NO. 9							
GLoads	10	-.4262E+04	-.1660E+04	.0000E+00	.0000E+00	.0000E+00	.4366E+07

```

GLoads 11 .4431E+04 .8301E+03 .0000E+00 .0000E+00 .0000E+00 .5239E+07
***BEAM NO. 10***
GLoads 11 -.4431E+04 -.8301E+03 .0000E+00 .0000E+00 .0000E+00 .5239E+07
GLoads 12 .4600E+04 -.2158E-03 .0000E+00 .0000E+00 .0000E+00 .4020E+07
***BEAM NO. 11***
GLoads 12 -.4600E+04 .2158E-03 .0000E+00 .0000E+00 .0000E+00 .4020E+07
GLoads 13 .4431E+04 -.8301E+03 .0000E+00 .0000E+00 .0000E+00 .5239E+07
***BEAM NO. 12***
GLoads 13 -.4431E+04 .8301E+03 .0000E+00 .0000E+00 .0000E+00 .5239E+07
GLoads 14 .4262E+04 -.1660E+04 .0000E+00 .0000E+00 .0000E+00 .4366E+07
***BEAM NO. 13***
GLoads 14 -.4262E+04 .1660E+04 .0000E+00 .0000E+00 .0000E+00 .4366E+07
GLoads 15 .4093E+04 -.2490E+04 .0000E+00 .0000E+00 .0000E+00 .1401E+07
***BEAM NO. 14***
GLoads 15 -.4093E+04 .2490E+04 .0000E+00 .0000E+00 .0000E+00 .1401E+07
GLoads 16 .3924E+04 -.3320E+04 .0000E+00 .0000E+00 .0000E+00 .3655E+07
***BEAM NO. 15***
GLoads 16 -.3924E+04 .3320E+04 .0000E+00 .0000E+00 .0000E+00 .3655E+07
GLoads 17 .3755E+04 -.4150E+04 .0000E+00 .0000E+00 .0000E+00 .1080E+08
***BEAM NO. 16***
GLoads 17 -.3755E+04 .4150E+04 .0000E+00 .0000E+00 .0000E+00 .1080E+08
GLoads 18 .3727E+04 -.4290E+04 .0000E+00 .0000E+00 .0000E+00 .1360E+08
***BEAM NO. 17***
GLoads 18 -.3727E+04 .4290E+04 .0000E+00 .0000E+00 .0000E+00 .1360E+08
GLoads 19 .3723E+04 -.4290E+04 .0000E+00 .0000E+00 .0000E+00 .1211E+08
***BEAM NO. 18***
GLoads 19 -.3723E+04 .4290E+04 .0000E+00 .0000E+00 .0000E+00 .1211E+08
GLoads 20 .3539E+04 -.4290E+04 .0000E+00 .0000E+00 .0000E+00 .1044E+08
***BEAM NO. 19***
GLoads 20 -.3539E+04 .4290E+04 .0000E+00 .0000E+00 .0000E+00 .1044E+08
GLoads 21 .3139E+04 -.4290E+04 .0000E+00 .0000E+00 .0000E+00 .7099E+07
***BEAM NO. 20***
GLoads 21 -.3139E+04 .4290E+04 .0000E+00 .0000E+00 .0000E+00 .7099E+07
GLoads 22 .2043E+04 -.4290E+04 .0000E+00 .0000E+00 .0000E+00 .1659E-08

```

GLOBAL SPRING LOADS (N, Nmm)

Type	Node	Fx	Fy	Fz	Mx	My	Mz
SPRG NO. 1							
GLoads	5	.3727E+04	.0000E+00	.0000E+00	.0000E+00	.0000E+00	.0000E+00
GLoads	6	.3727E+04	.0000E+00	.0000E+00	.0000E+00	.0000E+00	.0000E+00
SPRG NO. 2							
GLoads	5	.0000E+00	-.4290E+04	.0000E+00	.0000E+00	.0000E+00	.0000E+00
GLoads	6	.0000E+00	.4290E+04	.0000E+00	.0000E+00	.0000E+00	.0000E+00
SPRG NO. 3							
GLoads	5	.0000E+00	.0000E+00	.0000E+00	.0000E+00	.0000E+00	-.1360E+08
GLoads	6	.0000E+00	.0000E+00	.0000E+00	.0000E+00	.0000E+00	.1360E+08
SPRG NO. 4							
GLoads	18	-.3727E+04	.0000E+00	.0000E+00	.0000E+00	.0000E+00	.0000E+00
GLoads	19	.3727E+04	.0000E+00	.0000E+00	.0000E+00	.0000E+00	.0000E+00
SPRG NO. 5							
GLoads	18	.0000E+00	.4290E+04	.0000E+00	.0000E+00	.0000E+00	.0000E+00
GLoads	19	.0000E+00	-.4290E+04	.0000E+00	.0000E+00	.0000E+00	.0000E+00
SPRG NO. 6							
GLoads	18	.0000E+00	.0000E+00	.0000E+00	.0000E+00	.0000E+00	-.1360E+08
GLoads	19	.0000E+00	.0000E+00	.0000E+00	.0000E+00	.0000E+00	.1360E+08

GLOBAL REACTIONS (N, Nmm)

Node	Fx	Fy	Fz	Mx	My	Mz
1	-.2043E+04	-.4290E+04	.0000E+00	.0000E+00	.0000E+00	.0000E+00
23	.2043E+04	.4290E+04	.0000E+00	.0000E+00	.0000E+00	.0000E+00

LOAD CASE 1 ($K_\theta = 1 \text{ E12 Nmm/radian}$)

EXTERNAL PRESSURE $p_e = C_{p,e} \times K_a (\theta = 0^\circ)$ (i.e. $q_z = 1 \text{ kPa}$, $b = 1 \text{ m}$)

GLOBAL DISPLACEMENTS (mm, radians)

Node	Translations			/	Rotations		
	X	Y	Z		X	Y	Z
1	.0000E+00	.0000E+00	.0000E+00	/	.0000E+00	.0000E+00	-.8567E-03
2	.2285E+01	.1827E-01	.0000E+00	/	.0000E+00	.0000E+00	-.4788E-03
3	.2800E+01	.2208E-01	.0000E+00	/	.0000E+00	.0000E+00	-.3114E-03
4	.2985E+01	.2369E-01	.0000E+00	/	.0000E+00	.0000E+00	-.2465E-03
5	.3083E+01	.2376E-01	.0000E+00	/	.0000E+00	.0000E+00	-.2443E-03
6	.3083E+01	.2376E-01	.0000E+00	/	.0000E+00	.0000E+00	-.2260E-03
7	.3110E+01	-.1024E+00	.0000E+00	/	.0000E+00	.0000E+00	-.1443E-03
8	.2864E+01	.1217E+01	.0000E+00	/	.0000E+00	.0000E+00	.9448E-03
9	.2188E+01	.4660E+01	.0000E+00	/	.0000E+00	.0000E+00	.1641E-02
10	.1307E+01	.9127E+01	.0000E+00	/	.0000E+00	.0000E+00	.1837E-02
11	.4973E+00	.1326E+02	.0000E+00	/	.0000E+00	.0000E+00	.1451E-02
12	.4526E-01	.1567E+02	.0000E+00	/	.0000E+00	.0000E+00	.5652E-03
13	.8413E-01	.1568E+02	.0000E+00	/	.0000E+00	.0000E+00	-.8076E-03
14	-.5612E+00	.1236E+02	.0000E+00	/	.0000E+00	.0000E+00	-.1852E-02
15	-.1565E+01	.7299E+01	.0000E+00	/	.0000E+00	.0000E+00	-.2066E-02
16	-.2499E+01	.2591E+01	.0000E+00	/	.0000E+00	.0000E+00	-.1451E-02
17	-.2977E+01	.1378E+00	.0000E+00	/	.0000E+00	.0000E+00	-.1354E-03
18	-.2996E+01	.3372E-01	.0000E+00	/	.0000E+00	.0000E+00	-.2920E-04
19	-.2996E+01	.3372E-01	.0000E+00	/	.0000E+00	.0000E+00	-.4824E-05
20	-.2998E+01	.3362E-01	.0000E+00	/	.0000E+00	.0000E+00	-.1846E-05
21	-.2926E+01	.3134E-01	.0000E+00	/	.0000E+00	.0000E+00	.8987E-04
22	-.2578E+01	.2593E-01	.0000E+00	/	.0000E+00	.0000E+00	.3443E-03
23	.0000E+00	.0000E+00	.0000E+00	/	.0000E+00	.0000E+00	.1006E-02

} 'knee' joint
} on East side

'ridge' joint

} 'knee' joint
} on West side

GLOBAL BEAM LOADS (N, Nmm)

GLoads	Node	Fx	Fy	Fz	Mx	My	Mz
BEAM NO. 1							
GLoads	1	-.3298E+04	-.4436E+04	.0000E+00	.0000E+00	.0000E+00	-.1892E-08
GLoads	2	.4120E+04	.4436E+04	.0000E+00	.0000E+00	.0000E+00	.1016E+08
BEAM NO. 2							
GLoads	2	-.4120E+04	-.4436E+04	.0000E+00	.0000E+00	.0000E+00	-.1016E+08
GLoads	3	.4420E+04	.4436E+04	.0000E+00	.0000E+00	.0000E+00	.1443E+08
BEAM NO. 3							
GLoads	3	-.4420E+04	-.4436E+04	.0000E+00	.0000E+00	.0000E+00	-.1443E+08
GLoads	4	.4558E+04	.4436E+04	.0000E+00	.0000E+00	.0000E+00	.1650E+08
BEAM NO. 4							
GLoads	4	-.4558E+04	-.4436E+04	.0000E+00	.0000E+00	.0000E+00	-.1650E+08
GLoads	5	.4561E+04	.4436E+04	.0000E+00	.0000E+00	.0000E+00	.1832E+08
BEAM NO. 5							
GLoads	6	-.4561E+04	-.4436E+04	.0000E+00	.0000E+00	.0000E+00	-.1832E+08
GLoads	7	.4587E+04	.4310E+04	.0000E+00	.0000E+00	.0000E+00	.1554E+08
BEAM NO. 6							
GLoads	7	-.4587E+04	-.4310E+04	.0000E+00	.0000E+00	.0000E+00	-.1554E+08
GLoads	8	.4739E+04	.3562E+04	.0000E+00	.0000E+00	.0000E+00	.8315E+07
BEAM NO. 7							
GLoads	8	-.4739E+04	-.3562E+04	.0000E+00	.0000E+00	.0000E+00	-.8315E+07
GLoads	9	.4891E+04	.2814E+04	.0000E+00	.0000E+00	.0000E+00	.2971E+07
BEAM NO. 8							
GLoads	9	-.4891E+04	-.2814E+04	.0000E+00	.0000E+00	.0000E+00	-.2971E+07
GLoads	10	.5043E+04	.2066E+04	.0000E+00	.0000E+00	.0000E+00	-.4881E+06
BEAM NO. 9							
GLoads	10	-.5043E+04	-.2066E+04	.0000E+00	.0000E+00	.0000E+00	.4881E+06


```

GLoads 11 .5195E+04 .1319E+04 .0000E+00 .0000E+00 .0000E+00 .2062E+07
***BEAM NO. 10***
GLoads 11 -.5195E+04 -.1319E+04 .0000E+00 .0000E+00 .0000E+00 .2062E+07
GLoads 12 .5348E+04 .5707E+03 .0000E+00 .0000E+00 .0000E+00 .1753E+07
***BEAM NO. 11***
GLoads 12 -.5348E+04 -.5707E+03 .0000E+00 .0000E+00 .0000E+00 .1753E+07
GLoads 13 .5077E+04 .7579E+03 .0000E+00 .0000E+00 .0000E+00 .4093E+07
***BEAM NO. 12***
GLoads 13 -.5077E+04 -.7579E+03 .0000E+00 .0000E+00 .0000E+00 .4093E+07
GLoads 14 .4807E+04 .2086E+04 .0000E+00 .0000E+00 .0000E+00 .3085E+07
***BEAM NO. 13***
GLoads 14 -.4807E+04 -.2086E+04 .0000E+00 .0000E+00 .0000E+00 .3085E+07
GLoads 15 .4537E+04 .3415E+04 .0000E+00 .0000E+00 .0000E+00 .1271E+07
***BEAM NO. 14***
GLoads 15 -.4537E+04 -.3415E+04 .0000E+00 .0000E+00 .0000E+00 .1271E+07
GLoads 16 .4266E+04 .4744E+04 .0000E+00 .0000E+00 .0000E+00 .8975E+07
***BEAM NO. 15***
GLoads 16 -.4266E+04 -.4744E+04 .0000E+00 .0000E+00 .0000E+00 .8975E+07
GLoads 17 .3996E+04 .6072E+04 .0000E+00 .0000E+00 .0000E+00 .2003E+08
***BEAM NO. 16***
GLoads 17 -.3996E+04 -.6072E+04 .0000E+00 .0000E+00 .0000E+00 .2003E+08
GLoads 18 .3950E+04 .6296E+04 .0000E+00 .0000E+00 .0000E+00 .2437E+08
***BEAM NO. 17***
GLoads 18 -.3950E+04 -.6296E+04 .0000E+00 .0000E+00 .0000E+00 .2437E+08
GLoads 19 .3957E+04 .6296E+04 .0000E+00 .0000E+00 .0000E+00 .2279E+08
***BEAM NO. 18***
GLoads 19 -.3957E+04 -.6296E+04 .0000E+00 .0000E+00 .0000E+00 .2279E+08
GLoads 20 .4279E+04 .6296E+04 .0000E+00 .0000E+00 .0000E+00 .2090E+08
***BEAM NO. 19***
GLoads 20 -.4279E+04 -.6296E+04 .0000E+00 .0000E+00 .0000E+00 .2090E+08
GLoads 21 .4979E+04 .6296E+04 .0000E+00 .0000E+00 .0000E+00 .1627E+08
***BEAM NO. 20***
GLoads 21 -.4979E+04 -.6296E+04 .0000E+00 .0000E+00 .0000E+00 .1627E+08
GLoads 22 .6897E+04 .6296E+04 .0000E+00 .0000E+00 .0000E+00 .7451E-08

```

GLOBAL SPRING LOADS (N, Nmm)

Type	Node	Fx	Fy	Fz	Mx	My	Mz
SPRG NO. 1 (axial, East)							
GLoads	5	.4561E+04	.0000E+00	.0000E+00	.0000E+00	.0000E+00	.0000E+00
GLoads	6	.4561E+04	.0000E+00	.0000E+00	.0000E+00	.0000E+00	.0000E+00
SPRG NO. 2 (shear, East)							
GLoads	5	.0000E+00	-.4436E+04	.0000E+00	.0000E+00	.0000E+00	.0000E+00
GLoads	6	.0000E+00	.4436E+04	.0000E+00	.0000E+00	.0000E+00	.0000E+00
SPRG NO. 3 (bending-rotation, East)							
GLoads	5	.0000E+00	.0000E+00	.0000E+00	.0000E+00	.0000E+00	-.1832E+08
GLoads	6	.0000E+00	.0000E+00	.0000E+00	.0000E+00	.0000E+00	.1832E+08
SPRG NO. 4							
GLoads	18	-.3950E+04	.0000E+00	.0000E+00	.0000E+00	.0000E+00	.0000E+00
GLoads	19	.3950E+04	.0000E+00	.0000E+00	.0000E+00	.0000E+00	.0000E+00
SPRG NO. 5							
GLoads	18	.0000E+00	.6296E+04	.0000E+00	.0000E+00	.0000E+00	.0000E+00
GLoads	19	.0000E+00	-.6296E+04	.0000E+00	.0000E+00	.0000E+00	.0000E+00
SPRG NO. 6							
GLoads	18	.0000E+00	.0000E+00	.0000E+00	.0000E+00	.0000E+00	-.2437E+08
GLoads	19	.0000E+00	.0000E+00	.0000E+00	.0000E+00	.0000E+00	.2437E+08

GLOBAL REACTIONS (N, Nmm)

Node	Fx	Fy	Fz	Mx	My	Mz
1	-.3298E+04	-.4436E+04	.0000E+00	.0000E+00	.0000E+00	.0000E+00 (East, ground)
23	.6897E+04	-.6296E+04	.0000E+00	.0000E+00	.0000E+00	.0000E+00 (West, ground)

LOAD CASE 2 ($K_{\theta} = 1 \text{ E}12 \text{ Nmm/radian}$)

EXTERNAL PRESSURE $p_e = C_{p,e} \times K_a$ ($\theta = 90^\circ$) (i.e. $q_x = 1 \text{ kPa}$, $b = 1 \text{ m}$)

GLOBAL DISPLACEMENTS (mm, radians)

Node	Translations			/	Rotations		
	X	Y	Z		X	Y	Z
1	.0000E+00	.0000E+00	.0000E+00	/	.0000E+00	.0000E+00	-.5862E-03
2	.1565E+01	.1767E-01	.0000E+00	/	.0000E+00	.0000E+00	-.2832E-03
3	.1885E+01	.2136E-01	.0000E+00	/	.0000E+00	.0000E+00	-.1438E-03
4	.1990E+01	.2291E-01	.0000E+00	/	.0000E+00	.0000E+00	-.8895E-04
5	.2025E+01	.2298E-01	.0000E+00	/	.0000E+00	.0000E+00	-.8711E-04
6	.2025E+01	.2298E-01	.0000E+00	/	.0000E+00	.0000E+00	-.7142E-04
7	.2028E+01	.1694E-01	.0000E+00	/	.0000E+00	.0000E+00	-.2718E-05
8	.1769E+01	.1391E+01	.0000E+00	/	.0000E+00	.0000E+00	.8611E-03
9	.1202E+01	.4291E+01	.0000E+00	/	.0000E+00	.0000E+00	.1300E-02
10	.5600E+00	.7572E+01	.0000E+00	/	.0000E+00	.0000E+00	.1241E-02
11	.9858E-01	.9984E+01	.0000E+00	/	.0000E+00	.0000E+00	.6959E-03
12	-.7646E-06	.1064E+02	.0000E+00	/	.0000E+00	.0000E+00	-.1297E-09
13	-.9858E-01	.9984E+01	.0000E+00	/	.0000E+00	.0000E+00	-.6959E-03
14	-.5600E+00	.7572E+01	.0000E+00	/	.0000E+00	.0000E+00	-.1241E-02
15	-.1202E+01	.4291E+01	.0000E+00	/	.0000E+00	.0000E+00	-.1300E-02
16	-.1769E+01	.1391E+01	.0000E+00	/	.0000E+00	.0000E+00	-.8611E-03
17	-.2028E+01	.1694E-01	.0000E+00	/	.0000E+00	.0000E+00	.2718E-05
18	-.2025E+01	.2298E-01	.0000E+00	/	.0000E+00	.0000E+00	.7142E-04
19	-.2025E+01	.2298E-01	.0000E+00	/	.0000E+00	.0000E+00	.8711E-04
20	-.1990E+01	.2291E-01	.0000E+00	/	.0000E+00	.0000E+00	.8895E-04
21	-.1885E+01	.2136E-01	.0000E+00	/	.0000E+00	.0000E+00	.1438E-03
22	-.1565E+01	.1767E-01	.0000E+00	/	.0000E+00	.0000E+00	.2832E-03
23	.0000E+00	.0000E+00	.0000E+00	/	.0000E+00	.0000E+00	.5862E-03

GLOBAL BEAM LOADS (N, Nmm)

GLoads	Node	Fx	Fy	Fz	Mx	My	Mz
BEAM NO. 1							
GLoads	1	-.2499E+04	-.4290E+04	.0000E+00	.0000E+00	.0000E+00	.8440E-09
GLoads	2	.3595E+04	.4290E+04	.0000E+00	.0000E+00	.0000E+00	.8348E+07
BEAM NO. 2							
GLoads	2	-.3595E+04	-.4290E+04	.0000E+00	.0000E+00	.0000E+00	-.8348E+07
GLoads	3	.3995E+04	.4290E+04	.0000E+00	.0000E+00	.0000E+00	.1214E+08
BEAM NO. 3							
GLoads	3	-.3995E+04	-.4290E+04	.0000E+00	.0000E+00	.0000E+00	-.1214E+08
GLoads	4	.4179E+04	.4290E+04	.0000E+00	.0000E+00	.0000E+00	.1402E+08
BEAM NO. 4							
GLoads	4	-.4179E+04	-.4290E+04	.0000E+00	.0000E+00	.0000E+00	-.1402E+08
GLoads	5	.4183E+04	.4290E+04	.0000E+00	.0000E+00	.0000E+00	.1570E+08
BEAM NO. 5							
GLoads	6	-.4183E+04	-.4290E+04	.0000E+00	.0000E+00	.0000E+00	-.1570E+08
GLoads	7	.4211E+04	.4150E+04	.0000E+00	.0000E+00	.0000E+00	.1297E+08
BEAM NO. 6							
GLoads	7	-.4211E+04	-.4150E+04	.0000E+00	.0000E+00	.0000E+00	-.1297E+08
GLoads	8	.4380E+04	.3320E+04	.0000E+00	.0000E+00	.0000E+00	.6050E+07
BEAM NO. 7							
GLoads	8	-.4380E+04	-.3320E+04	.0000E+00	.0000E+00	.0000E+00	-.6050E+07
GLoads	9	.4549E+04	.2490E+04	.0000E+00	.0000E+00	.0000E+00	.1218E+07
BEAM NO. 8							
GLoads	9	-.4549E+04	-.2490E+04	.0000E+00	.0000E+00	.0000E+00	-.1218E+07
GLoads	10	.4718E+04	.1660E+04	.0000E+00	.0000E+00	.0000E+00	-.1522E+07
BEAM NO. 9							
GLoads	10	-.4718E+04	-.1660E+04	.0000E+00	.0000E+00	.0000E+00	.1522E+07

```

GLoads 11 .4887E+04 .8301E+03 .0000E+00 .0000E+00 .0000E+00 .2170E+07
***BEAM NO. 10***
GLoads 11 -.4887E+04 -.8301E+03 .0000E+00 .0000E+00 .0000E+00 .2170E+07
GLoads 12 .5056E+04 .5880E-04 .0000E+00 .0000E+00 .0000E+00 .7268E+06
***BEAM NO. 11***
GLoads 12 -.5056E+04 .5880E-04 .0000E+00 .0000E+00 .0000E+00 .7268E+06
GLoads 13 .4887E+04 .8301E+03 .0000E+00 .0000E+00 .0000E+00 .2170E+07
***BEAM NO. 12***
GLoads 13 -.4887E+04 .8301E+03 .0000E+00 .0000E+00 .0000E+00 .2170E+07
GLoads 14 .4718E+04 .1660E+04 .0000E+00 .0000E+00 .0000E+00 .1522E+07
***BEAM NO. 13***
GLoads 14 -.4718E+04 .1660E+04 .0000E+00 .0000E+00 .0000E+00 .1522E+07
GLoads 15 .4549E+04 .2490E+04 .0000E+00 .0000E+00 .0000E+00 .1218E+07
***BEAM NO. 14***
GLoads 15 -.4549E+04 .2490E+04 .0000E+00 .0000E+00 .0000E+00 .1218E+07
GLoads 16 .4380E+04 .3320E+04 .0000E+00 .0000E+00 .0000E+00 .6050E+07
***BEAM NO. 15***
GLoads 16 -.4380E+04 .3320E+04 .0000E+00 .0000E+00 .0000E+00 .6050E+07
GLoads 17 .4211E+04 .4150E+04 .0000E+00 .0000E+00 .0000E+00 .1297E+08
***BEAM NO. 16***
GLoads 17 -.4211E+04 .4150E+04 .0000E+00 .0000E+00 .0000E+00 .1297E+08
GLoads 18 .4183E+04 .4290E+04 .0000E+00 .0000E+00 .0000E+00 .1570E+08
***BEAM NO. 17***
GLoads 18 -.4183E+04 .4290E+04 .0000E+00 .0000E+00 .0000E+00 .1570E+08
GLoads 19 .4179E+04 .4290E+04 .0000E+00 .0000E+00 .0000E+00 .1402E+08
***BEAM NO. 18***
GLoads 19 -.4179E+04 .4290E+04 .0000E+00 .0000E+00 .0000E+00 .1402E+08
GLoads 20 .3995E+04 .4290E+04 .0000E+00 .0000E+00 .0000E+00 .1214E+08
***BEAM NO. 19***
GLoads 20 -.3995E+04 .4290E+04 .0000E+00 .0000E+00 .0000E+00 .1214E+08
GLoads 21 .3595E+04 .4290E+04 .0000E+00 .0000E+00 .0000E+00 .8348E+07
***BEAM NO. 20***
GLoads 21 -.3595E+04 .4290E+04 .0000E+00 .0000E+00 .0000E+00 .8348E+07
GLoads 22 .2499E+04 .4290E+04 .0000E+00 .0000E+00 .0000E+00 .1746E+08

```

GLOBAL SPRING LOADS (N, Nmm)

Type	Node	Fx	Fy	Fz	Mx	My	Mz
SPRG NO. 1							
GLoads	5	.4183E+04	.0000E+00	.0000E+00	.0000E+00	.0000E+00	.0000E+00
GLoads	6	.4183E+04	.0000E+00	.0000E+00	.0000E+00	.0000E+00	.0000E+00
SPRG NO. 2							
GLoads	5	.0000E+00	.4290E+04	.0000E+00	.0000E+00	.0000E+00	.0000E+00
GLoads	6	.0000E+00	.4290E+04	.0000E+00	.0000E+00	.0000E+00	.0000E+00
SPRG NO. 3							
GLoads	5	.0000E+00	.0000E+00	.0000E+00	.0000E+00	.0000E+00	-.1570E+08
GLoads	6	.0000E+00	.0000E+00	.0000E+00	.0000E+00	.0000E+00	.1570E+08
SPRG NO. 4							
GLoads	18	-.4183E+04	.0000E+00	.0000E+00	.0000E+00	.0000E+00	.0000E+00
GLoads	19	.4183E+04	.0000E+00	.0000E+00	.0000E+00	.0000E+00	.0000E+00
SPRG NO. 5							
GLoads	18	.0000E+00	.4290E+04	.0000E+00	.0000E+00	.0000E+00	.0000E+00
GLoads	19	.0000E+00	-.4290E+04	.0000E+00	.0000E+00	.0000E+00	.0000E+00
SPRG NO. 6							
GLoads	18	.0000E+00	.0000E+00	.0000E+00	.0000E+00	.0000E+00	-.1570E+08
GLoads	19	.0000E+00	.0000E+00	.0000E+00	.0000E+00	.0000E+00	.1570E+08

GLOBAL REACTIONS (N, Nmm)

Node	Fx	Fy	Fz	Mx	My	Mz
1	-.2499E+04	-.4290E+04	.0000E+00	.0000E+00	.0000E+00	.0000E+00
23	.2499E+04	.4290E+04	.0000E+00	.0000E+00	.0000E+00	.0000E+00

APPENDIX G. MOMENT - ROTATION Calculations

SPREADSHEET FORMULAE:

Combining the calibration test results for measured strains $\Delta\epsilon_m$ ('B' and 'T') of

$$\epsilon_m(B) = -3.9574 \times \text{mV output (in microstrain)} \text{ and } \Delta\epsilon_m(T) = -4.1952 \times \text{mV output,}$$

with the extreme fibre strain strain $\Delta\epsilon$ ('B' and 'T') expressions derived in Section 5.2.4. gave:

$$\begin{aligned}\Delta\epsilon(B) &= \left(\frac{D+a}{D+a+b} \right) \Delta\epsilon_m(B) + \left(\frac{D+a}{D+a+b} - 1 \right) \Delta\epsilon_m(T) \\ &= 0.99415 \times -3.9574 \Delta\epsilon_m(B) + -0.00585 \times -4.1592 \Delta\epsilon_m(T) \\ &= -3.934 \Delta\epsilon_m(B) + 0.0243 \Delta\epsilon_m(T)\end{aligned}$$

and

$$\begin{aligned}\Delta\epsilon(T) &= \left(\frac{a}{D+a+b} \right) \Delta\epsilon_m(B) + \left(\frac{a}{D+a+b} - 1 \right) \Delta\epsilon_m(T) \\ &= -0.00585 \times -3.9574 \Delta\epsilon_m(B) + 0.99415 \times -4.1592 \Delta\epsilon_m(T) \\ &= 0.0232 \Delta\epsilon_m(B) - 4.135 \Delta\epsilon_m(T)\end{aligned}$$

Bending strain was taken as half the difference between the two extreme fibre strains, and axial strain as the average. Moment was then the product of bending (micro)strain, LVL Young's Modulus ($E = 13,200 \text{ MPa}$) and Section Modulus ($Z = 6.065E6 \text{ mm}^3$).

[NB. it was noticed *after* all analysis was complete that the negative signs in the '0.00585' terms above had been omitted during analysis. This was found to have caused an error of about 1.1% in the calculated top and bottom extreme fibre strains, so was neglected.]

For rotations, the calibrated RVDT output signal was converted to radians as follows:

$$\begin{aligned}\Delta\text{rotation } (\theta) \text{ in milliradians} &= 8.135 \times (\text{milli})\text{Voltage output} \times \frac{\pi}{180} \\ &= 0.142 \times \text{mV output}\end{aligned}$$

Raw data (instrument output) is shown in columns C, E and F for RVDT and top and bottom 'plastic' strain gauges respectively, free of any calibration or conversion.

Stiffness was simply calculated as the quotient of the maximum values for rafter moment (column M) and joint rotation (column D), thereby representing a 'secant' stiffness (column N). An estimate for the 'true' node point stiffness would be 1.23 times this value.

"Filename" convention was as follows: "SJ" stood for "Signature Joinery" to distinguish this 1992 data from "KT" data of 1991, when the building occupants traded as "Kent Town Gate Centre". The *next four* digits give the date of the collection of wind events. For example, 'SJ0708' represented data collected on the 7th of August, 1992. The *fifth* digit is always a '4' for wind data, as it abbreviates "40 Hz sampling rate": other rates were used for thermal strain monitoring or 'frequency of response' measurements. A final 'b' denoted the second file taken on the same day.

"Event" times are shown for a 12 hour clock, and denote the time at which the event record is at time zero. Varying length records were taken, all being for a nominal 10 seconds *after* the preset velocity 'trigger' value was exceeded, but having between zero and 1.5 seconds of data collected *before* this occurred (see 5.1.4.). Where *two* times are shown for an event, this represents the case when the time history record for a 'significant' change in strain response 'straddled' two of these data "windows".

	A	B	C	D	E	F	G	H	I	J	K	L	M	N
352		3:57:06	2.83	-0.4019	-5.52	6.76	22.96	-26.75	22.67	-26.46	-24.56	-1.90	-1.97	4.894
353			-4.28	0.6078	6.21	-7.78	-25.83	30.79	-25.50	30.46	-27.98	2.48	2.24	3.685
354		4:00:53	3.55	-0.5041	-5.94	6.81	24.71	-26.95	24.40	-26.65	-25.53	-1.12	-2.04	4.054
355		4:01:27	-3.48	0.4942	6.11	-6.78	-25.41	26.83	-25.11	26.53	25.82	0.71	2.07	4.182
356			5.18	-0.7356	-7.94	8.45	33.02	-33.44	32.64	-33.05	-32.84	-0.21	-2.63	3.575
357			-4.18	0.5936	7.25	-9.06	-30.15	35.85	-29.77	35.47	32.62	2.85	2.61	4.399
358		4:02:42	-4.33	0.6149	6.92	-8.55	-28.78	33.84	-28.42	33.47	30.94	2.53	2.48	4.029
359		4:03:23	-2.25	0.3195	3.46	-5.03	-14.39	19.91	-14.19	19.71	16.95	2.76	1.36	4.246
360			2.2	-0.3124	-3.91	4.98	16.26	-19.71	16.05	-19.50	-17.77	-1.72	-1.42	4.555
361		4:05:32	2	-0.284	-5.76	6.74	23.96	-26.67	23.66	-26.38	-25.02	-1.36	-2.00	7.052
362		4:07:03	3.45	-0.4899	-4.46	5.88	18.55	-23.27	18.31	-23.02	-20.67	-2.36	-1.65	3.377
363		4:07:16	2.15	-0.3053	-5.05	6.22	21.00	-24.62	20.74	-24.35	-22.54	-1.81	-1.80	5.911
364			-1.38	0.196	5.41	-6.32	-22.50	25.01	-22.22	24.73	23.48	1.25	1.88	9.591
365		4:07:27	2.33	-0.3309	-6.1	7.36	25.37	-29.13	25.05	-28.81	-26.93	-1.88	-2.16	6.516
366			-3.5	0.497	6.25	-7.56	-26.00	29.92	-25.67	29.59	27.63	1.96	2.21	4.450
367			4.98	-0.7072	-6.47	8.27	26.91	-32.73	26.56	-32.38	-29.47	-2.91	-2.36	3.336
368		4:07:43	-3.78	0.5368	6.53	-8.23	-27.16	32.57	-26.81	32.22	29.52	2.70	2.36	4.402
369		4:10:10	-6.83	0.9699	11.4	-13.5	-47.41	53.42	-46.82	52.83	49.83	3.01	3.99	4.113
370			5.38	-0.764	-10.01	12.6	41.63	-49.86	41.10	-49.33	-45.21	-4.11	-3.62	4.738
371		4:10:52	1.45	-0.2059	-4.71	5.23	19.59	-20.70	19.35	-20.46	-19.91	-0.55	-1.59	7.740
372		4:11:21	3.18	-0.4516	-5.46	6.65	22.71	-26.32	22.42	-26.03	-24.23	-1.80	-1.94	4.295
373			-2.83	0.4019	4.88	-6.32	-20.30	25.01	-20.03	24.75	22.39	2.36	1.79	4.460
374		4:11:21,4:11:35	-7.1	1.0082	11.39	-12.76	-47.37	50.50	-46.80	49.92	48.36	1.56	3.87	3.840
375		4:11:35	-4.65	0.6603	5.64	-6.52	-23.46	25.80	-23.17	25.51	24.34	1.17	1.95	2.951
376		4:11:57	-4.78	0.6788	6.63	-8.11	-27.58	32.09	-27.23	31.75	29.49	2.26	2.36	3.478
377			4.38	-0.622	-5.77	6.98	24.00	-27.62	23.70	-27.32	-25.51	-1.81	-2.04	3.283
378		4:12:27	2.48	-0.3522	-5.69	6.71	23.67	-26.55	23.37	-26.26	-24.82	-1.44	-1.99	5.641
379			-6.45	0.9159	12.78	-15.12	-53.15	59.84	-52.49	59.17	55.83	3.34	4.47	4.880
380			4.85	-0.6887	-9.96	11.88	41.43	-47.01	40.91	-46.50	-43.70	-2.79	-3.50	5.080
381			-9.05	1.2851	12.65	-15.22	-52.61	60.23	-51.95	59.57	55.76	3.81	4.46	3.474
382		4:12:43	-4.4	0.6248	7.52	-8.18	-31.28	32.37	-30.90	32.00	31.45	0.55	2.52	4.030
383		4:15:27	2.55	-0.3621	-4.91	6.21	20.42	-24.58	20.16	-24.31	-22.24	-2.08	-1.78	4.916
384		4:16:04	2.13	-0.3025	-6.59	7.45	27.41	-29.48	27.08	-29.15	-28.11	-1.04	-2.25	7.441
385		4:17:21	2.65	-0.3763	-5.43	6.7	22.58	-26.51	22.30	-26.23	-24.26	-1.97	-1.94	5.162
386		4:17:21,4:17:35	-2	0.284	5.68	-6.44	-23.62	25.49	-23.34	25.20	24.27	0.93	1.94	6.841
387		4:19:35	2.4	-0.3408	-4.81	5.95	20.01	-23.55	19.75	-23.29	-21.52	-1.77	-1.72	5.055
388			-2.25	0.3195	4.2	-5.18	-17.47	20.50	-17.25	20.28	18.76	1.52	1.50	4.701
389	SJ28094b	4:27:06	2.13	-0.3025	-5.59	6.37	23.25	-25.21	22.97	-24.93	-23.95	-0.98	-1.92	6.338
390		4:27:21	3.48	-0.4942	-3.68	4.68	15.31	-18.52	15.11	-18.32	-16.72	-1.61	-1.34	2.708
391			-5.18	0.7356	7.78	-8.58	-32.36	33.95	-31.97	33.57	32.77	0.80	2.62	3.566
392		4:29:10	-2.78	0.3948	6.96	-8.07	-28.95	31.94	-28.59	31.58	30.09	1.49	2.41	6.101
393			2.1	-0.2982	-6.62	8.29	27.53	-32.81	27.18	-32.45	-29.82	-2.64	-2.39	8.005
394		4:32:11	-4.15	0.5893	6.25	-7.11	-26.00	28.14	-25.68	27.82	26.75	1.07	2.14	3.634
395		4:33:02	3.33	-0.4729	-5.36	6.82	22.29	-26.99	22.01	-26.70	-24.35	-2.35	-1.95	4.123
396			-2.38	0.338	6.39	-8.95	-26.58	35.42	-26.21	35.06	30.64	4.42	2.45	7.257
397		4:33:39	-2.13	0.3025	4.08	-5.38	-16.97	21.29	-16.75	21.07	18.91	2.16	1.51	5.004
398		4:35:35	-3.15	0.4473	6.35	-7.54	-26.41	29.84	-26.08	29.51	27.80	1.71	2.23	4.975
399			3.73	-0.5297	-6.79	9.3	28.24	-36.80	27.86	-36.42	-32.14	-4.28	-2.57	4.858
400		4:37:23	3.08	-0.4374	-5.9	6.9	24.54	-27.31	24.24	-27.00	-25.62	-1.38	-2.05	4.689
401		5:09:24	-1.98	0.2812	5.18	-5.73	-21.54	22.68	-21.29	22.42	21.85	0.57	1.75	6.222
402		5:54:19	-4.6	0.6532	6.7	-8.45	-27.87	33.44	-27.51	33.08	30.29	2.79	2.43	3.713
403		6:19:11	-3.43	0.4871	5	-6.08	-20.80	24.06	-20.53	23.80	22.17	1.63	1.77	3.643
404		7:18:37	3.03	-0.4303	-4.38	5.25	18.22	-20.78	17.99	-20.55	-19.27	-1.28	-1.54	3.585
405			-3.05	0.4331	4.63	-6.45	-19.26	25.53	-19.00	25.26	22.13	3.13	1.77	4.090
406		7:19:09	-6.1	0.8662	5.28	-4.382	-21.96	17.34	-21.73	17.11	19.42	-2.31	1.55	1.795
407		8:50:39	-3.3	0.4686	5.4	-4.482	-22.46	17.74	-22.22	17.50	19.86	-2.36	1.59	3.393
408		8:51:12	-2.28	0.3238	4.13	-3.428	-17.18	13.57	-17.00	13.39	15.19	-1.81	1.22	3.756
409		10:39:14 PM	-4.3	0.6106	2.05	-1.702	-8.53	6.73	-8.44	6.64	7.54	-0.90	0.60	989
410														
411			max	4.11				max	68.58	122.10	115.89	6.21	9.28	15.694
412			min	-2.37				min	-109.68	-79.85	-74.22	-6.02	-5.94	779
413			mean	0.0945				mean			2.65	0.12	0.21	4082.29
414									Δ top extm	Δ bot extm	Δ bend strn	Δ axial strn	$\partial M = \partial \sigma Z$	stiffness
415			Assumes linear-elastic stress-strain distribution, $E = 13,200 \text{ MPa}$											
416			top and bott strain gauges (SG) located 4.5mm remote from extreme fibres											
417			negative Δ bott strain (mV) indicates "opening" joint, equivalent to positive ∂ Moment											
418			Depth of tapering rafter at midpoint of SG gauge length is approx. 760mm											
419														
420	SHADINGS:	Column A	denotes one of the "best" data records											
421		Column E, F	means "off scale" strain value, so estimate based on											
422			the other strain gauge value and their relationship											
423			during the particular wind event is shown											

BIBLIOGRAPHY

- Australian Standard 1170.2-1989, "SAA Loading Code, (Minimum design loads on structures), Part 2: Wind Loads", Sydney, 1988.
- Australian Standard 1720.1-1988, "SAA Timber Structures Code, Part 1: Design Methods".
- ABENDROTH,R.E., WIPF,T.J. (1989). "Cyclic load behaviour of bolted timber joint", *Journal of Structural Engineering, ASCE*, **115**(10), 2496-2510.
- ANTONIDES,C.E., VANDERBILT,M.D., GOODMAN,J.R. (1980). "Interlayer gap effect on nailed joint stiffness", *Wood Science*, **13**(1), 41-46.
- ATHERTON,G.H., ROWE,K.E., BASTENDORFF,K.M.(1980). "Damping and slip of nailed joints", *Wood Science*, **12**(4), 218-226. (Also Paper 1353, *Forest Research Lab., School of Forestry, Oregon State University*).
- AUNE,P., PATTON-MALLORY,M. (1986a,b). "Lateral load-bearing capacity of nailed joints based on the yield theory-(a) theoretical development and (b) experimental verifications", *US Department of Agriculture, Forest Service, Forest Products Laboratory Research Paper FPL (a) 469,(b) 470*.
- BATCHELAR,M.K. (1984). "Improved plywood gusset joints for timber portal frames", *Proceedings, Pacific Timber Engineering Conf., Auckland, May 1984*, Vol. 2, 655-666.
- BATCHELAR,M.K., CAVANAGH,G.J. (1984). "Nailed plywood gusset joints for timber portal frames", *Proc., Pacific Timber Engineering Conference, Auckland, NZ, May 1984*, Vol. 2, 631-642.
- BATCHELAR,M.L., HUNT,R.D. (1991). "Composite plywood and steel plates for moment-resisting joints in timber frames", *Proc., International Timber Engineering Conf., London, UK*, Vol. 3, 3.104-110.
- BOULT,B.F. (1987). "Moment resisting joints", *New Zealand Journal of Timber Construction*, **3**(2), 265-276.
- BUCHANAN,A.H., DEAN,J.A. (1988). "Practical design of timber structures to resist earthquakes", *Proceedings, 1988 International Conference on Timber Engineering, Seattle, Washington USA, Sept 1988*, 813-822.
- CECCOTTI,A., VIGNOLI,A. (1988). "Dynamic tests on full-scale structures of glue-laminated timber: theoretical and experimental studies", *Journal of Testing and Evaluation*, **16**(2), 178-189.
- CHOU,C., POLENSEK,A. (1987). "Damping and stiffness of nailed joints: response to drying", *Wood and Fiber Science*, **19**(1), 48-58.
- CREWS,K. (1992). "Research and development trends in structural applications of timber for expansion of the non-residential market for forest products in Australia - 1990 Gottstein Fellowship Report", National Educational Trust of the Australian Forest Products Industry.
- CRUZ,H.M.P., HILSON,B.O., WHALE,L.R.J. (1991). "Dynamic behaviour of nailed timber joints-embedment tests under cyclic load", *Proceedings, International Timber Engineering Conference, London, UK*, Vol. 3, 3.11-3.19.
- DOWRICK,D.J. (1986). "Hysteresis loops for timber structures", *Bulletin of the New Zealand National Society for Earthquake Engineering*, **19**(2), 143-152.
- DUTT,A.J. (1983). "Simplification of the dynamic characteristics of the wind loading on a low-rise structure", *Proceedings, Sixth International Conference on Wind Engineering, Gold Coast, Qld, March 1983, Journal of Wind Engineering and Industrial Aerodynamics*, **13**, 301-312. Also published as "Wind Engineering 1983", Part A (Sessions 1-8), J.D.Holmes et al (eds), Elsevier Science Publishers, Amsterdam, The Netherlands, 1984.
- FOSCHI,R.O., FOLZ,B.R., YAO,F.Z.(1989). "Reliability based design of wood structures", Structural Research Series, Report No. 34, Department of Civil Engineering, University of British Columbia, Vancouver, Canada.
- FOSCHI,R.O., LONGWORTH,J. (1975). "Analysis and design of griplam nailed connections", *Journal of Structural Engineering, ASCE*, **101**(12), 2537-

- GERHARDS,C.C., LINK,C.L. (1987). "A cumulative damage model to predict load duration characteristics of lumber", *Wood and Fiber Science*, **19**(2), 147-164.
- GIRHAMMAR,U.A., ANDERSSON,H. (1988). "Effect of loading rate on nailed timber joint capacity", *Journal of Structural Engineering, ASCE*, **114**(11), 2439-2456.
- GRIFFITH,M.C., HIRST,M.J.S., LEE,D.S-C., STEVENS,W.B. (1992). "Dynamic Loading of Nailed Plywood Gusset Plate Joints", *Proceedings, Australian Timber Bridge Engineering Conference, Melbourne, VIC, November 1992*.
- HANSEN,F.T., MORTENSEN,N.L. (1991). "Full-scale testing of prefabricated timber frames subjected to dynamic load", *Proceedings, International Timber Engineering Conference, London, UK, Vol. 3*, 3.97-3.103.
- HILSON,B.O., WHALE,L.R.J. (1990). "Developments in the design of timber joints", *Structural Engineer*, **68**(8), 148-150.
- HIRAI,T. (1987). "Deformation of wooden gabled roof-frame, nailed-jointed with plywood gusset plates", *Mokuzai Gakkaishi, (Journal of the Japan Wood Research Society)*, **33**(9), 689-693.
- HIRST,M.J.S. (1990). "The thermal loading of structures", *Proceedings, Special Symposium on the Occasion of George Sved's 80th Birthday*, Civil Engineering Department, Adelaide University, 1 June 1990
- HOLMES,J.D., MELBOURNE,W.H., WALKER,G.R. (1990). "A Commentary on the Australian Standard for Wind Loads", The Australian Wind Engineering Society, Melbourne, AUST.
- HOLMES,J.D. (1988). "Distribution of peak wind loads on a low rise building", *Proceedings, Seventh International Conference on Wind Engineering, Aachen, FRG, July 1987, Vol 2, Journal of Wind Engineering and Industrial Aerodynamics*, **29**, 59-67 & 128-129.
- HOXEY,R.P. (1986). "A rationalised approach to the analysis of wind pressure measurements on buildings", Sixth Colloquium on Industrial and Buildings Aerodynamics, Aachen, FRG, June 1985, *Journal of Wind Engineering and Industrial Aerodynamics*, **23**, 193-209.
- HUMPHREY,P.E., OSTMAN,L.J. (1988). "Bolted timber connections.Part 1. A wafer technique to model wood deformation around bolts", *Wood and Fiber Science*, **21**(3), 239-251.
- HUNT,R.D., BRYANT,A.H. (1988). "Stresses in region of moment resisting joints in timber structures", *Eleventh Australasian Conference on the Mechanics of Structures and Materials, Auckland, August, 1988*, 115-120. (Also as "Moment resisting nail plate joints - recent developments at Auckland University", *Proc., 1988 International Conference on Timber Engineering, Seattle, Washington USA, Sept 1988*, 251-255.)
- HUNT,R.D., BRYANT,A.H. (1989). "Strength of timber members in joint regions", *Proceedings, Second Pacific Timber Engineering Conference, Auckland, May 1984*, 77-81.
- HUNT,R.D., BRYANT,A.H. (1990). "Strength of laminated timber members", *Proceedings, 1990 International Conference on Timber Engineering, Tokyo, 1990*, 163-169.
- HUNT,R.D., BRYANT,A.H. (1990). "Laterally loaded nail joints in wood", *Journal of Structural Engineering, ASCE*, **116**(1), 111-124.
- JANG,S., POLENSEK,A. (1989). "Theoretical models for creep slip of nailed joints between wood and wood based materials", *Wood Science and Technology*, **23**(3), 237-249.
- JEARY,A.P., LEE,B.E., SPARKS,P.R.(1979). "The determination of modal wind loads from full-scale building response measurements", *Proceedings of the Fifth International Conference on Wind Engineering, Fort Collins, Colorado, USA, Vol 1*, 577-591. Published as "Wind Engineering", J.E.Cermak (ed), Pergamon Press, UK, 1980.
- JENKINS,J.L., POLENSEK,A., BASTENDORFF,K.M. (1979). "Stiffness of nailed wall joints under short and long term lateral loads", *Wood Science*, **11**(3), 145-154.
- KARACABEYLI,E., FOSCHI,R.O. (1987). "Glulam rivet connections under eccentric loading", *Canadian Journal of Civil Engineering*, **14**(5),621-630. Discussion by I.SMITH and L.WHALE, **16**(1),90-91 and reply by the authors, **16**(1),91.
- KAREEM,A. (1984). "Model for predicting the acrosswind response of buildings", *Engineering Structures*, **6**(2), 136-141.

- KIVELL,B.T., MOSS,P.J., CARR,A.J. (1982). "The cyclic load behaviour of two timber portal frames with moment-resisting nailed joints", *Transactions, Institution of Professional Engineers, New Zealand*, 9(2/CE), 55-64.
- KLOPP,G.M., GRIFFITH,M.C. (1993). "Dynamic characteristics of unreinforced masonry buildings" (accepted for publication in *Civil Engineering Transactions, Institution of Engineers, Australia*).
- KNAP,F., LAKOMY,M. (1988). "Effect of the nail shaft cross-section on the strength of wooden nailed joints", *Wire*, 38(4), 462-463. <not available at time of Thesis publication>.
- KOHOUTEK,R. (1990). "Static and dynamic stabilities for structures with semi-rigid joints", *Twelfth Australasian Conference on the Mechanics of Structures and Materials, Brisbane, Qld., Sept 1990*, 191-196.
- KOMATSU,K. (1989). "Behaviour of nailed timber joints with steel side plates", *Proceedings, Second Pacific Timber Engineering Conference, Auckland, Vol 2*, 89-94.
- KOMATSU,K. (1989). "Performance of timber moment-resisting joints", *Proceedings, Second Pacific Timber Engineering Conference, Auckland, NZ, Vol 2*, 25-30.
- KOMATSU,K., KAMIYA,F., HIRASHIMA,Y. (1988). "Full size test and analysis on Glulam two storied portal frames subjected to horizontal load", *The 31st Japan Congress on Materials Research*, 185-191. (also as "Two storey Glulam portal frames", *New Zealand Journal of Timber Construction*, 4(2), 9-12.)
- KOMATSU,K., KAWAMOTO,N., HORIE,K., HARADA,M. (1991). "Modified Glulam moment-resisting joints", *Proc., 1991 International Conf. on Timber Engineering, London, UK, Vol. 3*, 3.111-118.
- LHEUDE,E.P. (1990). "A reappraisal of nailed timber joint design loads", *Proceedings, 2nd. National Structural Engineering Conference, Adelaide, October 1990.*, Vol 1, 361-365.
- LHEUDE,E.P. (1988). "Nail Loads for Plywood/Solid Wood Connections", *Proceedings, 1988 International Conf. on Timber Engrg, Seattle, Washington USA, Sept 1988*, Vol. 1, 3-10.
- LIU,J.Y., SOLTIS,L.A. (1984). "Lateral resistance of nailed joints- A test method", *Forest Products Journal*, 34(1), 55-60.
- LEE,D.S-C. (1993). "Fatigue Effects on Nailed Plywood Gusset Plate Joints", Thesis submitted for Master of Engineering Science Degree, Civil Engineering Department, Adelaide University. [see also Griffith et al (1992)].
- LOFERSKI,J.R., McLAIN,T.E. (1991). "Static and impact flexural properties of common wire nails", *Journal of Testing and Evaluation*, 19(4), 297-304.
- LOFERSKI,J.R., STERN,E.G. (1991) "Understanding impact testing of pallet nails and staples", *Journal of Testing and Evaluation*, 19(5), 379-393.
- LOWE,P.G., EDWARDS,M.R. (1984). "Aspects of ductility in nailed timber connections", *Proc., Pacific Timber Engineering Conference, Auckland, May 1984.*, Vol. 2, 622-630.
- MACK,J.J. (1966). "The strength and stiffness of nailed joints under short duration loading", *CSIRO Australia, Division of Forest Products Research Technical Paper No.40*.
- MACK,J.J. (1981). "Intermittent Loading of Nailed Joints", *CSIRO Australia, Division of Building Research Technical Paper (Second Series) No.40*.
- MALHOTRA,S.K., THOMAS,B. (1984). "Effect of interface characteristics on behaviour of timber joints with multiple nails", *Proceedings, Pacific Timber Engineering Conference, Auckland, May 1984.*, Vol 3, 892-898.
- MALHOTRA,S.K., RITCHIE,R.A.G. (1980). "Behaviour and reliability analysis of nailed timber connections under cyclic loads", *Proceedings, International Conference, Engineering for Protection from Natural Disasters, Bangkok, Thailand, Jan. 1980*, John Wiley & Sons Ltd., Chichester, England and New York, NY, pp 261-272.
- MASSE,D.I., SALINAS,J.J. (1989). "Structural reliability of nailed connections", *Canadian Agricultural Engineering*, 31(2), 195-203.
- McLAIN,T.E., THANGJITHAM,A.M. (1984). "Bolted wood-joint yield model", *Journal of Structural Engineering, ASCE*, 109(8), 1820-1835.
- MELBOURNE,W.H. (1977). "Probability distributions associated with the wind loading of structures", *Civil Engineering Transactions, Inst. of Engineers, Australia*, 19(1),58-67.

- MELCHERS,R.E., KAUR,D. (1982). "The behaviour of frames with flexible connections", *Proceedings, Eighth Australasian Conference on the Mechanics of Structures and Materials, Newcastle, NSW, August 1982, Paper 27.*
- MORIARTY,W.W. (1985). "On the directional uncertainty of strong wind gusts", *Journal of Wind Engineering and Industrial Aerodynamics*, 21(2), 155-166.
- MOSS,P.J. (1984). "Seismic performance of a multistoried timber frame having moment-resisting nailed joints", *Proceedings, Pacific Timber Engineering Conference, Auckland, May 1984., Vol 2, 559-568.*
- MOSS,P.J., CARR,A.J., BUCHANAN,A.H. (1986). "Seismic response of low-rise buildings", *Bulletin of the New Zealand Society for Earthquake Engineering*, 19(3), 180-199.
- NATIONAL ASSOCIATION OF FOREST INDUSTRIES or NAFI (1988), "Timber Datafile SSI - Timber Portal Frames", pp. 14-18.
- NICHOLLS,K. (1990). "Nail Plated Timber Connections", Final Year Research Project Report submitted in partial fulfilment of Bachelor of Engineering Degree, *Department of Civil Engineering, University of Adelaide, November 1990.*
- OEHLERS,D.J. (1991). "Residual strength of structural components subjected to cyclic loads", paper accepted for publication in *Journal of Structural Engineering, ASCE*, revised Dec '91.
- OEHLERS,D.J. (1992). "Design and assessment of shear connectors in composite bridge beams", paper accepted for publication in *Journal of Structural Engineering.*
- OHASHI,Y., SAKAMOTO,I. (1989). "Study on laminated timber moment-resisting joint", *Proceedings, Second Pacific Timber Engineering Conference, Auckland, NZ, Vol 2, 37-42.*
- PELLICANE,P.J. (1991). "Mechanical behaviour of nailed joints with various side member materials", *Journal of Testing and Evaluation*, 19(2), 97-106.
- PELLICANE,P.J., BODIG,J. (1984). "Comparison of nailed joint test methods", *Journal of Testing and Evaluation*, 12(5), 261-267.
- PELLICANE,P.J., BODIG,J., MUTUKU,R.N. (1989). "Modelling the moment-rotation behaviour of bolted joints subject to rotational loading", *Proceedings, Second Pacific Timber Engineering Conference, Auckland, NZ, Vol 2, 43-47.*
- POLENSEK,A. (1988). "Effects of testing variables on damping and stiffness of nailed wood-to-sheathing joints", *Journal of Testing and Evaluation*, 16(5), 474-480.
- POLENSEK,A. (1982). "Creep prediction for nailed joints under constant and increasing loading", *Wood Science*, 15(2), 183-192.
- POLENSEK,A., BASTENDORFF,K.M. (1987). "Damping in nailed joints of light-frame wood buildings", *Wood and Fibre Science*, 19(2), 110-125.
- POLENSEK,A., JANG,S.(1989). "Predicting creep of nailed lumber-to-plywood joints", *Journal of Engineering Mechanics, ASCE*, 115(10),2182-2198.
- RAPHANEL,J.L., SYMONDS,P.S. (1983). "The estimation of large deflections of a portal frame under asymmetric pulse loading", *Journal of Applied Mechanics.*, 51(3),494-500.
- REARDON,G.F. (1989). "The effect of claddings on the response of houses to wind forces", *Proc., Second Pacific Timber Engineering Conference, Auckland, NZ, Vol 2, 101-105.*
- SACHS,P. (1978). "Wind Forces in Engineering"(Second Edition), Pergamon Press, UK.
- SAFAK,E., FOUTCH,D.A. (1987). "Coupled vibrations of rectangular buildings subjected to normally-incident random wind loads", *Journal of Wind Engineering and Industrial Aerodynamics*, 26(2), 129-148.
- SIGRIST,C. (1989). "Nailed joints in timber construction", *Proceedings, Second Pacific Timber Engineering Conference, Auckland, NZ, Vol 2, 71-76.*
- SILVESTER, F.D. (1967). "TIMBER. Its Mechanical Properties and Factors Affecting its Structural Use", Pergamon Press, London, UK, p23.
- SLIKER,A. (1989). "Measurement of the smaller poisson's ratios and related compliances for wood", *Wood Science*, 21(3), 252-262.
- SMITH,I. (1988). "An integrated approach to modelling load-slip behaviour of timber joints with dowel type fasteners", *Proceedings, 1988 International Conference on Timber Engineering, Seattle, Washington USA, Sept 1988. Vol. 2, 285-293.*

- SMITH,I., WHALE,L.R.J., ANDERSON,C., HILSON,B.O., RODD,P.D., POPE,D.J., (1987, 4 parts). "Characteristic properties of nailed and bolted joints under short-term lateral load", *UK Timber Research and Development Association Research Paper*; Part 3 also published by *Journal of the Institute of Wood Science*, 11(2) Issue 62.
- SMITH,I., WHALE,L.R.J., ANDERSON,C., HILSON,B.O., RODD,P.D. (1988). "Design properties of laterally loaded nailed or bolted wood joints", *Canadian Journal of Civil Engineering*, 15(4), 633-643.
- SOLTIS,L.A., HUBBARD,F.K., WILKINSON,T.L. (1986). "Bearing strength of bolted timber joints", *Journal of Structural Engineering, ASCE*, 112(9), 2141-2154.
- SOLTIS,L.A., MTENGA,P.V.A. (1985). "Strength of nailed wood joints subjected to dynamic load", *Forest Products Journal*, 35(11/12), 14-18.
- STATHOPOLOUS,T. (1984). "Wind loads on low-rise buildings: a review of the state of the art", *Engineering Structures*, 6(2), 119-135. 82 refs.
- STERN,E.G., LOFERSKI,J.R. (1989). "Assembly of wood framed structures with helically threaded, hardened-steel nails and spikes", *Proceedings, Second Pacific Timber Engineering Conference, Auckland, Vol 2*, 249-257.
- STEVENS,W.B., GRIFFITH,M.C., HIRST,M.J.S. (1993). "Actual Deformations in Nailed Plywood Gusset Plate Joints due to Dynamic Loading", *Proceedings, 13th Australasian Conference on the Mechanics of Structures and Materials*, Wollongong, NSW, July 5-7, 1993.
- SURRY,D., STATHOPOLOUS,T., DAVENPORT,A.G. (1983). "Simple measurement techniques for area wind loads", *Journal of Engineering Mechanics, ASCE*, 109(4), 1058-1071.
- SURRY,D., STOPAR,E.M.F. (1989). "Wind loading of large low buildings", *Canadian Journal of Civil Engineering*, 16(4), 526-542.
- THOMAS,B., MALHOTRA,S.K. (1985). "Behaviour of timber joints with multiple nails", *Journal of Structural Engineering, ASCE*, 111(5), 973-991.
- TOKUDA,M. (1987). "Fatigue properties of nailed joints under reversed cyclic loading", *Mokuzai Gakkaishi, (Journal of the Japan Wood Research Society)*, 33(7),605-609.
- TSUJINO,T. (1988). "Deformation analysis of wooden frames assembled with nailed plywood gusset-plates", *Mokuzai Gakkaishi*, 34(5), 395-400.
- WALFORD,G.B. (1988). "Analysis of timber portal frame gusset joints", *Proceedings, 1988 International Conference on Timber Engineering, Seattle, Washington USA, Sept 1988, Vol. 1*, 428-431.
- WALFORD,G.B. (1988). "Analysis of timber portal frame gusset joints", *Proc., Institution of Professional Engineers, New Zealand, Annual Conference 1988: "Power of Engineering"*, Vol 1: Civil, New Plymouth, NZ, Feb. 1988, 317-326.
- WHITE,M.S., McLAIN,T.E., PADLA,D. (1990). "Relationships between the results of nail impact bend tests and selected nail material properties", *Journal of Testing and Evaluation*, 18(3), 219-226.
- WILKINSON,T.L. (1971). "Theoretical lateral resistance of nailed joints", *Journal of Structural Engineering, ASCE*, 97(5),1381-1398.
- WILKINSON,T.L. (1976). "Vibrational loading of mechanically fastened wood joints", *US Dept. of Agriculture, Forest Service, Forest Products Laboratory Research Paper FPL 274*.
- WILKINSON,T.L. (1986). "Load distribution among bolts parallel to load", *Journal of Structural Engineering, ASCE*, 112(4), 835-852.
- WILLIAMS,R.L. (1984). "Design of timber structures to resist high wind and earthquake", *Proceedings, Pacific Timber Engineering Conference, Auckland, May 1984., Vol 2*, 439-445.
- WOLFE,R.W., HALL,M., LYLES,D. (1991). "Test apparatus for simulating interactive loads on metal plate wood connections", *Journal of Testing and Evaluation*, 19(6), 421-428.
- YTRUP,P.J. (1990). "The Scrimber International Buildings, Mount Gambier", *Proc., 2nd National Structural Engineering Conference, Adelaide, October 1990, Vol. 1*, 167-172. (also in *Proc., 2nd Pacific Timber Engineering Conference, Auckland, NZ, Vol 3*, 35-39.)